(None) = RL-2000

REPORT NO. FAA-RD-75-32

IMPROVED SIDELOBE SUPPRESSION MODE PERFORMANCE OF ATCRBS WITH VARIOUS ANTENNAS

Dipak L. Sengupta
Jovan Zatkalik
Chen-To Tai

FEBRUARY 1975

INTERIM REPORT

Prepared for
U.S. DEPARTMENT OF TRANSPORTATION
FEDERAL AVIATION ADMINISTRATION
Systems Research and Development Service
Washington DC 20591

Technical Report Documentation Page

1. Report No.	2. Government Accession No.	3. Recipient's Catalog No.
FAA-RD-75-32		

4. Title and Subtitle	5. Report Date
IMPROVED SIDELOBE SUPPRESSION MODE PERFORMANCE OF ATCRBS WITH VARIOUS ANTENNAS	February 1975
	6. Performing Organization Code
	8. Performing Organization Report No.
7. Author(s) Dipak L. Sengupta, Jovan Zatkalik, and Chen-To Tai*	DOT-TSC-FAA-75-4
9. Performing Organization Name and Address The University of Michigan College of Engineering Dept. of Electrical and Computer Engineering Radiation Laboratory Ann Arbor MI 48105	10. Work Unit No. (TRAIS) FA519/R5119
	11. Contract or Grant No. DOT-TSC-717
	13. Type of Report and Period Covered Interim Report July 1973-June 1974
12. Sponsoring Agency Name and Address U.S. Department of Transportation Federal Aviation Administration Systems Research and Development Service Washington DC 20591	14. Sponsoring Agency Code

15. Supplementary Notes

*Under contract to: U.S. Department of Transportation
Transportation Systems Center
Kendall Square
Cambridge MA 02142

16. Abstract

The ISLS mode performance of terminal and enroute ATCRBS using existing and various improved antennas in the presence of perfectly dielectric flat ground are investigated theoretically. Necessary analytical expressions for various quantities characterizing the system performance have been derived. A computer program has been developed for the computation and tabulation of these quantities as functions of the elevation angle of the observation point for different combinations of heights of the directional and omnidirectional antennas. For each antenna combination results are given for the following seven quantities: the P1 and P2 pulse intensities, the pulse ratio P1/P2, the mainbeam killing and sidelobe punch-through zones in space, the effective azimuth beamwidth, the number of replies and the coverage diagram. Short discussions of results are given wherever appropriate.

17. Key Words	18. Distribution Statement
Improved Sidelobe Suppression, ATCRBS, Sidelobe, Vertical Lobing, Main Beam Killing	DOCUMENT IS AVAILABLE TO THE PUBLIC THROUGH THE NATIONAL TECHNICAL INFORMATION SERVICE, SPRINGFIELD, VIRGINIA 22161

19. Security Classif. (of this report)	20. Security Classif. (of this page)	21. No. of Pages	22. Price
Unclassified	Unclassified	168	

Form DOT F 1700.7 (8-72) Reproduction of completed page authorized

II

Preface

This report investigates theoretically the ISLS mode performance of ATCRBS using the existing and various improved beacon antennas in terminal and enroute configurations. The beacon antennas are assumed to be located above a perfectly dielectric flat ground having a relative dielectric constant of 3. The report is a preliminary attempt to theoretically evaluate the performance of each antenna so that the improvements of ATCRBS performance, if any, may be properly assessed. On the basis of the present study it has been found that unless the relative phase between the directional and omnidirectional antennas is properly adjusted the ISLS mode performance of ATCRBS can be considerably worse than that for the SLS mode.

We are pleased to acknowledge the benefit of several discussions with Mr. Frank LaRussa and Dr. Rudy Kalafus of DOT/TSC, Cambridge. We also acknowledge the valuable counsel and suggestions of Professor Ralph E. Hiatt. We wish to acknowledge with thanks the work of Dr. Mohammed Hidayet and Mr. Min Han who prepared the computer programming for this report.

TABLE OF CONTENTS

Table of Contents (cont'd)

LIST OF ILLUSTRATIONS

List of Illustrations (cont'd)

List of Illustrations (cont'd)

List of Illustrations (cont'd)

List of Illustrations (cont'd)

LIST OF TABLES

1. INTRODUCTION

1.1 Preliminary Remarks

This is the second Technical Report on Contract DOT-TSC-717 entitled "Volumetric Study in Support of ATCRBS". The effects of ground on the improved interrogator sidelobe suppression (ISLS) mode performance of ATCRBS using various antennas are theoretically investigated in the present report. A similar investigation of the SLS mode performance of ATCRBS has been reported in our first Technical Report [1]. The results obtained in [1] will be used frequently in the present study and, in fact, the present report should be studied in the context of [1].

1.2 Functional Characteristics of Interrogation Schemes

The basic principles of different interrogation schemes used in ATCRBS are discussed in detail in the open literature [2 - 6]. Here we mention only those aspects which are appropriate for the present investigation.

The ground interrogator of ATCRBS has a number of interrogation modes to accommodate its various uses [5]. Each interrogation consists of a pair of 0.8μs wide pulses (P1, P3) transmitted at 1030 MHz by the directional antenna of the beacon. An additional pulse (P2 pulse) is transmitted 2μs after the initial P1 pulse from the interogator equipped with sidelobe suppression system (SLS). The P2 pulse is transmitted by the omnidirectional antenna of the beacon. The ATCRBS interrogation signal format on mode 3/A, assigned to common ATC, is shown in Fig. 1. Ordinarily this interrogation signal is transmitted by the ground interrogator antenna system equipped with sidelobe suppression system (SLS). The pulse P2 is transmitted in order to suppress the aircraft responses to the signals received via the sidelobes of the directional antenna of the beacon. The effective radiated power of the P2 pulse is designed to be greater than that of any (P1 pulse) radiated via the sidelobe of the directional antenna. The aircraft transponder is designed not to respond if P2 > P1. When the transponder detects a

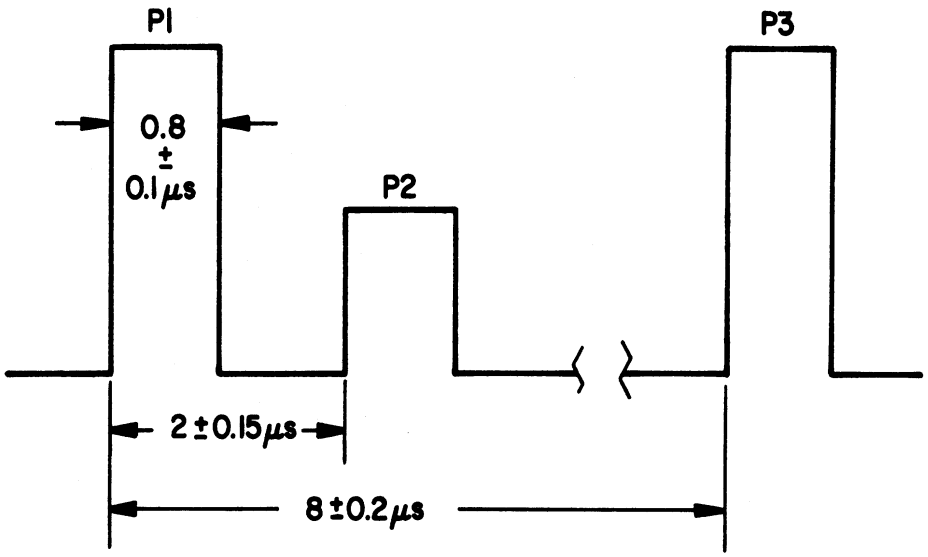

FIG. 1: ATCRBS interrogation signal format on mode 3/A.

sidelobe interrogation, it is inhibited for a period of 35 ± 10 μs, during which time a received interrogation cannot elicit a reply. The radiated power level of P2 is nominally set at 18 dB below the peak level of the directional beam radiating the P1 and P3 pulses. In order to accommodate reasonable manufacturing tolerances, the U.S. National Standard designates that a transponder shall be inhibited with high probability whenever the amplitude of the P2 pulse exceeds that of the P1 pulse and shall respond with high probability whenever the amplitude of P1 exceeds that of P2 by 9 dB or more.

The SLS scheme works satisfactorily in the absence of multipath sources on ground between the interrogator and the transponder. However, if the main beam of the antenna illuminates a large reflection surface, e.g., a hill, building, hangar, etc., which in turn reflects the transmitted energy at a level sufficient to trigger the transponder in an aircraft not in the main beam of the antenna, a false target indication will occur.

Consider a situation shown in Fig. 2 where the aircraft is receiving a direct signal as well as a strong signal reflected by a multipath source. The direct and

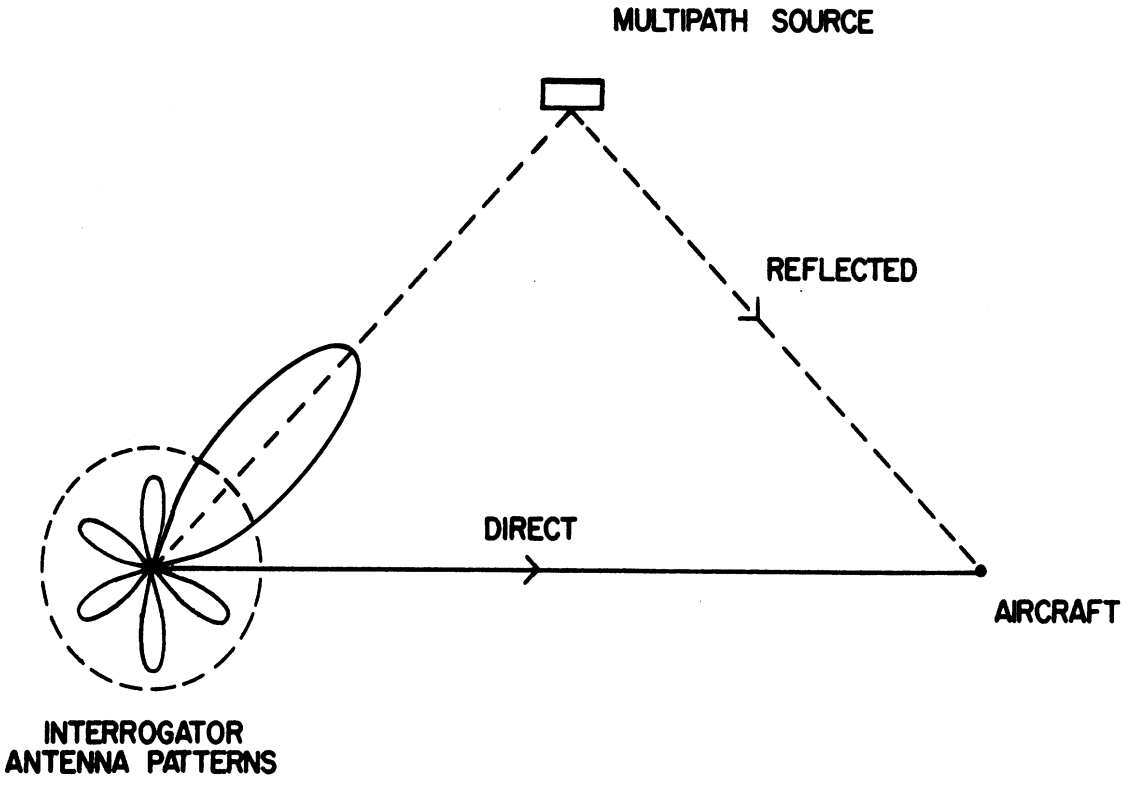

FIG. 2: Geometry of the interrogator, multipath source and an aircraft.

the reflected SLS signals arriving at the aircraft is shown in Fig. 3a. The direct signal is a sidelobe interrogation received from the interrogator. The main beam interrogation signal is received at a time delayed by τ via the reflected path. If the direct signal is recognized as a side-lobe interrogation the transponder will be suppressed for at least $25\mu s$ ($35 \pm 10\mu s$) and if $\tau < 25\mu s$ then the reflected main beam interrogation will not elicit a reply from the transponder. Frequently it happens that P1 pulse amplitude received by the direct path is not of sufficient amplitude to be recognized by the transponder. In such cases the direct path

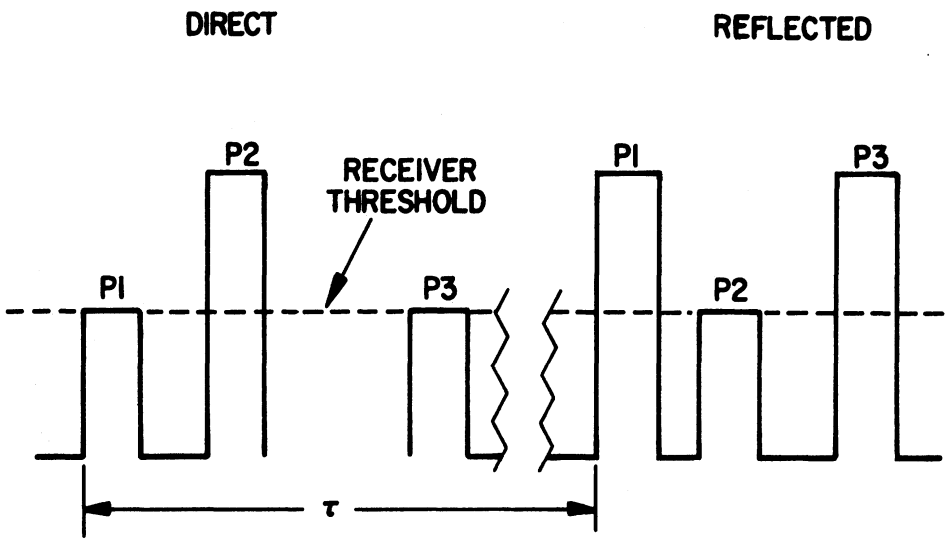

(a) SLS signal

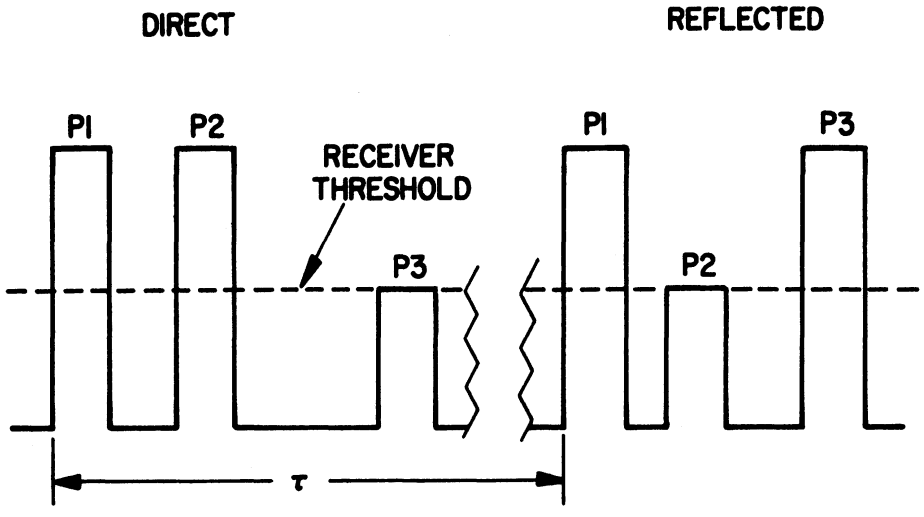

(b) ISLS signal

FIG. 3: SLS and ISLS signals received by the transponder.

interrogation does not cause suppression and the reflected interrogation elicits a reply, thereby giving a false target indication.

To increase the probability of direct path suppression, a fraction of the P1 pulse energy is radiated from the omnidirectional antenna. This increases the range at which the direct path interrogation will reliably suppress the transponder. This technique is termed the improved sidelobe suppression (ISLS). Figure 3 b shows the interrogation signal at the transponder corresponding to Fig. 2 in the ISLS case. The typical P1 pulse amplitude in the omni pattern is 18 dB below the peak main beam P1 pulse, i.e., equivalent to the P2 pulse. The ISLS direct signal in Fig. 3 b will now be recognized by the transponder as a sidelobe suppression signal and the transponder reply will be suppressed for at least 25μs and if $\tau < 25\mu s$ the multipath signal will not elicit any reply. Since ISLS increases the total number of sidelobe suppressions that occurs, it reduces by a small amount the probability of reply to valid interrogation.

1.3 Outline of the Report

The purpose of the present report is to investigate theoretically the effects of ground on the improved sidelobe suppression mode of operation of the ATCRBS for nine different interrogator antennas and for various combinations of heights of directional and omnidirectional antennas located above a flat infinite ground. The basic theoretical formulations of various quantities of interest are given in Section 2. The quantities of interest are the intensities of the radiated pulses at a far field point where a transponder is located, the received pulse ratio at the transponder, the potential main beam killing and sidelobe punch-through zones in space, the effective azimuth beamwidth of the interrogator directional antenna, the effective number of replies elicited from the transponder and the coverage diagram appropriate for the beacon system.

The various antennas along with their free space patterns are discussed in detail in [1]. For simplicity of computation approximate analytical expressions have been developed for the free space radiation patterns of all the test antennas. Since they have been discussed elsewhere, we only quote the appropriate expressions in Section 3.

Numerical results and discussion of pertinent quantities are given in Section 4.

A general discussion of the results along with our conclusions are given in Section 5.

The computer program used for obtaining the numerical results is given in Appendix A.

1.4 Basic Assumptions

It is appropriate to give here the basic assumptions and approximations on which the present investigation is based. These should be noted when applying the results to an actual system. The theoretical formulations used make the following assumptions and approximations:

1.4.1 The directional and omnidirectional interrogator antennas have definite phase centers located at different heights above ground. The displacement between the two antennas can take place in both the vertical and horizontal directions.

1.4.2 For most of the antennas, the free space directional and omnidirectional elevation plane patterns are ideally matched with the exceptions of the NADIF Fix antenna with the Westinghouse omni and the NADIF Fix antenna with the existing small omni (called the NADIF Fix II and the NADIF Fix III antennas, respectively).

1.4.3 The elevation plane antenna pattern profile at different azimuth sections is the same. This implies that the elevation pattern profile in the region of the azimuthal sidelobe is of the same shape as in the region of the main beam. Consequently, if $f(\theta)$ is the elevation plane pattern profile in the plane of symmetry of the main beam, then $Lf(\theta)$ will be the elevation plane pattern profile of the azimuthal sidelobe, where L is the sidelobe level relative to the maximum of the main beam (note that $0 \leq L \leq 1$).

1.4.4 The nominal or 3 dB beamwidths of the azimuthal plane patterns of the directional antennas are independent of the elevation angle. For small

elevation angles (say $\theta \leq 5^{o}$), this assumption is quite acceptable. The azimuthal plane patterns of the directional antennas are assumed to be given by universal Gaussian curves.

1.4.5 For the purpose of radiating the P1 pulse, equal amounts of P1 pulse power are fed into the directional and omnidirectional antennas. To radiate the P2 pulse an amount of P2 pulse power equal to that of the P1 pulse is fed into the omnidirectional antenna.

1.4.6 The horizontal displacements between the phase centers of the directional and omnidirectional antennas are assumed to be such that the P1 pulses radiated by them arrive at the transponder either in phase or out of phase with each other. The former is referred to as the maximum envelope case and the latter the minimum envelope case.

1.4.7 For most of the antennas the elevation plane patterns are available. For the purpose of computational simplicity we have developed approximate analytical expressions for the elevation plane patterns of all the antennas.

1.4.8 The ground is assumed to be flat and a pure dielectric with permittivity $\epsilon = 3$.

1.4.9 The main beam killing takes place whenever the P1 and P2 pulse amplitudes at the transponder satisfy the relation $P1(dB) - P2(dB) \leq 9dB$.

1.4.10 In the azimuthal sidelobe region, sidelobe punch-through occurs whenever the P1 and P2 pulses at the transponder satisfy the relation $P1(dB) - P2(dB) \geq 0$.

2. BASIC THEORETICAL FORMULATIONS

2.1 Definition of the Problem

Let us consider the general case of the ISLS mode of operation where the directional and omnidirectional antennas of the beacon are at different heights and are displaced in the horizontal direction. Figure 4 represents the disposition of antennas and the excitations for the case of P1 pulse radiation. Generally, both

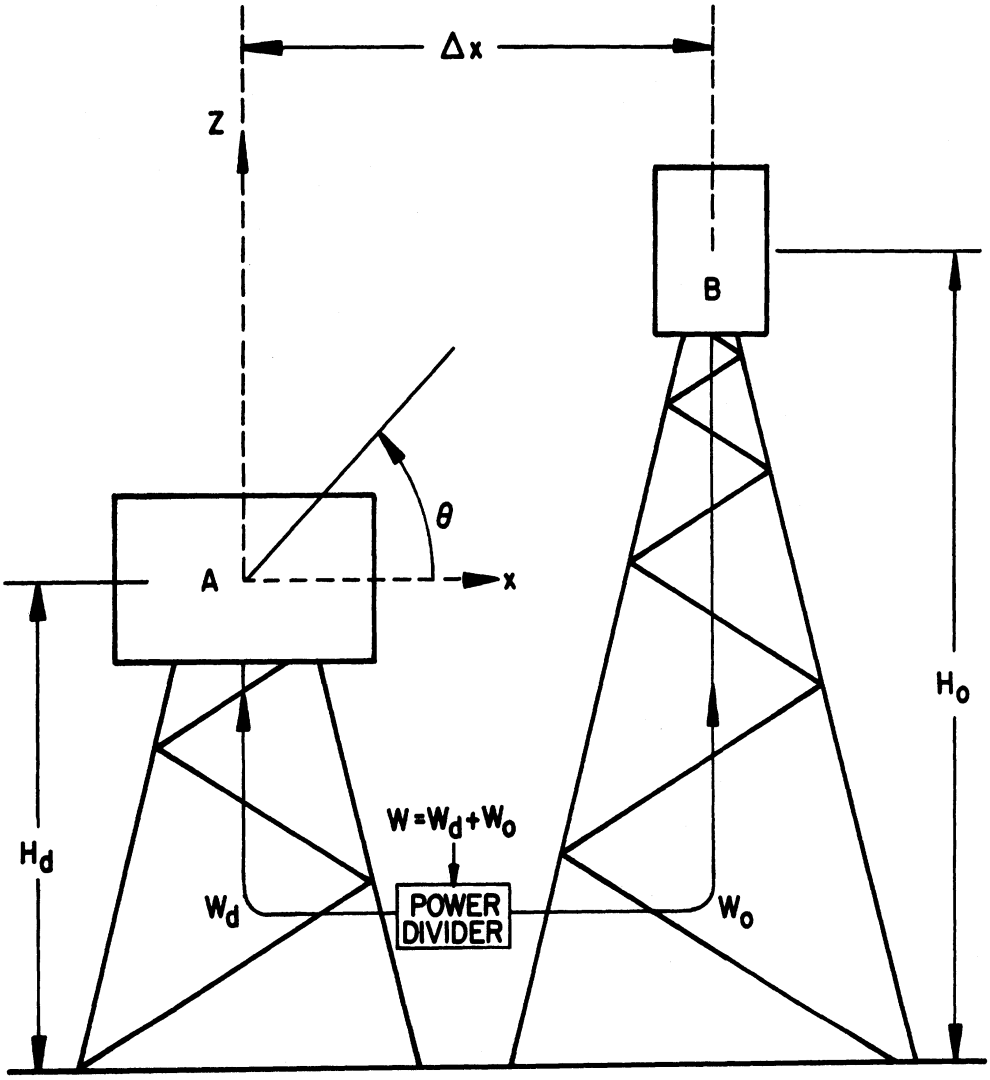

FIG. 4: Schematic arrangement of the antennas and the excitation of the P1 pulse radiation.

antennas are excited with different power and the relative phase of excitation is dependent on the difference in the cable lengths. Let the points A and B in Fig. 4 represent the phase centers of the directional and omnidirectional antennas respectively.

The main task is to calculate the intensities of P1 and P2 pulses at the transponder point produced by the antenna system shown in Fig. 4. The ground is assumed to be flat and a pure dielectric with relative dielectric constant $\epsilon_r = 3$. For the radiation of the P1 pulse the excitation of the antennas is as shown in Fig. 4. For the radiation of the P2 pulse only the omnidirectional antenna is excited with an appropriate amount of power.

2.2 The Intensities of P1 and P2 Pulses

Let the complex free space elevation plane pattern of the directional antenna with respect to the point A (Fig.4) be represented by $f_d(\theta)e^{j\phi_d(\theta)}$, where $f_d(\theta)$ and $\phi_d(\theta)$ are the amplitude and phase patterns, respectively, of the antenna in free space. It can be shown [1] that the corresponding patterns of the antenna in the presence of ground and with respect to the same point A are given by

$$F_d(\theta) = \left\{ \left[f_d(\theta) \right]^2 + 2\rho(\theta) f_d(\theta) f_d(-\theta) \cos \left[2\beta H_d \sin\theta + \phi_d(\theta) - \phi_d(-\theta) \right] + \left[\rho(\theta) f_d(-\theta) \right]^2 \right\}^{1/2} \tag{1}$$

$$\psi_d(\theta) = \arctan \frac{f_d(\theta) \sin\phi_d(\theta) + \rho(\theta) f_d(-\theta) \sin\left[\phi_d(-\theta) - 2\beta H_d \sin\theta\right]}{f_d(\theta) \cos\phi_d(\theta) + \rho(\theta) f_d(-\theta) \cos\left[\phi_d(-\theta) - 2\beta H_d \sin\theta\right]} \tag{2}$$

where: the complex pattern in the presence of ground is represented as

$F_d(\theta) \exp j\psi_d(\theta)$,

$\beta = 2\pi/\lambda$ is the free space propagation constant,

$\rho(\theta)$ is the reflection coefficient of ground for vertical polarization [1] and is given by

$$\rho(\theta) = \frac{3\sin\theta - \sqrt{2+\sin^2\theta}}{3\sin\theta + \sqrt{2+\sin^2\theta}} \quad . \tag{2a}$$

Eq. (2a) assumes that the ground is a perfect dielectric with dielectric constant 3 and is flat. Further discussion of $\rho(\theta)$ is given in [1].

Similarly, if $f_0(\theta)$ and $\phi_0(\theta)$ are the free space amplitude and phase patterns of the omnidirectional antenna with respect to point B (Fig. 4), the corresponding patterns in the presence of ground are given by the following:

$$F_0(\theta) = \left\{\left[f_0(\theta)\right]^2 + 2\rho(\theta) f_0(\theta) f_0(-\theta) \cos\left[2\beta H_0 \sin\theta + \phi_0(\theta) - \phi_0(-\theta)\right] + \left[\rho(\theta) f_0(-\theta)\right]^2\right\}^{1/2} \tag{3}$$

$$\psi_0(\theta) = \arctan \frac{f_0(\theta)\sin\left[\phi_d(\theta)\right] + \rho(\theta) f_0(-\theta)\sin\left[\phi_0(-\theta) - 2\beta H_0 \sin\theta\right]}{f_0(\theta)\cos\left[\phi_0(\theta)\right] + \rho(\theta) f_0(-\theta)\cos\left[\phi_0(-\theta) - 2\beta H_0 \sin\theta\right]} \tag{4}$$

In the ISLS mode of operation, the P1 pulse is radiated by a two-element array, with different element patterns, different excitation coefficients and with disposition of elements as represented in Fig. 5. The excitations of the elements

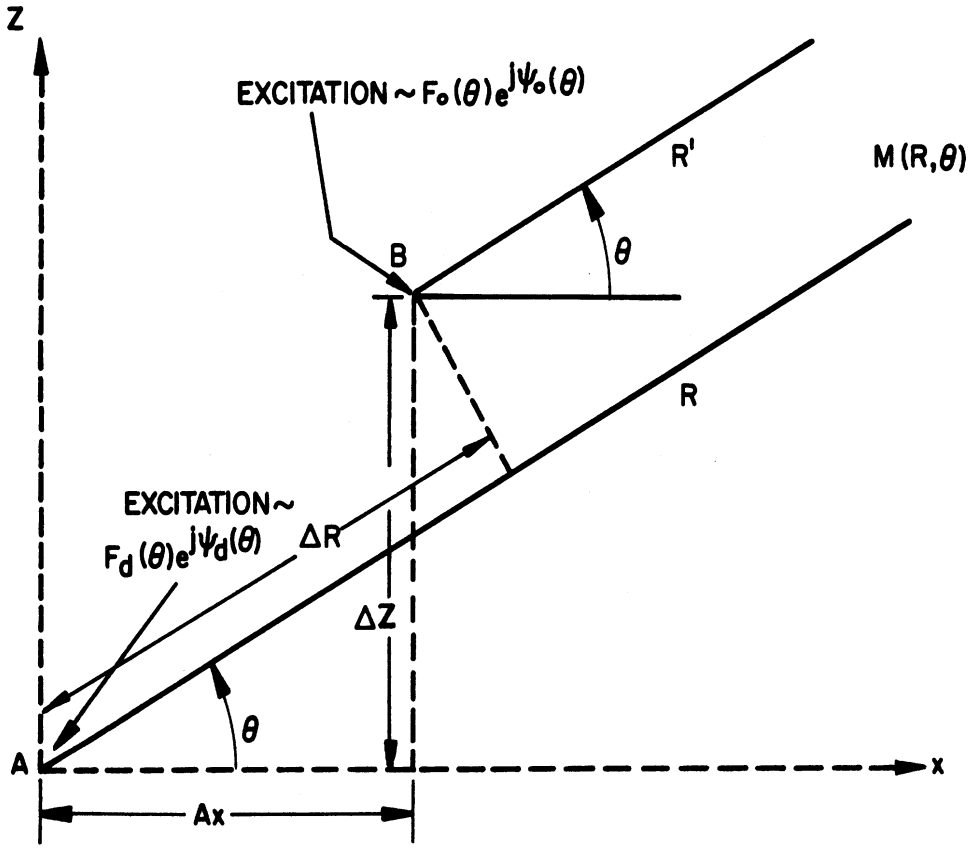

FIG. 5: Schematic representation of the two-element array radiating the P1 pulse.

A and B are proportional to Eqs. (1) - (2) and (3) - (4) respectively and are as shown in Fig. 5. From Fig. 5 it can be shown that the electric field produced by the array at a far field point $M(R,\theta)$ is given by the expression

$$E(\theta) = \frac{\sqrt{30 W_d G_d}}{R} F_d(\theta) e^{j\psi_d(\theta)} e^{-j\beta R} + \frac{\sqrt{30 W_0 G_0}}{R} F_0(\theta) e^{i\psi_0(\theta)} e^{-j[\beta(R-\Delta R)-\tau]} \tag{5}$$

where

the origin of the coordinates are assumed to be located at A,

W_d, G_d are the excitation power and maximum gain of the directional antenna,

W_0, G_0 are the excitation power and maximum gain of the omnidirectional antenna for P1 pulse,

τ is the phase difference in excitation caused by the difference in the cable length, etc.

ΔR is the path difference, as shown in Fig. 5, and is given by

$$\Delta R = \Delta x \cos\theta + \Delta z \sin\theta, \tag{5a}$$

where it is assumed that the point M is located such that its azimuth angle is zero.

Equation (5) can be written in the following form:

$$E(\theta) = A e^{-j\beta R}\left\{F_d(\theta) e^{j\psi_d(\theta)} + q F_0(\theta) \exp\left[j\left(\psi_0(\theta) + \beta\Delta R + \tau\right)\right]\right\}, \tag{6}$$

where

$$A = \frac{\sqrt{30 W_d G_d}}{R}, \tag{7}$$

$$q = \sqrt{\frac{W_0 G_0}{W_d G_d}}. \tag{8}$$

The constant q determines the level of the P1 pulse radiated through the omni antenna. With G_0, G_d given, this level can be adjusted to the proper value by adjusting the powers W_d, W_0. In free space, if it is assumed that the elevation plane patterns

of the two antennas are identical, the quantity $1/q$ gives the ratio of P1 pulse radiated by the directional antenna to the P1 pulse radiated by the omnidirectional antenna. Normally $1/q$ is taken to be 18 dB.

The voltage intensity of the P1 pulse at the far field point is proportional to the amplitude of the expression given by Eq. (6) and is given by

$$P1(\theta)_{ISLS} = |E(\theta)| = A\left\{\left[F_d(\theta)\right]^2 + 2qF_d(\theta)F_0(\theta)\cos\xi(\theta) + \left[qF_0(\theta)\right]^2\right\}^{1/2}, \qquad (9)$$

where

$$\left.\begin{aligned} \xi(\theta) &= \psi_d(\theta) - \psi_0(\theta) - \beta\Delta R - \tau \quad , \\ \Delta R &= \Delta x\cos\theta + \Delta z\sin\theta \\ \Delta z &= H_0 - H_d \quad . \end{aligned}\right\} \qquad (10)$$

Equation (9) gives the desired expression for the P1 pulse at the transponder for the ISLS mode of operation of the beacon. For further analysis it is convenient to use an alternate form of $P1(\theta)_{ISLS}$. Assume that the excitation powers of the directional antennas are the same for ISLS as well as SLS cases. It is known [1] that the voltage intensity of the P1 pulse in SLS mode is given by

$$P1(\theta)_{SLS} = \left|\frac{\sqrt{30\,W_d G_d}}{R} F_d(\theta)\, e^{j\psi_d(\theta)}\, e^{-j\beta R}\right| = AF_d(\theta) \quad , \qquad (11)$$

which can be obtained from Eq. (9) with $q = 0$.

In both ISLS and SLS modes of operation the P2 pulse is radiated by the omnidirectional antenna only. If the excitation power of the omni antenna when the P2 pulse is radiated is W_2 (in both modes) then we obtain the following expression for the voltage intensity of the P2 pulse at the far field point:

$$P2(\theta) = \left|\frac{\sqrt{30\,W_2 G_0}}{R} F_0(\theta)\, e^{j\psi_0(\theta)}\, e^{-j\beta R'}\right| = \frac{A}{K_0} F_0(\theta) \quad , \qquad (12)$$

where $$K_0 = \sqrt{\frac{W_d G_d}{W_2 G_0}} \tag{13}$$

We shall call the constant K_0 the nominal ratio of the P1 to P2 pulse. With G_d and G_0 given, this ratio can be adjusted to the proper value by adjusting the powers W_d and W_2. Normally K_0 is taken to be equal to 18 dB.

With the help of Eqs. (11) and (12), the expression for the $P1(\theta)_{ISLS}$ as given by Eq. (9) is transformed into

$$P1(\theta)_{ISLS} = \left\{ \left[P1(\theta)_{SLS} \right]^2 + 2qK_0 P1(\theta)_{SLS} P2(\theta) \cos \xi(\theta) + \left[qK_0 P2(\theta) \right]^2 \right\}^{1/2} \tag{14}$$

Equation (14) is the new, alternate expression for $P1(\theta)_{ISLS}$. It gives the relation between the intensity of the P1 pulse in the ISLS mode of operation, and the intensity of the same pulse in SLS mode of operation. From Eq. (14) it is evident that SLS mode can be theoretically treated as a special case of ISLS mode with the factor q equal to zero. The value of the constant qK_0 can be found from Eqs. (8) and (9) and is given by

$$qK_0 = \sqrt{W_0 / W_2} \quad , \tag{15}$$

which means that qK_0 is equal to the square root of the ratio of the excitation powers of the omnidirectional antenna radiating the $P1(\theta)$ pulse in ISLS mode and the $P2(\theta)$ pulse. These two powers are commonly equal ($qK_0 = 1$), but for the purpose of further analysis we shall take them to be different, i.e., $qK_0 \neq 1$.

Let us investigate the behavior of the $P1(\theta)_{ISLS}$ as a function of the horizontal displacement Δx of the two antennas. The functions $F_d(\theta)$ and $F_0(\theta)$ are independent of Δx. In Eqs. (9) and (14), the only function which depends on Δx is $\xi(\theta)$, as defined in Eq. (10). In a given situation, the factor $\cos \xi(\theta)$ will lie between +1 and -1. Thus in the ISLS mode the $P1(\theta)$ pulse amplitude will lie between a maximum envelope function $P1(\theta)_{MAX}$ and a minimum envelope function $P1(\theta)_{MIN}$. These two envelope functions are given by

$$P1(\theta)_{MAX} = A\left[F_d(\theta) + qF_0(\theta)\right] = P1(\theta)_{SLS} + qK_0 P2(\theta) \ , \qquad (16)$$

$$P1(\theta)_{MIN} = A\left[F_d(\theta) - qF_0(\theta)\right] = P1(\theta)_{SLS} - qK_0 P2(\theta) \ . \qquad (17)$$

The two envelope functions defined by Eqs. (16) and (17) are used to obtain the $P1(\theta)_{ISLS}$ pulses as functions of the elevation angle θ. The physical implications of the envelope functions are given in the next section.

2.3 Physical Implications of the Maximum and Minimum Envelope Functions

In the previous section we have said that the received P1 pulse amplitude lies between a maximum and a minimum envelope function. It is appropriate here to give a discussion on the physical implications of these functions.

Basically the maximum level is attained when the P1 pulses from the directional and omnidirectional antennas appear in phase at the transponder. The minimum level is obtained when they appear out of phase. The RF phase difference between the two P1 pulses is given by Eq. (10). In an ideal case $\psi_d(\theta) = \psi_0(\theta)$, i.e., the elevation plane phase patterns of the antennas are identical. Even if they are not identical, it is reasonable to assume that $\psi_d(\theta) - \psi_0(\theta)$ is a constant over a range of interest in θ, i.e., for $0 \leq \theta \leq 10^o$. Within this range $\sin\theta$ is a very small quantity and $\cos\theta \simeq 1$. Thus one can approximate Eq. (10) by

$$\xi(\theta) \simeq (c - \Delta x - \tau), \qquad (18)$$

where $c = \psi_d(\theta) - \psi_0(\theta) \simeq$ constant.

It is now conceivable that by properly choosing τ, one can adjust $\xi(\theta) = 0$ or π which will then yield the two envelope functions. In a practical situation this can be obtained by introducing the appropriate amount of phase difference between the two antennas.

2.4 The Pulse Ratio

From Eqs. (9) and (12) the following expression is obtained for the pulse ratio at a point located within the azimuthal main beam of the antenna:

$$\frac{P1(\theta)_{ISLS}}{P2(\theta)} = K(\theta)_{ISLS} = K_0 \left\{ \left[\frac{F_d(\theta)}{F_0(\theta)}\right]^2 + 2q \frac{F_d(\theta)}{F_0(\theta)} \cos\xi(\theta) + q^2 \right\}^{1/2} , \qquad (19)$$

where $K(\theta)_{SLS}$ is the ratio $P1(\theta)/P2(\theta)$ in the SLS mode of operation and is given by [1]:

$$K(\theta)_{SLS} = K_0 \frac{F_d(\theta)}{F_0(\theta)} \quad . \tag{20}$$

In addition to the true pulse ratio function $K(\theta)_{ISLS}$ we introduce here the concept of envelopes of pulse ratio functions $K_{MAX}(\theta)_{ISLS}$ and $K_{MIN}(\theta)_{ISLS}$ having the same meanings as discussed in the case of the $P1(\theta)$ function. Thus using Eqs. (18) and (19) with $\cos\xi(\theta) = \pm 1$, we obtain the following expressions for the pulse ratio envelopes:

$$K_{MAX}(\theta)_{ISLS} = K_0\left[\frac{F_d(\theta)}{F_0(\theta)} + q\right] = K(\theta)_{SLS} + qK_0 \quad , \tag{21}$$

$$K_{MIN}(\theta)_{ISLS} = K_0\left[\frac{F_d(\theta)}{F_0(\theta)} - q\right] = K(\theta)_{SLS} - qK_0 \quad . \tag{22}$$

If the far field point is located within an azimuthal sidelobe of the interrogator directional antenna, then the received pulse ratio can be obtained by the same expressions given above (Eqs. 18 - 22) provided their right hand sides are multiplied by the quantity L which represents the sidelobe level compared to the main beam amplitude (note: in general $0 \leq L \leq 1$).

With the known pulse ratio functions, the main beam killing and false target zones in space can be obtained in the same manner as in the SLS case [1]. In the present ISLS case there will be zones corresponding to each envelop of the pulse ratio. In general for given threshold levels of the receiver, the main beam killing zones will be more serious at the minimum envelopes and the sidelobe punch-through zones would be more serious at the maximum envelopes.

2.5 Effective Azimuth Beamwidth and Number of Replies

So far we have investigated the various field intensity functions in a vertical plane passing through the plane of symmetry of the azimuthal plane pattern of the

directional antenna of the beacon. In the present section we investigate the behavior of these functions with respect to the variation of the azimuth angle. It should be noted that the effective azimuth beamwidth and the number of replies elicited from a transponder depend on the azimuthal plane pattern of the directional antenna of the interrogator.

Suppose that the three dimensional pattern of the directional antenna in the presence of ground can be expressed by

$$F_{s_d}(\theta,\alpha) = F_d(\theta)\eta_d(\alpha) \tag{23}$$

where $F_d(\theta)$ is the elevation plane pattern of the antenna above ground as given in Eq. (1), and $\eta_d(\alpha)$ is the azimuthal plane pattern of the same antenna normalized such that

$$\eta_d(0) = 1 \quad . \tag{24}$$

For the omnidirectional antenna we shall take the ideal rotationally symmetric azimuthal plane pattern $\eta_0(\alpha) = 1$, and hence the three dimensional pattern of the omnidirectional antenna located above ground is

$$F_{s0}(\theta,\alpha) = F_0(\theta) \quad , \tag{25}$$

where $F_0(\theta)$ is given by Eq. (3).

Applying the same procedure as in Section 2.2, we can obtain an expression for the P1 pulse as a function of θ and α. After introducing $F_{sd}(\theta,\alpha)$ instead of $F_d(\theta)$, and $\xi(\theta,\alpha)$ instead of $\xi(\theta)$ in Eq. (9), we obtain

$$P1(\theta,\alpha)_{ISLS} = A\left\{\left[F_d(\theta)\eta_d(\alpha)\right]^2 + 2qF_d(\theta)\eta_d(\alpha)F_0(\theta)\cos\xi(\theta,\alpha) + \left[qF_0(\theta)\right]^2\right\}^{1/2} , \tag{26}$$

where $\xi(\theta,\alpha)$ can be obtained from $\xi(\theta)$ in Eq. (10) by taking the path difference $\Delta x \cos\alpha$ instead of Δx. The alternate expression corresponding to Eq. (14) is

$$P1(\theta,\alpha)_{ISLS} = \left\{P1(\theta)_{SLS}\eta_d(\alpha)^2 + 2qK_0 P1(\theta)_{SLS}\eta_d(\alpha)P2(\theta)\cos\xi(\theta,\alpha) + \left[qK_0 P2(\theta)\right]^2\right\}^{1/2} . \quad (27)$$

We again introduce the envelope functions $P1(\theta,\alpha)_{MAX}$ and $P1(\theta,\alpha)_{MIN}$ which correspond to $\cos\xi(\theta,\alpha) = +1$ and -1 respectively in Eqs. (36) and (27). We then have the following two general expressions for the pulse envelopes:

$$P1(\theta,\alpha)_{MAX} = A\left[F_d(\theta)\eta_d(\alpha) + qF_0(\theta)\right] = P1(\theta)_{SLS}\eta_d(\alpha) + qK_0 P2(\theta) , \quad (28)$$

$$P1(\theta,\alpha)_{MIN} = A\left[F_d(\theta)\eta_d(\alpha) - qF_0(\theta)\right] = P1(\theta)_{SLS}\eta_d(\alpha) - qK_0 P2(\theta) , \quad (29)$$

The effective azimuth beamwidth α_{eff} is defined as

$$\alpha_{eff} = 2\alpha_1 , \quad (30)$$

where α_1 is the positive solution of the equation

$$P1(\theta,\alpha_1)_{ISLS} = aP2(\theta) , \quad (31)$$

where a is the threshold of the transponder logic, which is nominally 9 dB. For the two envelope cases the corresponding beamwidths are $2\alpha_{1MAX}$ and $2\alpha_{1MIN}$ which correspond to Eqs. (28) and (29) respectively. α_{1MAX} and α_{1MIN} are the positive solutions of the following two equations:

$$P1(\theta)_{SLS}\eta_d(\alpha_{1MAX}) + qK_0 P2(\theta) = aP2(\theta) , \quad (32)$$

$$P1(\theta)_{SLS}\eta_d(\alpha_{1MIN}) - qK_0 P2(\theta) = aP2(\theta) . \quad (33)$$

As in [1] the azimuthal plane pattern of the directional antenna is taken to be the universal Gaussian function and is given by

$$\eta_d(\alpha) = \exp -1.39(\alpha/\alpha_0)^2 , \quad (34)$$

where α_0 is the total half-power beamwidth of the pattern.

After using Eqs. (34), (32) and (33) and some algebraic manipulations, we obtain the following:

$$\alpha_{1MAX}(\theta) = 2\alpha_0\left[\frac{K_1(\theta)_{SLS} - 20\log(a - K_0 q)}{12.0735}\right]^{1/2}, \tag{35}$$

$$\alpha_{1MIN}(\theta) = 2\alpha_0\left[\frac{K_1(\theta)_{SLS} - 20\log(a + qK_0)}{12.0735}\right]^{1/2} \tag{36}$$

where $K_1(\theta)_{SLS}$ is the dB ratio of P1(θ) to P2(θ) pulses in the SLS mode of operation, i.e.,

$$K_1(\theta)_{SLS} = 20\log\frac{P1(\theta)_{SLS}}{P2(\theta)} = 20\log\left[K_0\,\frac{F_d(\theta)}{F_0(\theta)}\right] \tag{37}$$

For the SLS case [1] we have, from Eq. (35) or (36), with $qK_0 = 0$,

$$\alpha_{eff}(\theta) = 2\alpha_0\left[\frac{K_1(\theta)_{SLS} - 20\log a}{12.0735}\right]^{1/2}. \tag{38}$$

Comparing Eq. (38) with Eqs. (35) and (36), we notice that the effect of ISLS mode of operation on the effective azimuth beamwidth is equivalent to a change in the threshold level for the SLS mode of operation by an amount $\pm qK_0$. The number of replies corresponding to the two envelope functions are

$$N_{MAX}(\theta) = \frac{f_i}{\Omega}\alpha_{1MAX}(\theta), \tag{39}$$

$$N_{MIN}(\theta) = \frac{f_i}{\Omega}\alpha_{1MIN}(\theta), \tag{40}$$

where f_i is the pulse repetition rate and Ω is the angular scanning speed in deg/sec. Typical values of f_i and Ω are

$f_i = 350$ pulses/sec

$\Omega = 90^\circ$/sec for terminal installation,

$\Omega = 36^\circ$/sec for enroute installation.

The number of replies from the SLS mode of operation has been discussed in [1] and is given below for comparison:

$$N(\theta)_{SLS} = \frac{f_i}{\Omega} \alpha_{eff}(\theta) \quad . \tag{41}$$

As explained in [1], the effective azimuth beamwidth and number of replies have practical meanings for relatively close targets such that the replies from them in the absence of SLS or ISLS mode of operation could be obtained in an azimuth angle range wider than the conventional 3 dB beamwidth azimuth range.

2.6 Coverage Diagram

The maximum range of a beacon system is a statistical quantity depending on the acceptable probability of detection and the tolerable probability of "false alarm". For the purpose of the present analysis we shall adopt the following convention which appears to be appropriate for practical purposes: Let R_0 denote the maximum free space range of a beacon system in the SLS mode for some given and convenient probabilities of detection and false alarm. Suppose that this range R_0 is given to us as a parameter. Then all unknown constants in the various field intensity expressions discussed in earlier sections (e.g., the excitation power, minimum detectable signal, etc.) can be expressed in terms of this parameter. If $P1(\theta)_{min}$ denotes the minimum detectable ISLS $P1(\theta)$ pulse at the transponder point, then it can be shown from Eq. (9) that the corresponding range is given by

$$R(\theta)_{ISLS} = \frac{(30 W_d G_d)^{1/2}}{P1(\theta)_{min}} \left\{ \left[F_d(\theta)\right]^2 + 2qF_d(\theta)F_0(\theta)\cos\xi(\theta) + \left[qF_0(\theta)\right]^2 \right\}^{1/2} , \tag{42}$$

where the range R is now expressed as a function of the elevation angle θ. The maximum free space range in SLS mode is evidently given by

$$R_0 = \frac{(30 W_d G_d)^{1/2}}{P1(\theta)_{min}} \tag{43}$$

where $P1(\theta)_{min}$ refers to the minimum detectable P1 pulse in the SLS mode. Combining Eqs. (42) and (43) we obtain the following expression for the range:

$$R(\theta)_{ISLS} = R_0\left\{\left[F_d(\theta)\right]^2 + 2qF_d(\theta)F_0(\theta)\cos\xi(\theta) + \left[qF_0(\theta)\right]^2\right\}^{1/2} \qquad (44)$$

where we have assumed that the minimum detectable P1 pulse amplitudes are the same in both ISLS and SLS modes of operation. Eq. (44) is the desired expression for the coverage diagram in ISLS mode of operation. After introducing the envelope functions we obtain the following two range equations appropriate for the maximum and minimum envelopes:

$$R_{MAX}(\theta) = R_0\left[F_d(\theta) + qF_0(\theta)\right] = R(\theta)_{SLS} + qR_0F_0(\theta) \quad , \qquad (45)$$

$$R_{MIN}(\theta) = R_0\left[F_d(\theta) - qF_0(\theta)\right] = R(\theta)_{SLS} - qR_0F_0(\theta) \quad , \qquad (46)$$

where $R(\theta)_{SLS}$ is the range at an angle θ in the SLS mode of operation. All curves which represent the true coverage diagrams in ISLS mode will always lie between the two envelope curves given in Eqs. (45) and (46). Typical values of R_0 are R_0 = 40 nautical miles for terminal stations and R_0 = 200 nautical miles for en-route stations.

3. FREE SPACE PATTERNS OF THE TEST ANTENNAS

In the previous chapter we have discussed theoretically the methods of obtaining the various quantities characterizing the ISLS mode performance of ATCRBS. To obtain quantitative results for any of these quantities the free space patterns of the interrogator antennas must be available. Detailed discussions of the analytical expressions for the free space patterns of various test antennas used in the present investigation have been given in [1] and will not be repeated. For completeness of the report and for quick reference we give here the final expressions for the free space patterns of the antennas.

3.1 Antennas Under Study [1].

Performance of the beacon system using nine different antennas are studied in the present investigation. These are the Westinghouse array antenna [7], Texas Instruments reflector antenna [8], Hazeltine open array antenna [9], the existing "hog-trough" antenna [10], Hazeltine E-scan antenna [11], enroute Texas Instruments Fix antenna (TI Fix Antenna) [8], enroute NADIF Fix with Texas Instruments omni antenna (NADIF Fix I) [8], enroute NADIF Fix with Westinghouse omni antenna (NADIF Fix II) [7], and enroute NADIF Fix with existing small omni antenna (NADIF Fix III) [10]. All these antennas are described in the references cited. The method of obtaining analytical expressions to approximate the given elevation plane patterns of all nine antennas mentioned above is discussed in [1]. In the following sections we quote the expressions appropriate for each antenna without giving their derivations.

3.2 Analytical Expressions for the Free Space Elevation Plane Patterns of Various Antennas [1]

3.2.1 Westinghouse Array Antenna.

The free space elevation plane pattern of the directional antenna is given by

$$f_d(\theta) = \frac{1}{15.86} \frac{\sin(\frac{\pi}{2}\cos\theta)\cos(\frac{\pi}{2}\sin\theta)}{\cos\theta} \left[5.4201 + \sum_{n=1}^{7} a_n \cos(n\beta d \sin\theta + \psi_n)\right], \quad (47)$$

where the coefficients a_n and ψ_n are given in Table 1.

TABLE 1: EXCITATION COEFFICIENTS OF THE ELEMENTS OF THE WESTINGHOUSE ARRAY ANTENNA

Element No.	Amplitude a_n	Phase in deg. ψ_n
7	0.8108	-91.27
6	0.6346	-47.04
5	0.2644	-151.88
4	1.1086	-64.65
3	0.4554	13.02
2	1.7039	-135.06
1	4.3738	-64.85
0	5.4201	00.00

It should be noted that the array has seven more elements numbered from -1 to -7 whose excitation may be obtained from Table 1 with $a_{-n} = a_n$ and $\psi_{-n} = -\psi_n$. A plot of $f_d(\theta)$ vs. θ may be found in [1]. The free space azimuthal pattern of the directional antenna is given by

$$\eta_d(\alpha) = \exp\left[-1.39(\alpha/2.25)^2\right] \quad , \tag{48}$$

where α is in degrees.

The free space elevation and azimuthal plane patterns of the omnidirectional antenna are given by the following:

$$\left.\begin{aligned} f_0(\theta) &= f_d(\theta) \text{ as given by Eq. (47)} \\ \eta_0(\alpha) &= 1 \end{aligned}\right\} \tag{49}$$

3.2.2 Texas Instruments Reflector Antenna.

The free space elevation plane pattern of the antenna is given by

$$f_d(\theta) = \sum_{n=-2}^{n=10} f_{d_1}(\theta_n) \frac{\sin\pi\left[\dfrac{\sin\theta}{0.07846} - n\right]}{\pi\left[\dfrac{\sin\theta}{0.07846} - n\right]} \quad , \tag{50}$$

The coefficients $f_{d_1}(\theta_n)$ and θ_n in Eq. (50) are given in Table 2.

TABLE 2: SAMPLED VALUES OF THE PATTERN FUNCTION FOR THE TEXAS INSTRUMENTS REFLECTOR ANTENNA

n	θ_n^o	$f_{d_1}(\theta_n)$
-2	-9.0	0.084
-1	-4.5	0.080
0	0.0	0.500
1	4.5	1.000
2	9.0	0.800
3	13.6	0.860
4	18.3	0.790
5	23.1	0.860
6	28.1	0.960
7	32.3	0.540
8	38.9	0.230
9	44.5	0.120
10	51.3	0.060

A plot of $f_d(\theta)$ vs. θ as given by Eq. (50) can be found in [1]. The free space azimuthal plane pattern of the antenna is given by

$$\eta_d(\alpha) = \exp\left[-1.39(\alpha/2.36)^2\right] \quad , \tag{51}$$

where α is in degrees.

The free space elevation and azimuthal plane patterns of the omnidirectional antenna are given by the following:

$$\left.\begin{aligned} f_0(\theta) &= f_d(\theta) \text{ as given by Eq. (50)} \\ \eta_0(\alpha) &= 1 \end{aligned}\right\} \tag{52}$$

3.2.3. Hazeltine Open Array Antenna.

The free space elevation plane pattern of the antenna is given by

$$f_d(\theta) = \sum_{n=0}^{3} f_{d_1}(\theta_n) \frac{\sin\pi\left[\frac{\sin\theta}{0.2250} - n\right]}{\pi\left[\frac{\sin\theta}{0.2250} - n\right]} \quad , \tag{53}$$

where θ_n and $f_{d_1}(\theta_n)$ are given in Table 3.

TABLE 3: SAMPLED VALUES OF THE PATTERN FUNCTION FOR THE HAZELTINE OPEN ARRAY ANTENNA

n	θ_n^o	$f_{d_1}(\theta)$
0	0.00	0.500
1	13.0	1.000
2	26.75	0.885
3	42.40	0.530

A plot of $f_d(\theta)$ vs. θ as given by Eq. (53) may be found in [1]. The free space azimuthal plane pattern of the antenna is given by

$$\eta_d(\alpha) = \exp\left[-1.39(\alpha/2.30)^2\right] \quad , \tag{54}$$

where α is in degrees.

The free space elevation and azimuthal plane patterns of the omnidirectional antenna are given by

$$\left.\begin{aligned} f_0(\theta) &= f_d(\theta) \text{ as given by Eq. (53)} \quad , \\ \eta_0(\alpha) &= 1 \end{aligned}\right\} \tag{55}$$

3.2.4 Existing Hog-Trough Antenna.

The free space elevation plane pattern of the directional antenna is given by

$$f_d(\theta) = \sum_{n=-2}^{n=+2} f_{d_1}(\theta_n) \frac{\sin\pi\left[\dfrac{\sin\theta}{0.47767} - n\right]}{\pi\left[\dfrac{\sin\theta}{0.47767} - n\right]} \quad , \tag{56}$$

where θ_n and $f_{d_1}(\theta)$ are given in Table 4.

TABLE 4: SAMPLED VALUES OF THE PATTERN FUNCTION FOR THE EXISTING HOG-TROUGH ANTENNA

n	θ_n^o	$f_{d_1}(\theta_n)$
-2	-72.80	0.084
-1	-28.55	0.510
0	0.00	0.966
1	28.55	0.780
2	72.80	0.045

A plot of $f_d(\theta)$ vs. θ, as given by Eq. (56), may be found in [1]. The free space azimuthal plane pattern of the directional antenna is given by

$$\eta_d(\theta) = \exp\left[-1.39(\alpha/2.27)^2\right] \quad , \tag{57}$$

where α is in degrees.

The free space elevation and azimuthal plane patterns of the omnidirectional antenna are given by

$$\left.\begin{aligned} f_0(\theta) &= f_d(\theta) \text{ as given by Eq. (56)} \\ \eta_0(\alpha) &= 1 \end{aligned}\right\} \quad , \tag{58}$$

3.2.5 Hazeltine E-Scan Antenna.

The free space elevation plane pattern of the directional antenna is given by

$$f_d(\theta) = \sum_{n=-3}^{n=6} f_{d_1}(\theta_n) \frac{\sin\pi\left[\frac{\sin\theta}{0.11942} - n\right]}{\pi\left[\frac{\sin\theta}{0.11942} - n\right]} \quad , \tag{59}$$

where θ_n and $f_{d_1}(\theta_n)$ are given in Table 5.

A plot of $f_d(\theta)$ vs. θ, as given by Eq. (59) may be found in [1]. The free space azimuthal plane pattern of the directional antenna is given by

$$\eta_d(\alpha) = \exp\left[-1.39(\alpha/2.33)^2\right] \tag{60}$$

where α is in degrees.

TABLE 5: SAMPLED VALUES OF THE PATTERN FUNCTION FOR THE HAZELTINE E-SCAN ANTENNA

n	θ_n^o	$f_{d_1}(\theta_n)$
-3	-21.00	0.079
-2	-13.80	0.072
-1	-6.85	0.030
0	0.00	0.530
1	6.85	0.915
2	13.80	0.945
3	2.100	0.845
4	28.55	0.845
5	36.70	0.315
6	45.80	0.034

The free space elevation and azimuthal plane patterns of the omnidirectional antenna are given by

$$\left.\begin{aligned} f_0(\theta) &= f_d(\theta) \text{ as given by Eq. (59)} \\ \eta_0(\alpha) &= 1 \quad . \end{aligned}\right\} \tag{61}$$

3.2.6 Enroute Texas Instruments Fix Antenna.

The free space elevation plane pattern of the directional antenna is given by

$$f_d(\theta) = \sum_{n=-2}^{n=12} f_{d_1}(\theta_n) \frac{\sin\pi\left[\frac{\sin\theta}{0.0583} - n\right]}{\pi\left[\frac{\sin\theta}{0.0583} - n\right]} \quad , \tag{62}$$

where θ_n and $f_{d_1}(\theta_n)$ are given in Table 6.

A plot of $f_d(\theta)$ vs. θ, as given by Eq. (62) may be found in [1]. The free space azimuthal plane pattern of the directional antenna is given by

$$\eta_d(\alpha) = \exp\left[-1.39(\alpha/1.5)^2\right] \quad , \tag{63}$$

where α is in degrees.

TABLE 6: SAMPLED VALUES OF THE PATTERN FUNCTION FOR THE ENROUTE TEXAS INSTRUMENTS FIX ANTENNA

n	θ_n^o	$f_{d_1}(\theta_n)$
-2	-6.70	0.010
-1	-3.33	0.039
0	0.00	0.561
1	3.33	0.990
2	6.70	0.482
3	10.10	0.450
4	13.50	0.435
5	17.00	0.420
6	20.50	0.355
7	24.10	0.417
8	27.80	0.342
9	31.65	0.350
10	35.70	0.334
11	39.90	0.240
12	44.40	0.120

The free space elevation and azimuthal plane patterns of the omnidirectional antenna are given by

$$\left.\begin{aligned} f_0(\theta) &= f_d(\theta) \text{ as given by Eq. 62)} \\ \eta_0(\theta) &= 1 \end{aligned}\right\} . \qquad (64)$$

3.2.7 Enroute NADIF Fix Antennas (NADIF Fix I, II and III).

The three enroute NADIF Fix antennas use the same directional antenna but different omnidirectional antennas. The equivalent vertical apertures of the NADIF Fix directional antennas are taken to be the same as that of the enroute Texas Instruments Fix antenna. Consequently the free space elevation plane patterns of the NADIF Fix directional antennas are given by Eq. (62) where the coefficients θ_n and $f_{d_1}(\theta_n)$ are given in Table 7.

A plot of $f_d(\theta)$ vs. θ, as given by Eq. (62) with coefficients of Table 7, may be found in [1]. The free space azimuthal plane patterns of NADIF Fix directional antennas are given by

$$\eta_d(\alpha) = \exp\left[-1.39(\alpha/1.53)^2\right] \quad , \tag{65}$$

where α is in degrees.

TABLE 7: SAMPLED VALUES OF THE PATTERN FUNCTION FOR THE ENROUTE NADIF FIX ANTENNAS

n	θ_n	$f_{d_1}(\theta_n)$
-2	-6.70	0.010
-1	-3.33	0.094
0	0.00	0.635
1	3.33	0.990
2	6.70	0.530
3	10.10	0.542
4	13.50	0.515
5	17.00	0.515
6	20.50	0.430
7	24.50	0.465
8	27.80	0.437
9	31.65	0.302
10	35.70	0.302
11	39.90	0.217
12	44.40	0.153

The free space elevation and azimuthal plane patterns of the NADIF Fix I omnidirectional antenna are given by

$$\left.\begin{aligned} f_0(\theta) &= f_d(\theta) \text{ given by Eq. (62) with coefficients in Table 7,} \\ \eta_0(\alpha) &= 1 \end{aligned}\right\} . \tag{66}$$

The free space elevation and azimuthal plane patterns of NADIF Fix II antenna are given by

$$\left.\begin{aligned} f_0(\theta) &= f_d(\theta) \text{ of the Westinghouse array antenna as given by Eq. (47) ,} \\ \eta_0(\alpha) &= 1 \end{aligned}\right\} . \tag{67}$$

The free space elevation and azimuthal plane patterns of NADIF Fix III antenna are given by

$$\left.\begin{aligned} f_0(\theta) &= f_d(\theta) \text{ of the existing hog-trough antenna, as given by Eq. (56)} \\ \eta_0(\alpha) &= 1 \end{aligned}\right\} . \quad (68)$$

Notice that the elevation plane patterns of the directional and omnidirectional antennas of NADIF Fix II and III antennas are not identical.

3.3 Summary of the Important System Parameters

The ISLS mode performance of the ATCRBS using all the antennas, discussed in the previous sections, are investigated in the present study. In each case the appropriate antenna pattern functions are used to obtain the desired performance parameters discussed in Section 2. In addition to the pattern functions, the following parameters characterize each system studied:

H_d is the height of the phase center of the directional antenna expressed in feet,

H_0 is the height of the phase center of the omnidirectional antenna expressed in feet,

K_0 is the nominal pulse ratio in dB, usually taken to be 18dB,

$1/q$ is the nominal ratio between the P1 pulse amplitudes radiated by the directional and omnidirectional antennas in free space, usually $1/q = 18$dB.

ϕ_0 is the total azimuthal half-power beamwidth of the directional antenna, expressed in degrees,

α_g is the field gradient at the horizon and is defined to be the rate of decay of the field in dB per 1^o below the horizon,

λ is the free space wavelength, $\lambda = 11.464$ inches at $f = 1.03$GHz,

f_i is the pulse repetition frequency,

Ω is the scanning rate in degrees per second.

The various antenna systems to be studied, along with the important parameters characterizing each system are shown in Table 8.

TABLE 8: SOME IMPORTANT PARAMETERS OF THE ANTENNA SYSTEMS

	Antenna Type	H_d	H_0	ϕ_0	α_g	K_0 or q	f_i	Ω
Terminal	Westinghouse Array	34	42	2.25	2.5	18	360	90
	Texas Inst. Reflector	34	43	2.36	3.4	18	360	90
	Hazeltine Open Array	33	37	2.30	1.6	18	360	90
	Existing Hog-Trough	41	43	2.27	0.37	18	360	90
	Hazeltine E-Scan	16	16	2.33	2.4	18	360	90
Enroute	Westinghouse Array	82	90	2.25	2.5	18	360	36
	Texas Inst. Reflector	82	91	2.36	3.4	18	360	36
	Existing Hog-Trough	108	110	2.27	0.37	18	360	36
	Texas Instruments Fix	92	112	2.2	5.0	18	360	36
	NADIF Fix I	92	112	1.53	5.0	18	360	36
	NADIF Fix II	92	111	1.53	5.0	18	360	36
	NADIF Fix III	92	110	1.53	5.0	18	360	36

All the terminal antennas, except the Hazeltine open array and the E-scan antennas, are mounted on a 27-foot tower. The Hazeltine antenna is mounted on a 17-foot tower. All the enroute antennas are mounted on a 75-foot tower.

4. NUMERICAL RESULTS AND DISCUSSION

In the present chapter we give the numerical results obtained for the various quantities of interest characterizing the performance of the ATCRBS using different antennas. Short discussions of results are given wherever appropriate.

4.1 The Computer Program

A computer program has been developed to obtain numerical and/or graphical results for the various quantities described in Section 2. The program is capable of handling simultaneous the SLS and ISLS mode of performance of the ATCRBS using the different test antennas discussed in Section 3. For the ISLS mode of operation, the computer output consists of the following:

4.1.1 free space elevation plane patterns of various ATCRBS antennas (tabulated numerical results),

4.1.2 $P1(\theta)_{MAX}$, $P1(\theta)_{MIN}$ and $P2(\theta)$ in dB as functions of the elevation angle θ (graphical).

4.1.3 pulse ratios $K_{MAX}(\theta)_{ISLS} = P1(\theta)_{MAX}/P2(\theta)$, $K_{MIN}(\theta)_{ISLS} = P1(\theta)_{MIN}/P2(\theta)$ in dB as functions of θ, normalized to the free space nominal value K_0 (= 18 dB) (graphical),

4.1.4 effective azimuth beamwidths $\alpha_{1MAX}(\theta)$ and $\alpha_{1MIN}(\theta)$ as functions of θ (tabulated),

4.1.5 number of replies $N_{MAX}(\theta)$ and $N_{MIN}(\theta)$ as functions of θ (graphical).

From the above results, the main beam killing and sidelobe punch-through zones and the coverage diagram for each antenna system are prepared using the methods described in [1].

The program can handle arbitrary combinations of H_d and H_0, arbitrary nominal pulse ratios K_0 and $1/q$, any values of f_i and Ω, for any chosen range of the elevation angle θ. The complete program is given in Appendix A.

4.2. Numerical Results for Terminal Installations

In this section numerical results are given for the terminal ATCRBS using different antenna systems. The method of obtainining some of the diagrams is described in more detail only for the Westinghouse antenna which is considered first. Since the same procedure is used to obtain the results for other antennas, the discussion of the method will not be repeated for the other systems.

4.2.1 Westinghouse Array Antenna.

The heights above ground of the phase centers of the directional and omnidirectional antennas are, respectively, $H_d = 34'$ and $H_0 = 42'$. The vertical aperture of each antenna is 8'. The free space elevation plane patterns of the directional and omnidirectional antennas are assumed to be identical.

Figure 6 shows $P1(\theta)_{MAX}$, $P1(\theta)_{MIN}$ and $P2(\theta)$ in dB as functions of θ, where the zero dB level is adjusted to coincide with the maximum $P1(\theta)_{SLS}$ level in the free space case. The corresponding free space curves (for $q = 0$) are also shown in Fig. 6 for comparison. Note that the two free space level curves are displaced from each other by the nominal pulse ratio of 18 dB. Observe that for the SLS case $q = 0$ and the $P1(\theta)_{SLS}$ curve for the same antenna would lie between the $P1(\theta)_{MAX}$ and $P1(\theta)_{MIN}$ curves shown in Fig. 6. (See also [1].) For the value of q used here it is found from Fig. 6 that the lobing structures of $P1(\theta)_{MAX}$ and $P1(\theta)_{MIN}$ are approximately the same and are displaced from each other by a certain amount. The amount of this displacement depends on the parameter q and the elevation plane pattern of the omnidirectional antenna in the presence of ground. The lobing structure of the $P2(\theta)$ curve is different from the two $P1(\theta)$ curves. The oscillations in the curves are found to be less than ± 1 dB for $\theta \sim 3^o$ and for $\theta > 5^o$ the P2 curve assumes the free space value, and $P1(\theta)_{MAX}$ and $P1(\theta)_{MIN}$ curves assume their respective saturation values above and below the free space value.

Figure 7 shows the envelopes of the pulse ratio $K_{MAX}(\theta)_{ISLS}$ and $K_{MIN}(\theta)_{ISLS}$ as functions of θ and normalized to the nominal free space value K_0 (= 18 dB). Observe that the maximum envelope curve lies above the minimum

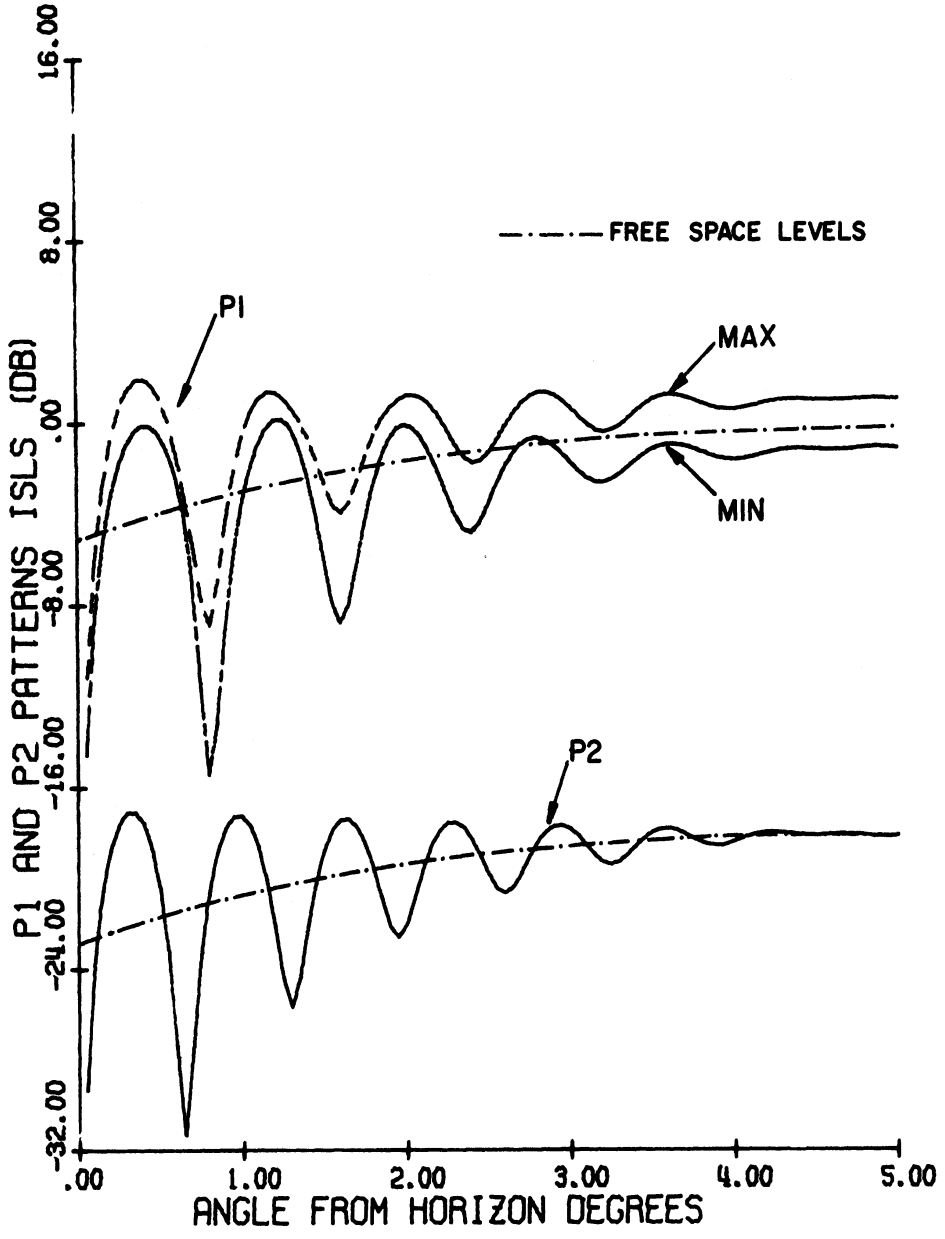

FIG. 6: $P1(\theta)_{MAX}$, $P1(\theta)_{MIN}$ and $P2(\theta)$ as functions of θ.

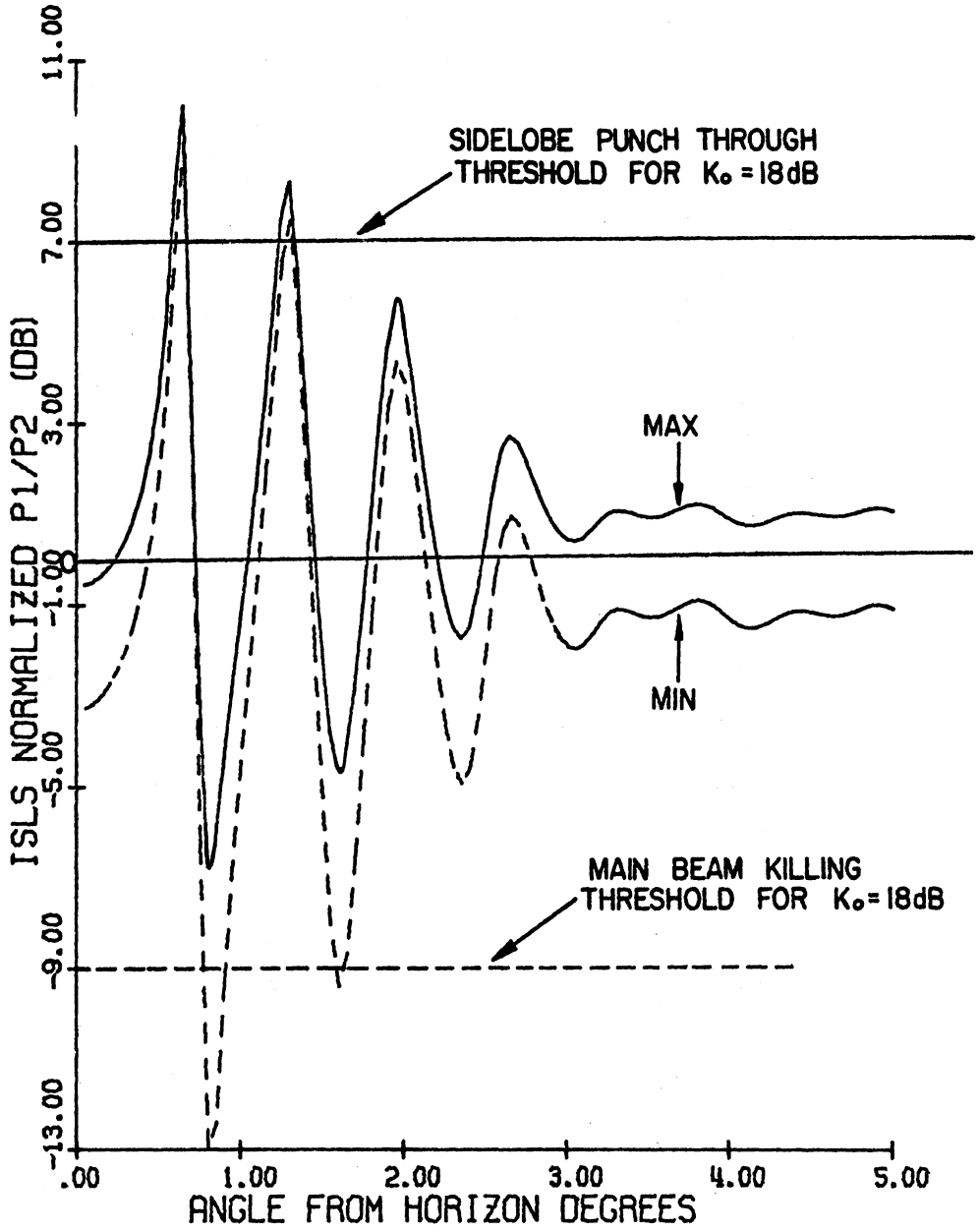

FIG. 7: Normalized pulse ratio envelopes as functions of θ.

envelope curve. As a result, the maximum and minimum values of $K_{MAX}(\theta)_{ISLS}$ are larger than those of $K_{MIN}(\theta)_{ISLS}$. This implies that the main beam killing would be more serious at the minima of $K_{MIN}(\theta)_{ISLS}$ and the sidelobe punch-through would be more serious at the maxima of $K_{MAX}(\theta)_{ISLS}$. For $\theta > 4^{o}$ the oscillations in the pulse ratio curves may be considered to be negligible.

The main beam killing and sidelobe punch-through zones for the antenna are obtained from the normalized pulse ratio curves shown in Fig. 7. The main beam killing zones in space are those regions in space where the pulse ratio falls below a given threshold level a [1]. For a pulse ratio curve normalized to the nominal free space value K_0, the main beam killing threshold occurs at $(a - K_0)$ dB. Thus with a = 9dB and K_0 = 19dB, the main beam killing threshold occurs at (9 - 18) = -9dB as shown in Fig. 7.

The sidelobe punch-through zones in space are those regions in space where the pulse ratio rises above the sidelobe punch-through threshold level b [1]. For a pulse ratio curve normalized to the nominal free space value of K_0 dB, if the azimuth sidelobe level of the antenna is -LdB, the sidelobe punch-through threshold level occurs at $(b + L - K_0)$ dB. With b = 0dB, L = 25dB and K_0 = 18dB, the sidelobe punch-through threshold level occurs at (0 + 25 - 18) = 7dB, as shown in Fig. 7.

Figure 8 shows the potential main beam killing and sidelobe punch-through zones as functions of the nominal pulse ratio K_0. These zones have been obtained from Fig. 7 with a = 9dB, b = 0dB and L = -25dB. It should be noticed that in Fig. 8 there are two sets of zones corresponding to the two pulse envelope ratio curves shown in Fig. 7. Observe that the main beam killing zones for the maximum envelope ratio lie within those for the minimum envelope ratio whereas the sidelobe punch-through zones for the maximum envelope ratio lie outside those of the minimum envelope ratio. As can be seen from Fig. 8, for K_0 = 18dB there are two main beam killing zones and two sidelobe punch-through zones for the range $0 \leq \theta \leq 3^{o}$.

Figure 9 shows the effective azimuth beamwidths $\alpha_{1MAX}(\theta)$, $\alpha_{1MIN}(\theta)$ as functions of θ for the threshold level a = 9dB and nominal pulse ratio K_0 = 18dB.

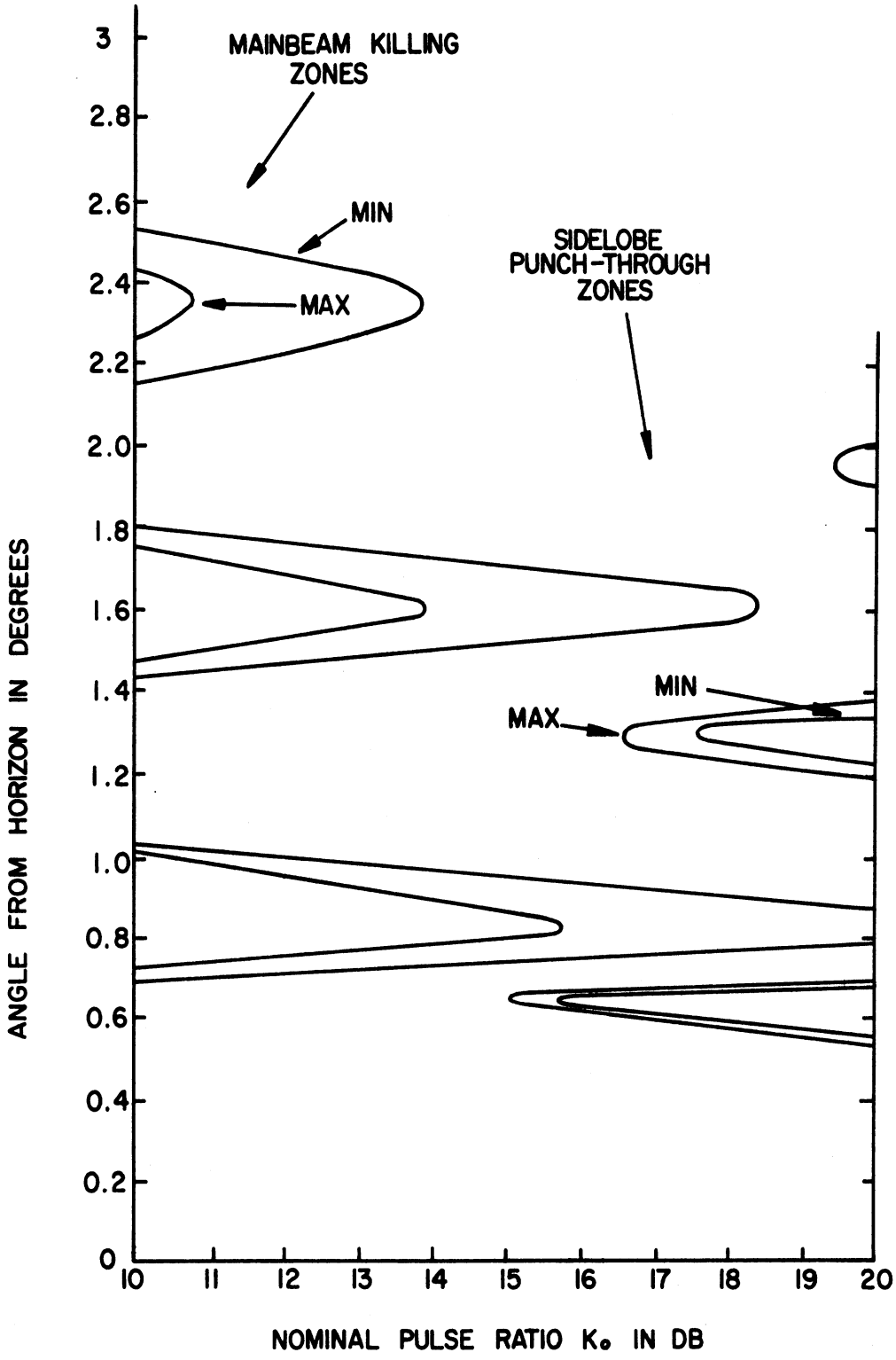

FIG. 8: Mainbeam killing and sidelobe punch-through zones as functions of the nominal pulse ratio for the Westinghouse array antenna. H_d = 34', H_0 = 42', f = 1030 MHz, P1 DIR/OMNI = 18.00 dB, a = 9 dB, b = 0 dB, L = -25 dB.

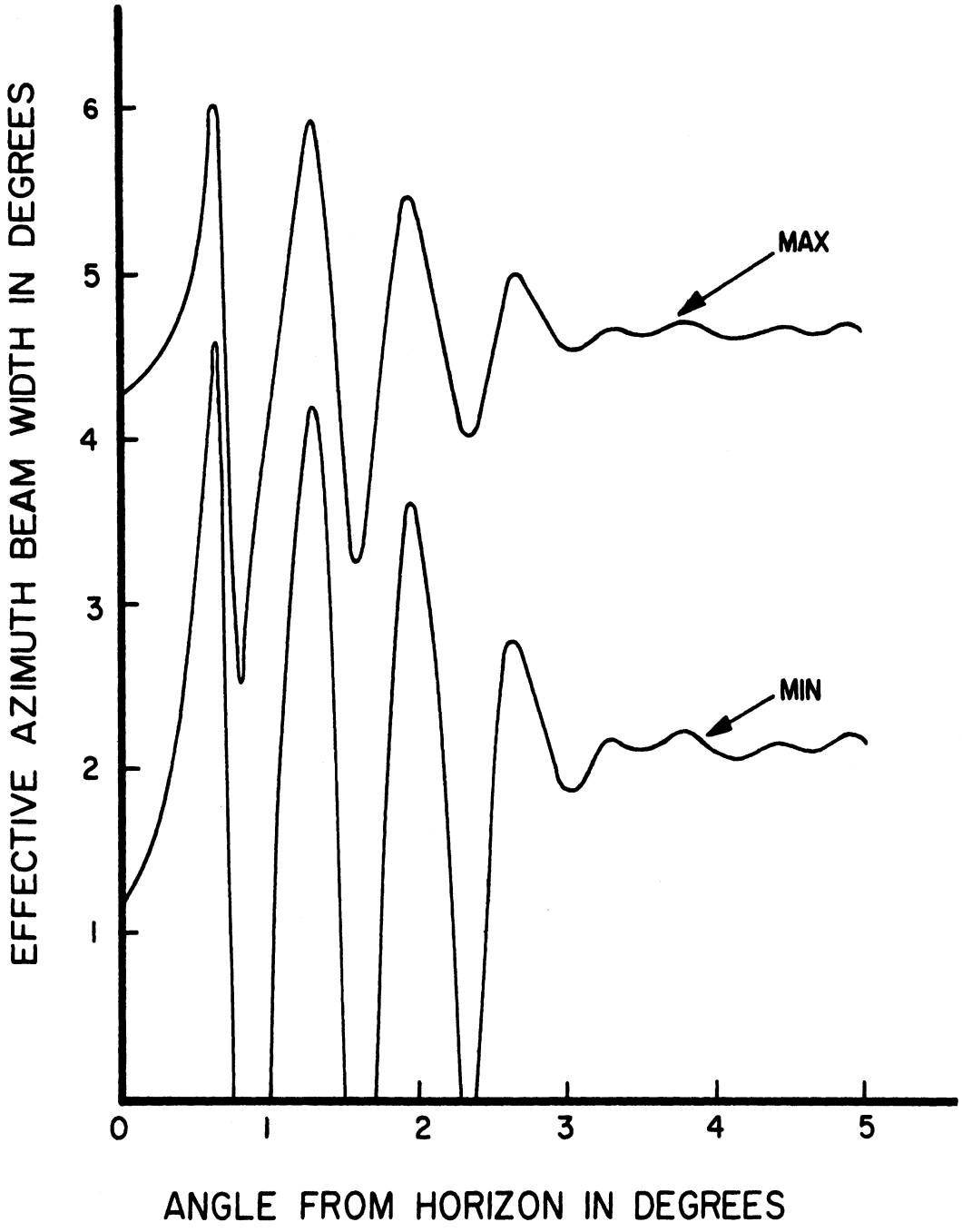

FIG. 9: Effective azimuth beamwidths as functions of the angle from the horizon for the Westinghouse array antenna. H_d = 34', H_0 = 42', f = 1030 MHz, nominal pulse ratio K_0 = 18dB, P1 DIR/OMNI = 18dB.

For $\theta \gtrsim 3^{o}$ the effective beamwidths assume constant values of about 4.6^{o} and 2.2^{o} at the maximum and minimum envelope cases respectively. In the SLS mode of operation with the same antenna the free space constant value of the effective azimuth beamwidth is about 3.9^{o}.

Figure 10 shows the number of replies $N_{MAX}(\theta)$, $N_{MIN}(\theta)$ as functions of θ. These have been obtained by using Eqs. (39) and (40) with f_i = 360 pulses/sec and Ω = 90 deg/sec (15 rpm). Since the number of replies is an integer, Fig. 10 is obtained by taking the first integer which is less than or equal to the solution of Eq. (39) or (40). It is found from Fig. 10 that at any angle θ the number of replies is larger for the maximum envelope case. Both $N_{MAX}(\theta)$ and $N_{MIN}(\theta)$ are oscillating functions of θ. For the antenna considered in Fig. 10 the numbers of replies assume constant values for $\theta \gtrsim 3.5^{o}$. The saturation values of N_{MAX} and N_{MIN} are found to be about 18 and 7 respectively. It should be noted that the saturation value of the number of replies is about 15 for the same antenna in the SLS case [1].

Figure 11 shows the coverage diagram for the antenna normalized to the maximum free space range of 40 nautical miles. The diagram has been prepared with the conventional 4/3 radius of the earth to take into account the normal refraction at the lower atmosphere. Equations (45) and (46) have been used to obtain the ranges as functions of θ. As shown in Fig. 11, for the maximum envelope case the maximum range of 50.5 nautical miles occurs at $\theta \sim 0.4^{o}$ and the minimum range of 14 nautical miles occurs at $\theta \sim 0.9^{o}$. The corresponding ranges for the minimum envelope case are 40 nautical miles at $\theta \sim 0.4^{o}$ and 7 nautical miles at $\theta \sim 0.9^{o}$, respectively. For comparison the SLS mode free space coverage diagram for the same antenna is also shown in Fig. 11.

4.2.2 Texas Instruments Reflector Antenna.

The heights above ground of the phase centers of the directional and omnidirectional antennas are, respectively, H_d = 34' and H_0 = 43'. The free space elevation plane patterns of the directional and omhidirectional antennas are assumed to be identical.

Figure 12 shows $P1(\theta)_{MAX}$, $P1(\theta)_{MIN}$ and $P2(\theta)$ in dB as functions of θ, where the 0 dB level is adjusted to coincide with the maximum $P1(\theta)_{SLS}$ level in the

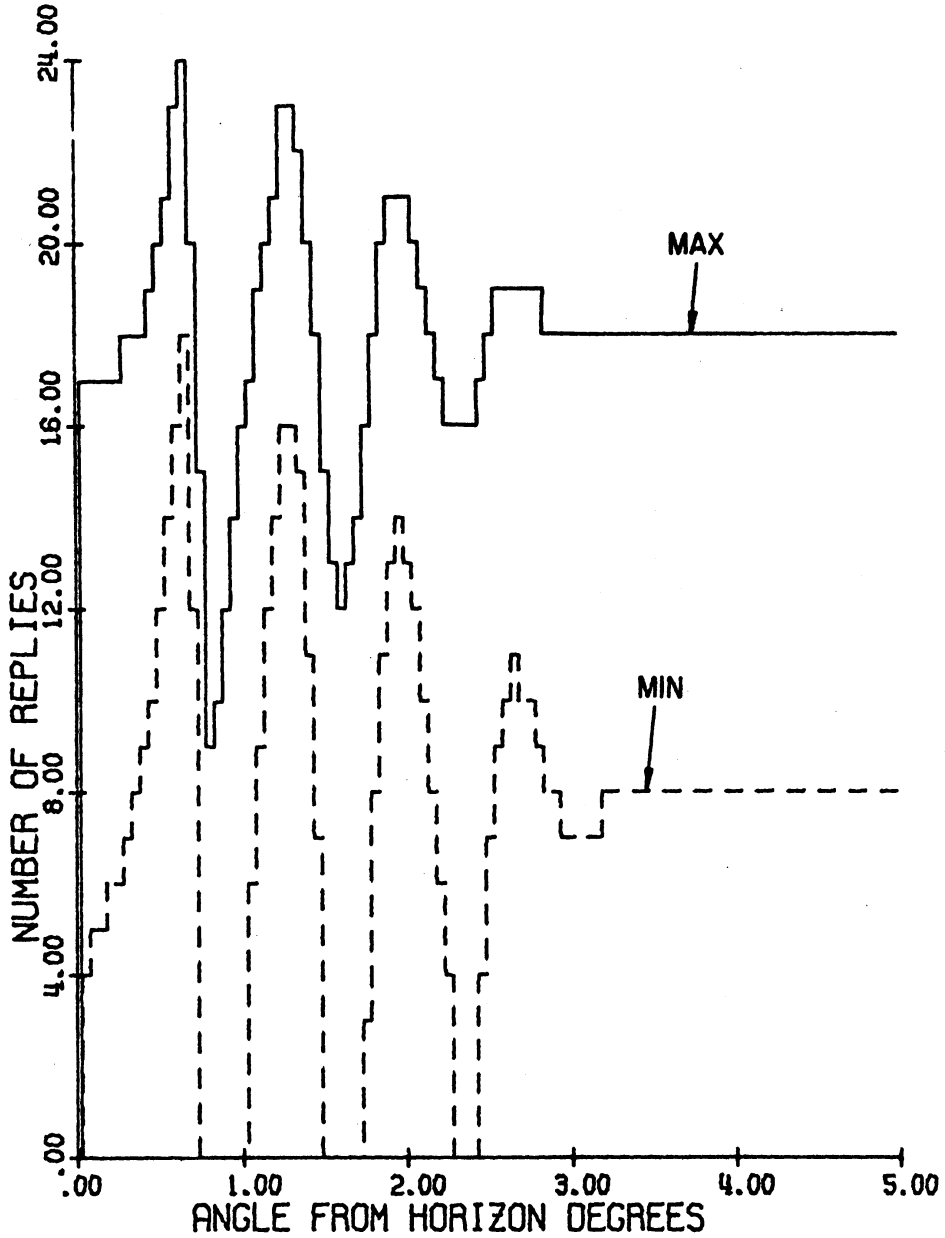

FIG. 10: Number of replies as functions of angle from the horizon.

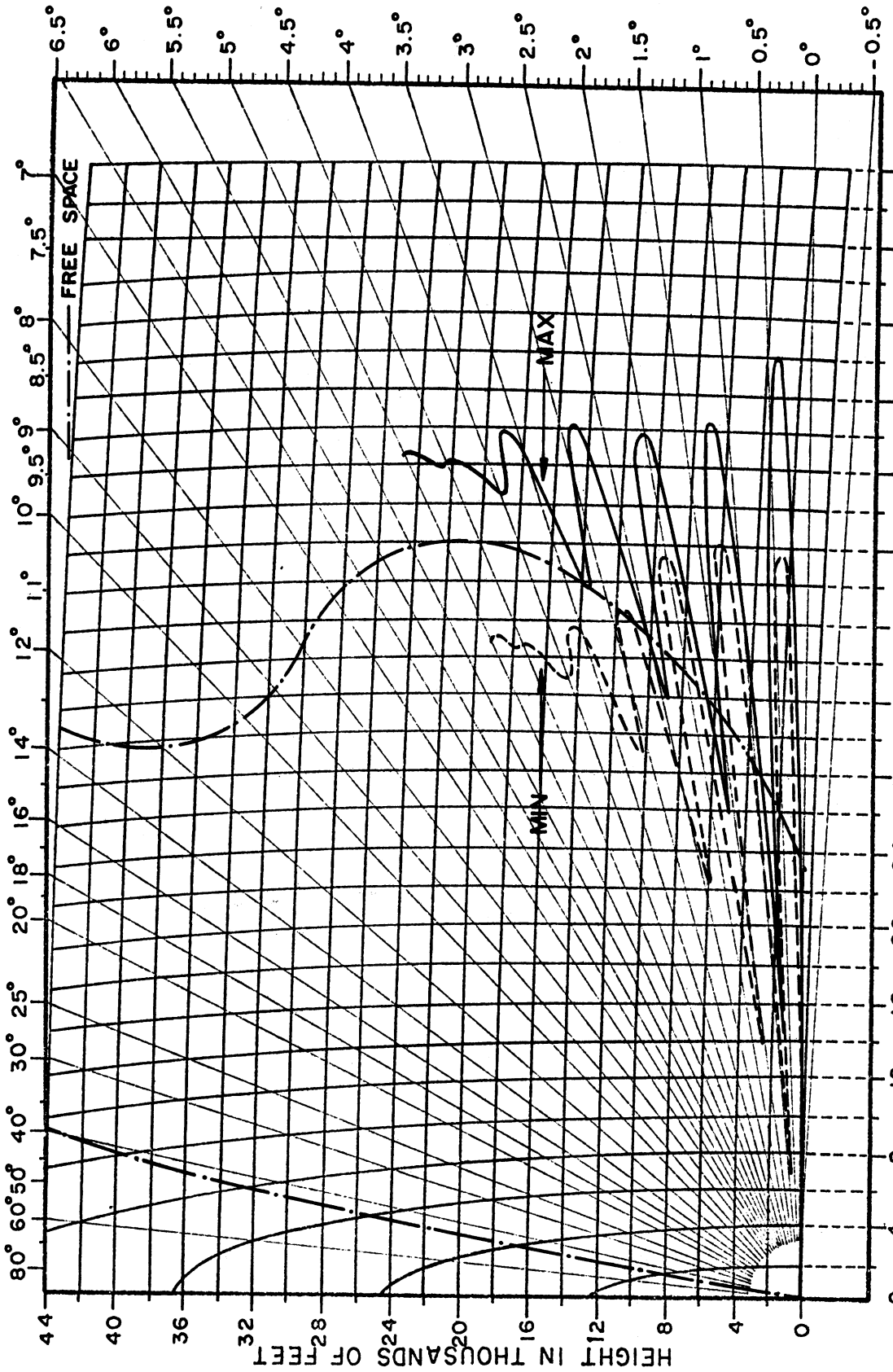

FIG. 11: Coverage diagram for the Westinghouse array antenna. $H_d = 34'$, $H_0 = 42'$, f = 1030 MHz.

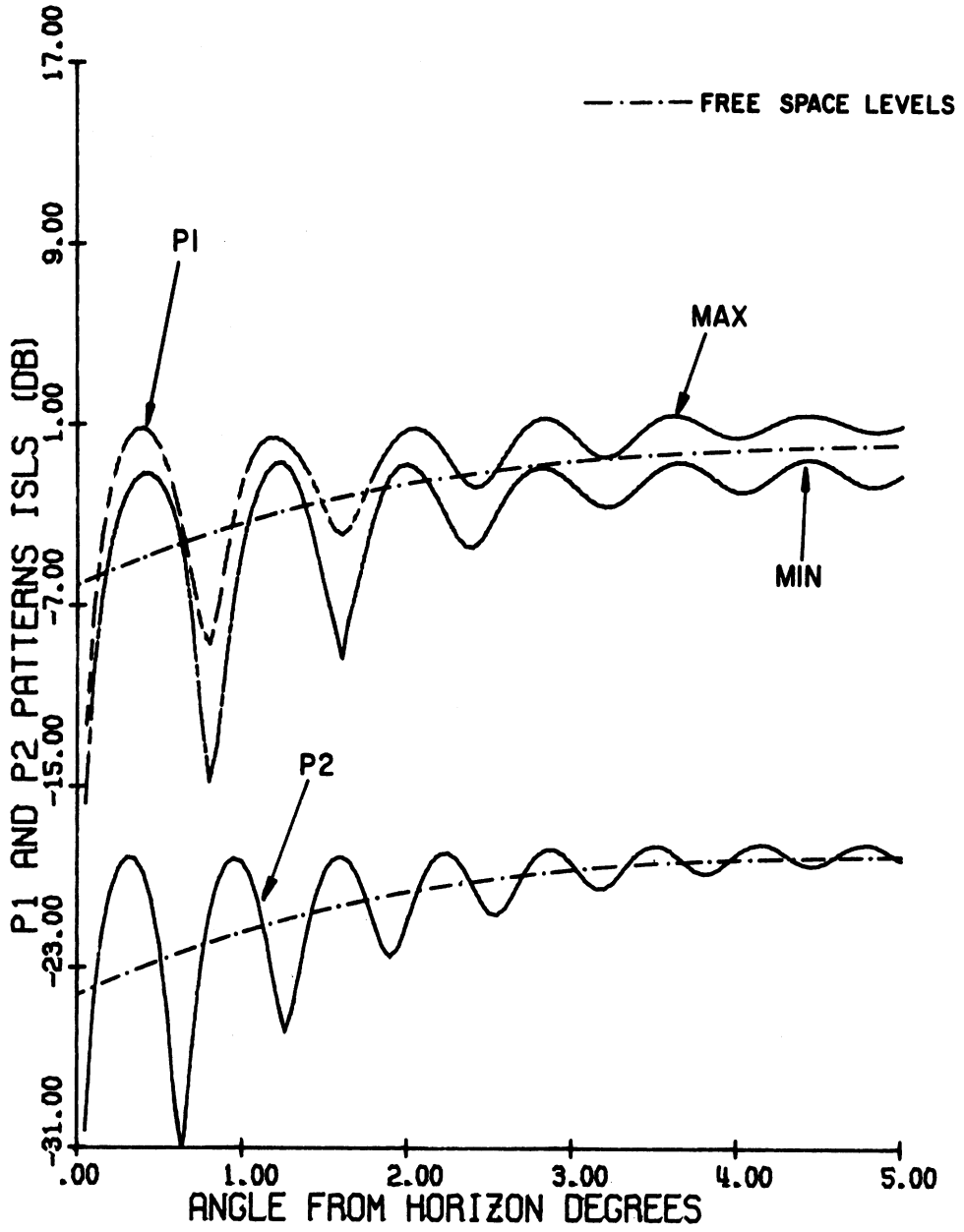

FIG. 12: $P1(\theta)_{MAX}$, $P1(\theta)_{MIN}$ and $P2(\theta)$ as functions of θ.

free space case. The corresponding free space curves (for q = 0) are also shown in Fig. 12 for comparison. The oscillations in the curves may be considered to be negligible for $\theta \gtrsim 4.5^{o}$. The general behavior of the curves is similar to Fig. 6 for the Westinghouse antenna.

Figure 13 shows the maximum and minimum envleope pulse ratios as functions of θ and normalized to the nominal free space value K_0 (= 18 dB). The oscillatory nature of the curves may be considered negligible for $\theta \gtrsim 4.5^{o}$.

The main beam killing and sidelobe punch-through zones as functions of nominal pulse ratio are shown in Fig. 14. For K_0 = 18 dB there is one main beam killing zone and two sidelobe punch-through zones within the range of θ shown in Fig. 14.

Figure 15 shows the effective azimuth beamwidths $\alpha_{1MAX}(\theta)$, $\alpha_{1MIN}(\theta)$ as functions of θ for the threshold level a = 9 dB and the nominal pulse ratio K_0 = 18 dB. For $\theta \gtrsim 4.5^{o}$ the curves assume constant values given by $\alpha_{1MAX} \simeq 4.8^{o}$ and $\alpha_{1MIN} \simeq 2.3^{o}$. In the SLS mode of operation with the same antenna, the free space value of the effective azimuth beamwidth is about 4^{o}.

Figure 16 shows the number of replies $N_{MAX}(\theta)$, $N_{MIN}(\theta)$ as functions of θ. For $\theta > 4.5^{o}$ $N_{MAX}(\theta) \sim 19$ and $N_{MIN} \sim 7$. For the same antenna the saturation value of the number of replies is about 16 in the SLS case [1].

Figure 17 shows the coverage diagram for the antenna normalized to the free space maximum range of 40 nautical miles. As shown in Fig. 17 for the maximum envelope case the maximum range of about 44 nautical miles occurs at $\theta \sim 0.4^{o}$ and the minimum range of about 6 nautical miles occurs at $\theta \sim 0.7^{o}$. The corresponding ranges for the minimum envelope case are about 34 and 3 nautical miles respectively.

4.2.3 Hazeltine Open Array Antenna.

The heights above ground of the phase centers of the directional and omnidirectional antennas are, respectively, H_d = 33' and H_0 = 37'. The vertical aperture of the antenna is 4' and it is assumed that the free space elevation plane patterns of the directional and omnidirectional antennas are identical.

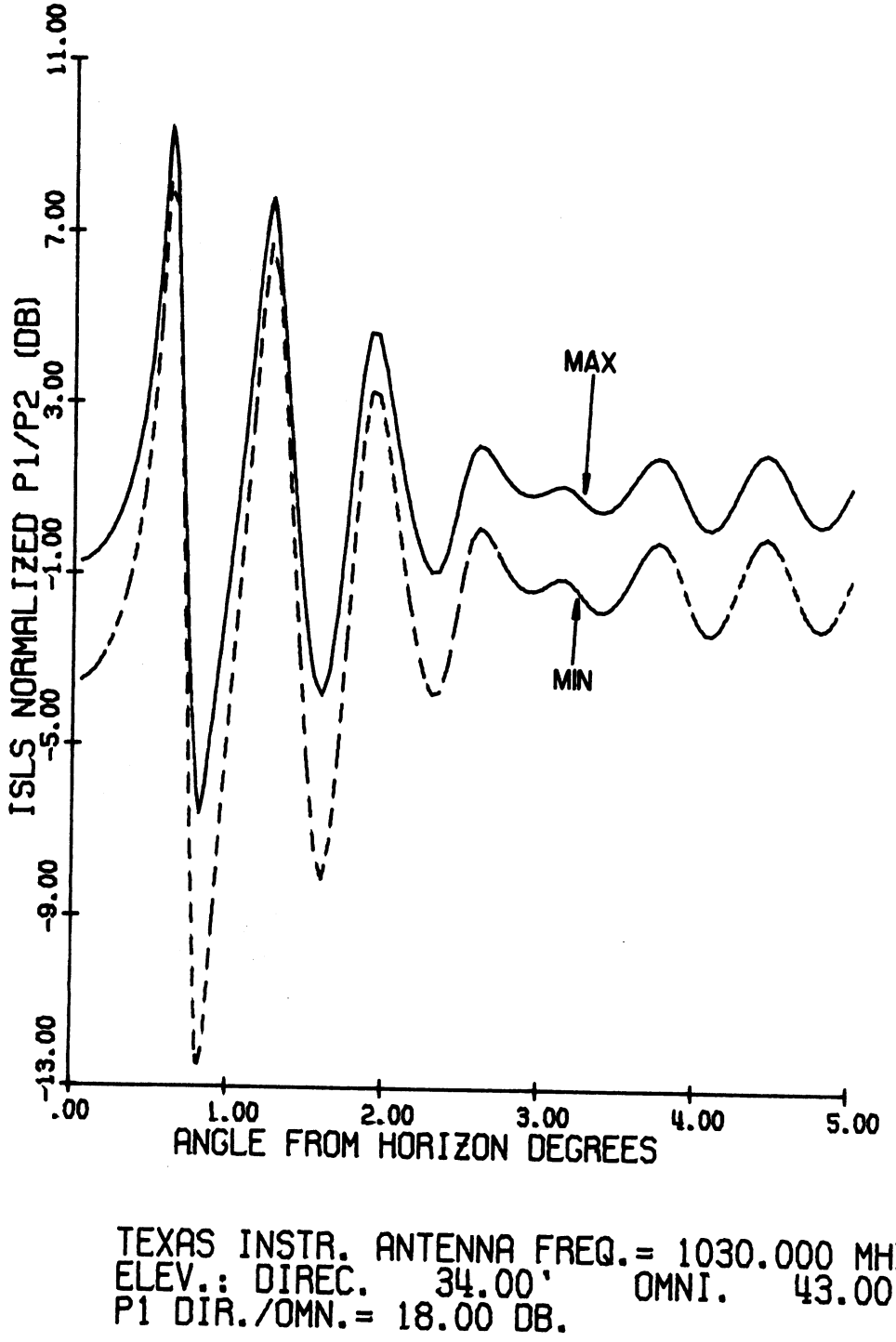

FIG. 13: Normalized pulse ratio envelopes as functions of θ.

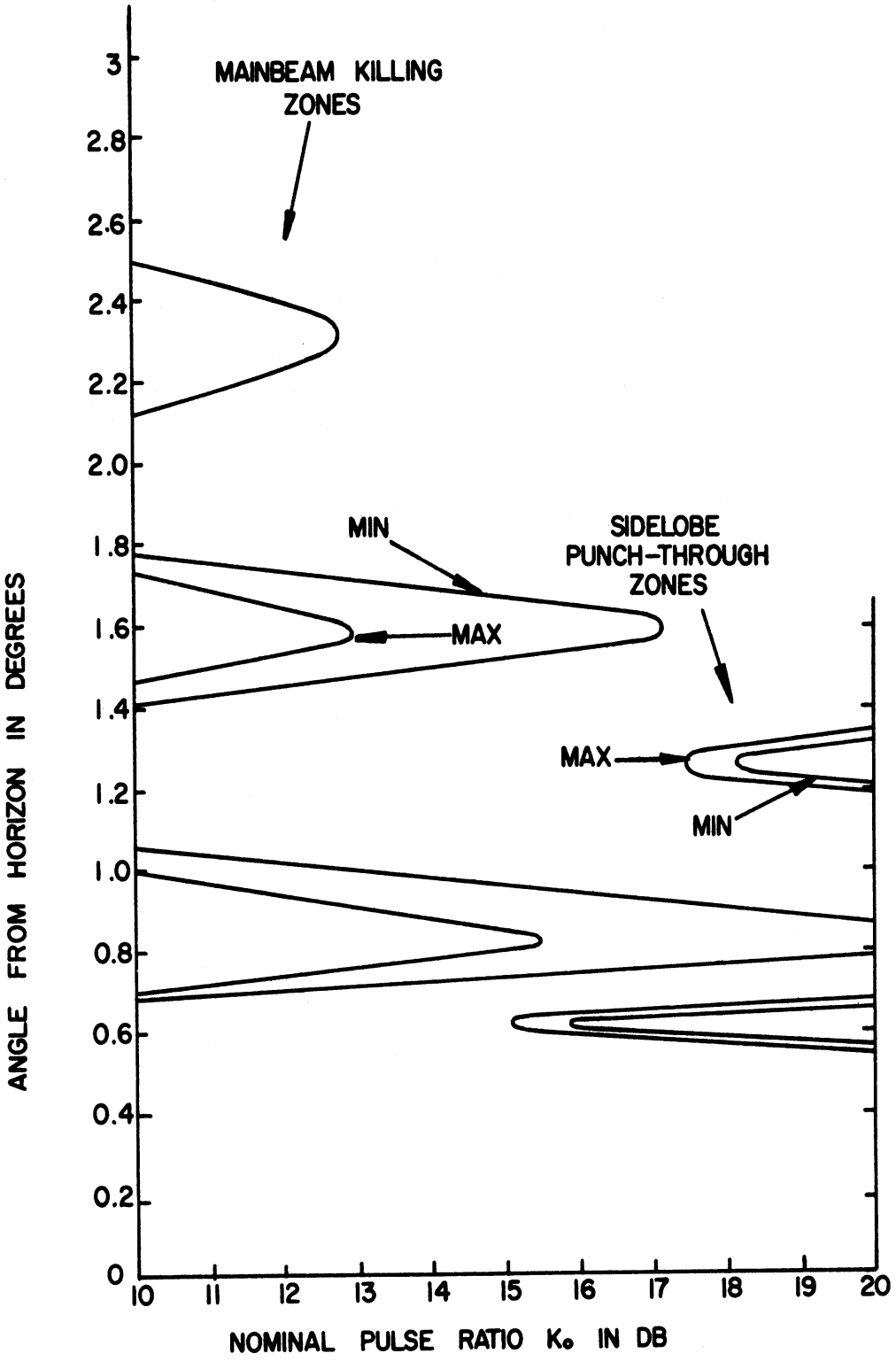

FIG. 14: Mainbeam killing and sidelobe punch-through zones as functions of the nominal pulse ratio for the Texas Instruments reflecting antenna. H_d = 34', H_0 = 43', f = 1030 MHz, P1 DIR/OMNI = 18.00 dB, a = 9dB, B = 0dB, L = -25dB.

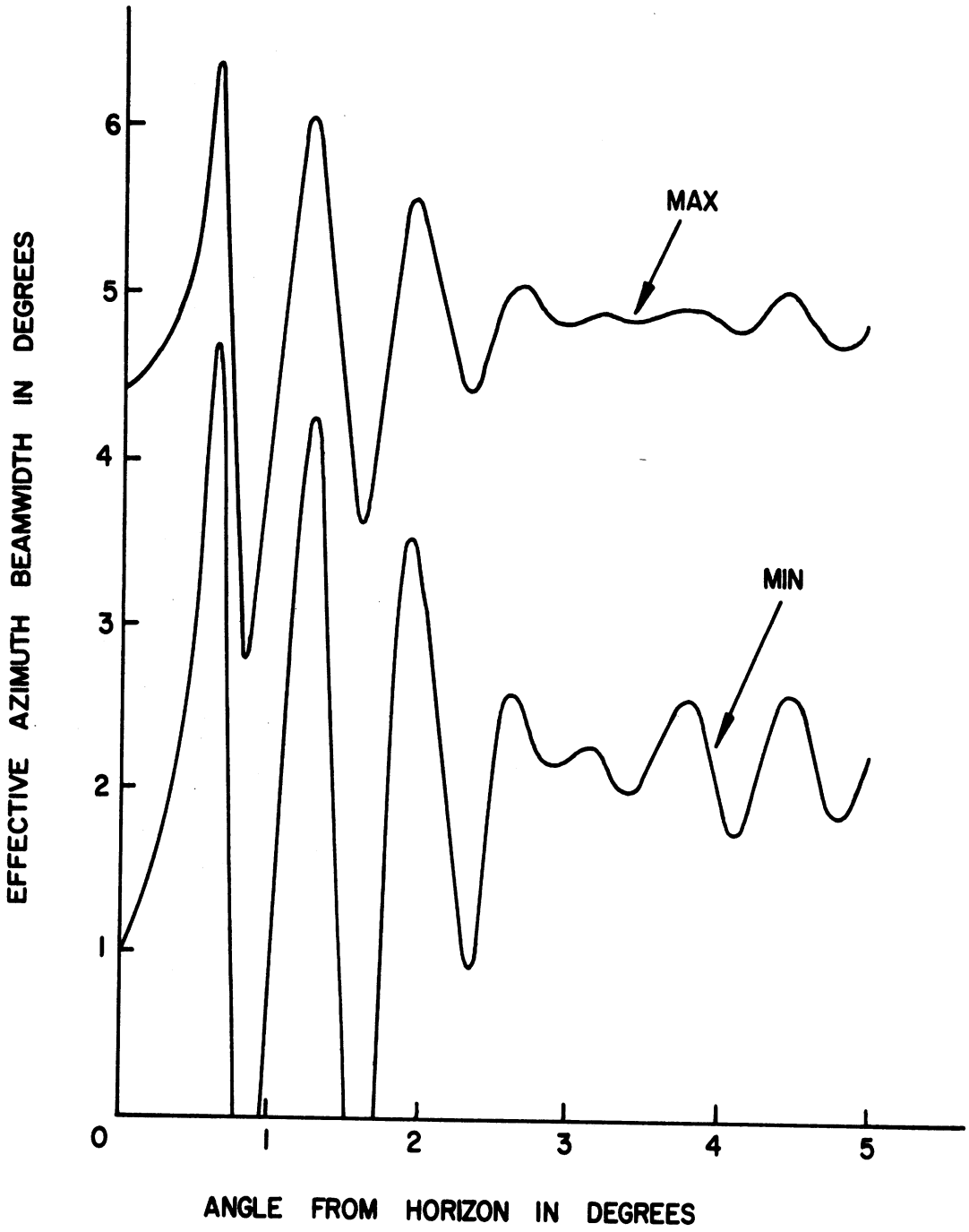

FIG. 15: Effective azimuth beamwidths as functions of the angle from the horizon for the Texas Instruments reflector antenna. H_d = 34', H_0 = 43', f = 1030 MHz, nominal pulse ratio K_0 = 18dB, P1 DIR/OMNI = 18dB.

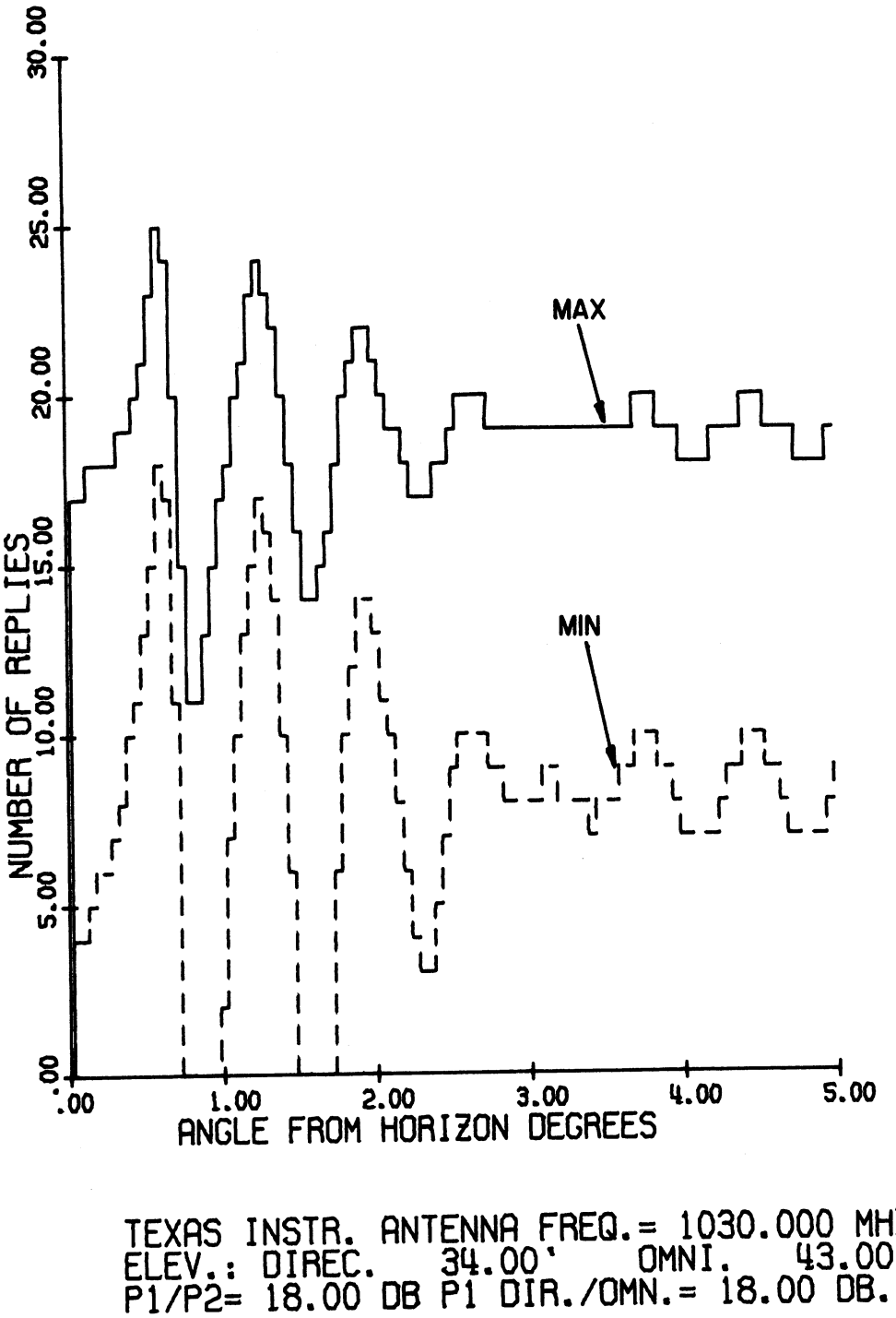

FIG. 16: Number of replies as functions of angle from the horizon.

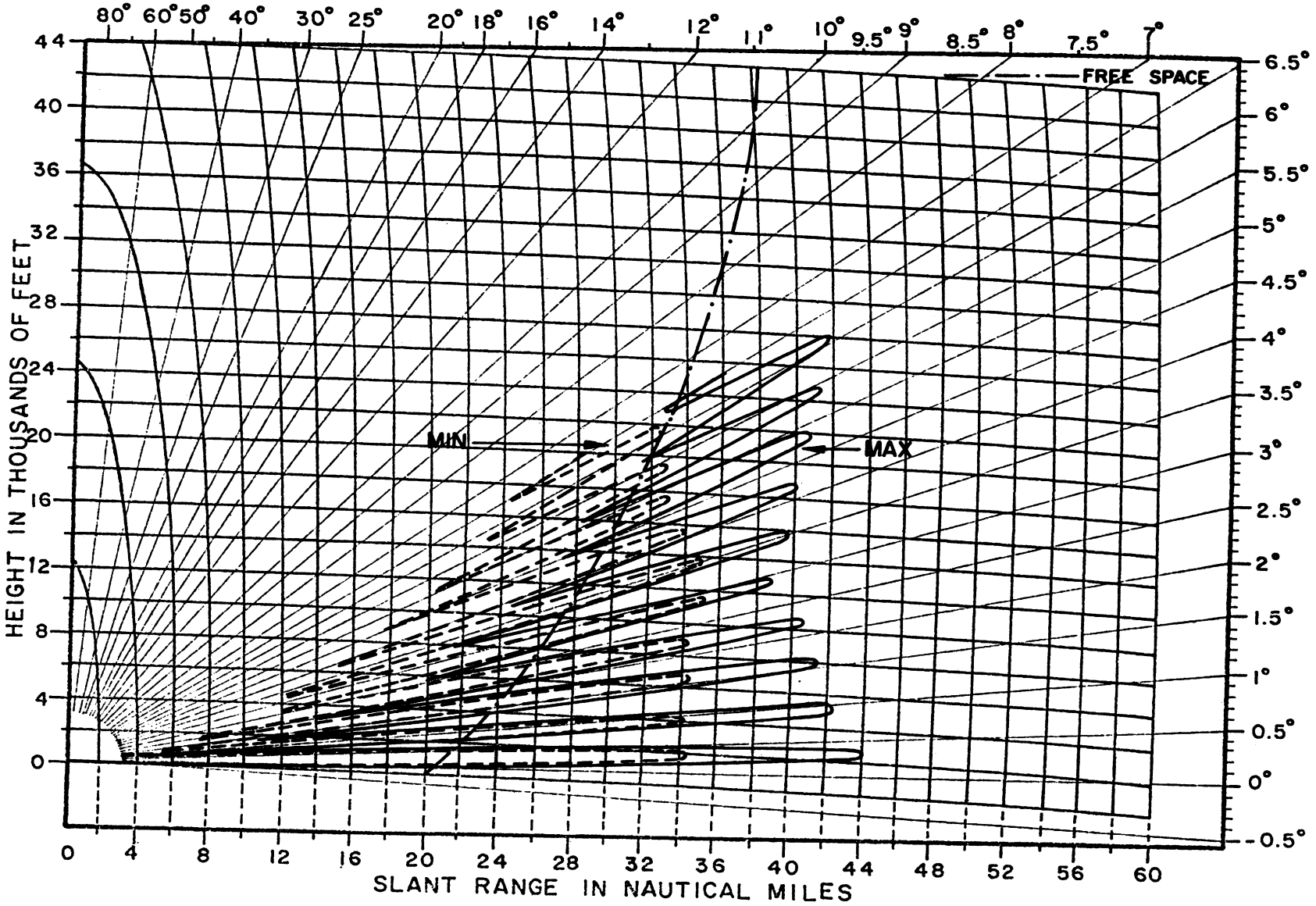

FIG. 17: Coverage diagram for the Texas Instruments reflector antenna. H_d = 34', H_0 = 43', f = 1030 MHz

Figure 18 a shows $P1(\theta)_{MAX}$, $P1(\theta)_{MIN}$ and $P2(\theta)$ pulses as functions of θ where the 0 dB level is adjusted to coincide with the maximum of $P1(\theta)_{SLS}$ level in the free space case. Due to the small field gradient ($\alpha_g = 8\,dB/5^o$) of the antenna, the oscillations of the patterns in Fig. 18 a are not so quickly damped out as in the case of the previous two antennas. For this reason, $P1(\theta)_{MAX}$, $P1(\theta)_{MIN}$, and $P2(\theta)$ curves in the extended region $5^o \leq \theta \leq 10^o$ are shown in Fig. 18 b. For $\theta > 10^o$ the oscillations in the curves are negligible.

The pulse ratios as functions of θ are shown in Figs. 19 a and 19 b for $0 \leq \theta \leq 5^o$ and $5^o \leq \theta \leq 10^o$ respectively.

The main beam killing and sidelobe punch-through zones as functions of nominal pulse ratio are shown in Figs. 20 a and 20 b. For $K_0 = 18\,dB$ there are four main beam killing zones and four sidelobe punch-through zones for the range of θ values shown .

Figures 21 a and b show the effective azimuth beamwidths as functions of θ for $0 \leq \theta \leq 5^o$ and $5^o \leq \theta \leq 10^o$. The oscillations in the curves continue up to $\theta \sim 10^o$ and beyond $\theta = 10^o$ they assume their respective saturation values. The saturation values for the maximum and minimum envelope cases are about 4.7 and 2.0 respectively. In the SLS mode of operation with the same antenna, the free space value of the effective azimuth beamwidth is about 4^o.

The number of replies as functions of θ are shown in Fig. 22 for the range $0 \leq \theta \leq 5^o$. The saturation values of $N_{MAX}(\theta) \sim 19$ and $N_{MIN}(\theta) \sim 8$, which occur for $\theta > 10^o$. For the same antenna operating in the SLS mode, the free space value of the number of replies is 16.

The coverage diagram normalized to the free space maximum range of 40 nautical miles is shown in Fig. 23. As shown in Fig. 23 for the maximum envelope case, the maximum range of about 44 nautical miles occurs at $\theta \sim 0.4^o$ and the minimum range of about 8 nautical miles occurs at $\theta \sim 0.8^o$. The corresponding ranges for the minimum envleope case are 34 nautical miles and 5 nautical miles respectively.

4.2.4. The Existing Hog-Trough Antenna.

The heights above ground of the phase centers of the directional and omnidirectional antennas are 41' and 43' respectively. The vertical aperture of each

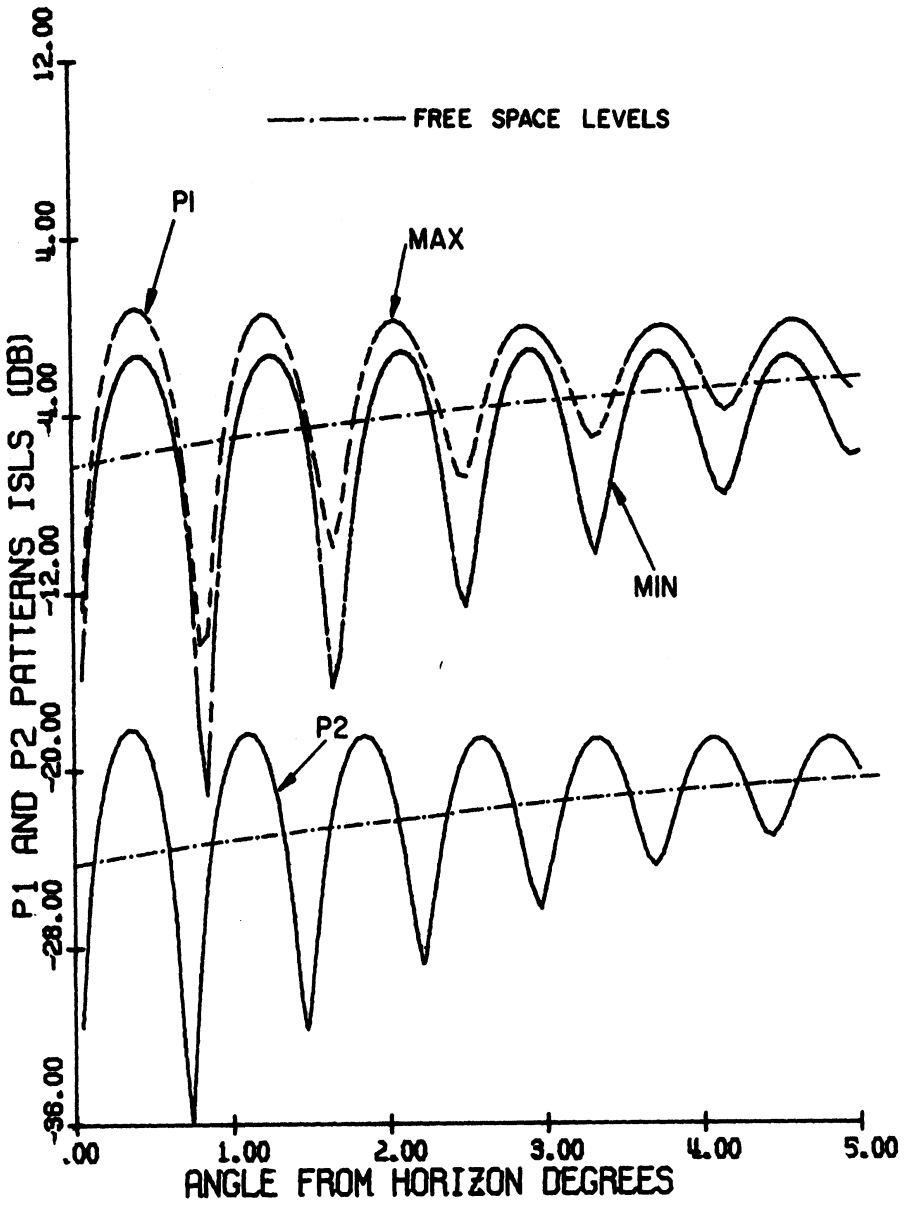

FIG. 18 a: $P1(\theta)_{MAX}$, $P1(\theta)_{MIN}$ and $P2(\theta)$ as functions of θ.

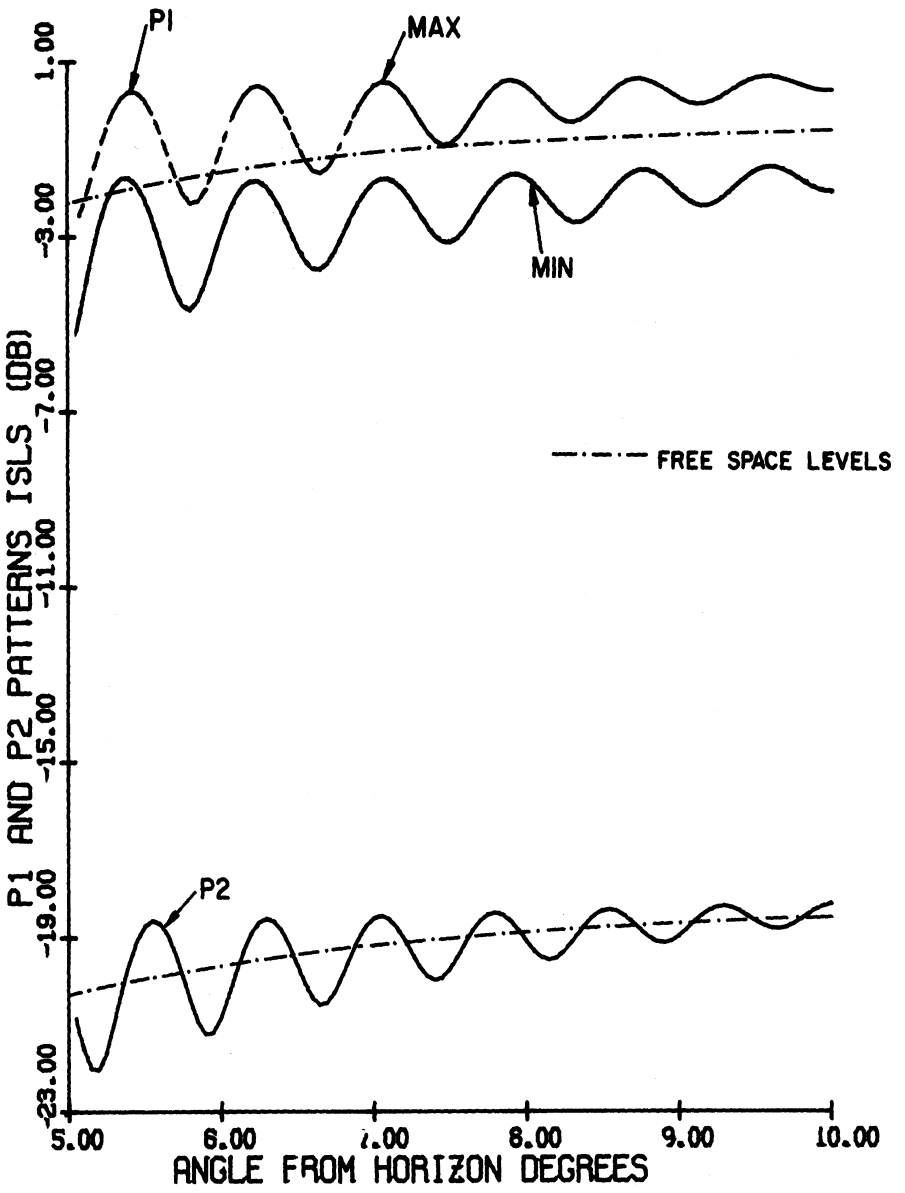

FIG. 18 b: $P1(\theta)_{MAX}$, $P1(\theta)_{MIN}$ and $P2(\theta)$ as functions of θ.

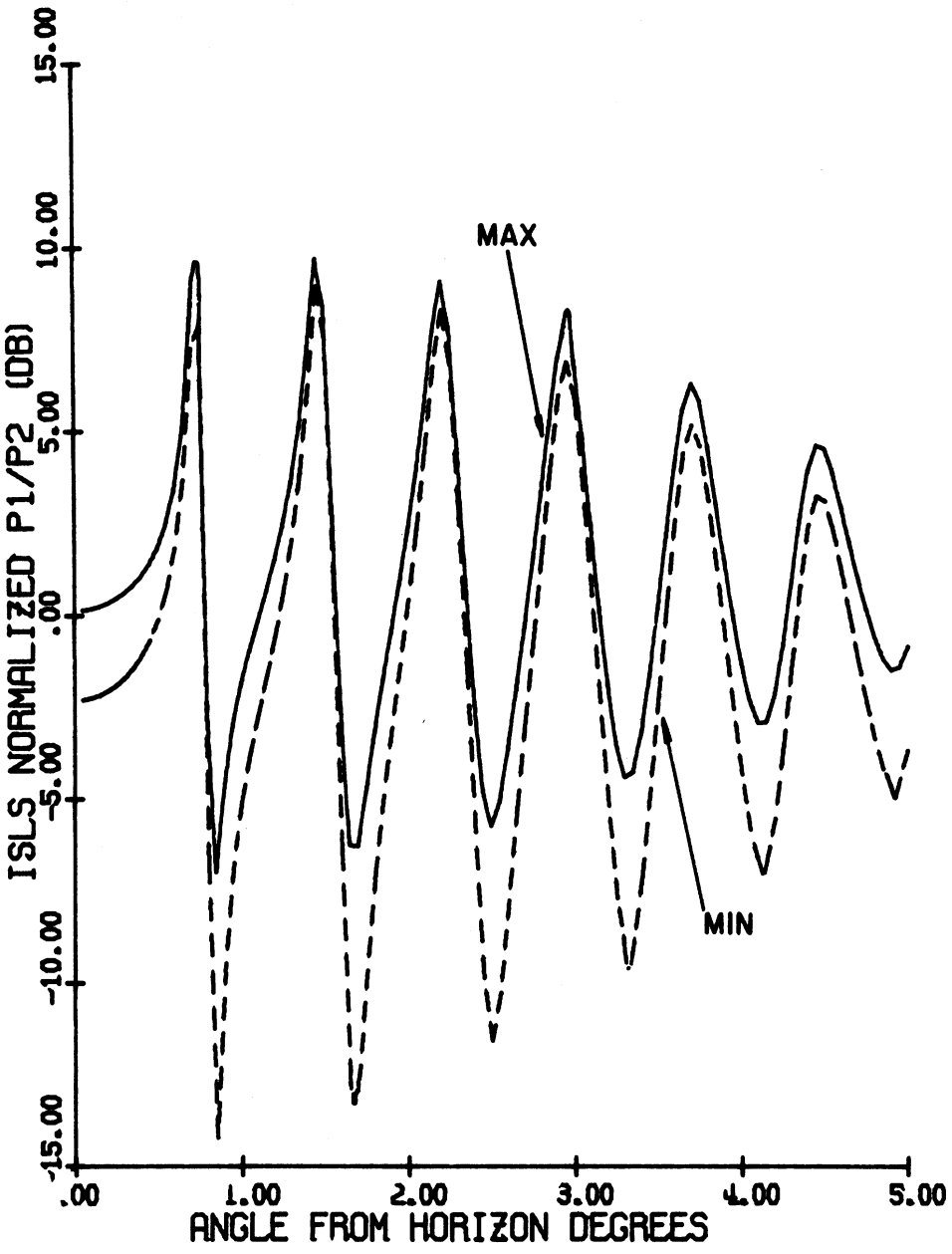

FIG. 19 a: Normalized pulse ratio envelopes as functions of θ.

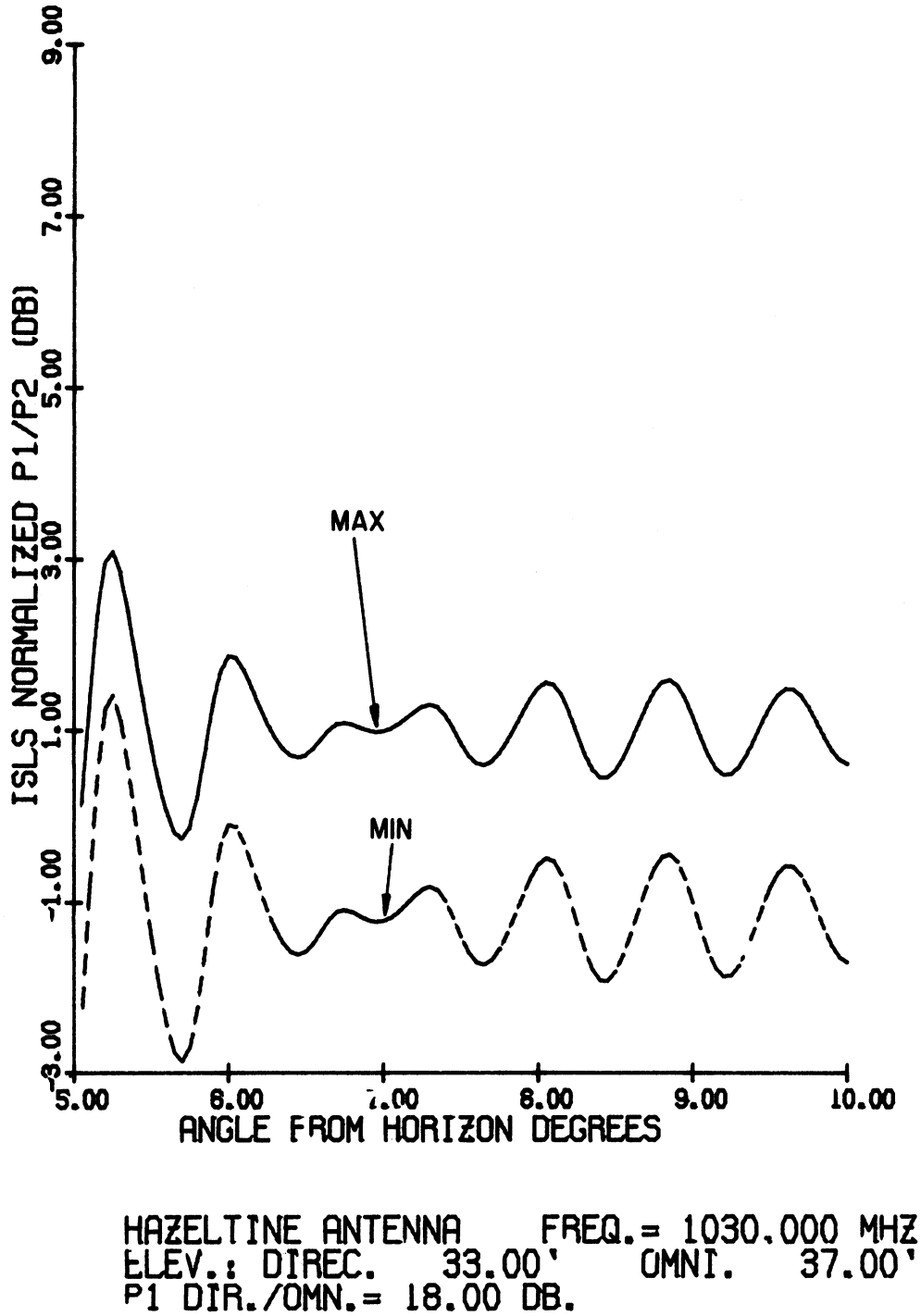

FIG. 19 b: Normalized pulse ratio envelopes as functions of θ.

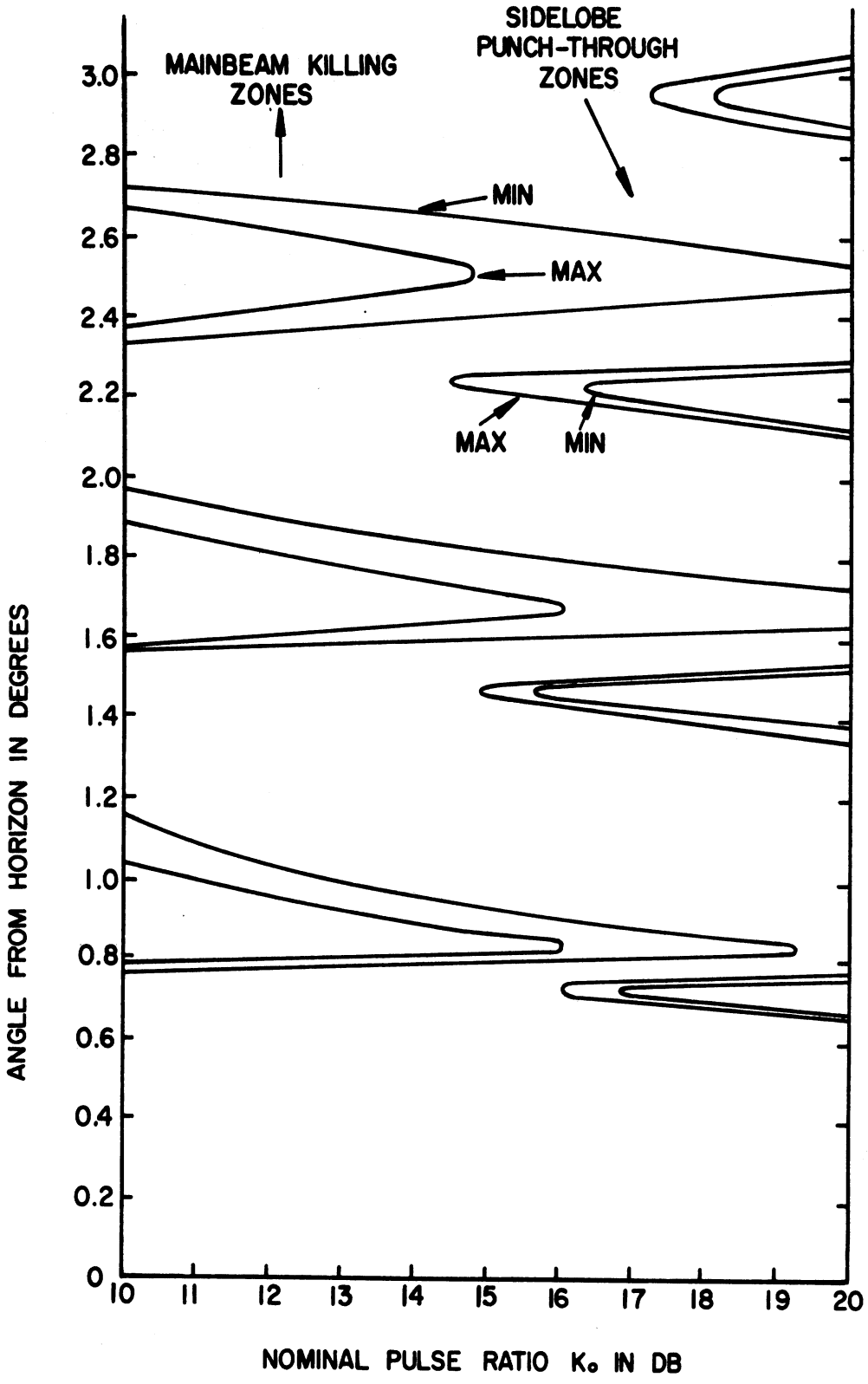

FIG. 20 a: Mainbeam killing and sidelobe punch-through zones as functions of the nominal pulse ratio for the Hazeltine open array. H_d = 33', H_0 = 37', f = 1030 MHz, P1 DIR/OMNI = 18 dB, a = 9 dB, b = -25 dB.

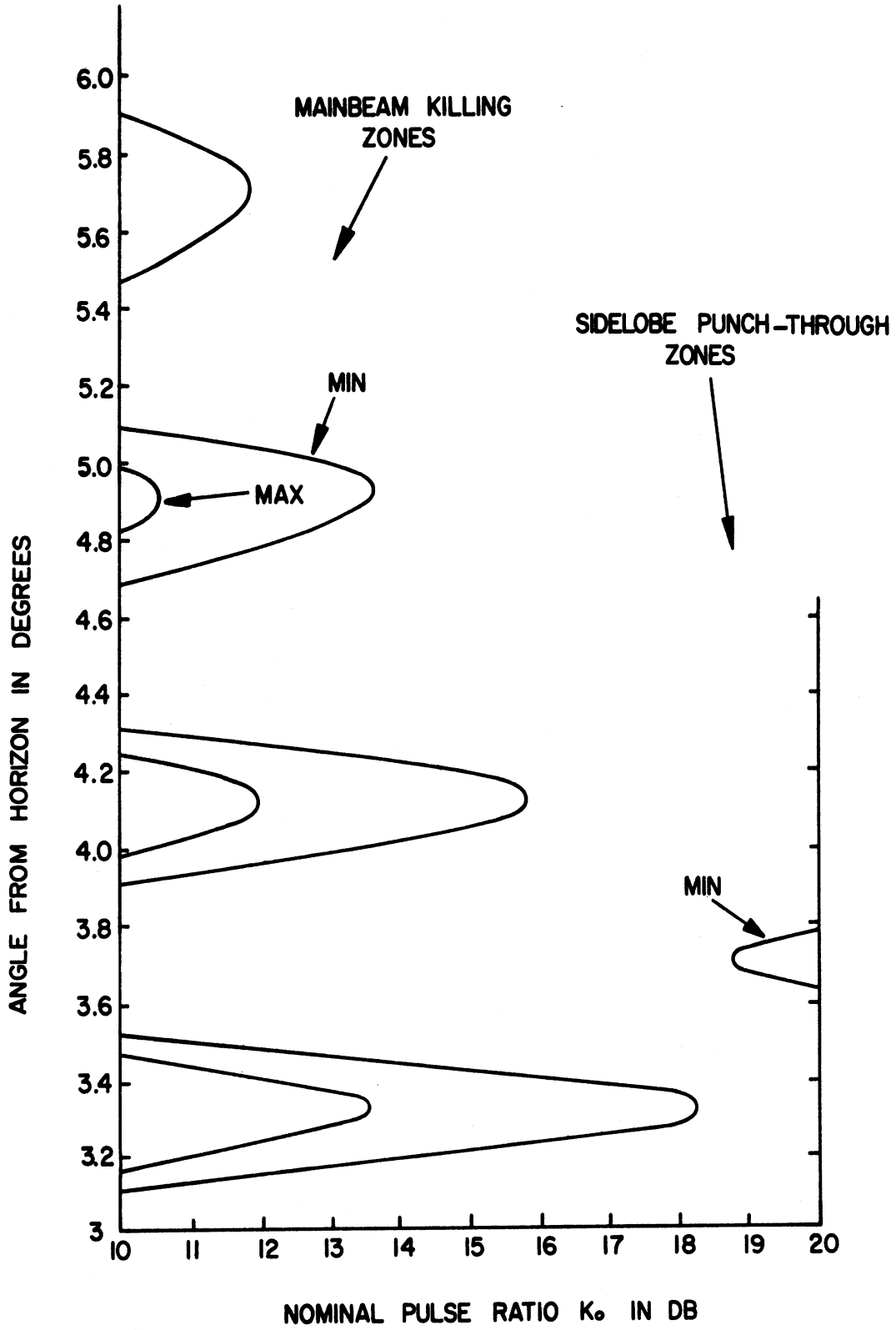

FIG. 20 b: Mainbeam killing and sidelobe punch-through zones as functions of θ for the Hazeltine open array. H_d = 33', H_0 = 37', f = 1030 MHz, P1 DIR/OMNI = 18dB, a = 9dB, b = 0dB, L = -25dB.

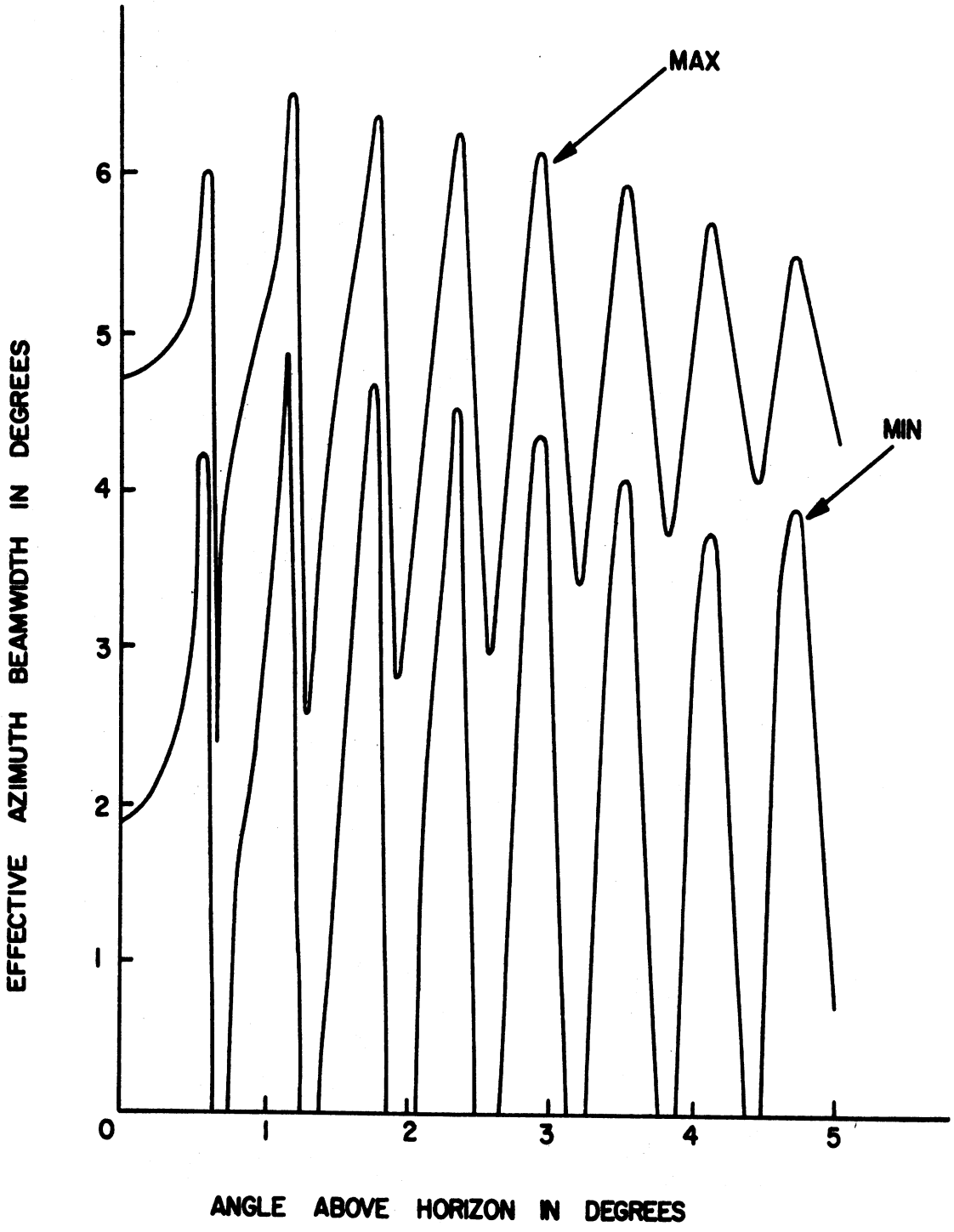

FIG. 21 a: Effective beamwidths as functions of angle from the horizon for the Hazeltine open array. H_d = 34', H_0 = 37', f = 1030 MHz, nominal pulse ratio K_0 = 18dB, P1 DIR/OMNI = 18dB.

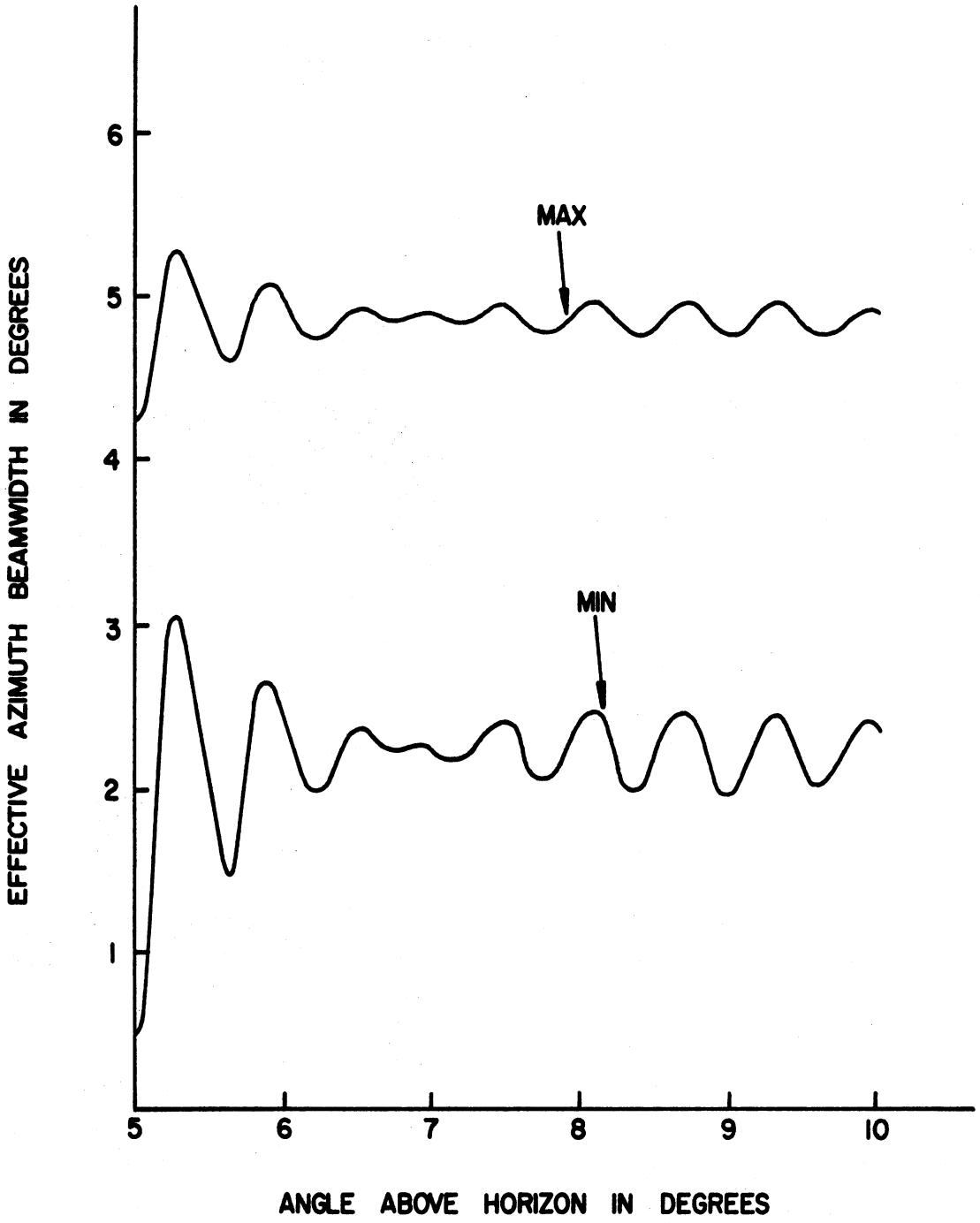

FIG. 21 b: Effective azimuth beamwidths as functions of angle from the horizon for the Hazeltine open array. H_d = 34', H_0 = 37', f = 1030 MHz, nominal pulse ratio K_0 = 18dB, P1 DIR/OMNI = 18dB.

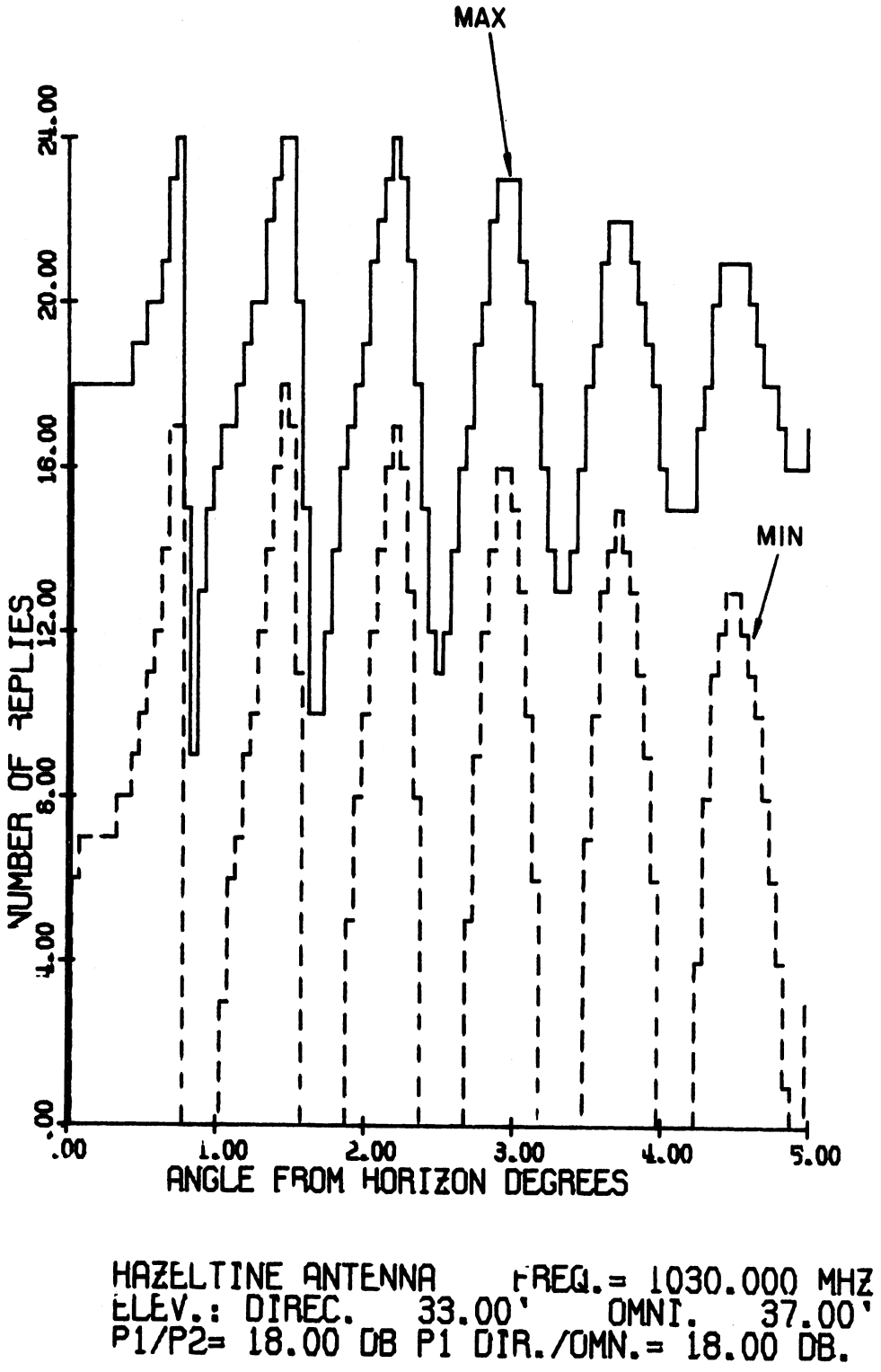

FIG. 22: Number of replies as functions of angle from the horizon.

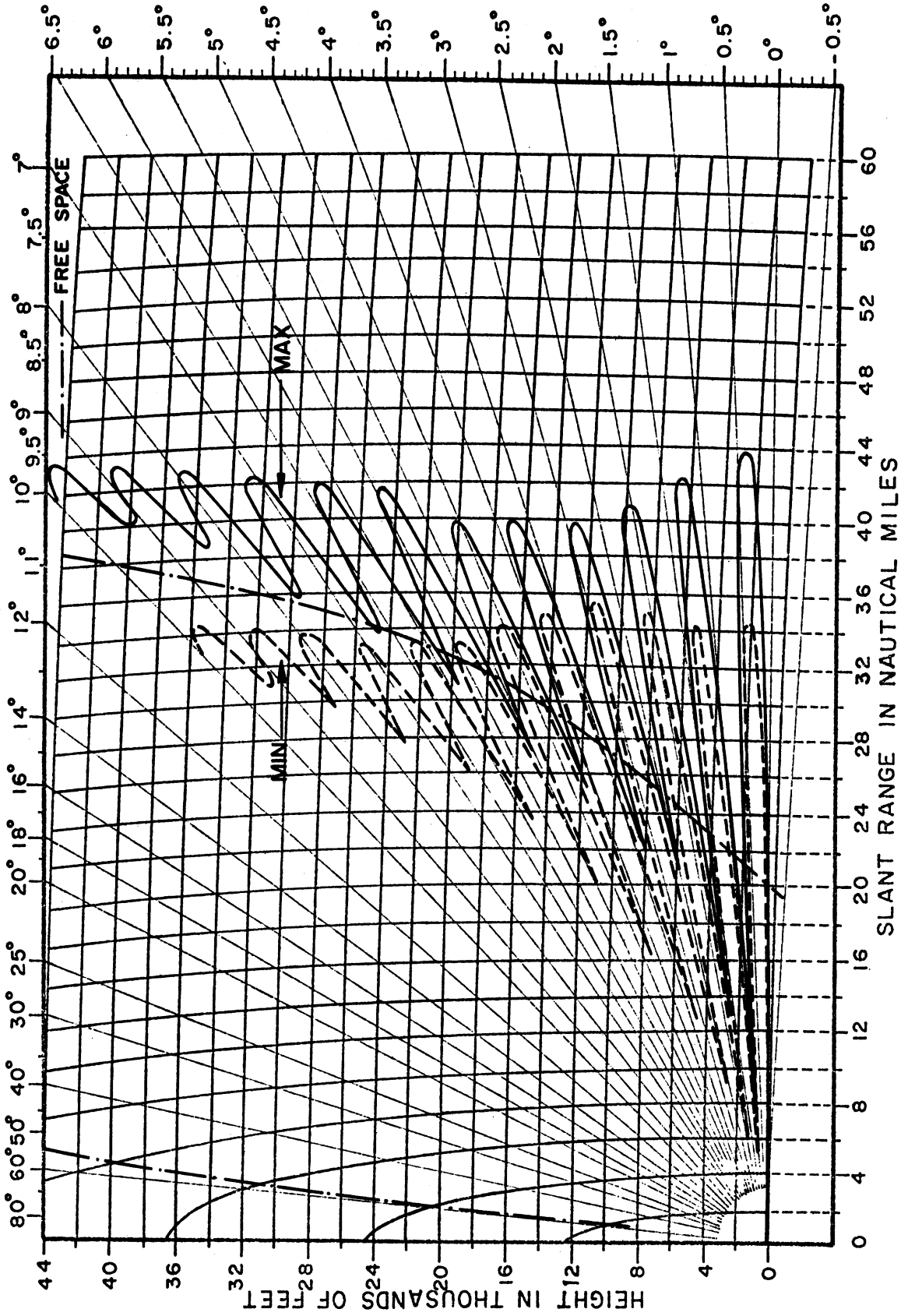

FIG. 23: Coverage diagram for the Hazeltine open array. H_d = 33', H_0 = 37', f = 1030 MHz.

antenna is about 2' and it is assumed that the free space elevation plane patterns of the directional and omnidirectional antennas are identical.

Figure 24 a shows the $P1(\theta)_{MAX}$, $P1(\theta)_{MIN}$, and $P2(\theta)$ pulses as functions of θ in the range $0 \leq \theta \leq 5^{o}$, where the 0 dB level is adjusted to coincide with the maximum of the $P1(\theta)_{SLS}$ level in the free space case. Because of the small field gradient of the antenna ($\alpha_{g} = 0.5\,dB/5^{o}$) the lobing structure in $P1(\theta)_{MAX}$, $P1(\theta)_{MIN}$ and $P2(\theta)$ are much more pronounced in the present case. The oscillations in the curves are found to be appreciable for values of θ up to about 20^{o}. Figs. 24 b through d show the variations of the respective pulses for three more regions of θ, $5^{o} \leq \theta \leq 10^{o}$, $10^{o} \leq \theta \leq 15^{o}$ and $15^{o} \leq \theta \leq 20^{o}$.

Figures 25 a through 25 d show the pulse ratios as functions of θ for four different ranges of θ. Here also the oscillations in the curve persist for θ values up to about 20^{o}.

Figures 26 a and 26 b show the main beam killing and sidelobe punch-through zones as functions of the nominal pulse ratio. It is anticipated that these zones exist for this antenna beyond the θ values shown in Fig. 26. If desired, they may be obtained from the corresponding pulse ratio curves for the ranges of θ shown in Figs. 26 a and b. There are seven main beam killing zones and eight sidelobe punch-through zones for $K_{0} = 18\,dB$.

Figure 27 shows the effective beamwidths as functions of θ for the range $0 \leq \theta \leq 5^{o}$. It is anticipated that the effective beamwidths would fluctuate for θ values up to about 20^{o}. For $\theta > 20^{o}$, $\alpha_{1MAX}(\theta) \sim 4.8^{o}$ and $\alpha_{1MIN}(\theta) \sim 2.5^{o}$. For the same antenna operating in the SLS mode [1] the free space value of the effective azimuth beamwidth is about 3.75^{o}, which occurs at $\theta > 20^{o}$.

Figure 28 shows the number of replies $N_{MAX}(\theta)$ and $N_{MIN}(\theta)$ as functions of θ. For $\theta > 20^{o}$, $N_{MAX}(\theta) \sim 19$ and $N_{MIN}(\theta) \sim 9$. For the same antenna the saturation value of the number of replies in the SLS mode is about 15.

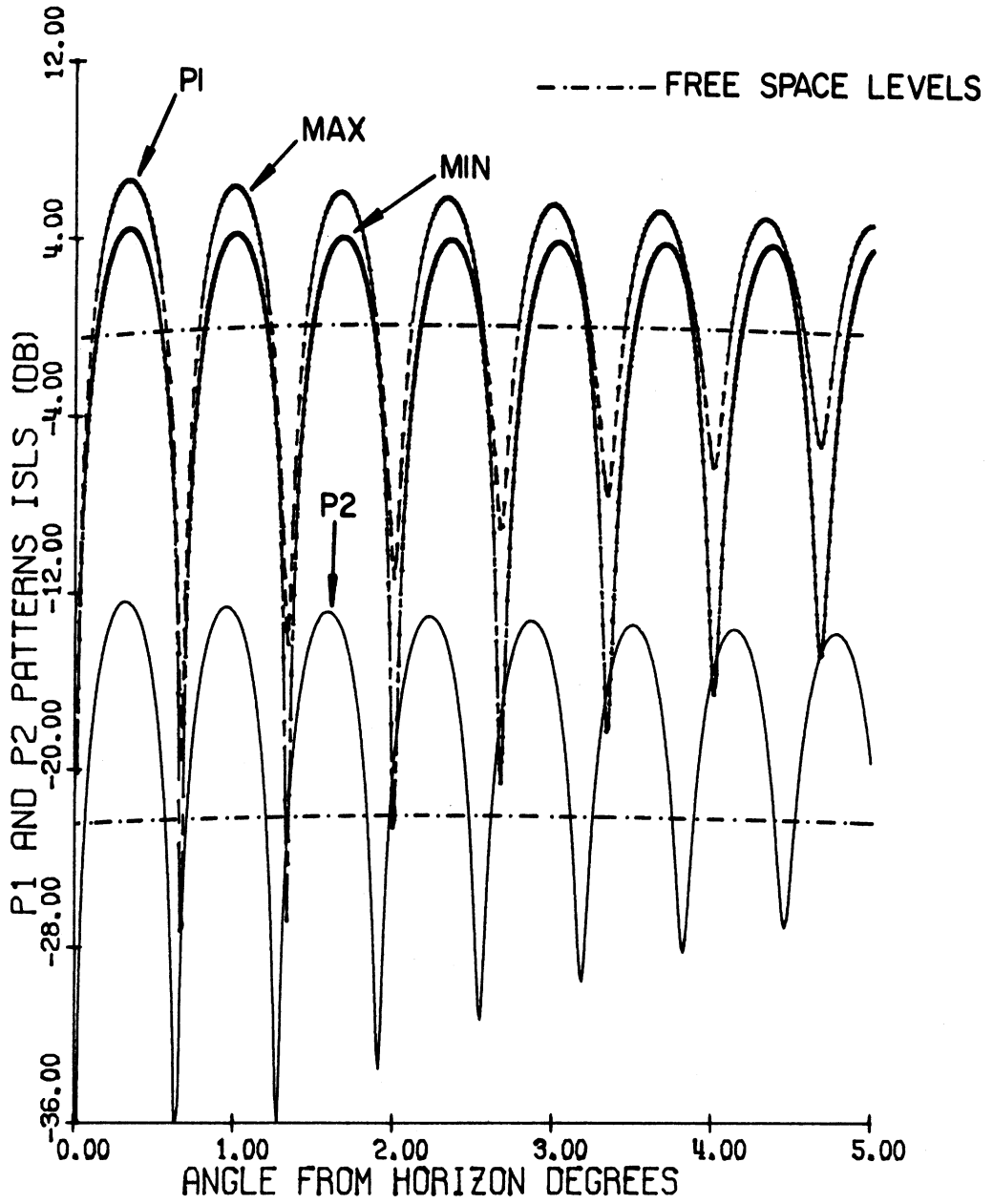

EXISTING ANTENNA TILTED ANGLE= 0.0 D
ELEV.: DIREC. 41.00' OMNI. 43.00'
P1/P2= 18.00 DB P1 DIR./OMN.= 18.00 DB.

FIG. 24 a: $P1(\theta)_{MAX}$, $P1(\theta)_{MIN}$ and $P2(\theta)$ as functions of θ.

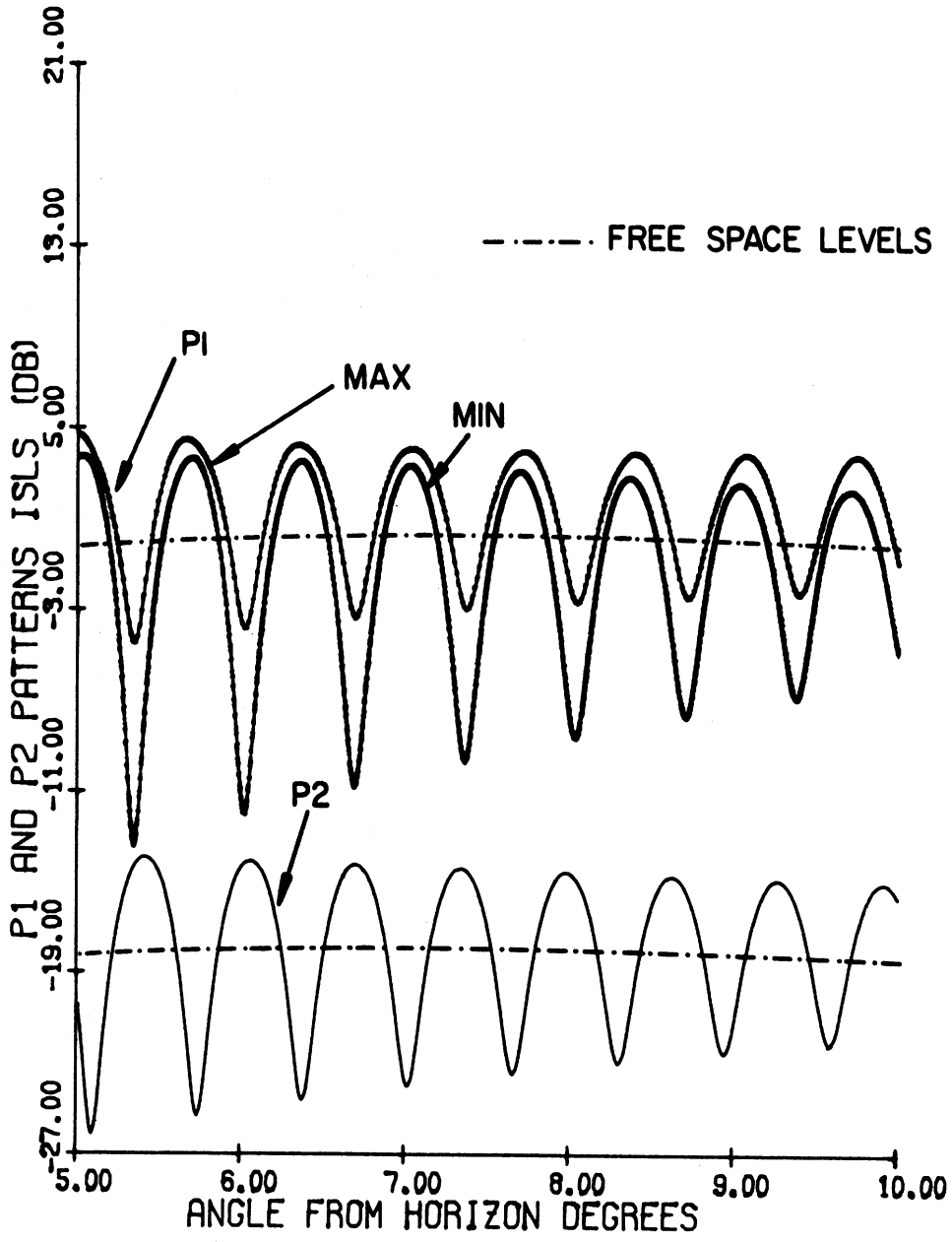

EXISTING ANTENNA TILTED ANGLE= 0.0 D
ELEV.: DIREC. 41.00' OMNI. 43.00'
P1/P2= 18.00 DB P1 DIR./OMN.= 18.00 DB.

FIG. 24 b: $P1(\theta)_{MAX}$, $P1(\theta)_{MIN}$ and $P2(\theta)$ as functions of θ.

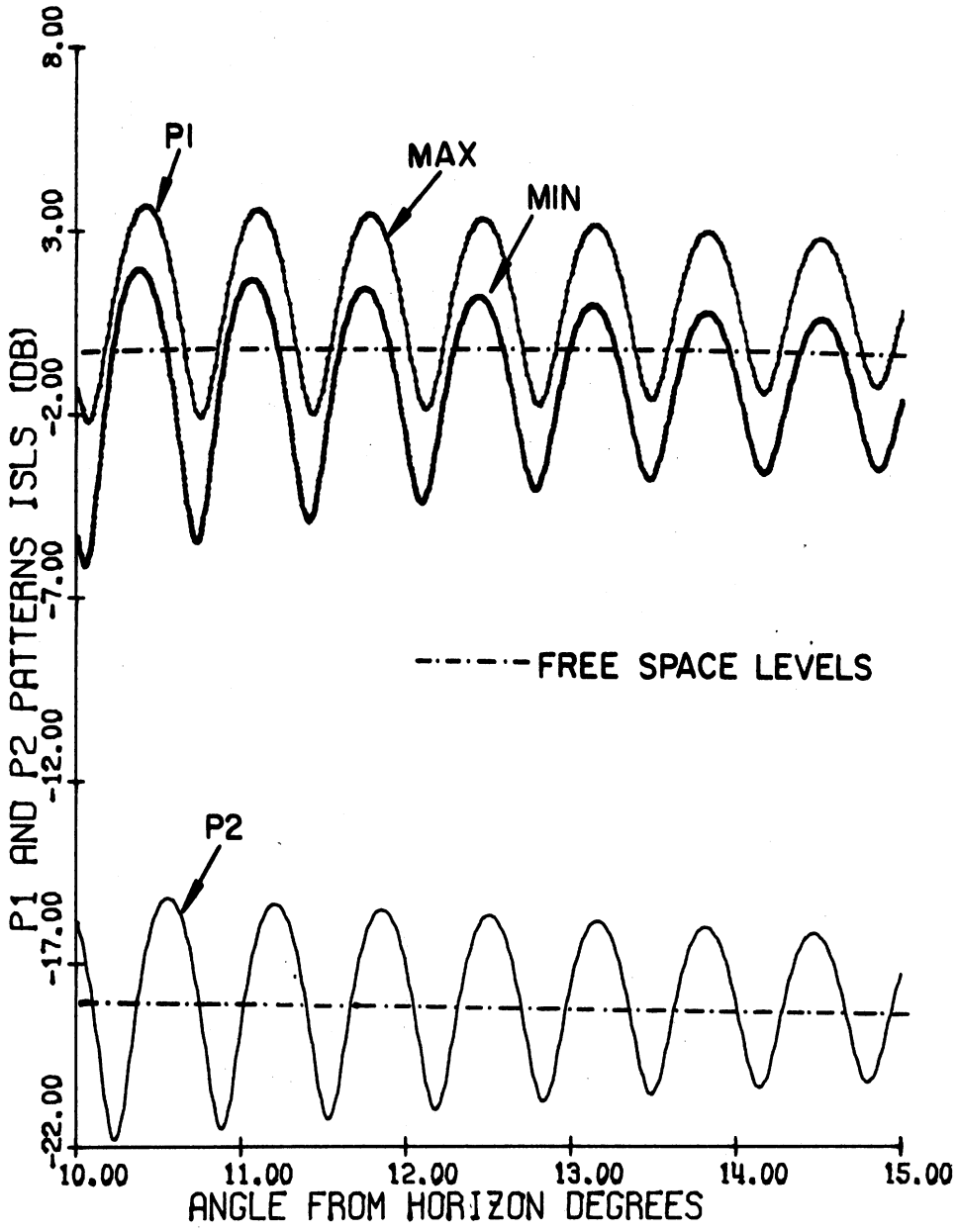

FIG. 24 c: $P1(\theta)_{MAX}$, $P1(\theta)_{MIN}$ and $P2(\theta)$ as functions of θ.

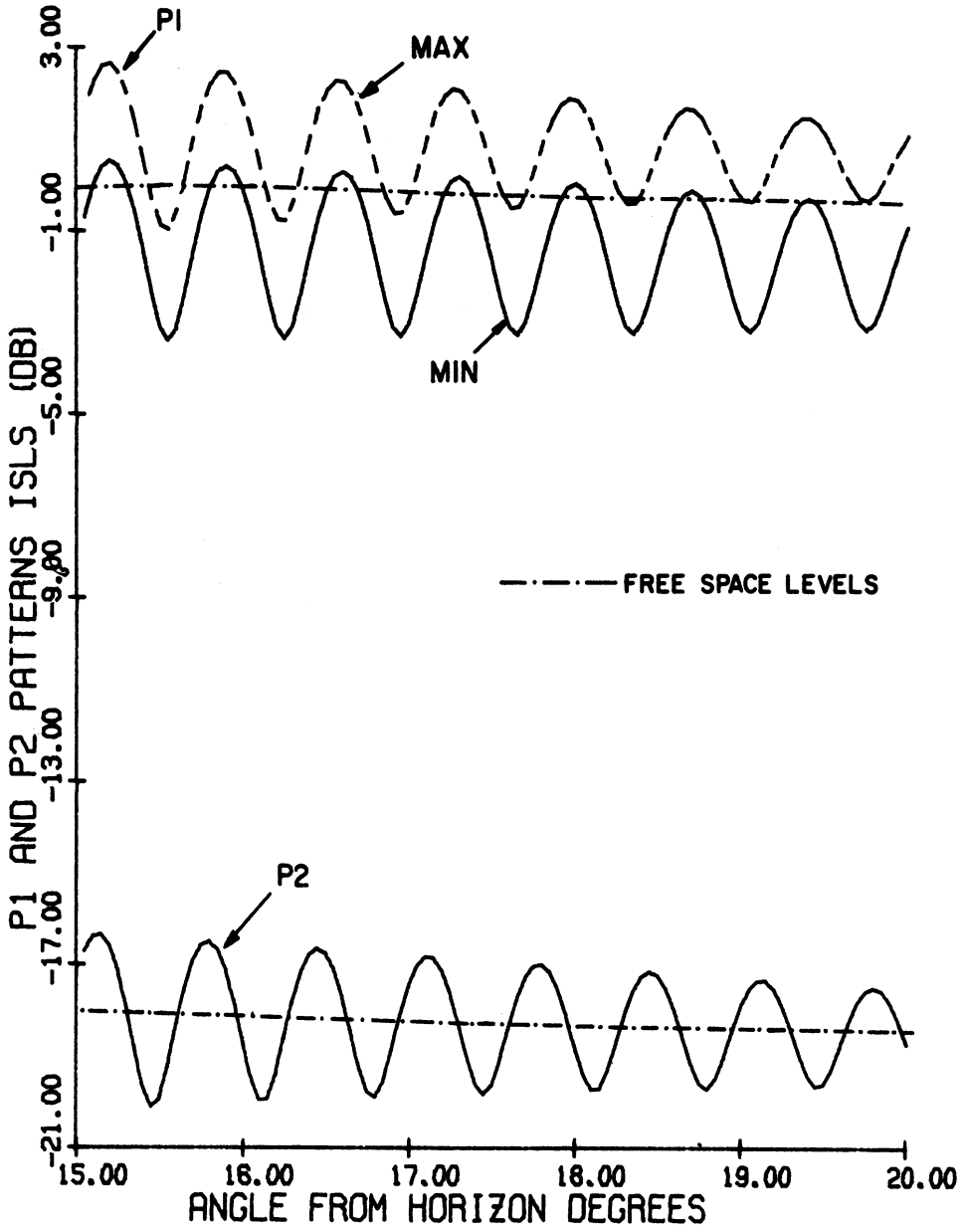

EXISTING ANTENNA FREQ.= 1030.000 MHZ
ELEV.: DIREC. 41.00' OMNI. 43.00'
P1/P2= 18.00 DB P1 DIR./OMN.= 18.00 DB.

FIG. 24 d: $P1(\theta)_{MAX}$, $P1(\theta)_{MIN}$ and $P2(\theta)$ as functions of θ.

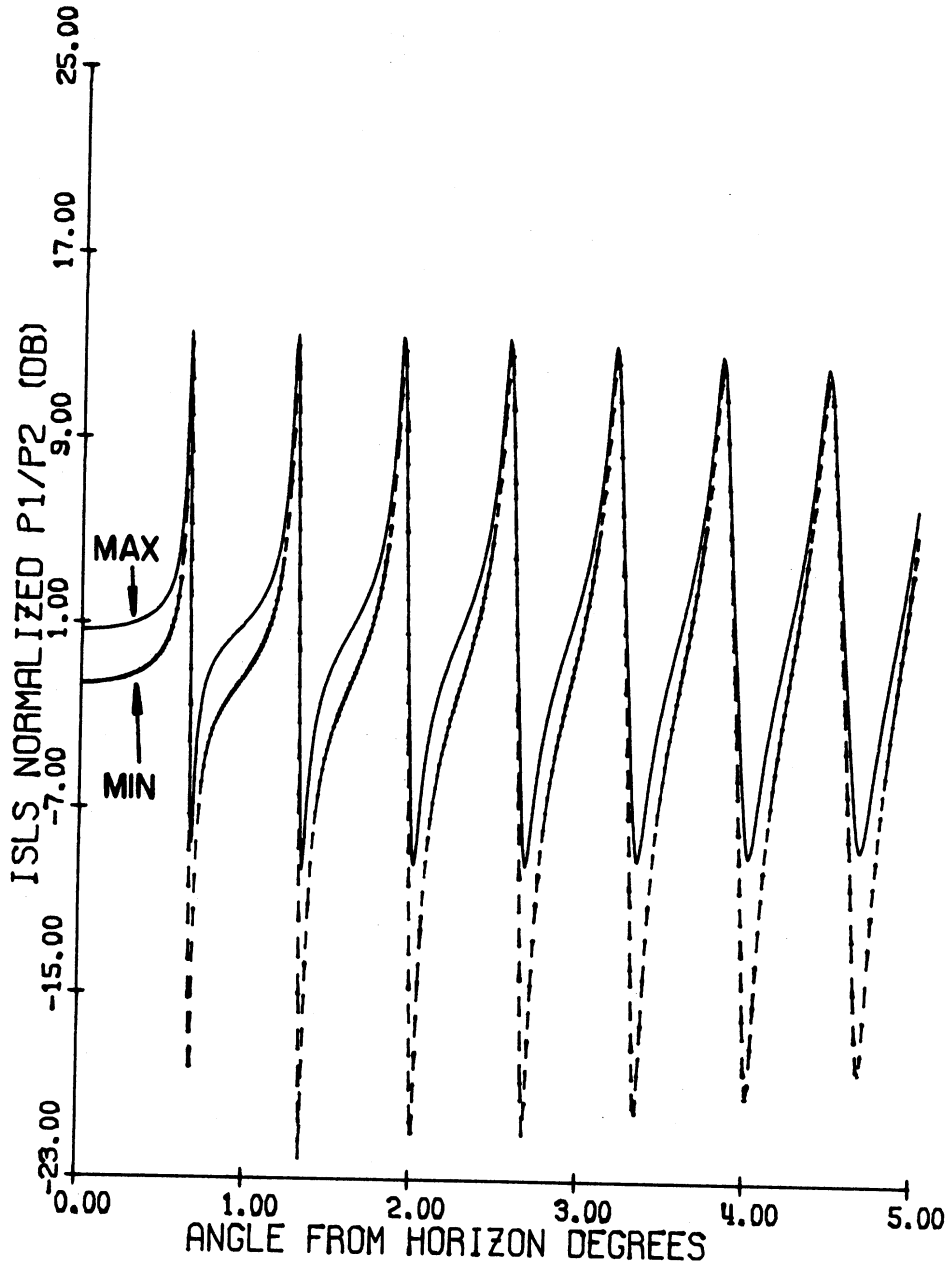

FIG. 25 a: Normalized pulse ratio envelopes as functions of θ.

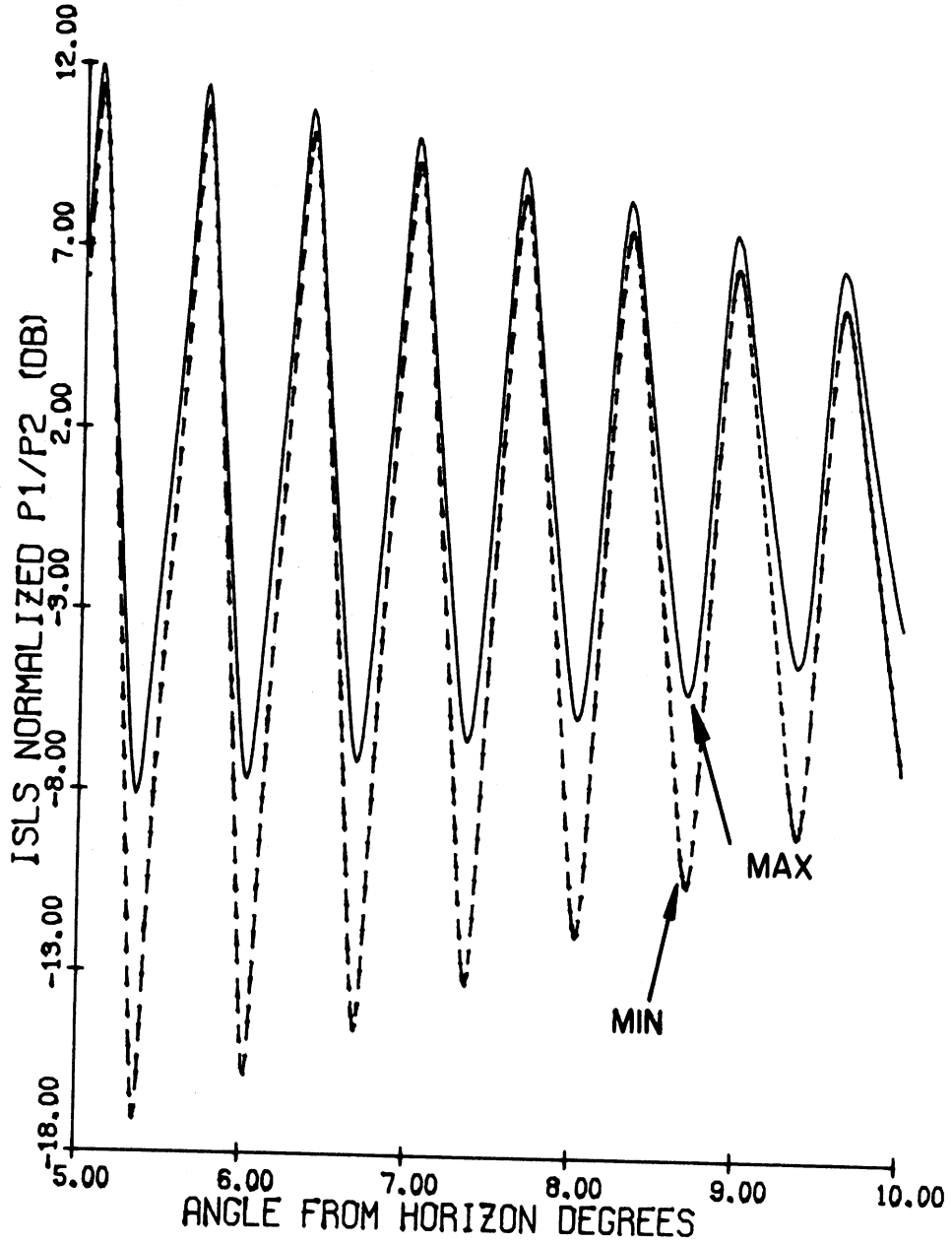

FIG. 25 b: Normalized pulse ratio envelopes as functions of θ.

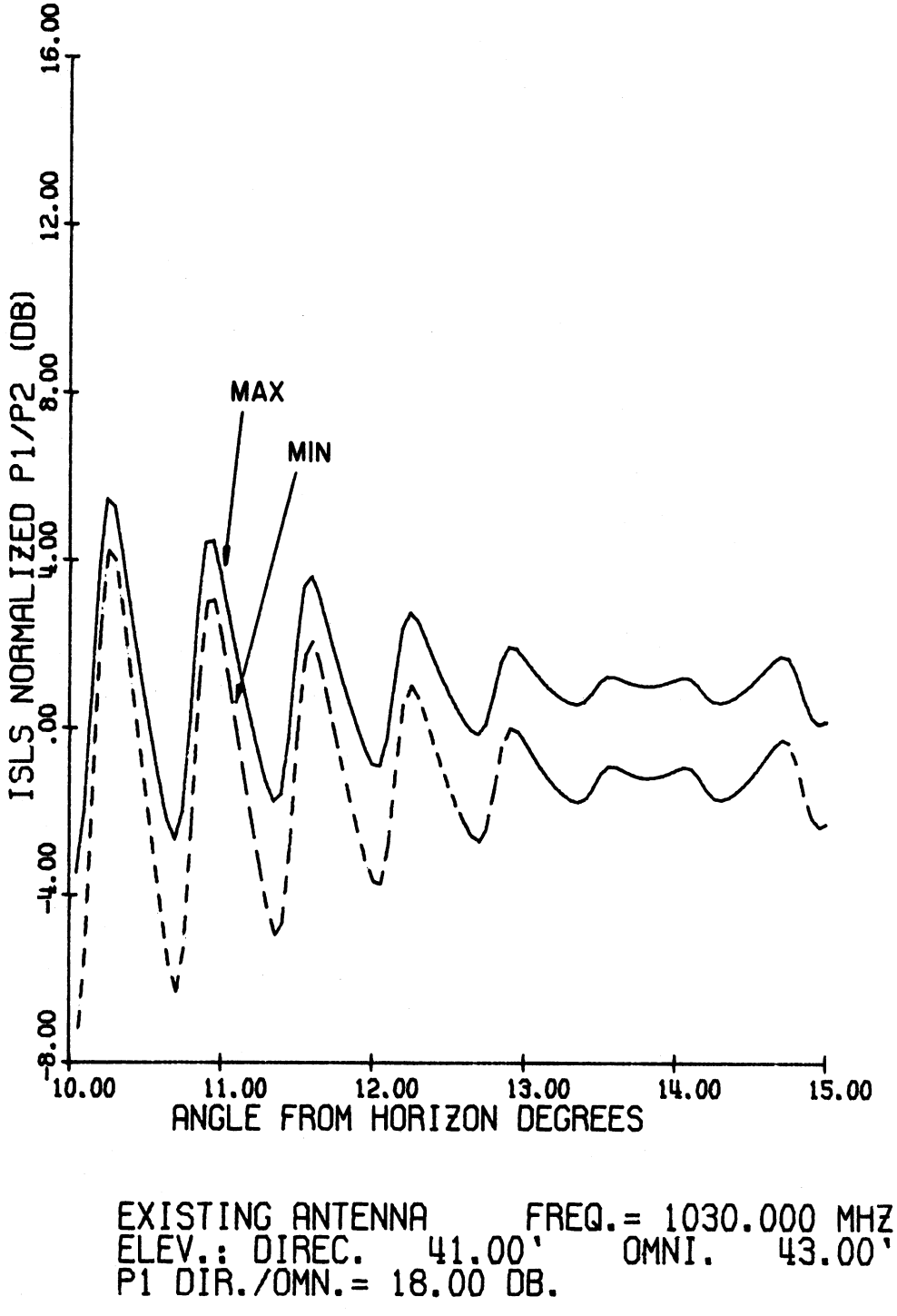

FIG. 25 c: Normalized pulse ratio envelopes as functions of θ.

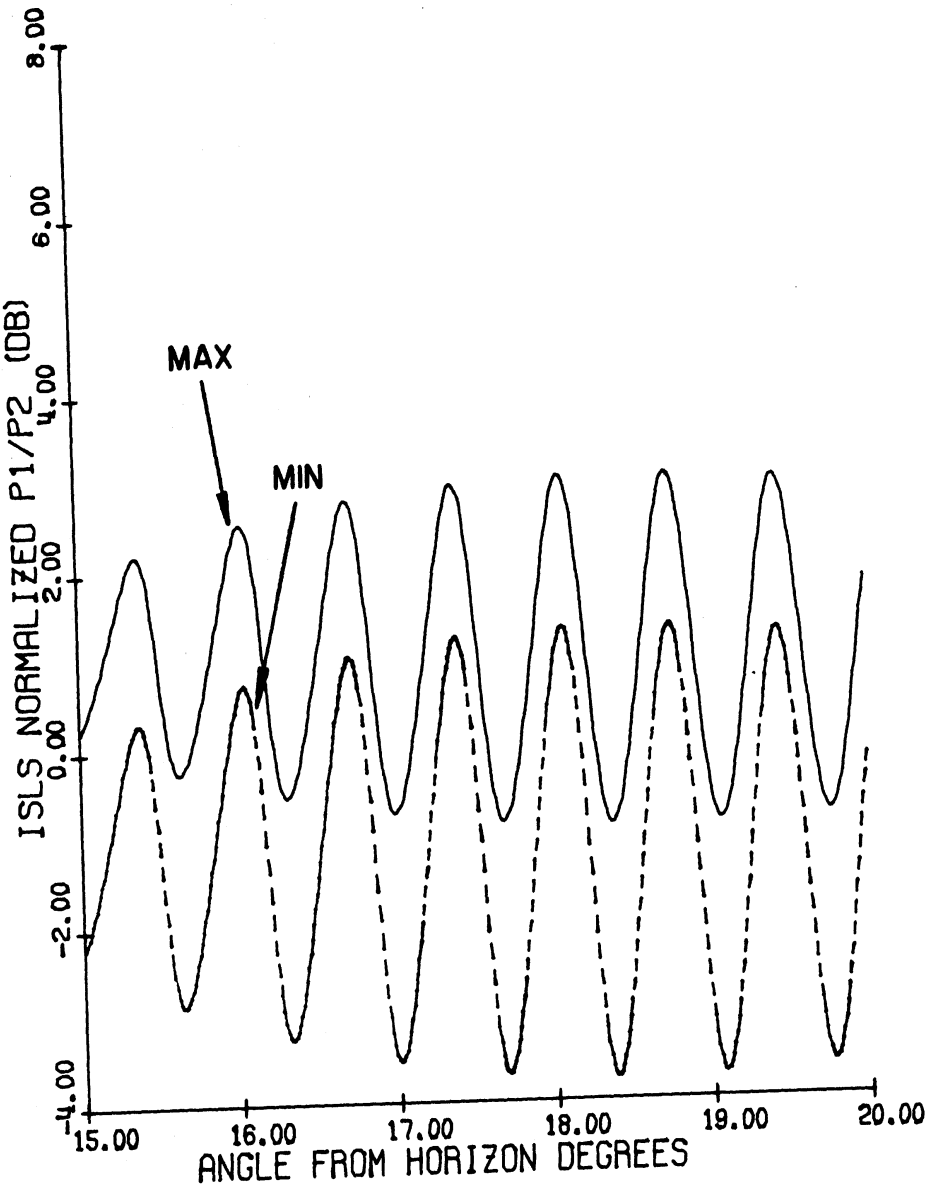

FIG. 25 d: Normalized pulse ratio envelopes as functions of θ.

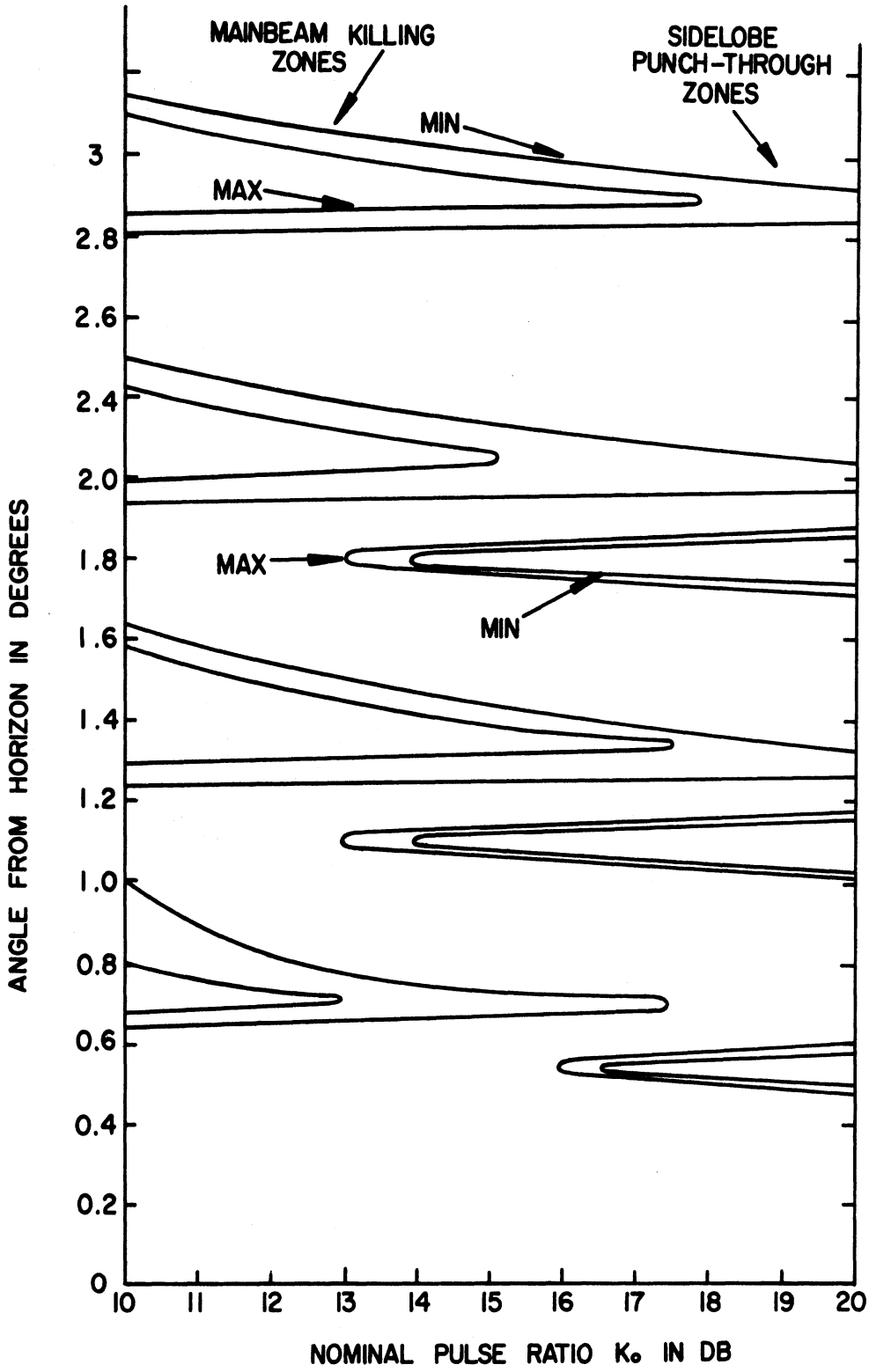

FIG. 26 a: Mainbeam killing and sidelobe punch-through zones as functions of the nominal pulse ratio for the existing hog-trough antenna. H_d = 41', H_0 = 43', f = 1030 MHz, P1 DIR/OMNI = 18 dB, a = 9 dB, b = 0 dB, L = -25 dB.

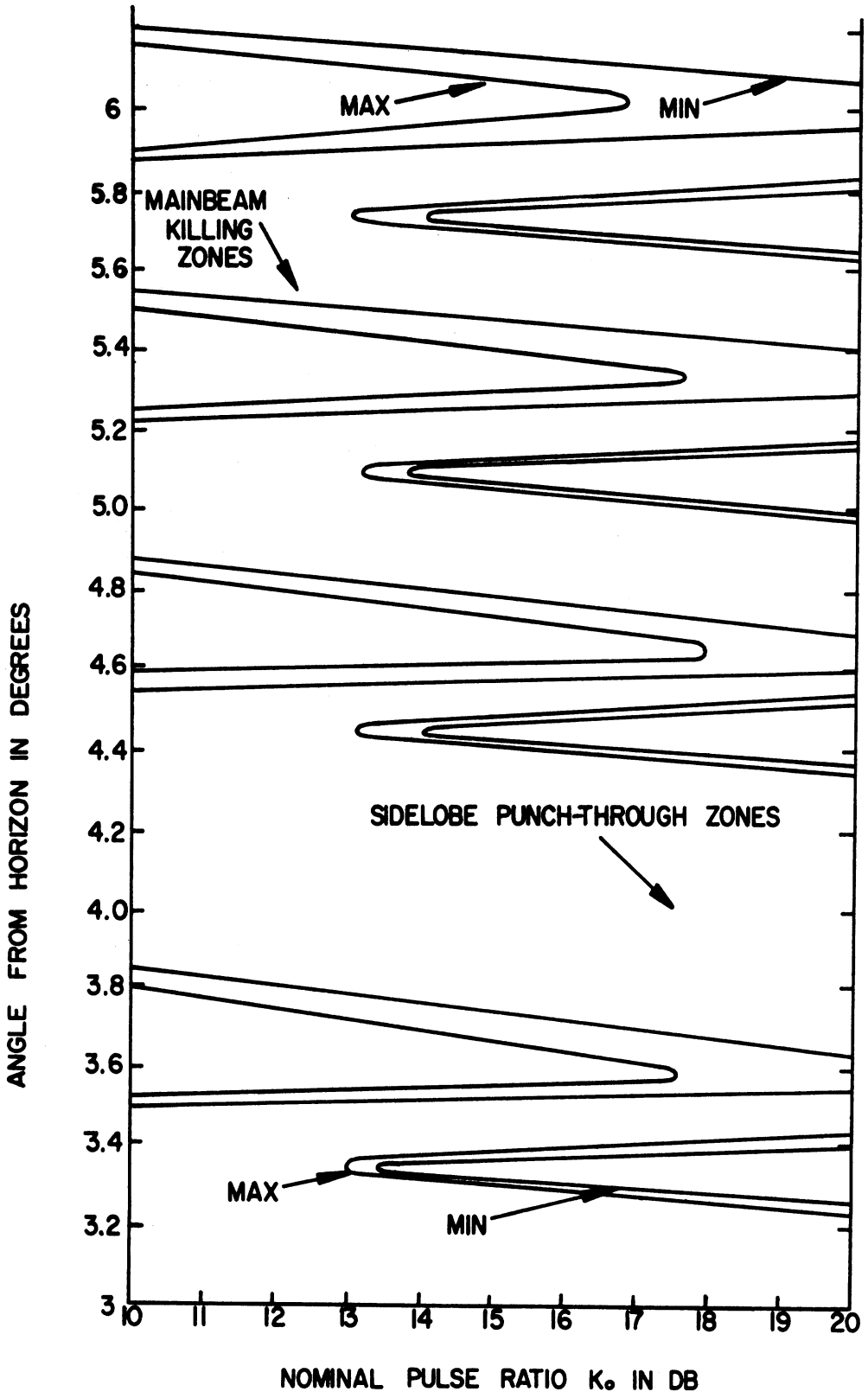

FIG. 26 b: Mainbeam killing and sidelobe punch-through zones as functions of the nominal pulse ratio for the existing hog-trough antenna. H_d = 41', H_0 = 43', f = 1030 MHz, P1 DIR/OMNI = 18dB, a = 9dB, b = 0dB, L = -25dB.

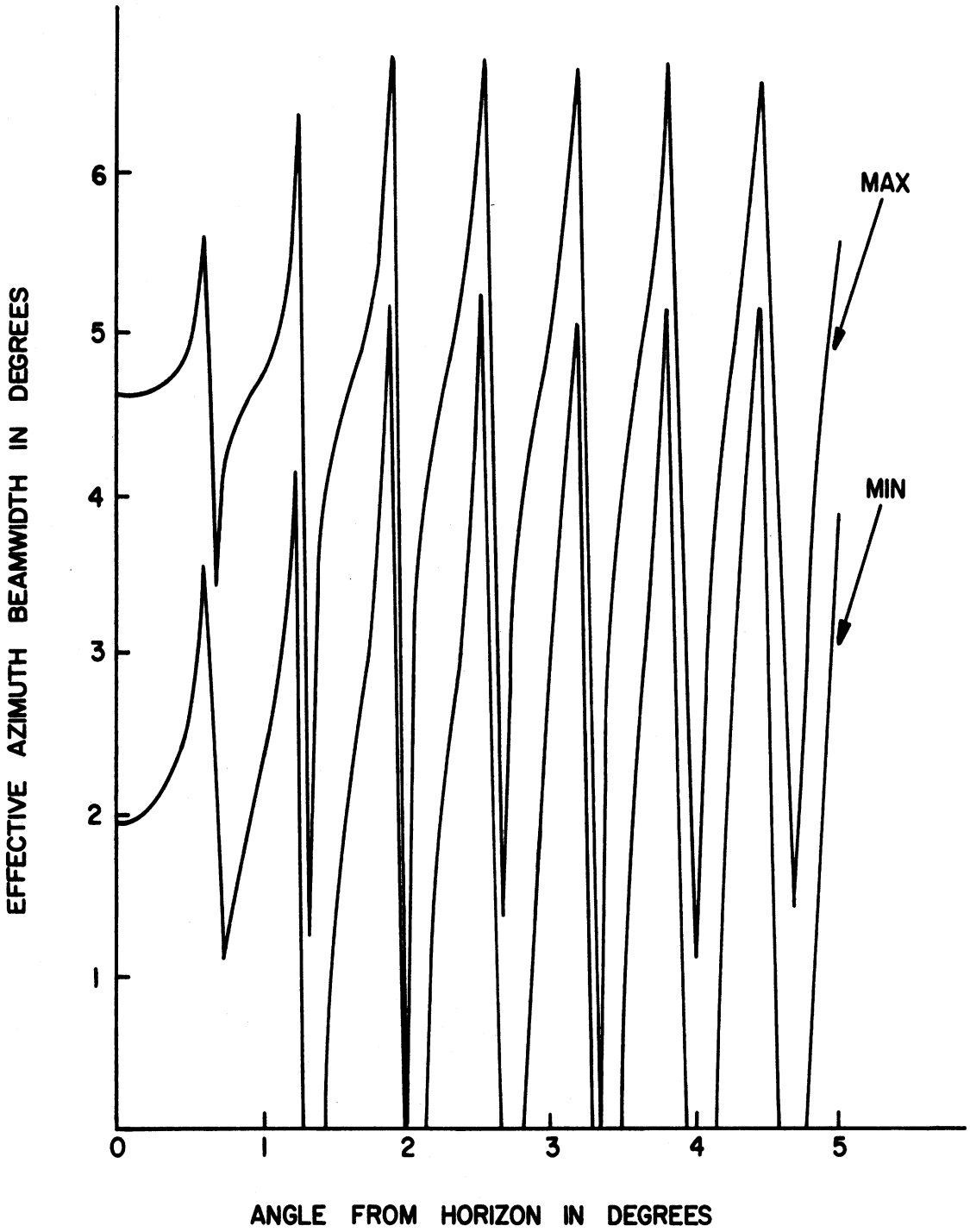

FIG. 27: Effective azimuth beamwidths as functions of the angle from the horizon for the existing hog-trough antenna. H_d = 41', H_0 = 43', f = 1030 MHz, nominal pulse ratio K_0 = 18dB, P1 DIR/OMNI = 18dB.

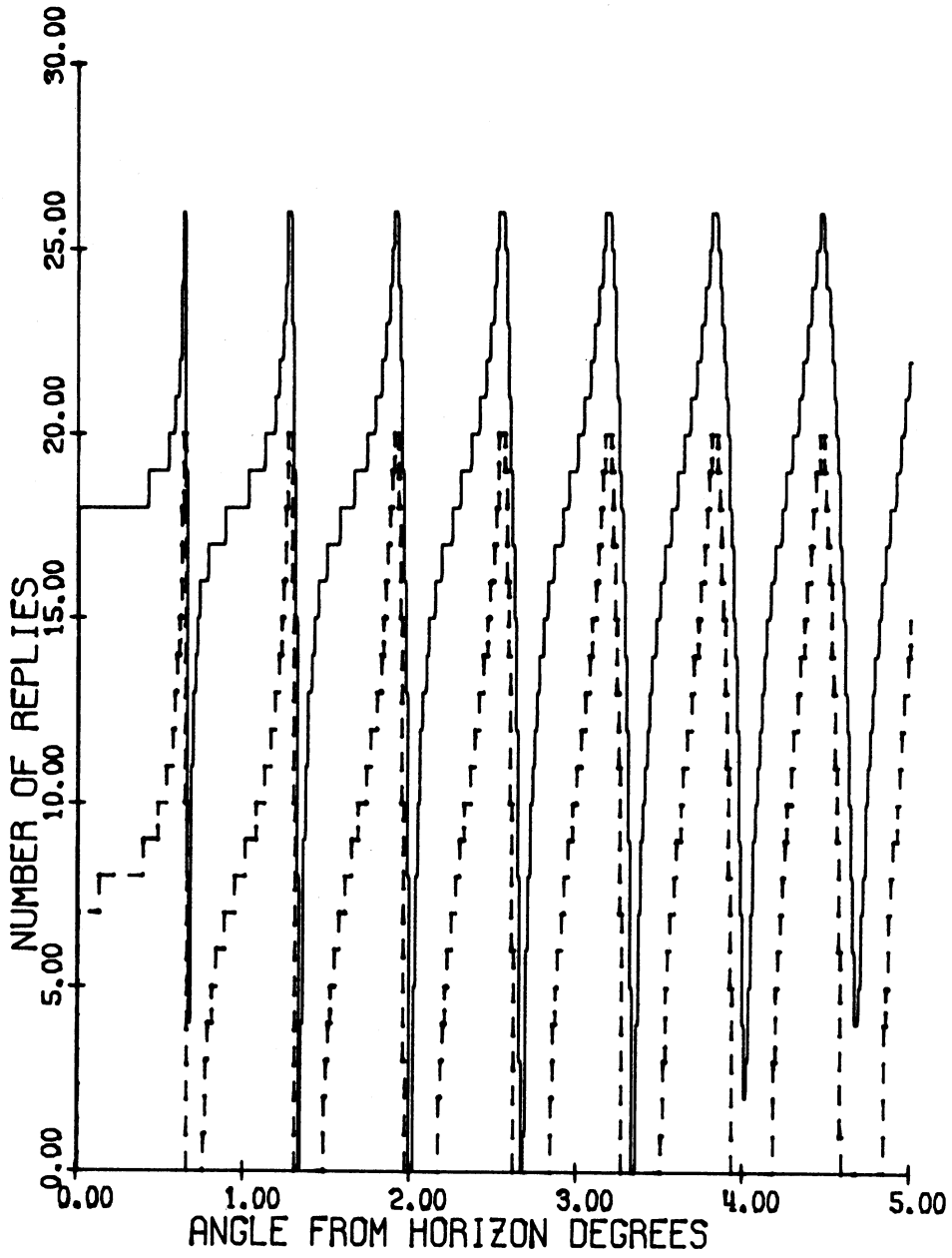

FIG. 28: Number of replies as functions of angle from the horizon.

Figures 29 a and 29 b show the coverage diagram for the antenna normalized to the free space maximum range of 40 nautical miles. As shown in Fig. 29(a) for the maximum envelope case, the maximum range of 81 nautical miles occurs at $\theta \sim 0.4^{o}$ and the minimum range of 5 nautical miles occurs at $\theta \sim 0.8^{o}$. The corresponding ranges for the minimum envelope case are 62 and 2 nautical miles respectively.

4.2.5. Hazeltine E-Scan Antenna.

This is a special beacon antenna with coincident phase centers of the directional and omnidirectional antennas. The heights of the two phase centers are $H_d = H_0 = 16'$. The vertical aperture of each antenna is 8' and it is assumed that their elevation plane patterns are identical.

Figure 30 shows the $P1(\theta)_{MAX}$, $P1(\theta)_{MIN}$ and $P2(\theta)$ pulses as functions of θ where the 0 dB level is adjusted to coincide with the maximum $P1(\theta)_{SLS}$ level in the free space case. As can be seen from Fig. 30, the lobing structures of the curves are identical for the present antenna. As a result, the pulse ratio curves are constants with respect to θ and the normalized values are approximately +1.19dB and -1.19dB respectively, as shown in Fig. 31.

There is no main beam killing or sidelobe punch-through region for this antenna.

The effective azimuth beamwidths $\alpha_{1MAX}(\theta)$ and $\alpha_{1MIN}(\theta)$ are constants with respect to θ. These are $\alpha_{1MAX}(\theta) \sim 4.75^{o}$ and $\alpha_{1MIN}(\theta) \sim 2^{o}$.

The number of replies $N_{MAX}(\theta)$, $N_{MIN}(\theta)$ as functions of θ are shown in Fig. 32. They are constants with $N_{MAX}(\theta) = 19$ and $N_{MIN}(\theta) = 8$. For the same antenna the number of replies is 16 in the SLS mode [1].

The coverage diagram for the antenna is shown in Fig. 33. As shown in the figure, for the maximum envelope case, the maximum range of about 4.5 nautical miles occurs at $\theta \sim 0.9^{o}$ and the minimum range of about 1.4 nautical miles occurs at $\theta \sim 1.7^{o}$. The corresponding ranges for the minimum envelope case are 36 nautical miles and about 1.2 nautical miles respectively.

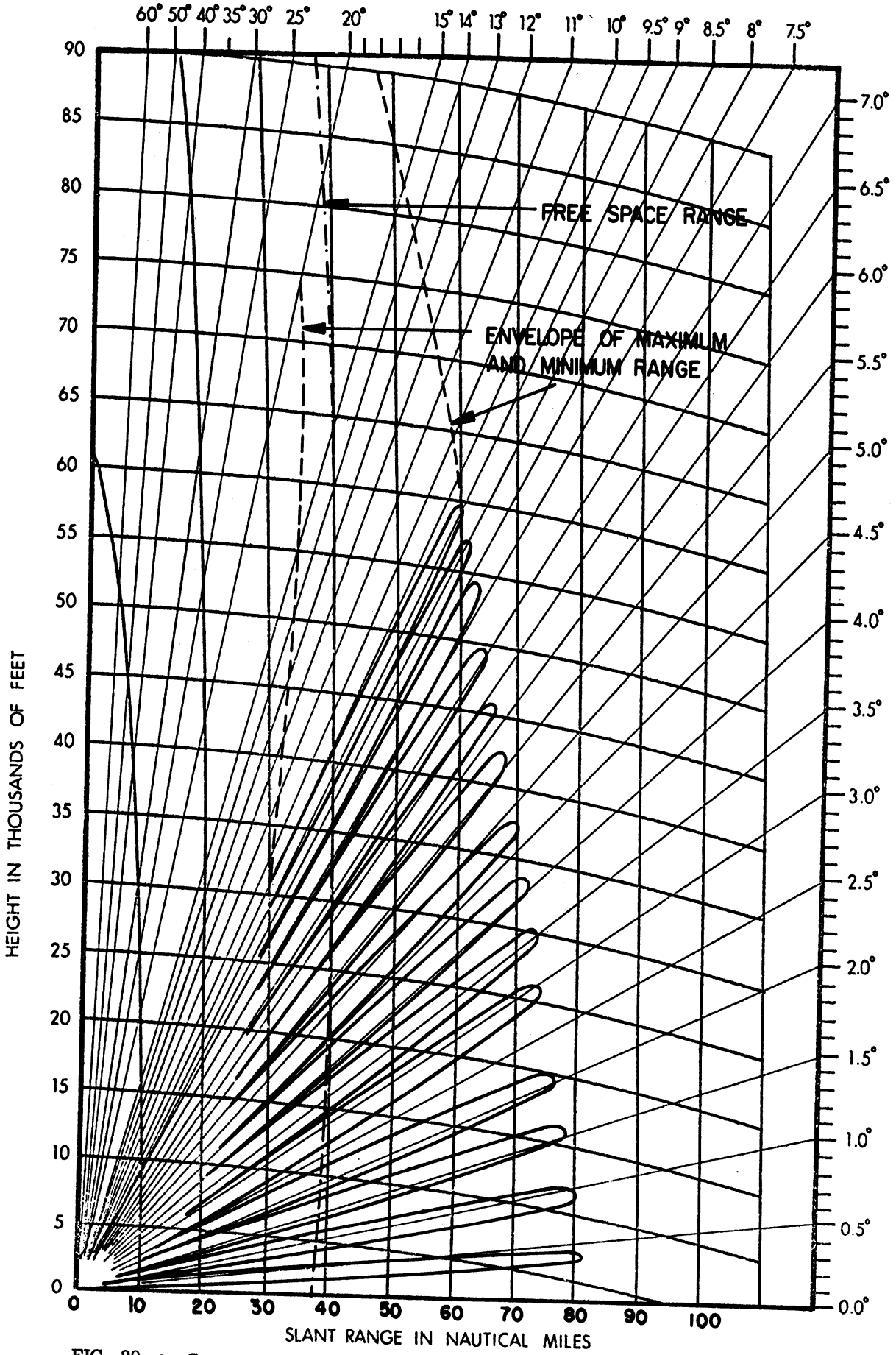

FIG. 29 a: Coverage diagram at the maximum envelope for the existing hog-trough antenna. H_d = 41', H_0 = 43', f = 1030 MHz.

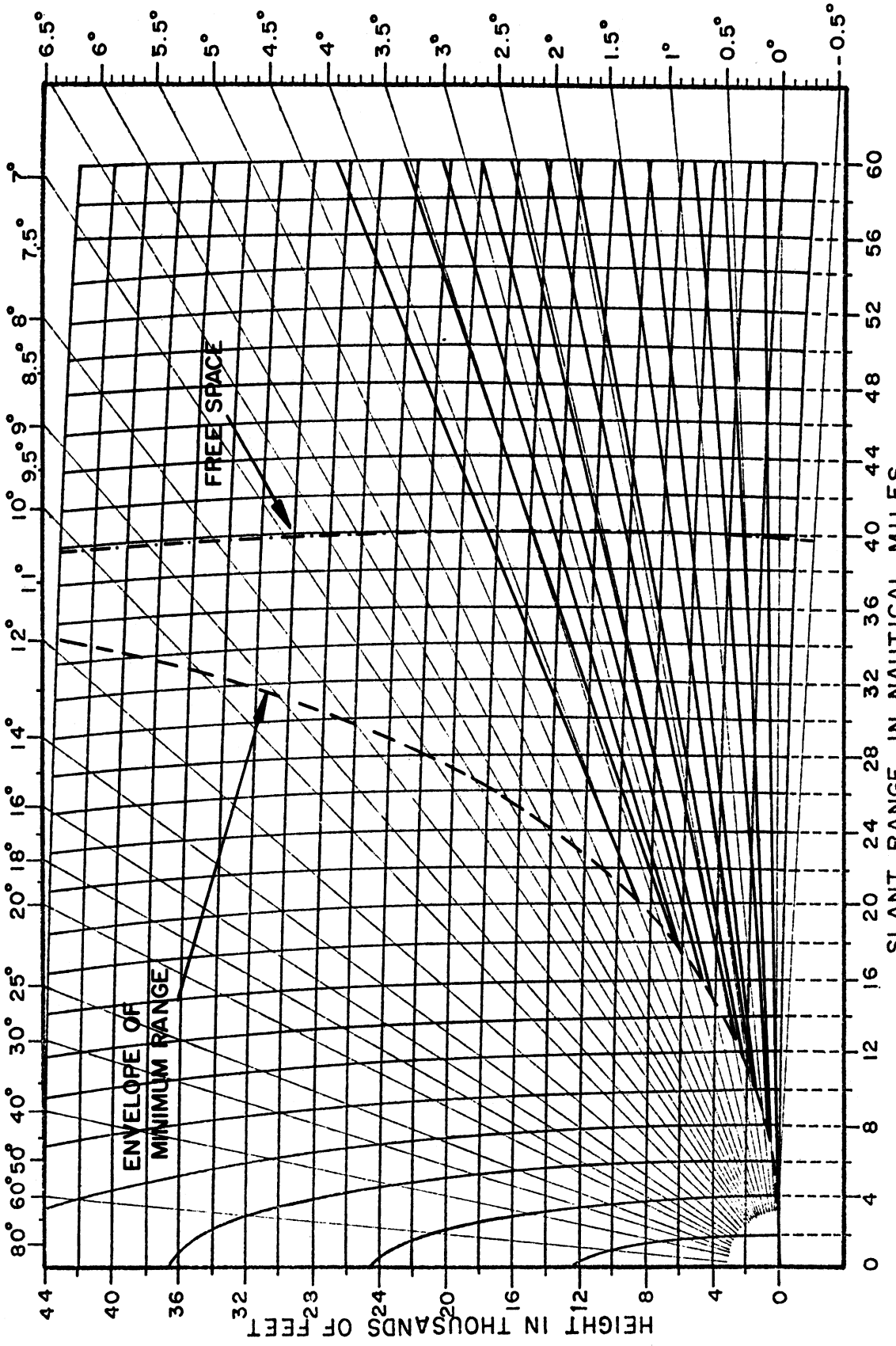

FIG. 29 b: Coverage diagram on expanded scale at the maximum envelope for the existing horn-trough antenna. $H_d = 41'$, $H_0 = 43'$, f = 1030 MHz.

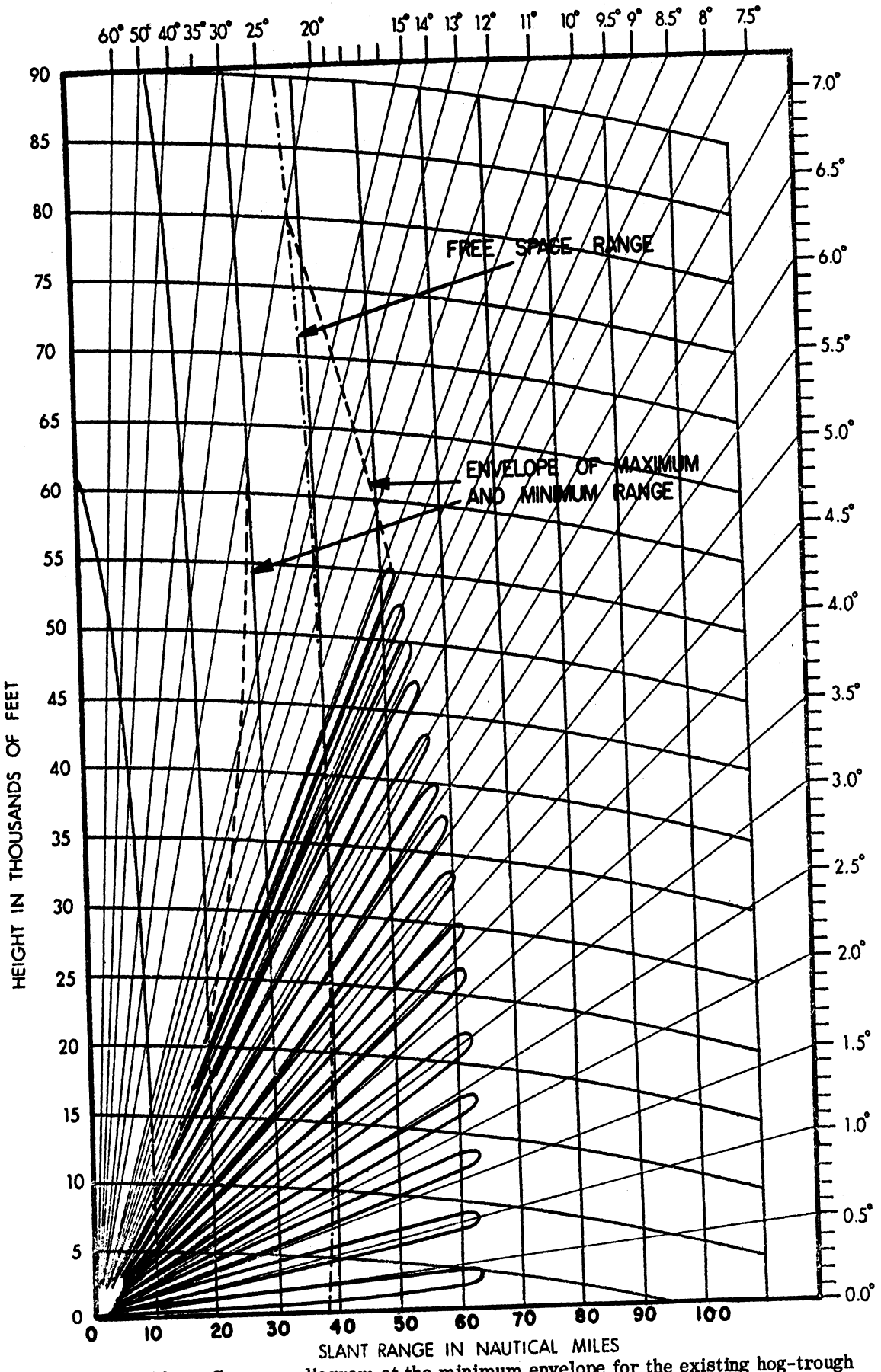

FIG. 29 c: Coverage diagram at the minimum envelope for the existing hog-trough antenna. H_d = 41', H_0 = 43', f = 1030 MHz.

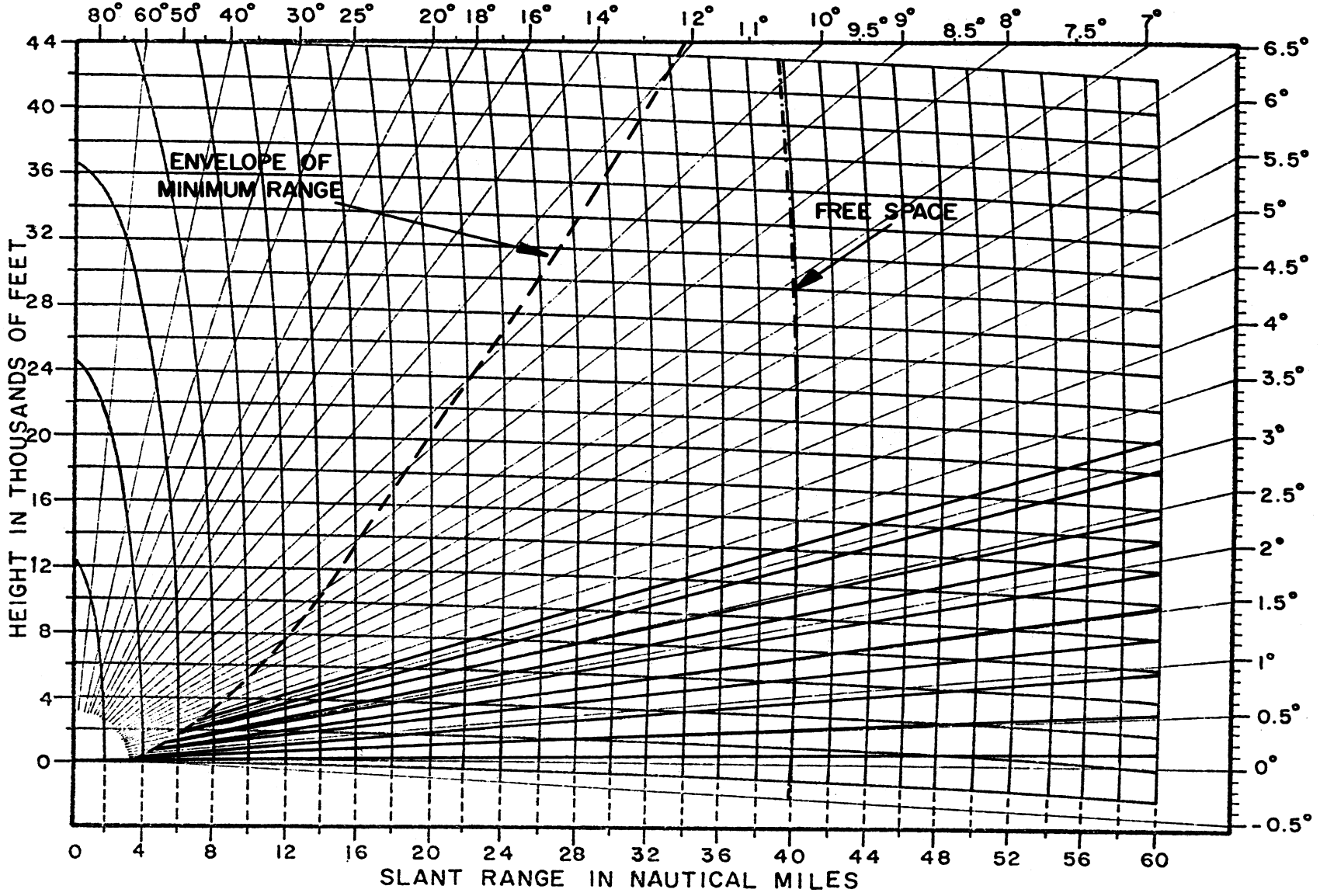

FIG. 29 d: Coverage diagram on expanded scale at the minimum envelope for the existing hog-trough antenna. H_d = 41', H_0 = 43', f = 1030 MHz.

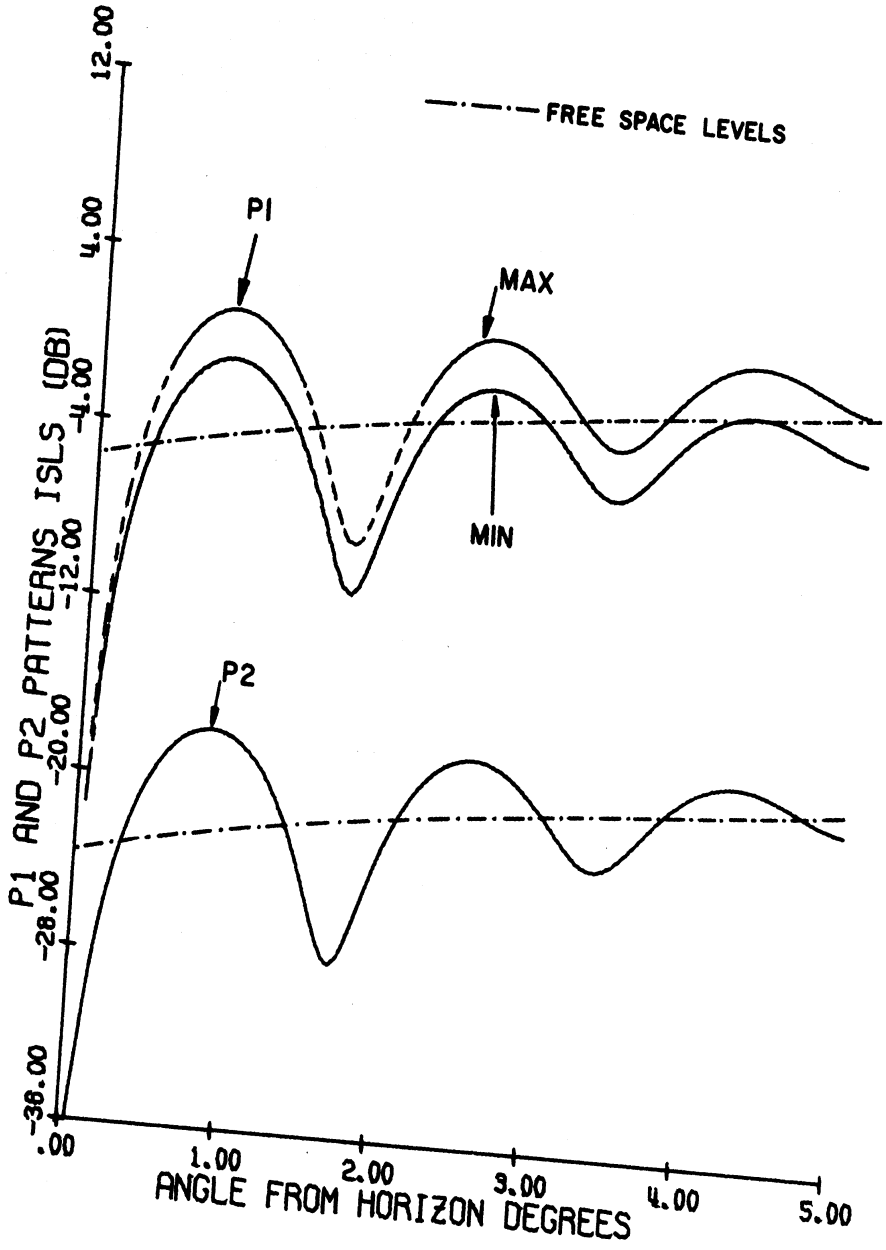

FIG. 30: $P1(\theta)_{MAX}$, $P1(\theta)_{MIN}$ and $P2(\theta)$ as functions of θ.

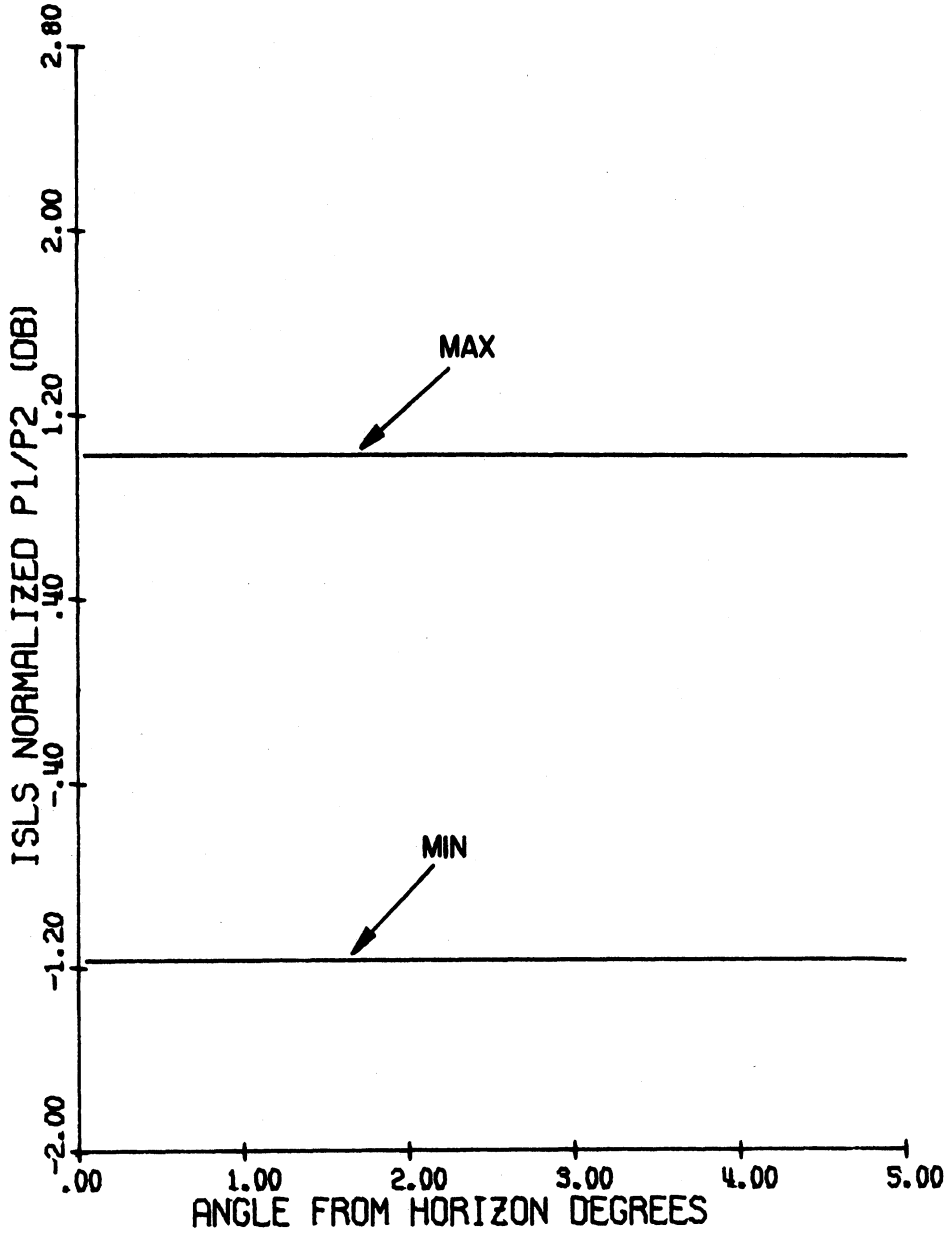

FIG. 31: Normalized pulse ratio envelopes as functions of θ.

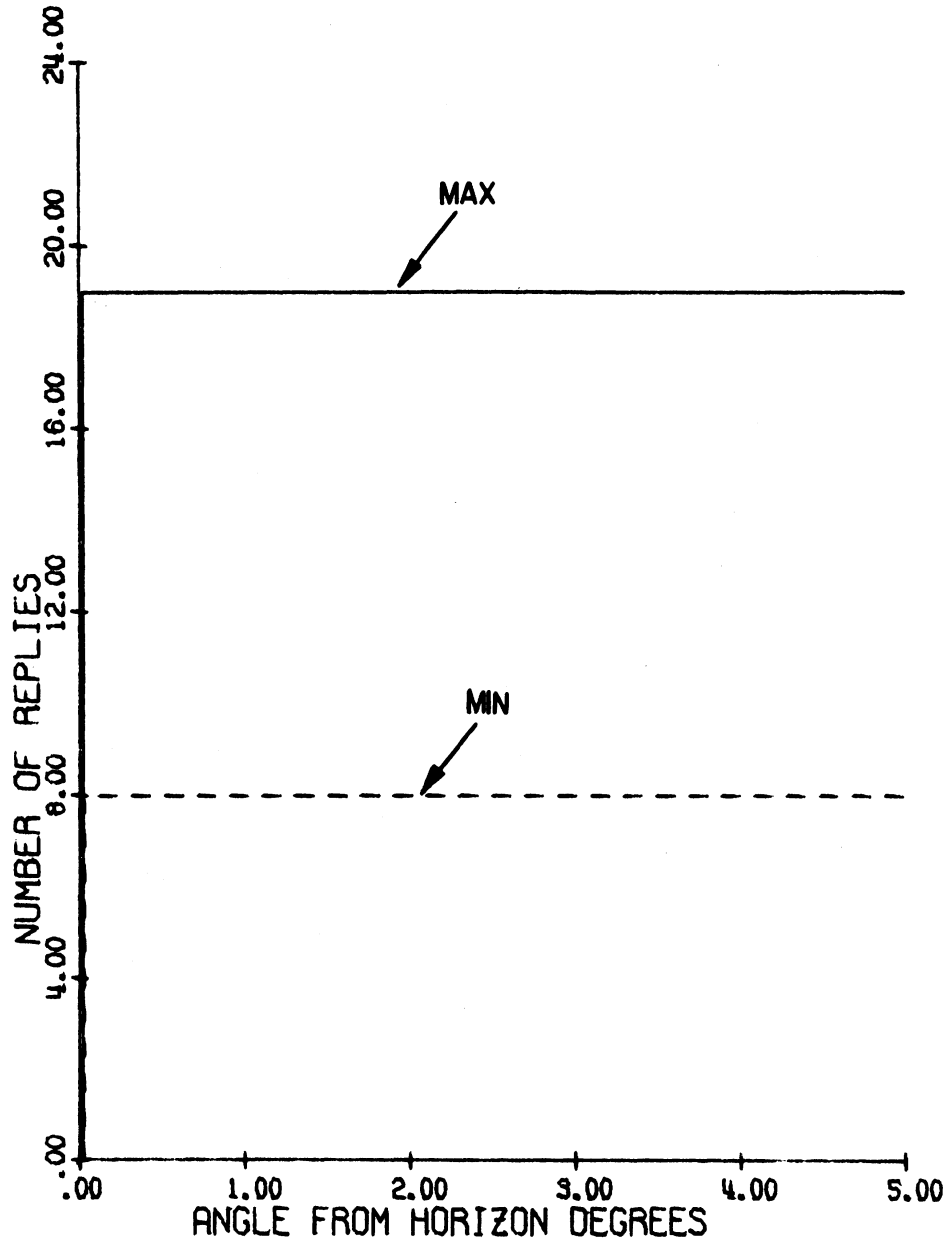

HAZELTINE ESCAN ANT. FREQ.= 1030.000 MHZ
ELEV.: DIREC. 16.00' OMNI. 16.00'
P1/P2= 18.00 DB P1 DIR./OMN.= 18.00 DB.

FIG. 32: Number of replies as functions of angle from the horizon.

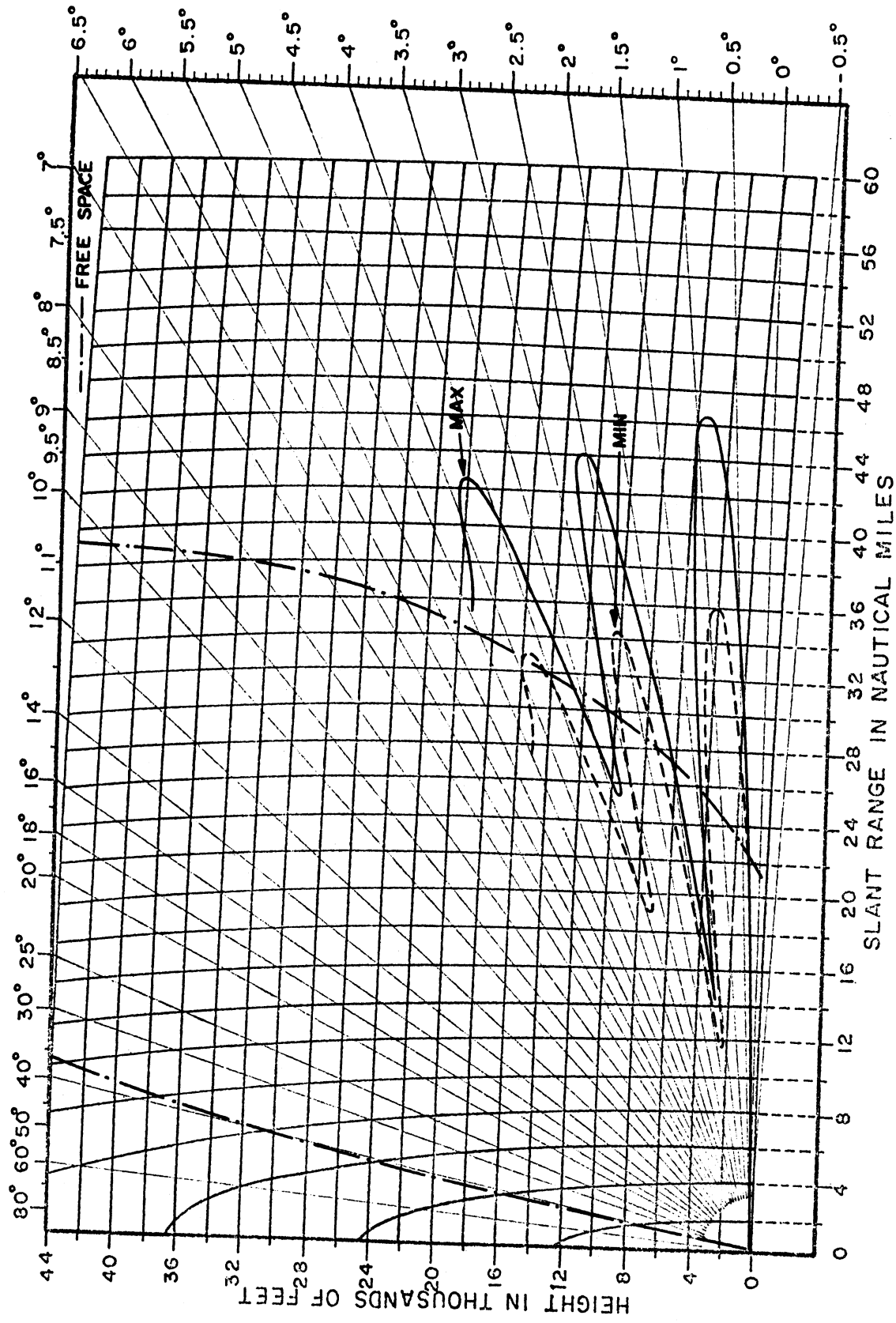

FIG. 33: Coverage diagram for the Hazeltine E-scan antenna. $H_d = 26'$, $H_0 = 26'$, $f = 1030$ MHz.

4.3 Numerical Results for Enroute Installations

In this section numerical results are given for the performance of enroute ATCRBS using different antenna systems. In general, all the enroute antenna systems are mounted on a 75' tower. The scanning rate of the enroute antenna is 6 rpm, i.e., $\Omega = 36^{o}/\text{sec}$.

4.3.1. Westinghouse Array Antenna.

The heights above ground of the phase centers of the directional and omnidirectional antennas are, respectively, $H_d = 82'$ and $H_0 = 90'$. The vertical aperture of each antenna is 8'. The free space elevation plane patterns of the directional and omnidirectional antennas are assumed to be identical.

Figure 34 shows $P1(\theta)_{MAX}$, $P1(\theta)_{MIN}$ and $P2(\theta)$ pulses as functions of θ where the zero dB level has been adjusted to coincide with the maximum of the $P1(\theta)_{SLS}$ level in the free space case. The corresponding free space curves (for $q = 0$) are also shown in Fig. 34 for comparison. As compared with the terminal installation with the same antenna (Fig. 6), in the enroute case the number of lobings within the same range of θ is much greater. This is because of the greater height of the antenna used in the enroute installation. However, the oscillations in the patterns become negligible for $\theta > 4.5^{o}$ as in the terminal case.

Figure 35 shows the envelopes of the normalized pulse ratio $K_{MAX}(\theta)_{ISLS}$ and $K_{MIN}(\theta)_{ISLS}$ as functions of θ. The oscillations in the curves become negligible for $\theta > 3^{o}$.

Figure 36 shows the main beam killing and sidelobe punch-through zones as functions of nominal pulse ratio. For $K_0 = 18\text{dB}$ ($a = 9\text{dB}$, $b = 0\text{dB}$) there are five main beam killing zones and four sidelobe punch-through zones within the range of θ shown in Fig. 36. Comparing Figs. 36 and 8, it is found that the number of both zones is increased by increasing the antenna height in the enroute case.

Figure 37 shows the effective azimuth beamwidths $\alpha_{1MAX}(\theta)$, $\alpha_{1MIN}(\theta)$ as functions of θ for the threshold level $a = 9\text{dB}$ and nominal pulse ratio $K_0 = 18\text{dB}$. For $\theta > 5^{o}$, $\alpha_{1MAX}(\theta) \sim 4.7^{o}$ and $\alpha_{1MIN}(\theta) \sim 2.2^{o}$. The corresponding value of the azimuth beamwidth in the SLS case is about 3.9^{o}.

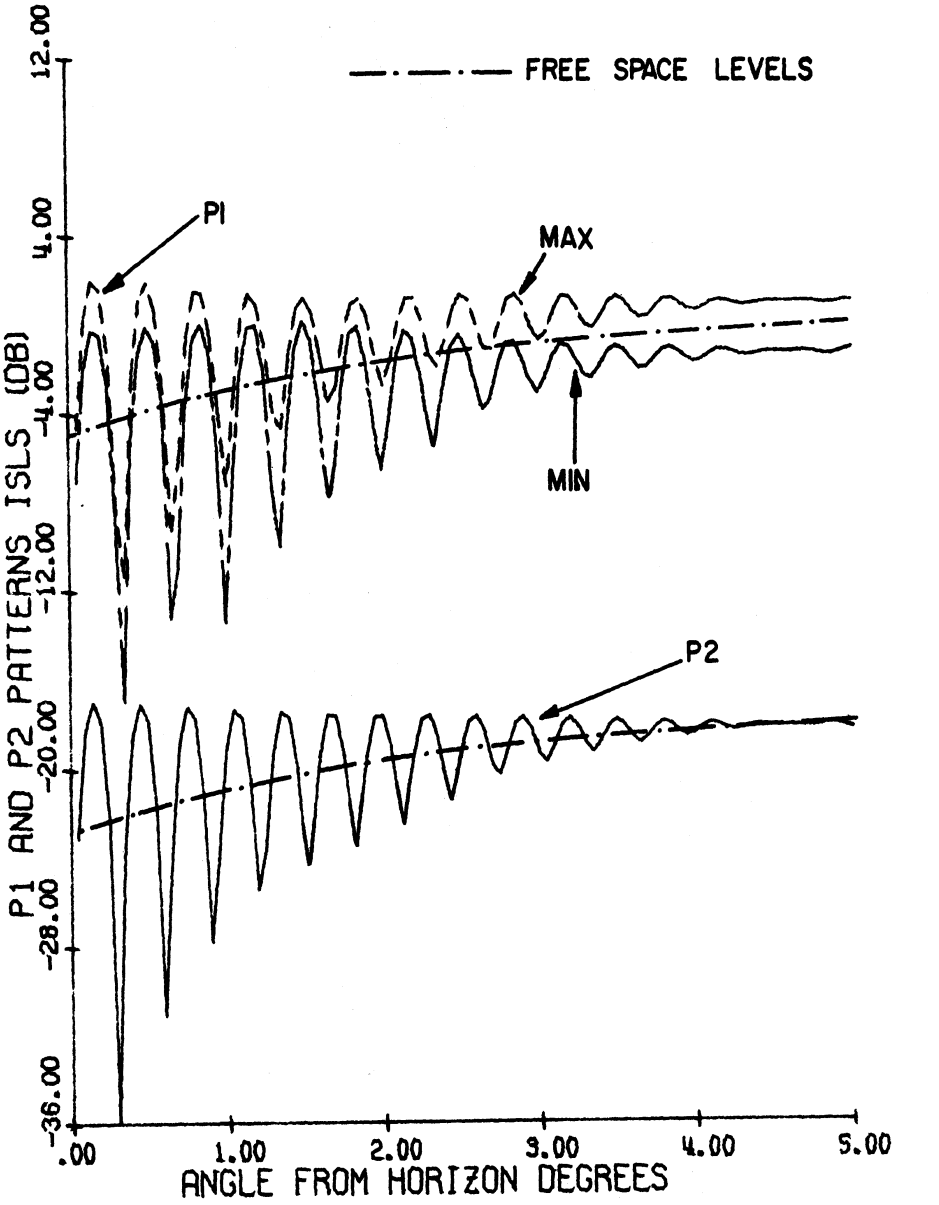

FIG. 34: $P1(\theta)_{MAX}$, $P1(\theta)_{MIN}$ and $P2(\theta)$ as functions of θ.

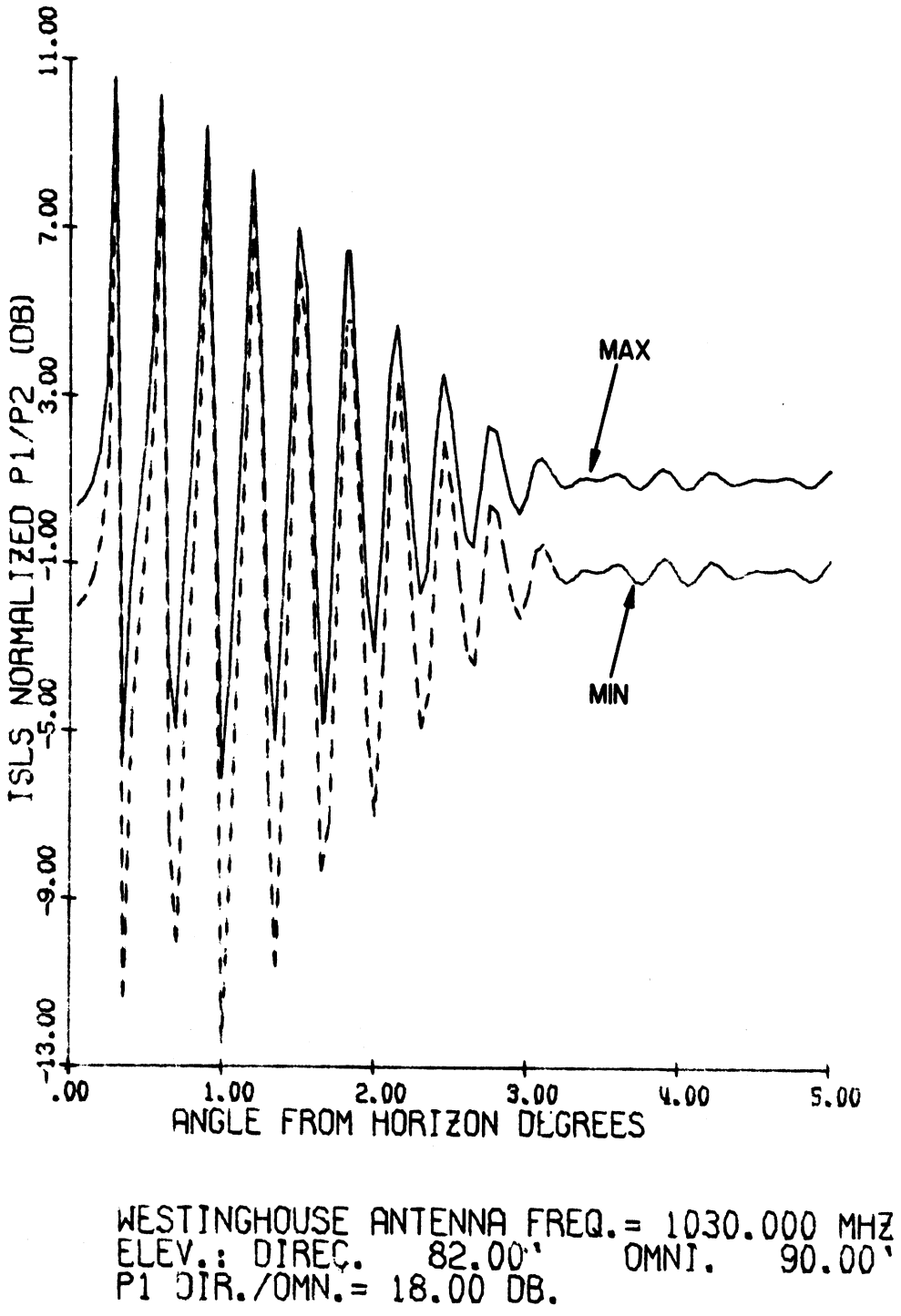

FIG. 35: Normalized pulse ratio envelopes as functions of θ.

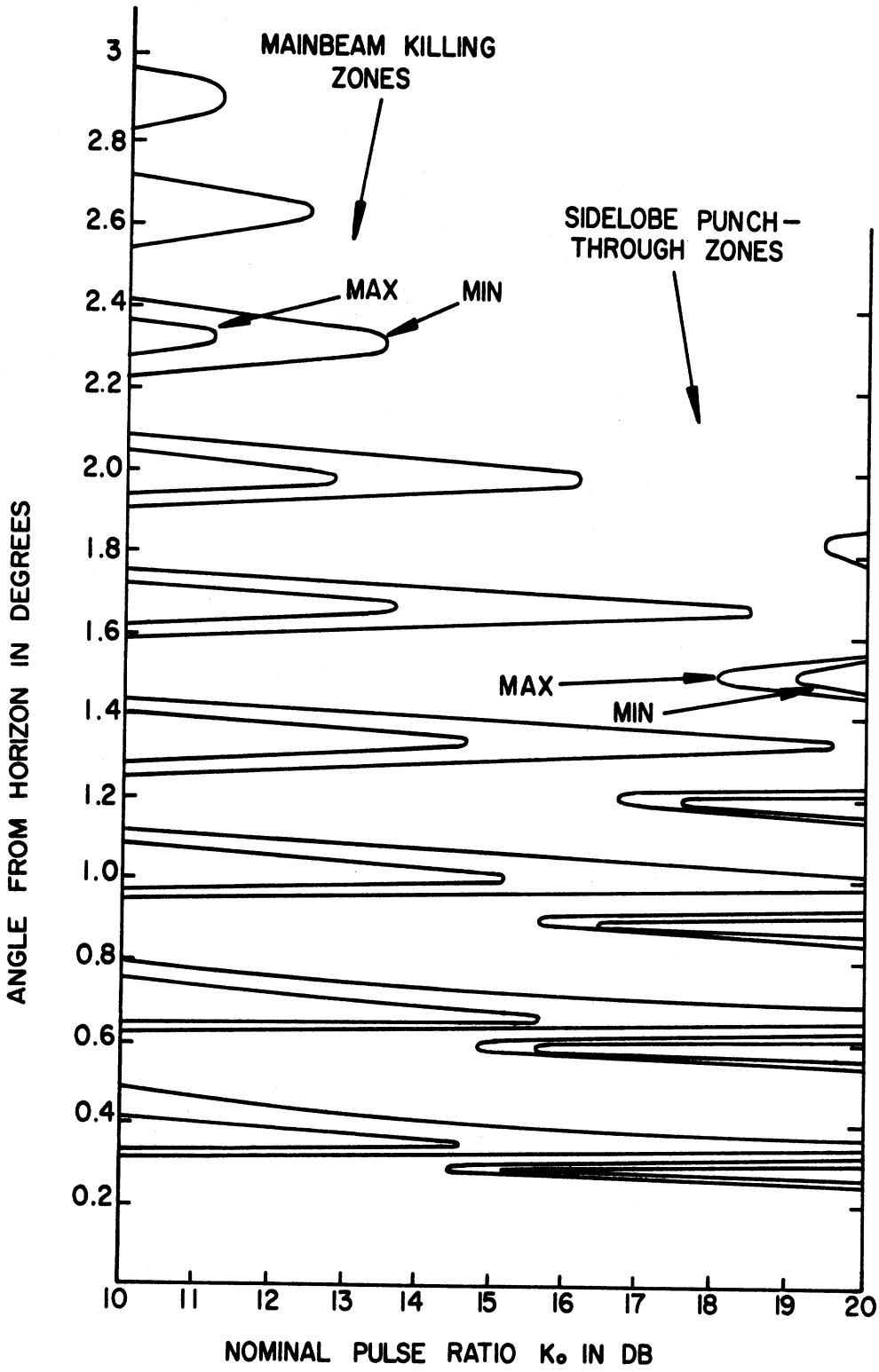

FIG. 36: Mainbeam killing and sidelobe punch-through zones as functions of the nominal pulse ratio for the Westinghouse array antenna. H_d = 82', H_0 = 90', f = 1030 MHz, P1 DIR/OMNI = 18dB, a = 9dB, b = 0dB, L = -25dB.

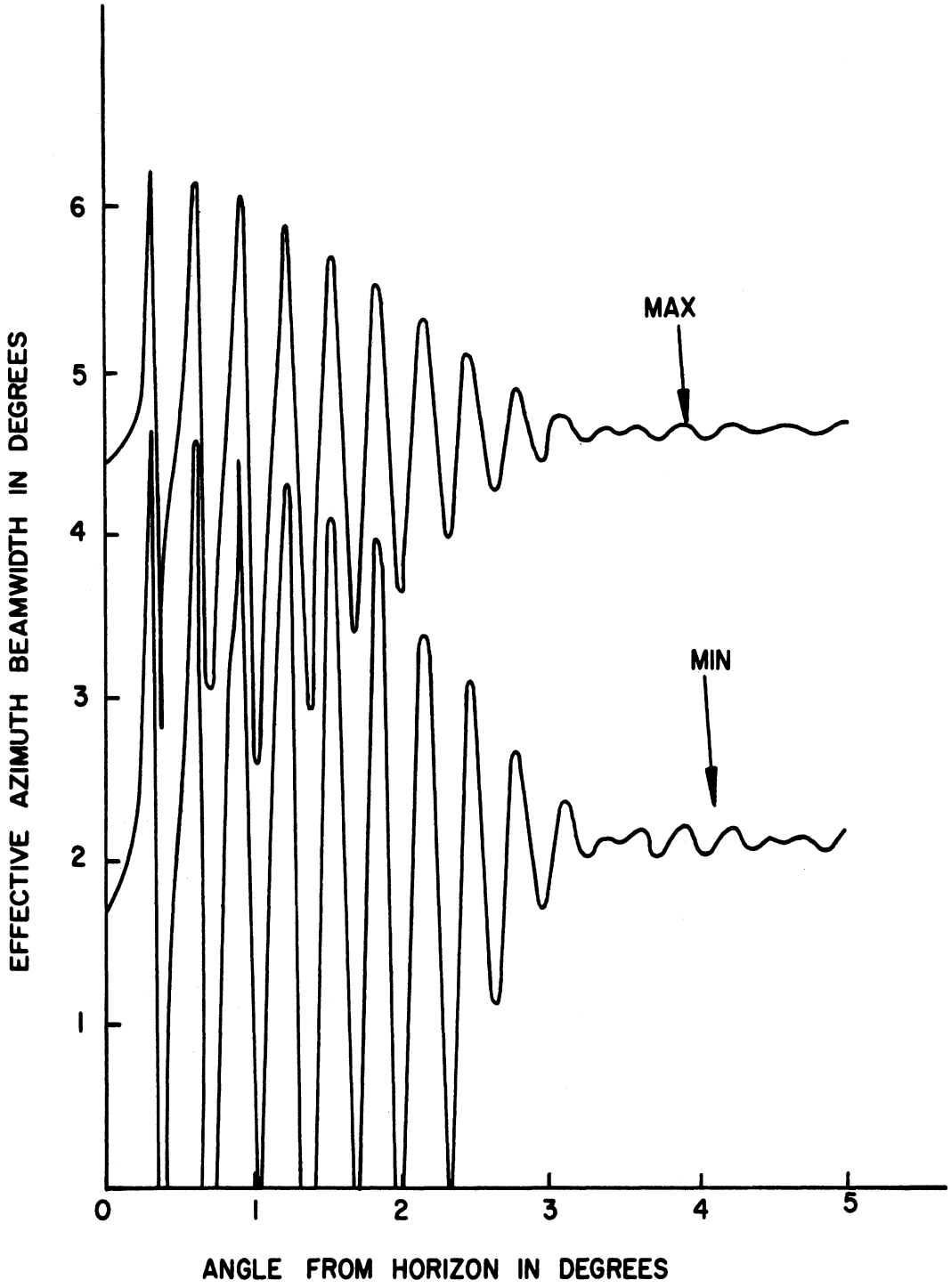

FIG. 37: Effective azimuth beamwidths as functions of the angle from the horizon for Westinghouse array antenna. H_d = 82', H_0 = 90', f = 1030 MHz, nominal pulse ratio K_0 = 18dB, P1DIR/OMNI = 18dB.

Figure 38 gives the number of replies $N_{MAX}(\theta)$, $N_{MIN}(\theta)$ as functions of θ. For $\theta > 3^{o}$ the number of replies assume constant values $N_{MAX}(\theta) \sim 37$, $N_{MIN}(\theta) \sim 17$. For the same antenna, the saturation value of the number of replies in the SLS case is about 31. For $\theta < 3^{o}$, $N_{MAX}(\theta)$ varies between 50 and 20 and $N_{MIN}(\theta)$ varies between 36 and 0.

Figure 39 shows the coverage diagram for the antenna normalized to the free space maximum range of 200 nautical miles. As shown in Fig. 38 for the maximum envelope case, the maximum range of 251 nautical miles occurs at $\theta \sim 0.18^{o}$ and the minimum range of 50 nautical miles occurs at $\theta \sim 0.3^{o}$. The corresponding ranges for the minimum envelope case are 192 and 28 nautical miles respectively.

4.3.2. Texas Instruments Reflector Antenna.

The heights above ground of the phase centers of the directional and omnidirectional antennas are, respectively, $H_d = 82'$ and $H_0 = 91'$. The free space elevation patterns of the directional and omnidirectional antennas are assumed identical.

Figure 40 shows $P1(\theta)_{MAX}$, $P1(\theta)_{MIN}$ and $P2(\theta)$ as functions of θ, where the 0 dB level is adjusted to coincide with the maximum $P1(\theta)_{SLS}$ level in the free space case. The corresponding free space curves (for $q = 0$) are also shown in Fig. 40 for comparison. The oscillations in the curves may be considered negligible for $\theta > 4.5^{o}$.

Figure 41 shows the normalized maximum and minimum envelope pulse ratios as functions of θ. The oscillations in the curves for $\theta \geq 4.5^{o}$ may be considered to be negligible.

Figure 42 shows the main beam killing and sidelobe punch-through zones as functions of the nominal pulse ratio. For $K_0 = 18$ dB ($a = 9$ dB, $b = 0$), there are six main beam killing zones and four sidelobe punch-through zones within the range of θ shown.

Figure 43 shows the effective azimuth beamwidths $\alpha_{1MAX}(\theta)$, $\alpha_{1MIN}(\theta)$ as functions of θ for the threshold level $a = 9$dB and nominal pulse ratio $K_0 = 1.8$dB. For $\theta > 4.5^{o}$, $\alpha_{1MAX}(\theta) \sim 4.7^{o}$ and $\alpha_{1MIN}(\theta) \sim 1.9^{o}$. The corresponding beamwidth is about 3.9^{o} in the SLS mode.

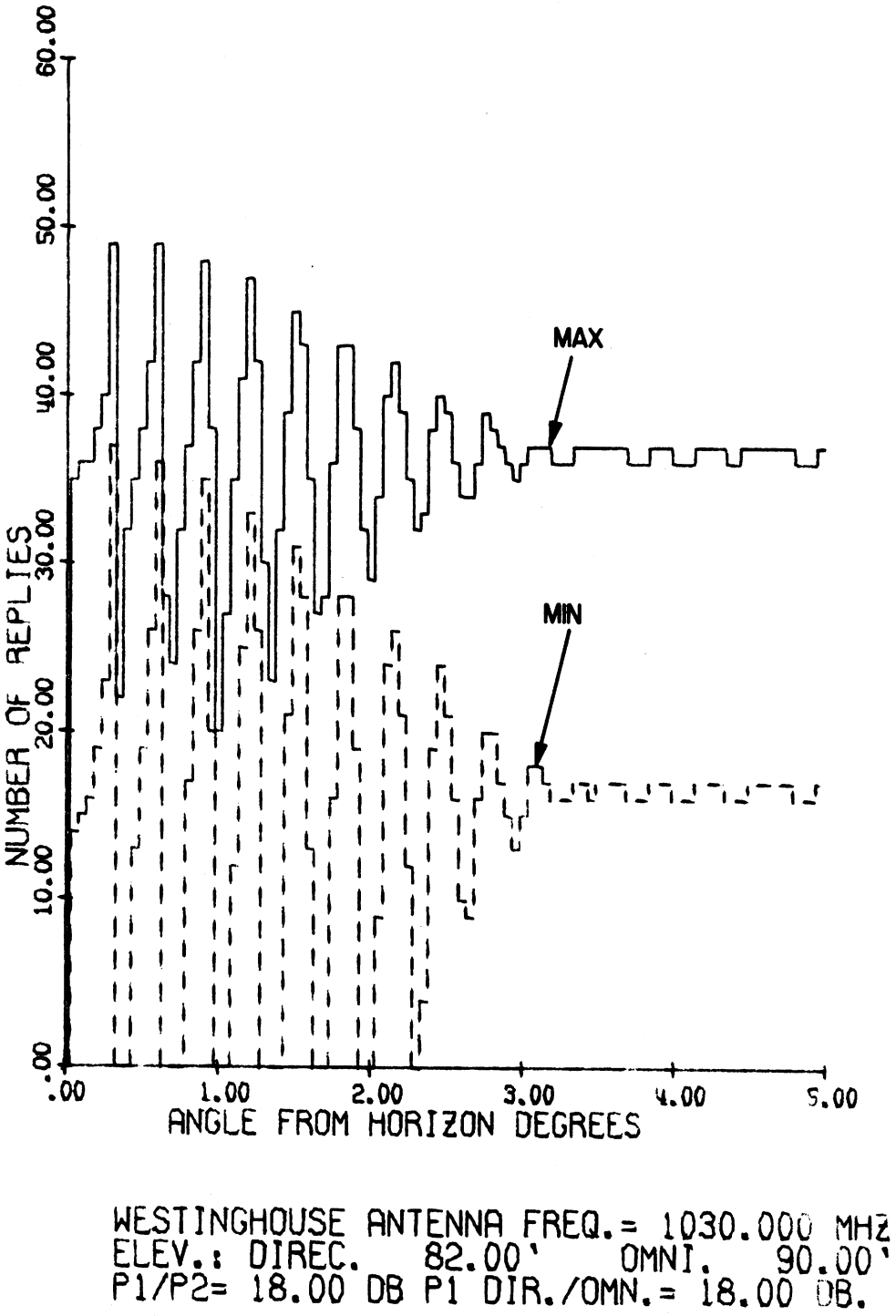

FIG. 38: Number of replies as functions of angle from the horizon.

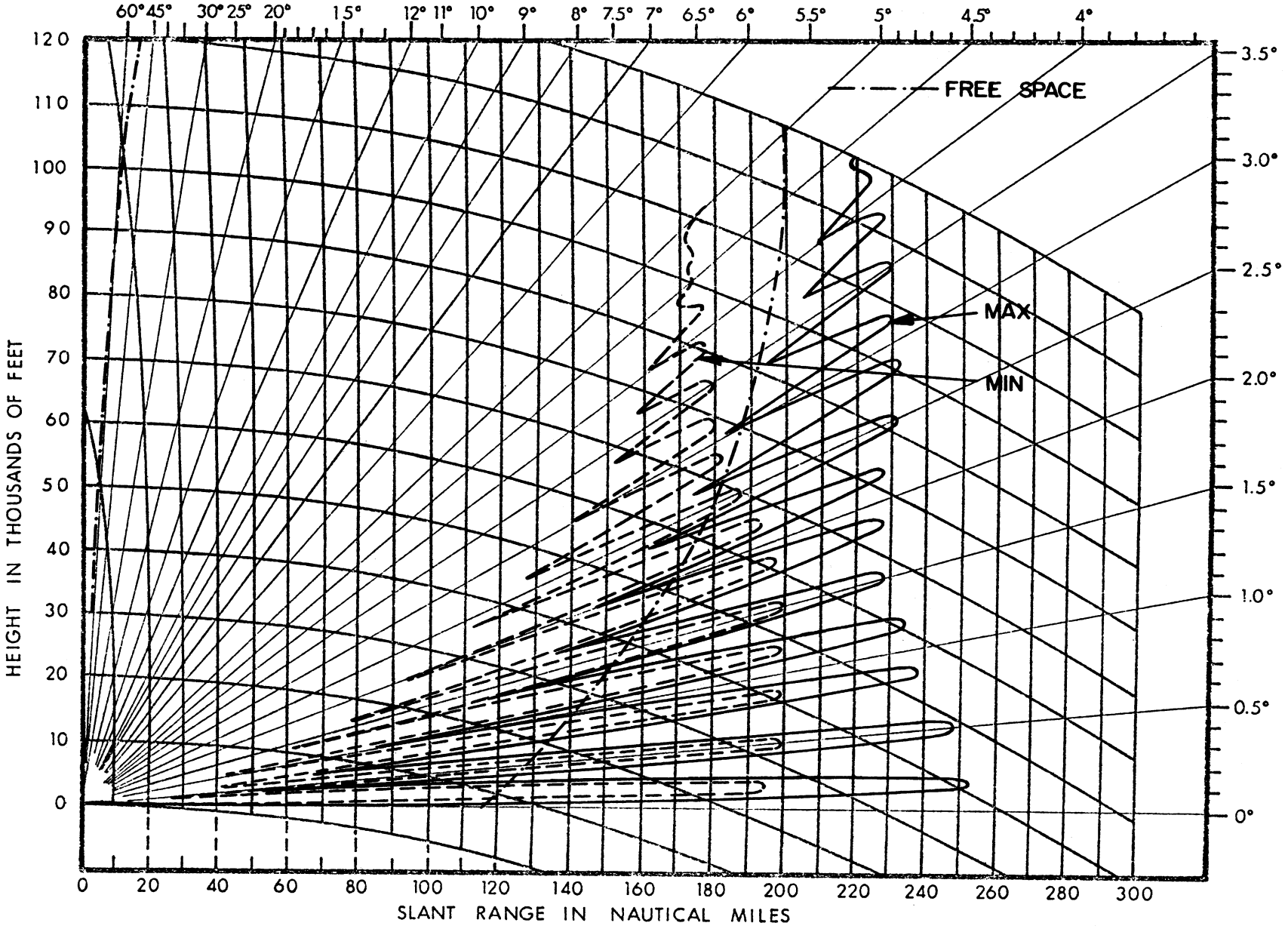

FIG. 39: Coverage diagram for the Westinghouse array. H_d = 82', H_0 = 90', f = 1030 MHz.

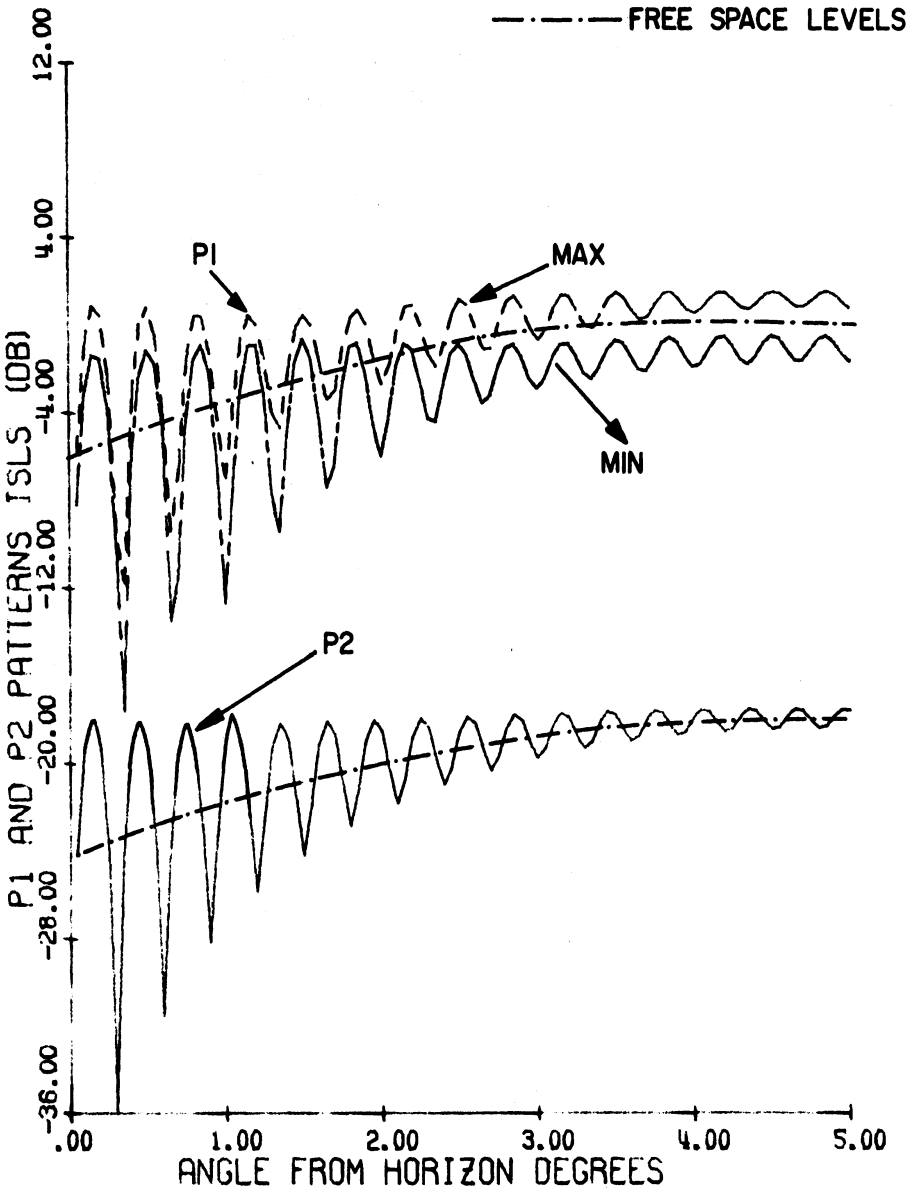

FIG. 40: $P1(\theta)_{MAX}$, $P1(\theta)_{MIN}$ and $P2(\theta)$ as functions of θ.

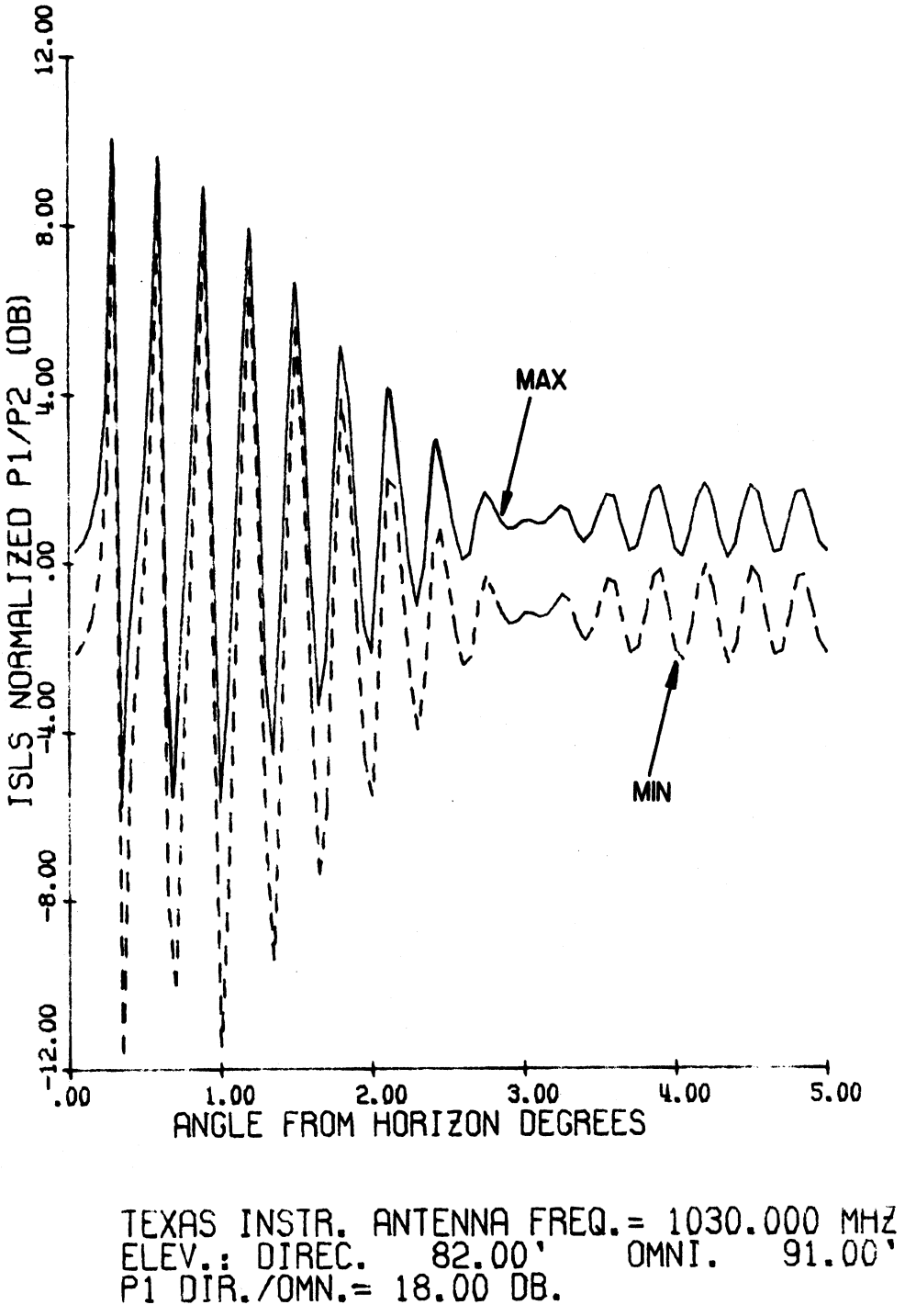

FIG. 41: Normalized pulse ratio envelopes as functions of θ.

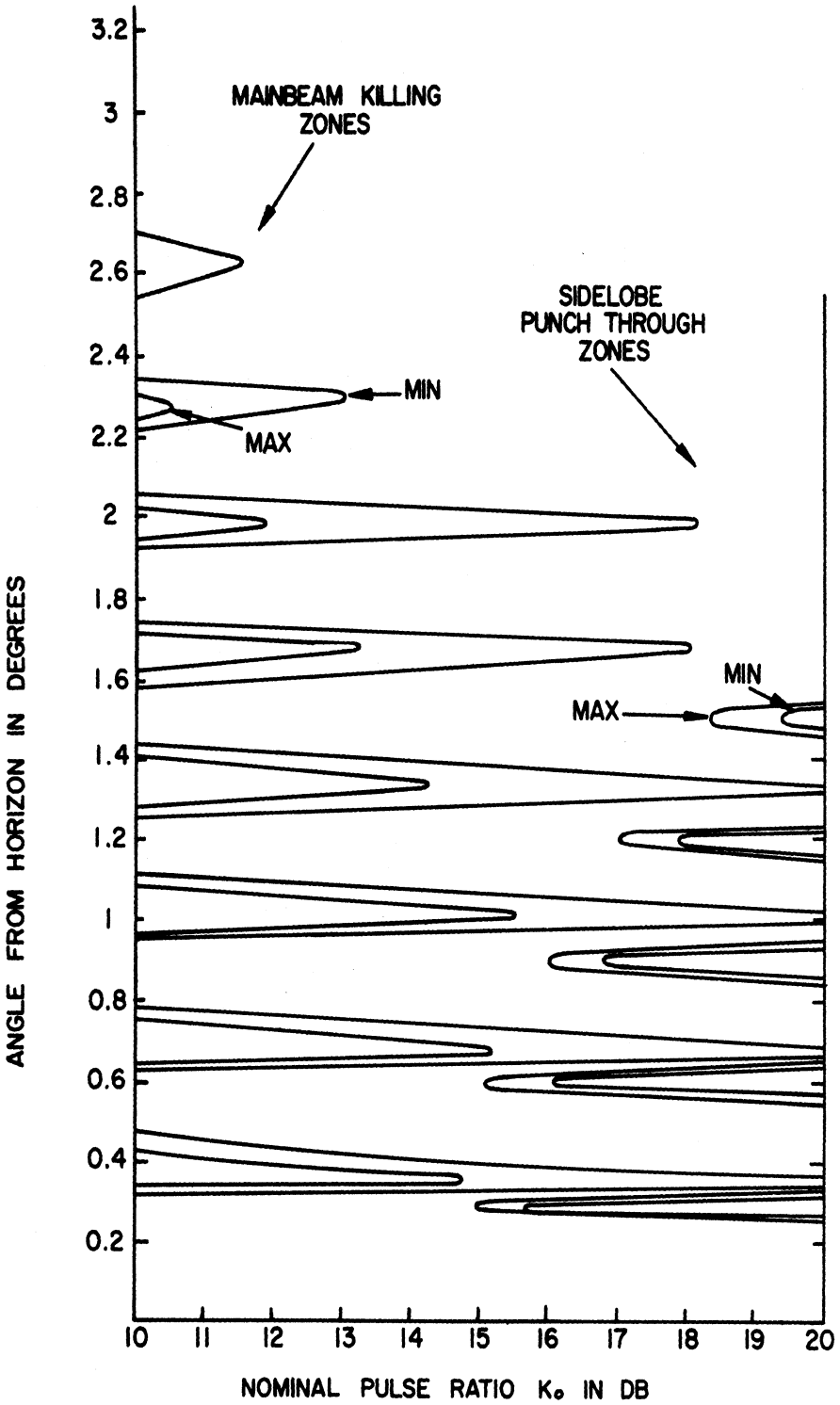

FIG. 42: Mainbeam killing and sidelobe punch-through zones as functions of the nominal pulse ratio for the Texas Instruments reflector antenna. H_d = 82', H_0 = 91', f = 1030 MHz, P1 DIR/OMNI = 18 dB, a = 9 dB, b = 0 dB, L = -25 dB.

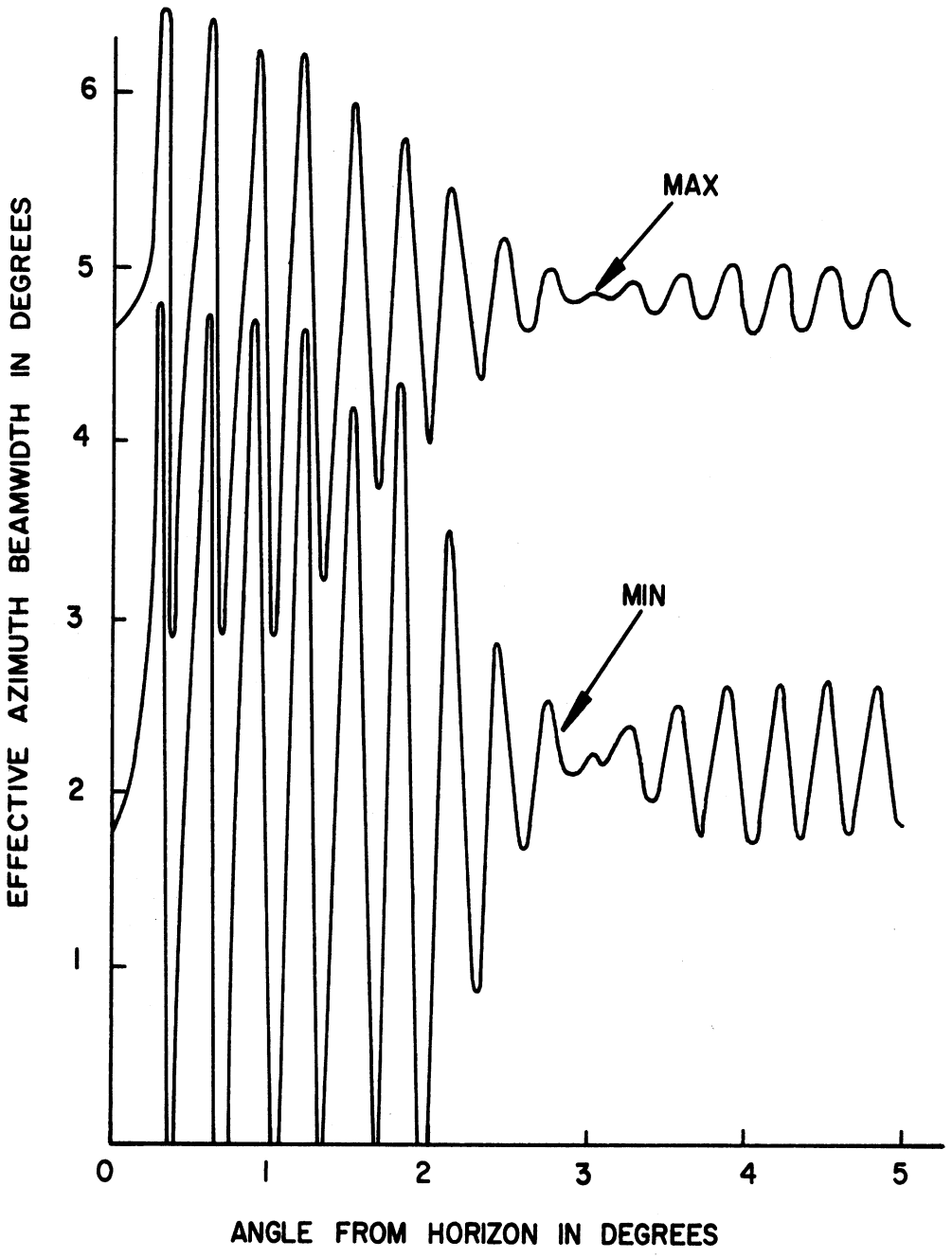

FIG. 43: Effective azimuth beamwidths as functions of the angle from the horizon for the Texas Instruments reflector antenna. H_1 = 82', H_0 = 91', f = 1030 MHz, nominal pulse ratio K_0 = 18dB, P1 DIR/OMNI = 18dB.

Figure 44 shows the number of replies $N_{MAX}(\theta)$, $N_{MIN}(\theta)$ as functions of θ. For $\theta > 3^{o}$ the numbers of replies assume essentially constant values $N_{MAX}(\theta) \sim 39$, $N_{MIN}(\theta) \sim 16$. For the same antenna in the SLS mode, the saturation value of the number of replies is about 32 and occurs for $\theta \gtrsim 3^{o}$. For $\theta < 3^{o}$ $N_{MAX}(\theta)$ varies between 51 and 22 and $N_{MIN}(\theta)$ varies between 39 and 0.

Figure 45 shows the coverage diagram for the antenna where the maximum free space range is adjusted to 200 nautical miles. As can be seen from Fig. 45 , for the maximum envelope case the maximum range of 220 nautical miles occurs at $\theta \sim 0.18^{o}$ and the minimum range of 52 nautical miles occurs at $\theta \sim 0.3^{o}$. The corresponding ranges for the minimum envelope case are 172 and 28 nautical miles respectively.

4.3.3. Existing Hog-Trough Antenna

The heights above ground of the phase centers of the directional and omnidirectional antennas are, respectively, H_d = 108' and H_0 = 110'. The free space elevation plane pattern of the directional and omnidirectional antennas are assumed to be identical.

Figure 46 a shows the variation of $P1(\theta)_{MAX}$, $P1(\theta)_{MIN}$ and $P2(\theta)$ as functions of θ in the range $0 \leq \theta \lesssim 5^{o}$, with the 0 dB level adjusted to coincide with the maximum $P1(\theta)_{SLS}$ in the free space case. Because of the small field gradient (α_g = 0.5dB/5^{o}) of the antennas, the number of lobings in the patterns is quite large. In fact, the oscillations in the curves are found to persist for values of θ up to about 20^{o}. Figures 46 b through d show the variations of the respective pulses for three more ranges of θ, $5^{o} \leq \theta \leq 10^{o}$, $10^{o} \leq \theta \leq 15^{o}$ and $15^{o} \leq \theta \leq 20^{o}$.

Figures 47 a through d give the variations of the pulse ratios as functions of θ for four ranges of θ within $0^{o} \leq \theta \leq 20^{o}$. The oscillations are found to be appreciable for θ values up to 20^{o}.

Figure 48 gives the main beam killing zones and sidelobe punch-through zones as functions of the nominal pulse ratio. As expected, compared to the terminal case within the same range of θ, the number of zones is increased in th enroute case. With the range $0 \leq \theta \leq 3^{o}$, there are 5 main beam killing

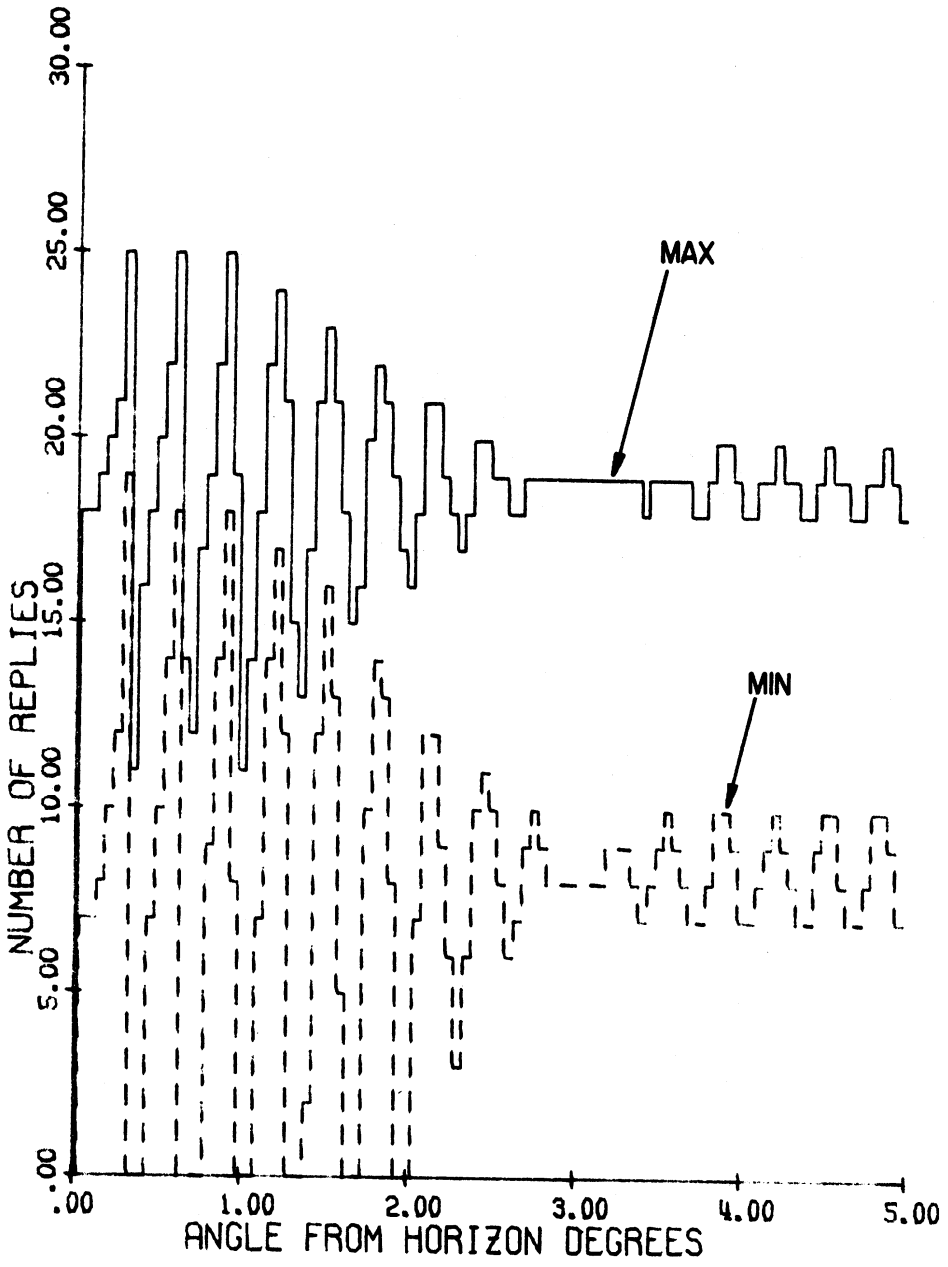

FIG. 44: Number of replies as functions of angle from the horizon.

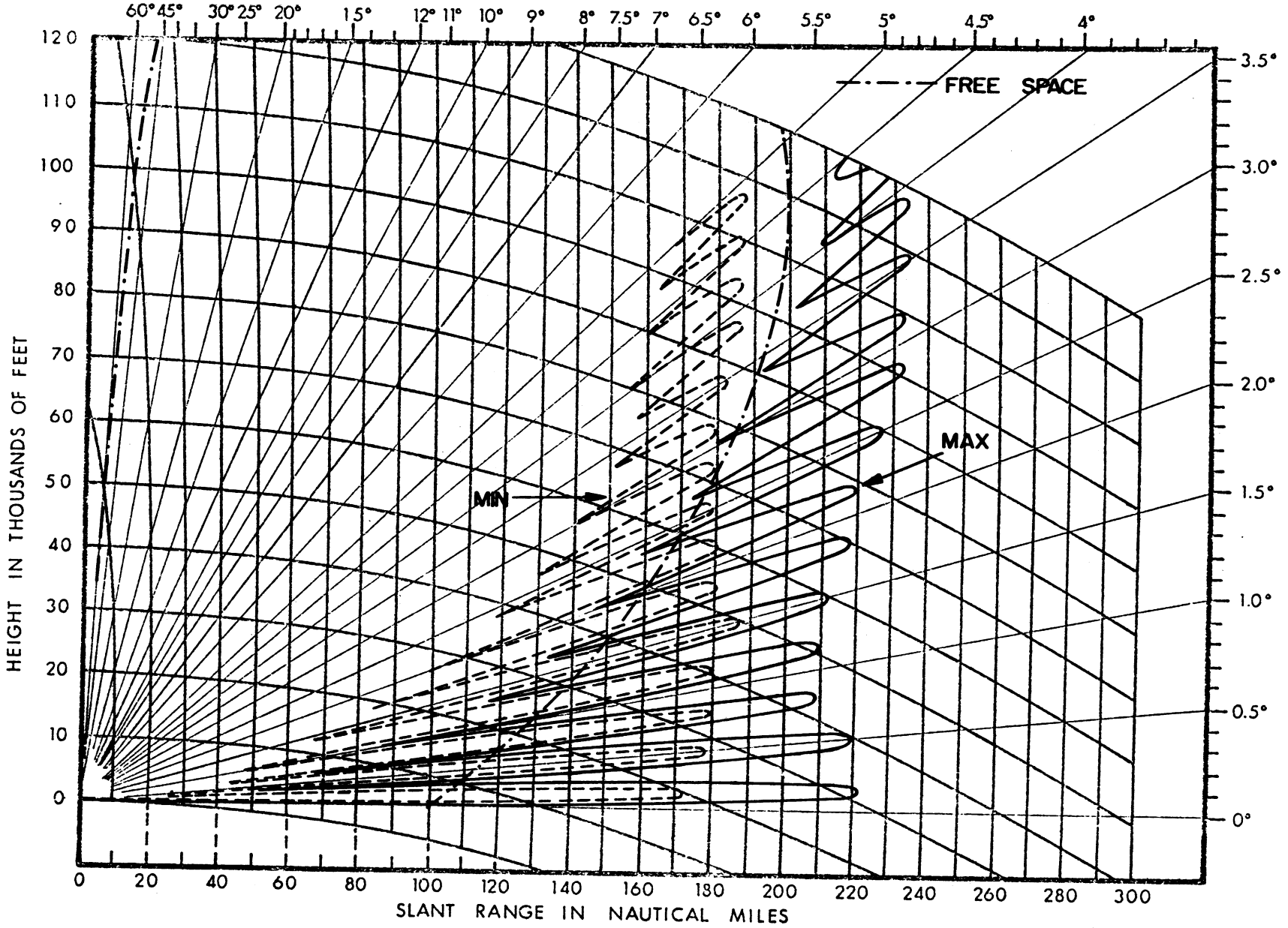

FIG. 45: Coverage diagram for the Texas Instruments reflector antenna. H_d = 82', H_0 = 91', f = 1030 MHz.

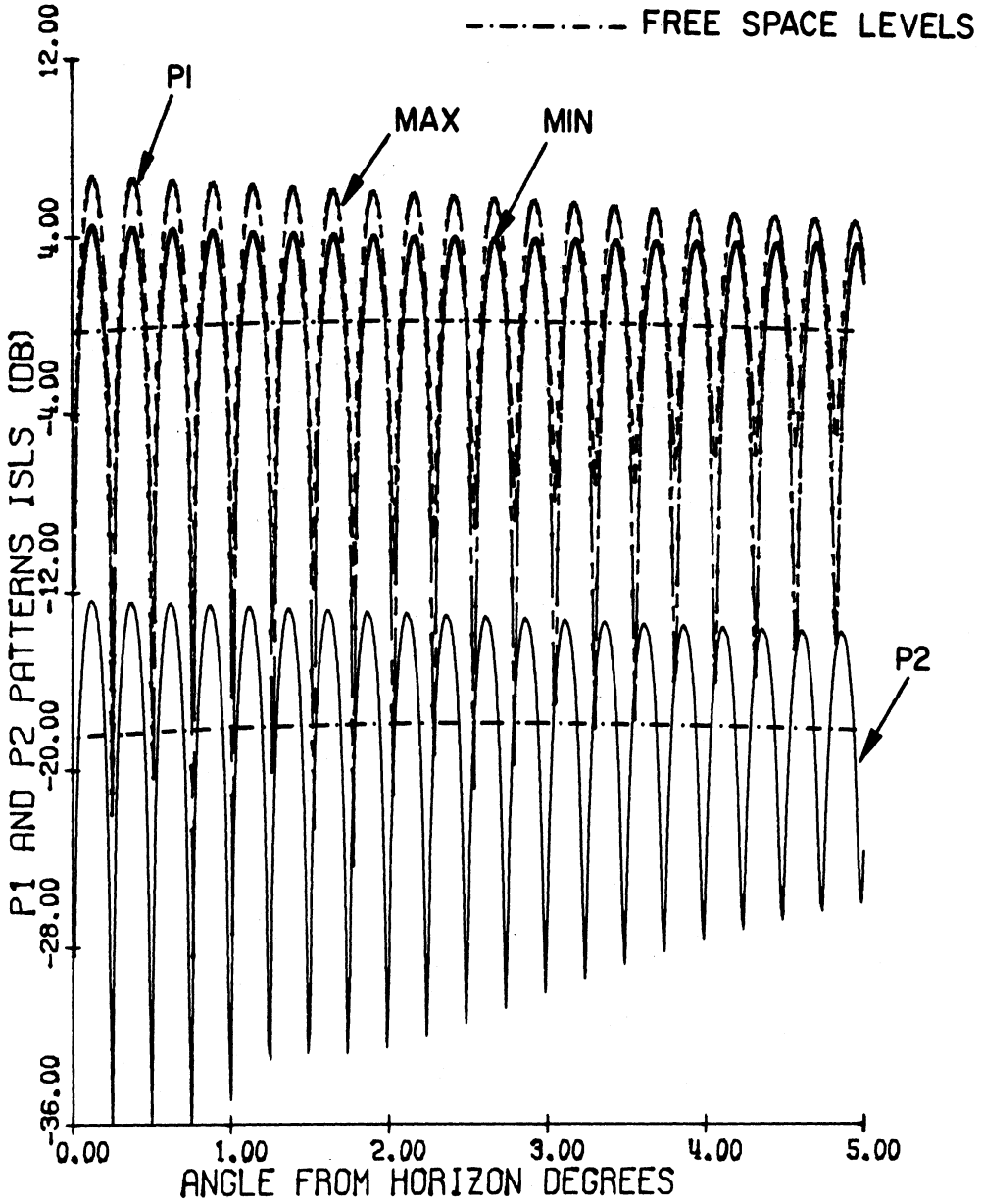

EXISTING ANTENNA TILTED ANGLE= 0.0 D
ELEV.: DIREC. 108.00' OMNI. 110.00'
P1/P2= 18.00 DB P1 DIR./OMN.= 18.00 DB.

FIG. 46 a: $P1(\theta)_{MAX}$, $P1(\theta)_{MIN}$ and $P2(\theta)$ as functions of θ.

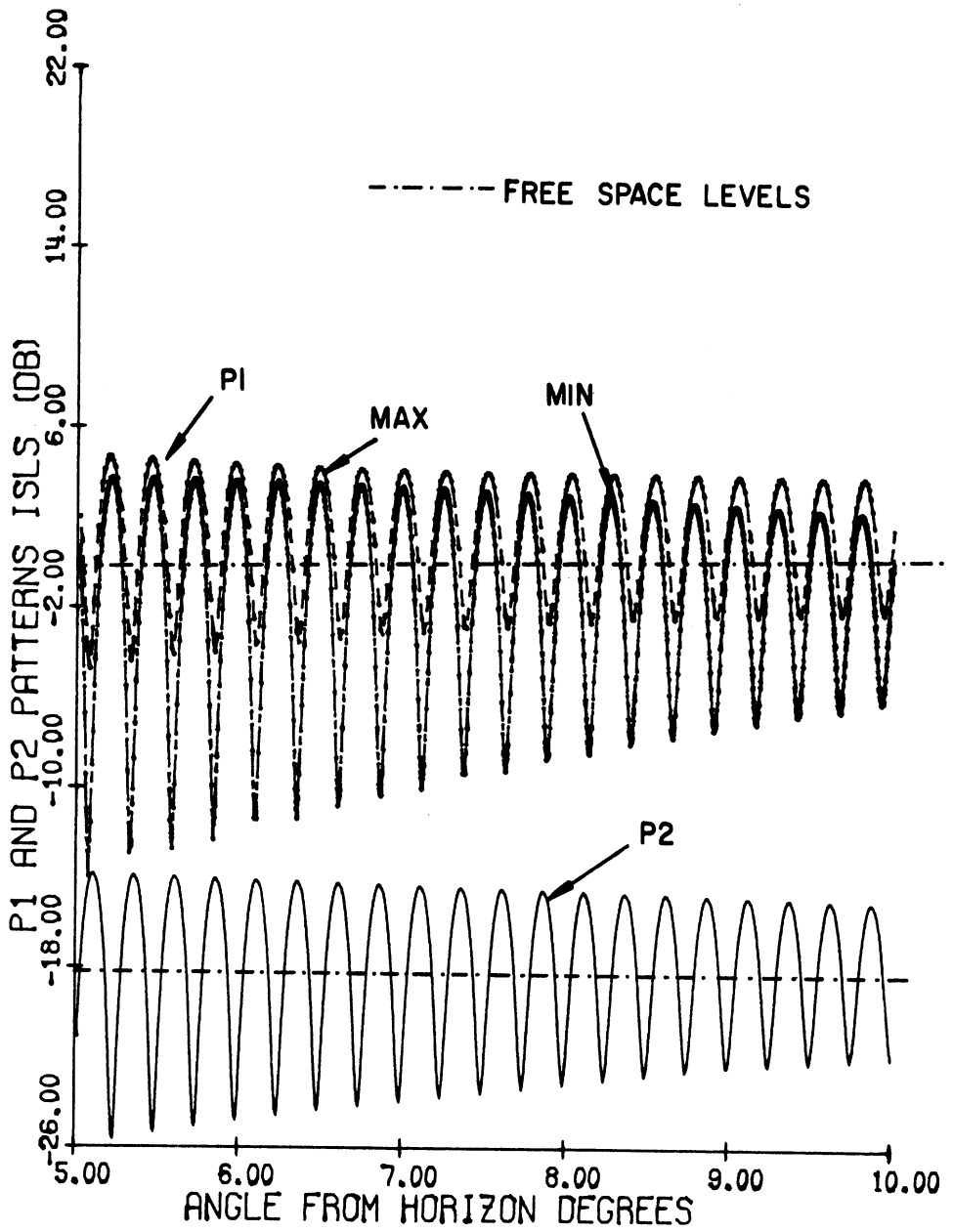

FIG. 46 b: $P1(\theta)_{MAX}$, $P1(\theta)_{MIN}$ and $P2(\theta)$ as functions of θ.

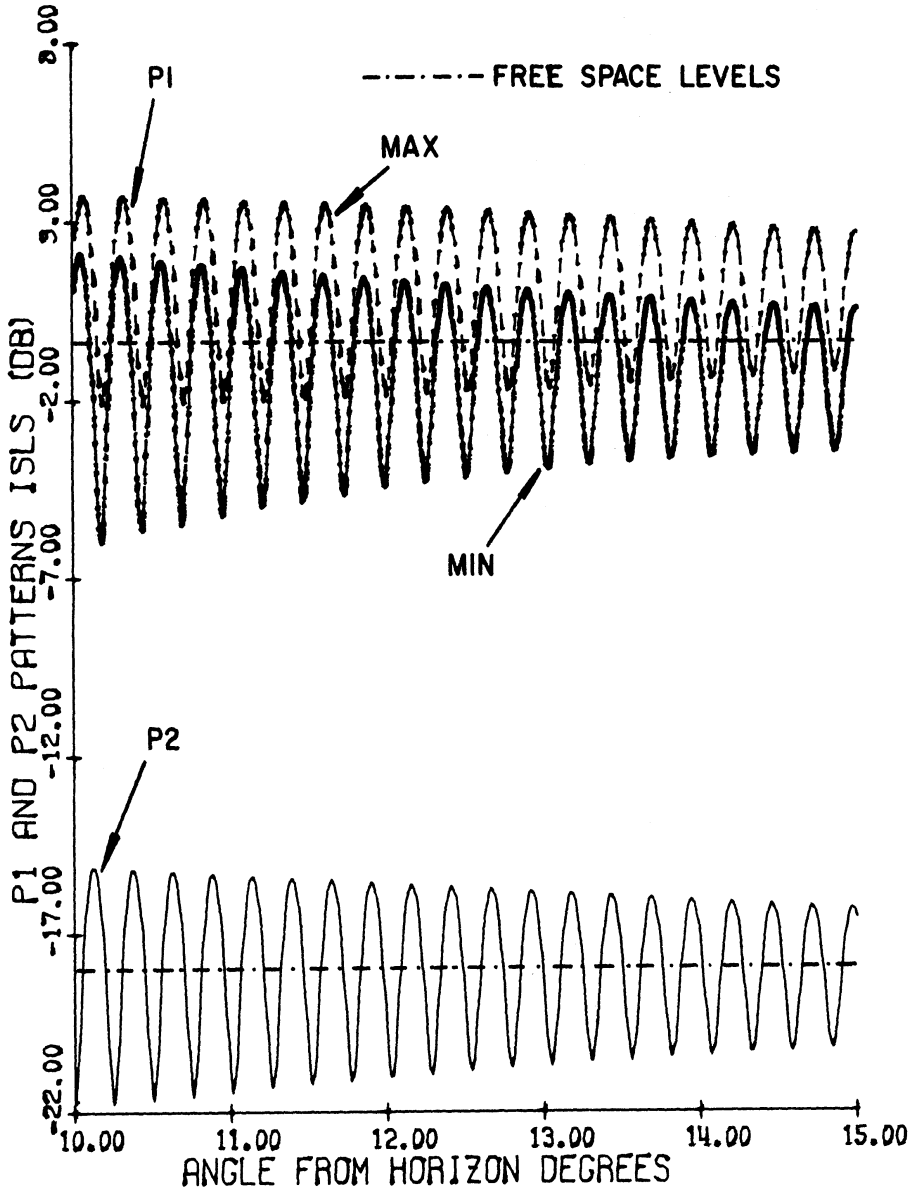

EXISTING ANTENNA TILTED ANGLE= 0.0 D
ELEV.: DIREC. 108.00' OMNI. 110.00'
P1/P2= 18.00 DB P1 DIR./OMN.= 18.00 DB.

FIG. 46 c: $P1(\theta)_{MAX}$, $P1(\theta)_{MIN}$ and $P2(\theta)$ as functions of θ.

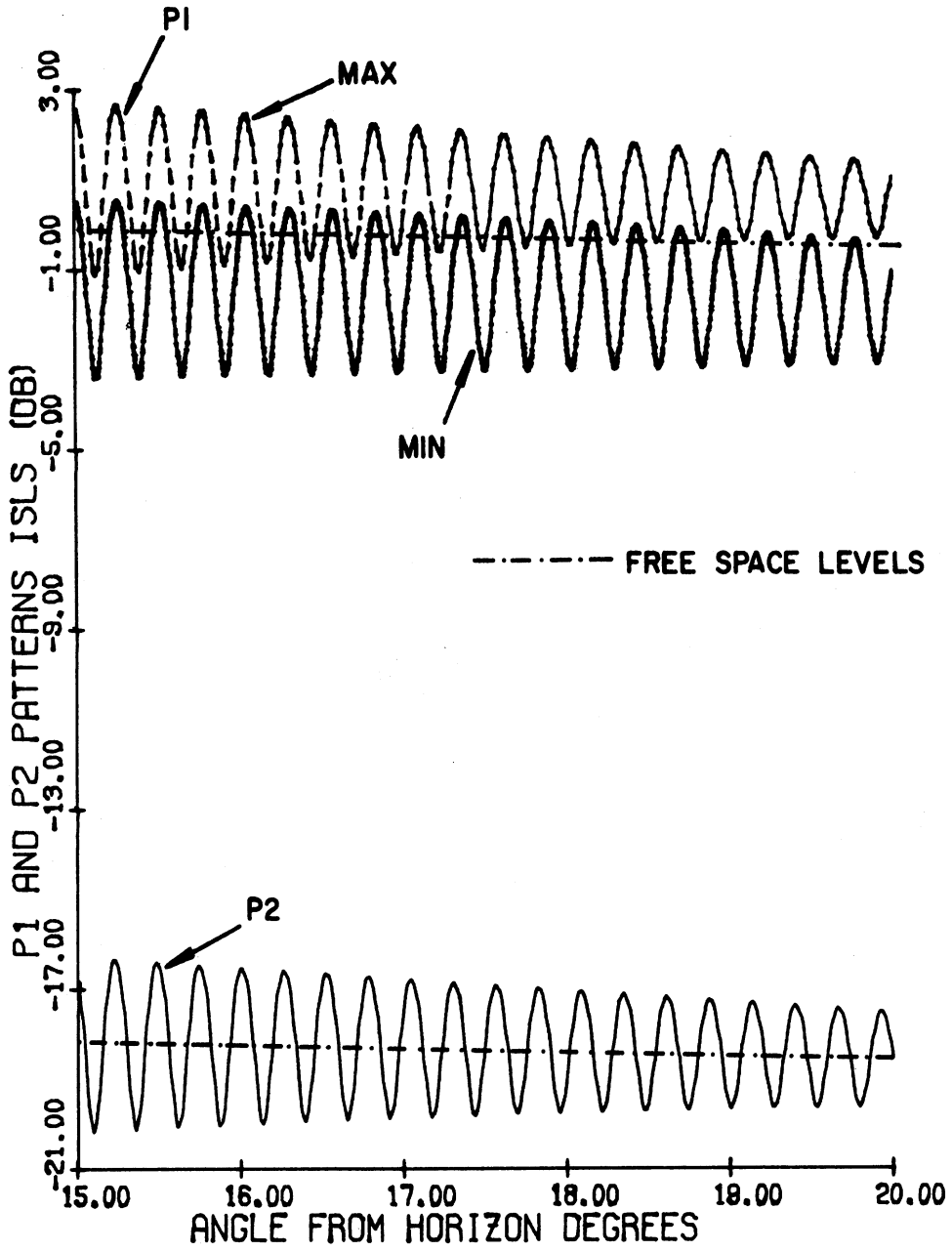

EXISTING ANTENNA TILTED ANGLE= 0.0 D
ELEV.: DIREC. 108.00' OMNI. 110.00'
P1/P2= 18.00 DB P1 DIR./OMN.= 18.00 DB.

FIG. 46 d: $P1(\theta)_{MAX}$, $P1(\theta)_{MIN}$ and $P2(\theta)$ as functions of θ.

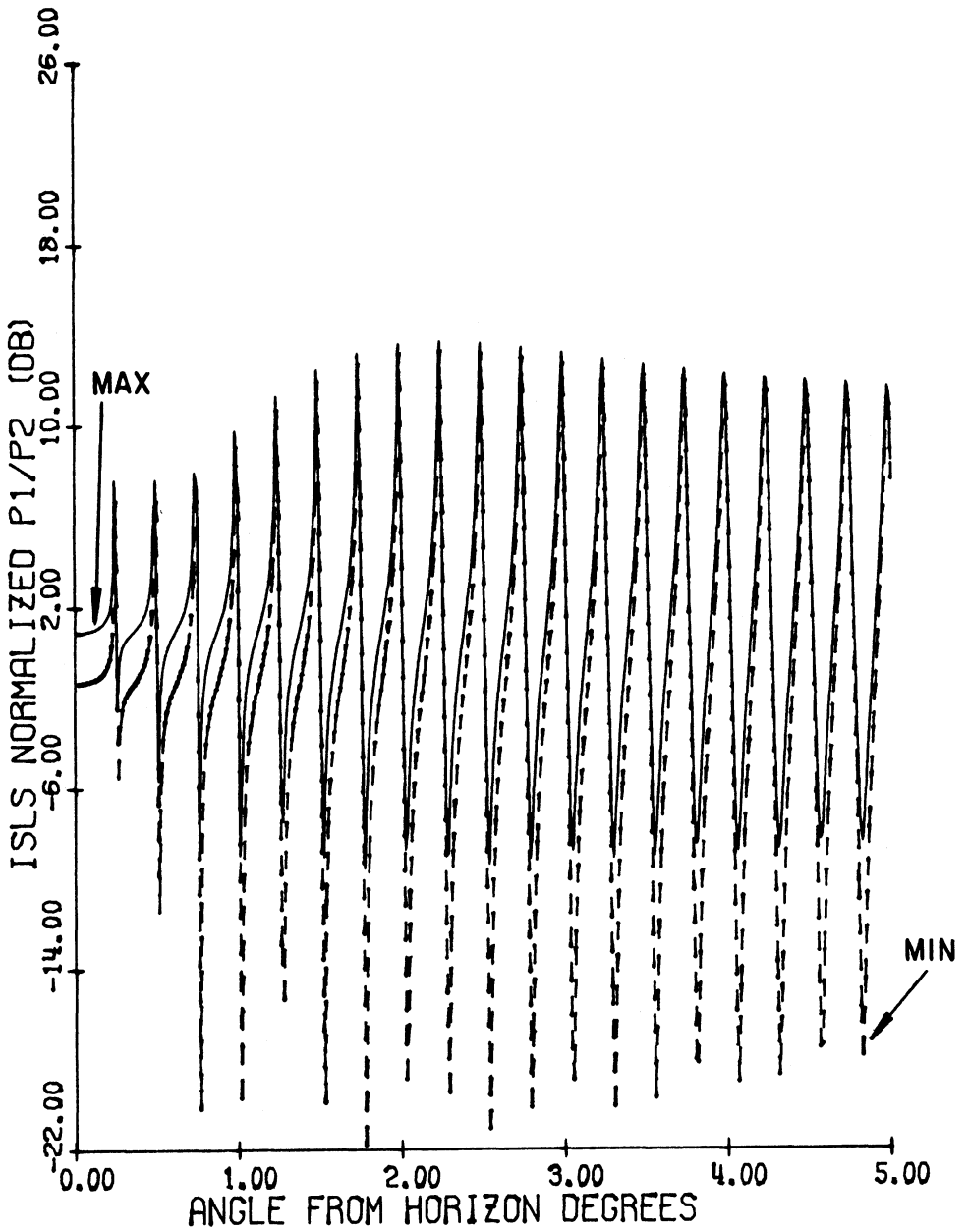

FIG. 47 a: Normalized pulse ratio envelopes as functions of θ.

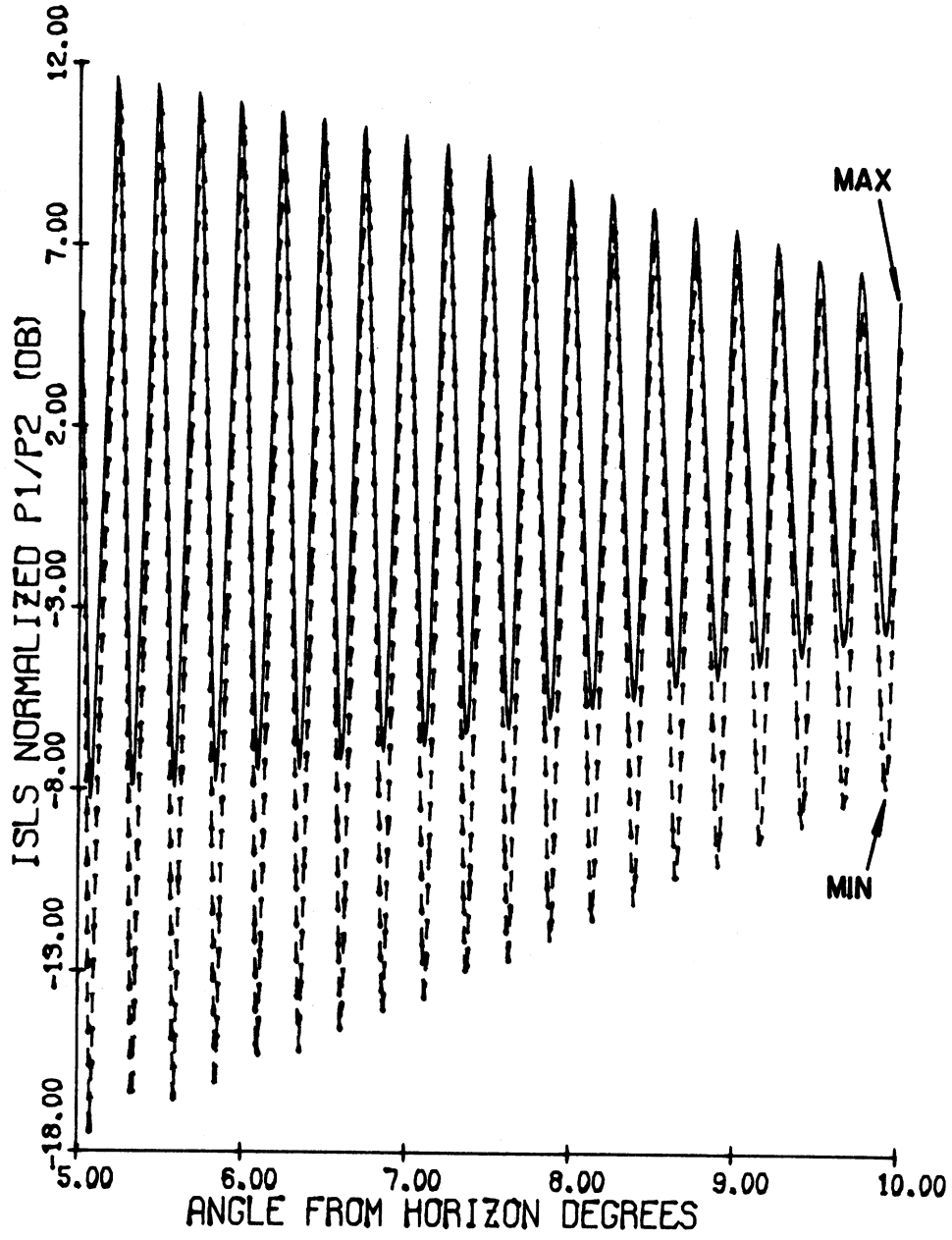

FIG. 47 b: Normalized pulse ratio envelopes as functions of θ.

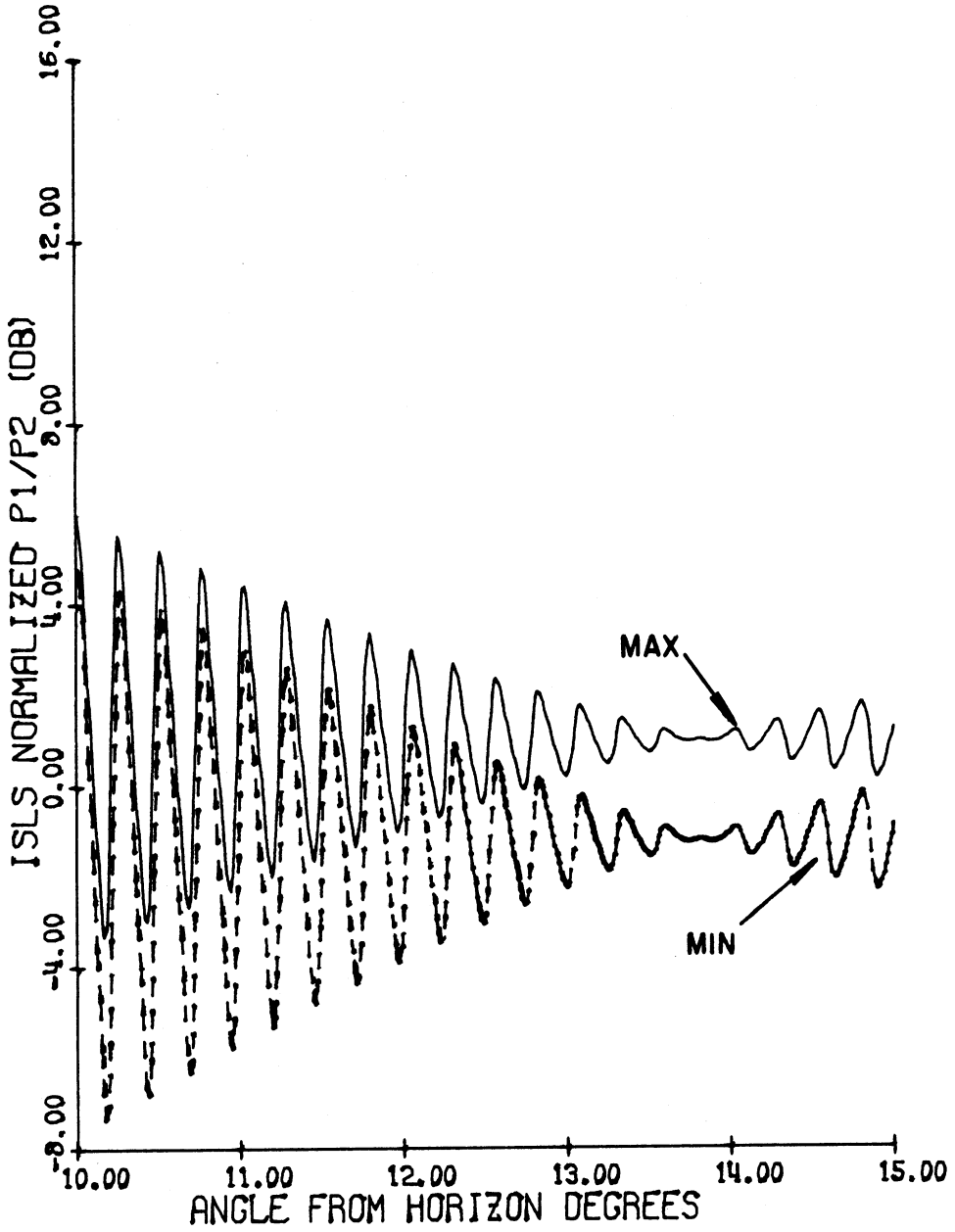

FIG. 47 c: Normalized pulse ratio envelopes as functions of θ.

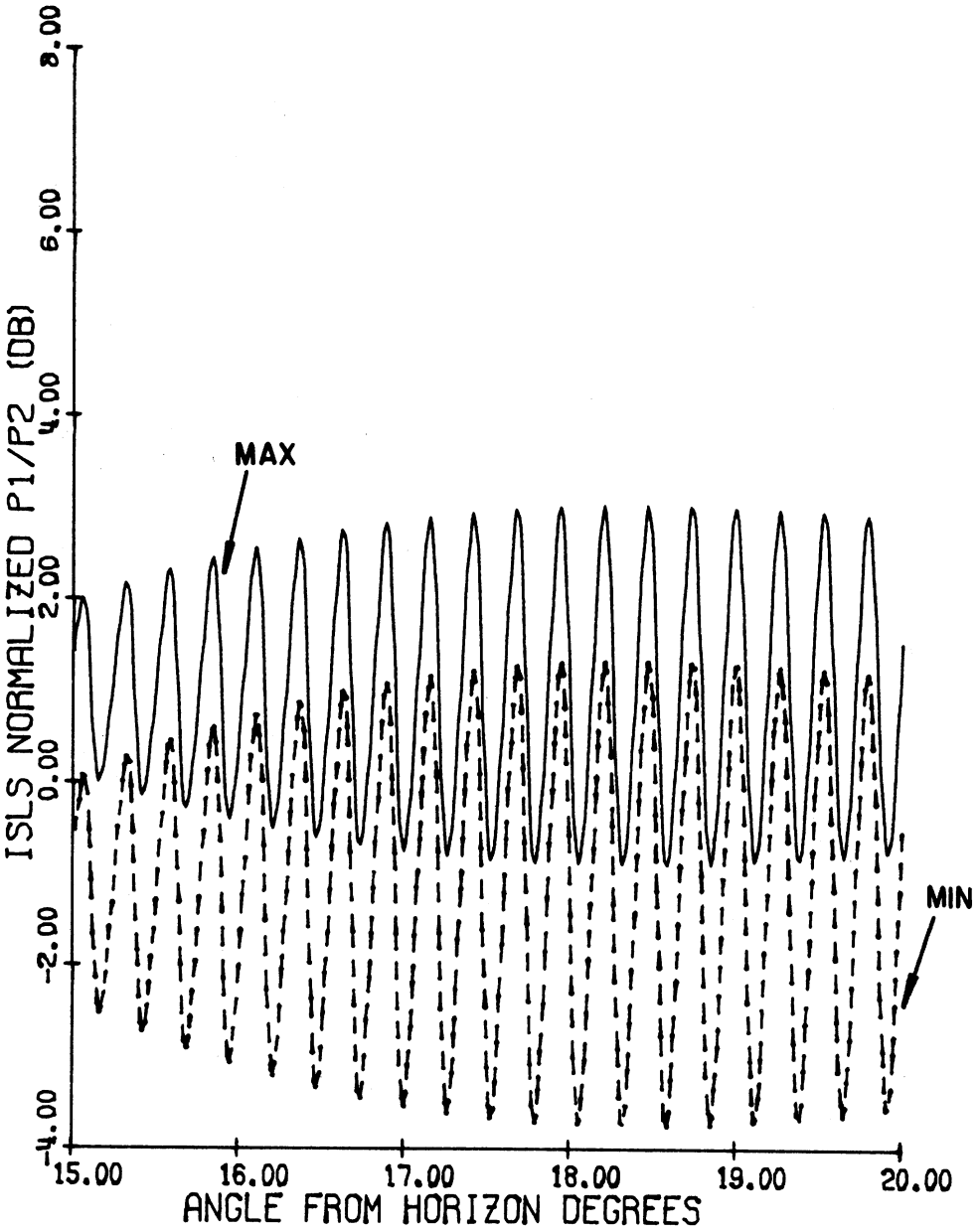

FIG. 47 d: Normalized pulse ratio envelopes as functions of θ.

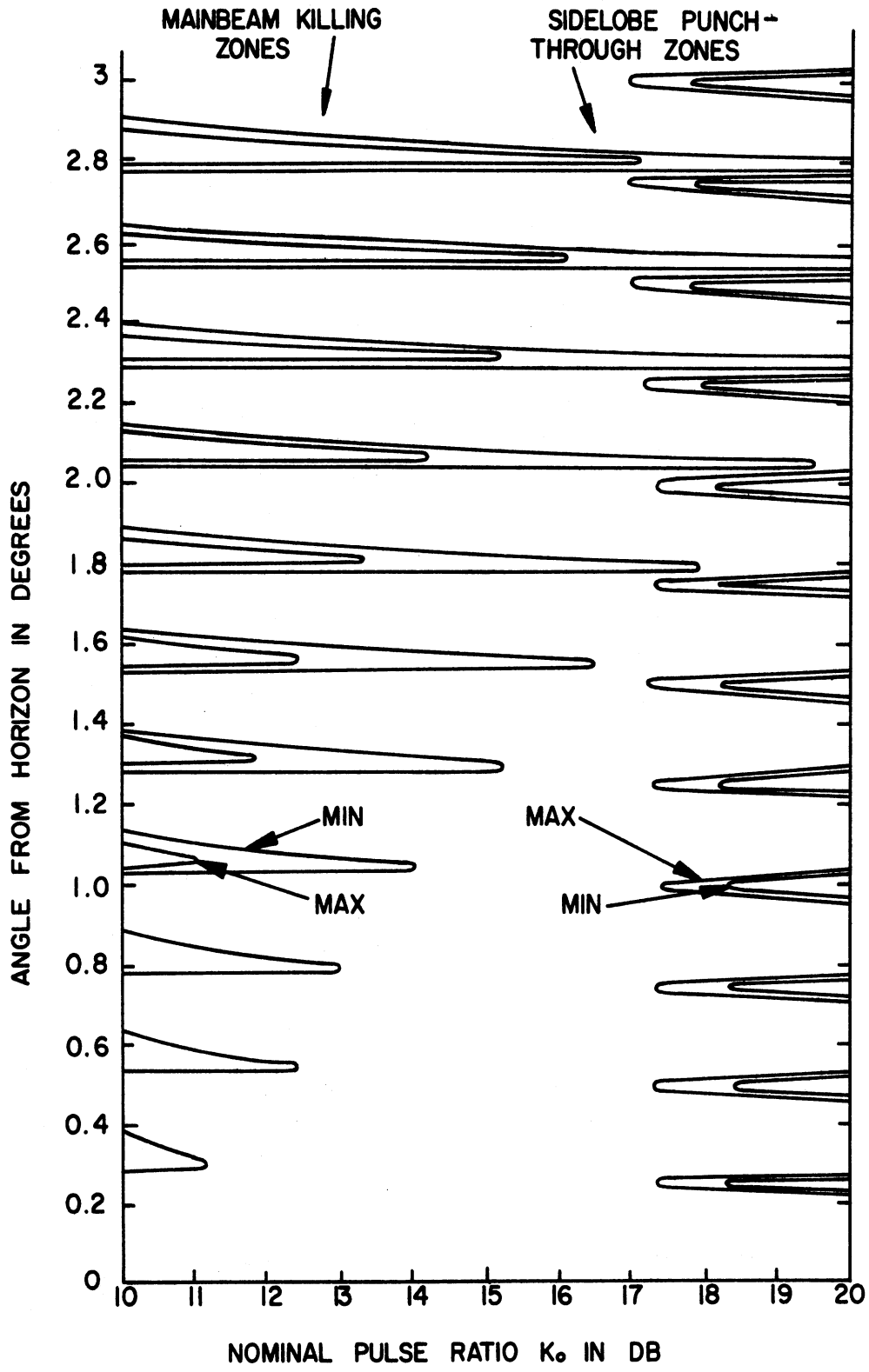

FIG. 48: Mainbeam killing and sidelobe punch-through zones as functions of the nominal pulse ratio for the existing hog-trough antenna. H_d = 108', H_0 = 110', f = 1030 MHz, P1 DIR/OMNI = 18dB, a = 9dB, b = 0dB, L = -25dB.

zones and 12 sidelobe punch-through zones for K_0 = 18 dB, a = 9 dB and b = 0 dB. If desired, zones for $\theta > 3^0$ may be obtained from the corresponding pulse ratios.

Figure 49 gives the effective beamwidths $\alpha_{1MAX}(\theta)$, $\alpha_{1MIN}(\theta)$ as functions of θ in the range $0 \leq \theta \leq 5^0$. The saturated values of the beamwidths are $\alpha_{1MAX}(\theta) \sim 4.8^0$ and $\alpha_{1MIN}(\theta) \sim 2.4^0$, and they occur for $\theta > 20^0$. The corresponding value of the effective beamwidth for the same antenna in the SLS mode is about 4.0^0.

Figure 50 gives the number of replies $N_{MAX}(\theta)$ and $N_{MIN}(\theta)$ as functions of θ, for four different ranges of θ in $0 \leq \theta \leq 20^0$. For $\theta > 20^0$, $N_{MAX}(\theta) \sim 38$ and $N_{MIN}(\theta) \sim 18$. For the same antenna the saturation value of the number of replies which occurs at $\theta > 20^0$ is about 32. For $\theta < 20^0$, $N_{MAX}(\theta)$ varies between 47 and 0, and $N_{MIN}(\theta)$ varies between 33 and 0.

Figures 51 a and 51 b show the coverage diagram for the antenna where the maximum free space range in the SLS case is adjusted to 200 nautical miles. It can been seen from Fig. 51 a that for the maximum envelope case the maximum range of 408 nautical miles occurs at $\theta \sim 0.18^0$ and the minimum range of 22 nautical miles occurs at $\theta \sim 0.3^0$. The corresponding ranges for the minimum envelope case are found to be 321 and 19 nautical miles respectively.

4.3.4. Texas Instruments Fix Antenna.

The heights above ground of the phase centers of the directional and omnidirectional antennas are H_d = 92' and H_0 = 112' respectively. The free space elevation plane patterns of the directional and omnidirectional antennas are assumed to be identical.

Figure 52 shows $P1(\theta)_{MAX}$, $P1(\theta)_{MIN}$ and $P2(\theta)$ as functions of θ, where the 0 dB level is adjusted to coincide with the maximum of $P1(\theta)_{SLS}$ level in the free space case. The corresponding free space curves (q = 0) are also shown in Fig. 52 for comparison. The oscillations in the curves may be considered to be negligible for $\theta > 3^0$.

Figure 54 shows the main beam killing and sidelobe punch-through zones as functions of the pulse ratio for K_0 = 18 dB (a = 9 dB, b = 0 dB). There are three main beam killing zones and three sidelobe punch-through zones within the range of θ shown.

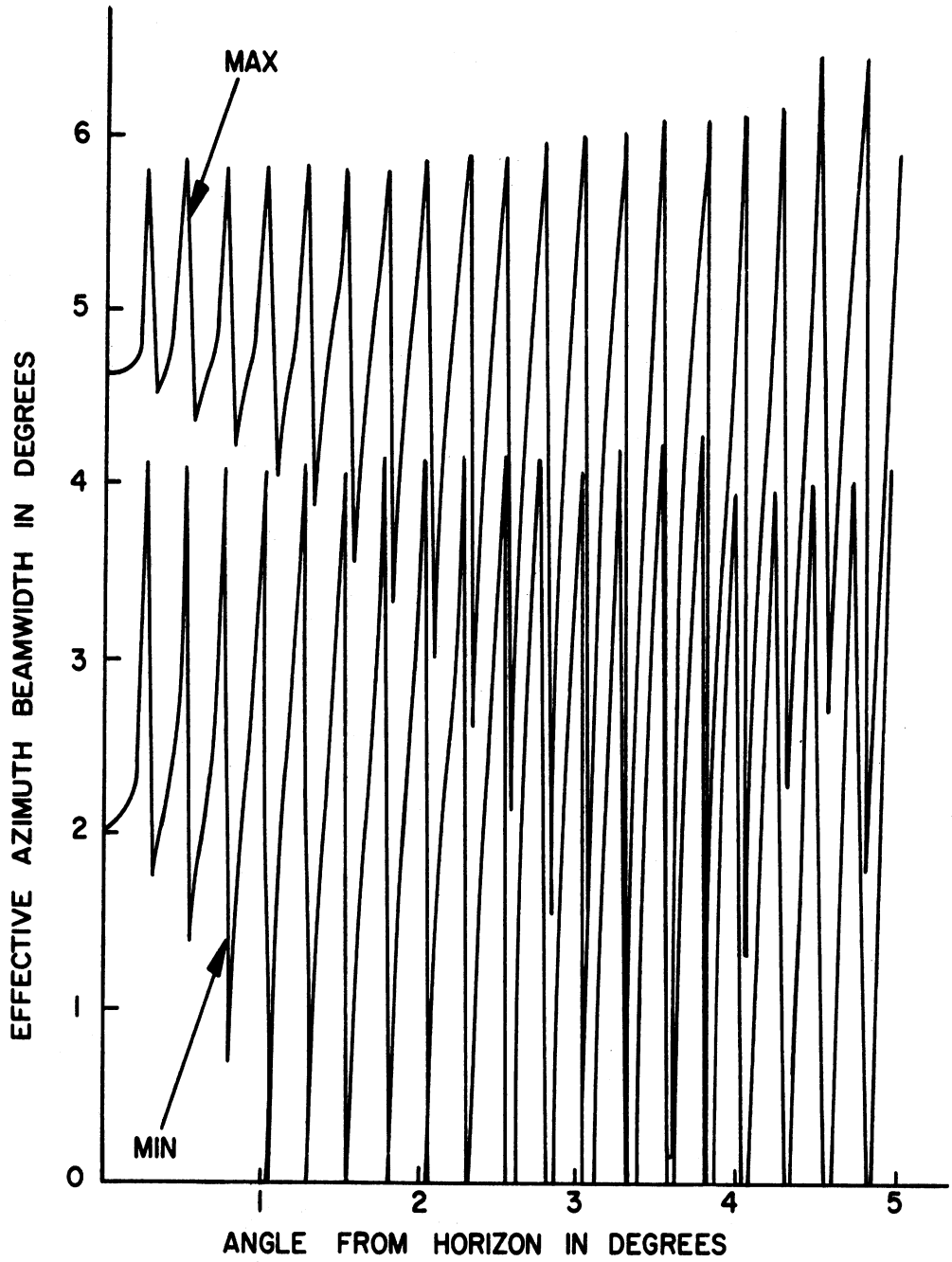

FIG. 49: Effective azimuth beamwidths as functions of the angle from the horizon for the existing hog-trough antenna. H_d = 108', H_0 = 110', f = 1030 MHz, nominal pulse ratio K_0 = 18dB, P1 DIR/OMNI = 18 dB.

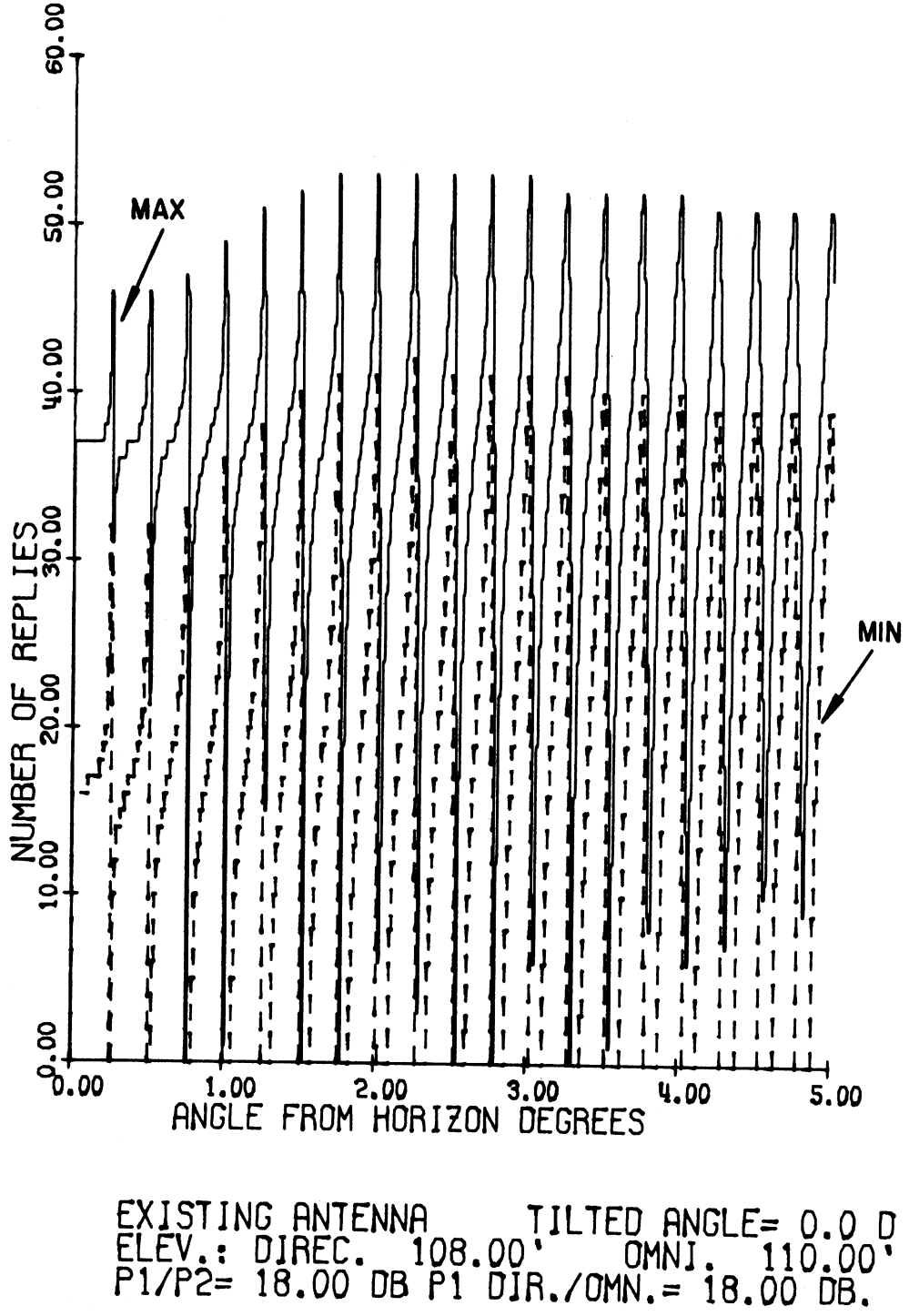

FIG. 50: Number of replies as functions of angle from the horizon.

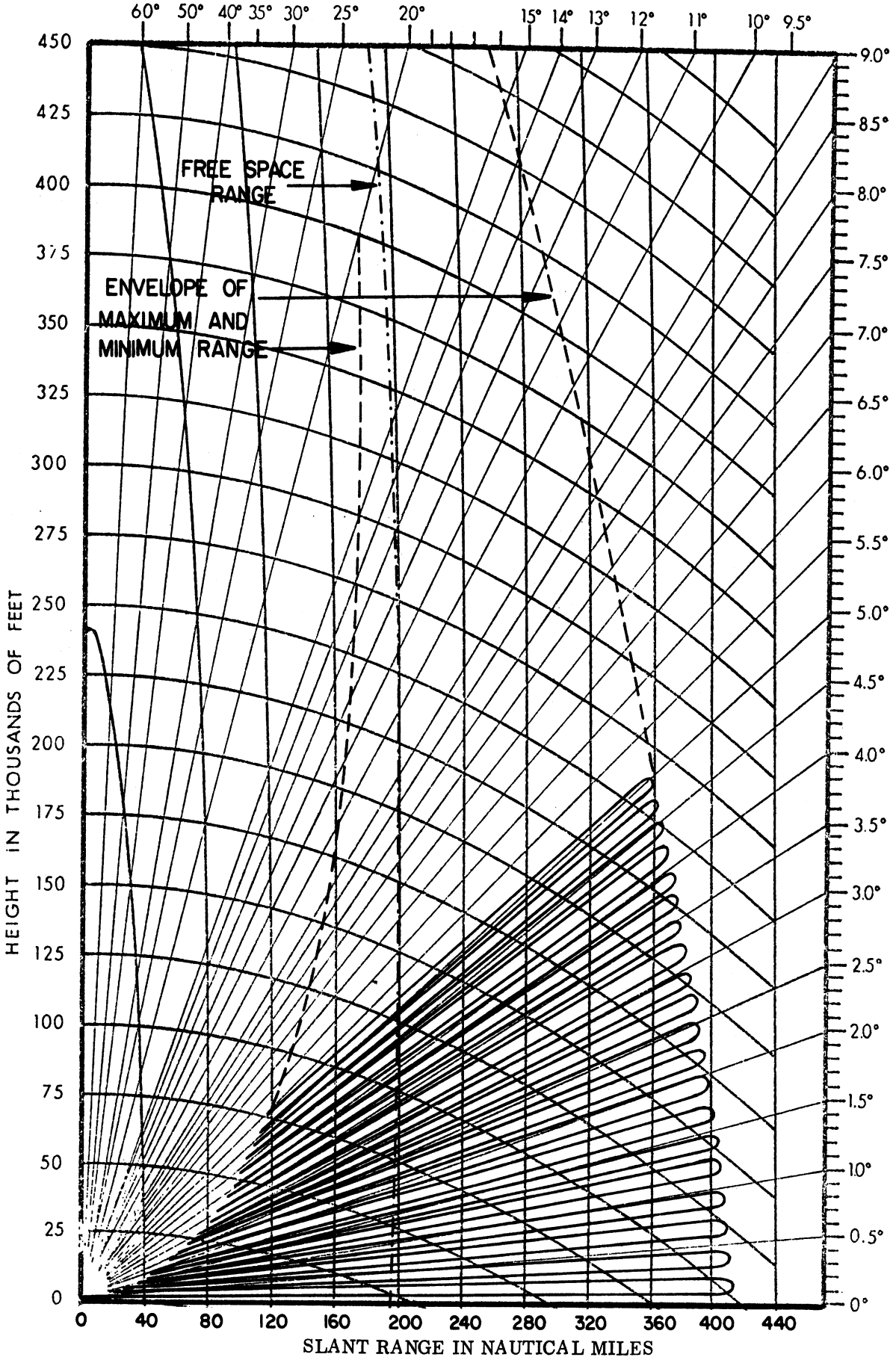

FIG. 51 a: Coverage diagram of the maximum envelope for the existing hog-trough antenna. H_d = 108', H_0 = 110', f = 1030 MHz.

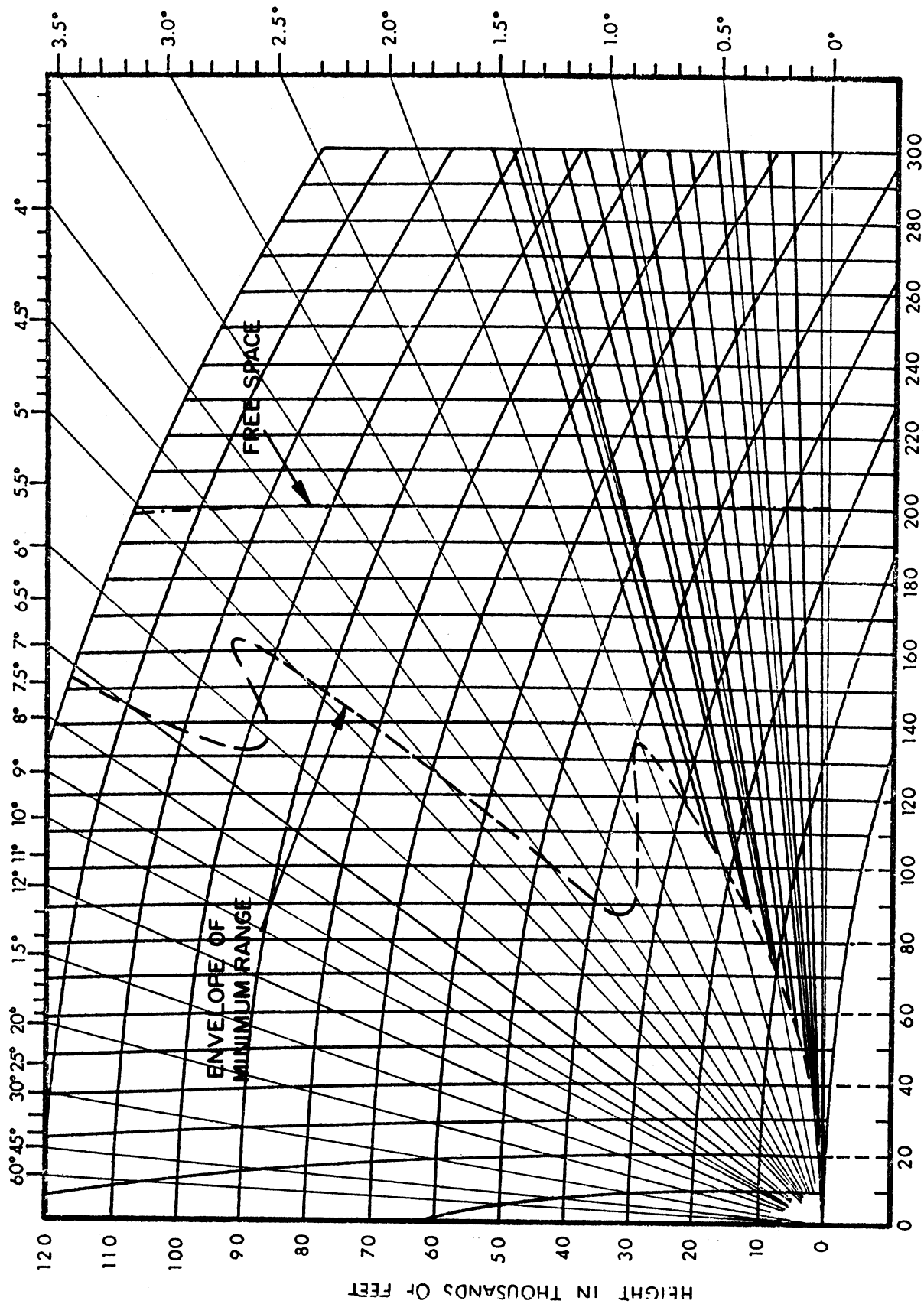

FIG. 51 b: Coverage diagram on expanded scale of the maximum envelope for the existing hog-trough antenna. H = 108', H = 110', f = 1030 MHz.

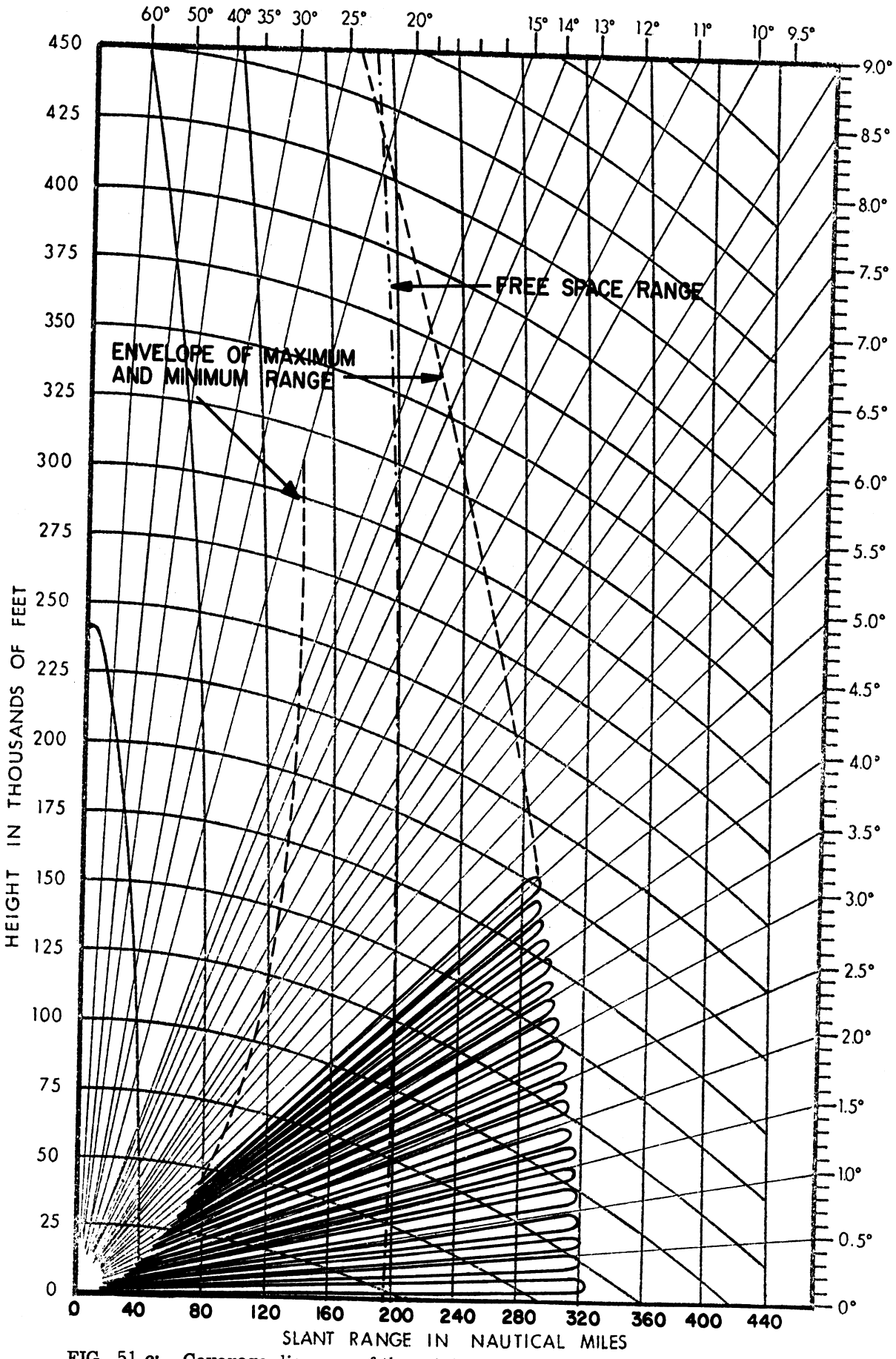

FIG. 51 c: Coverage diagram of the minimum envelope for the existing hog-trough antenna. $H_d = 108'$, $H_0 = 110'$, f = 1030 MHz.

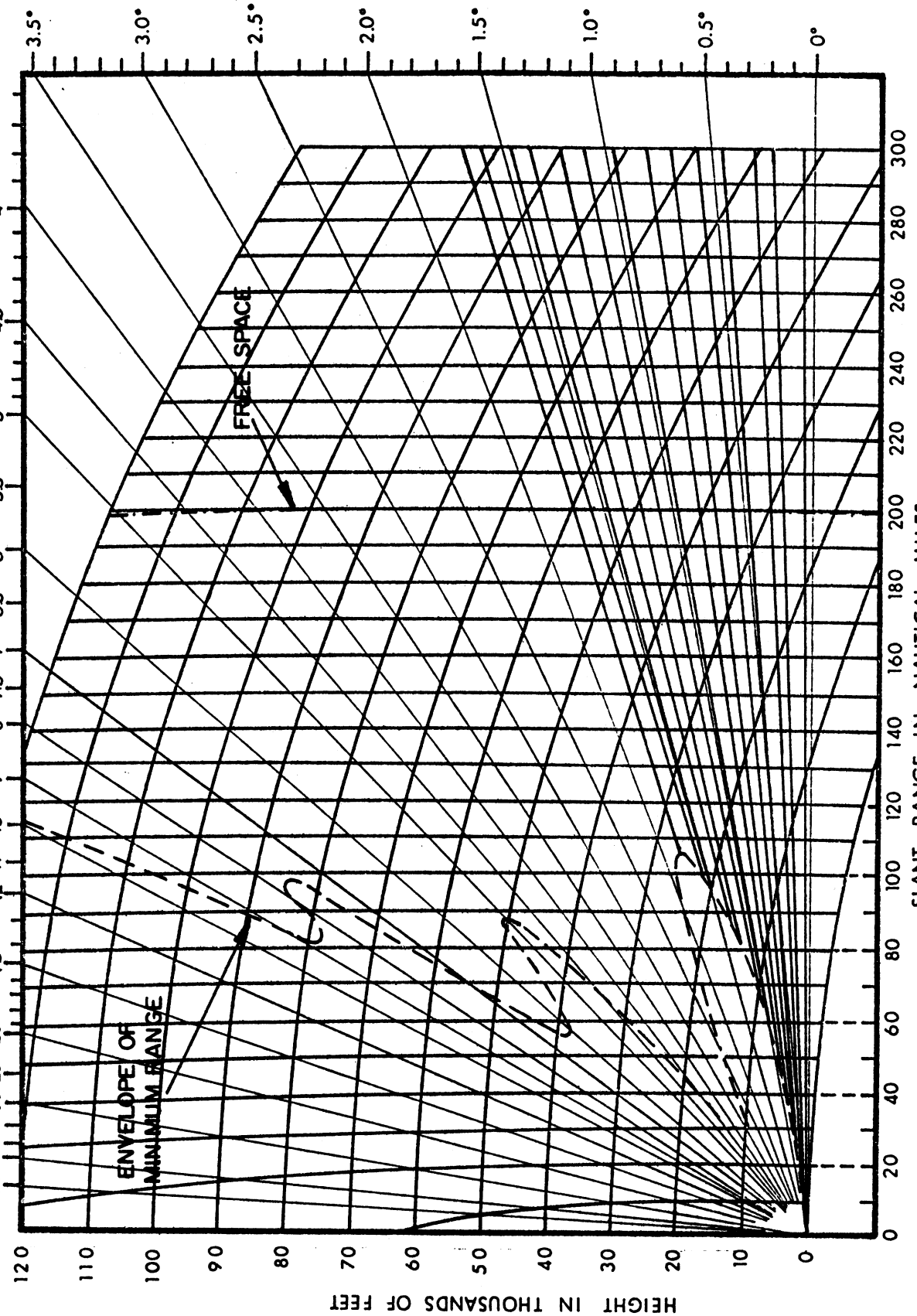

FIG. 51 d: Coverage diagram on expanded scale of the minimum envelope for the existing hog-trough antenna. $H_d = 108'$, $H_0 = 110'$, $f = 1030$ MHz.

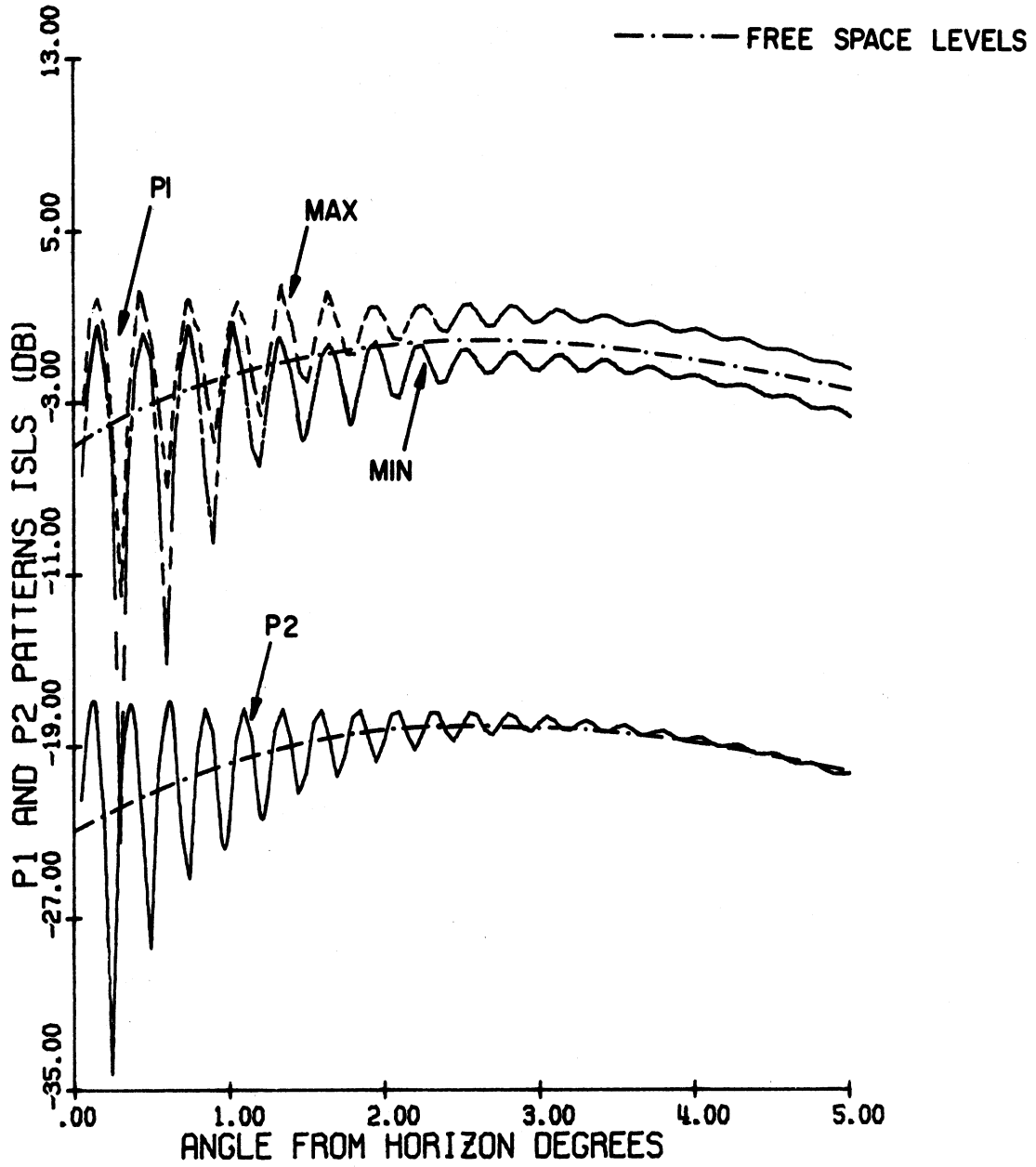

FIG. 52: $P1(\theta)_{MAX}$, $P1(\theta)_{MIN}$ and $P2(\theta)$ as functions of θ.

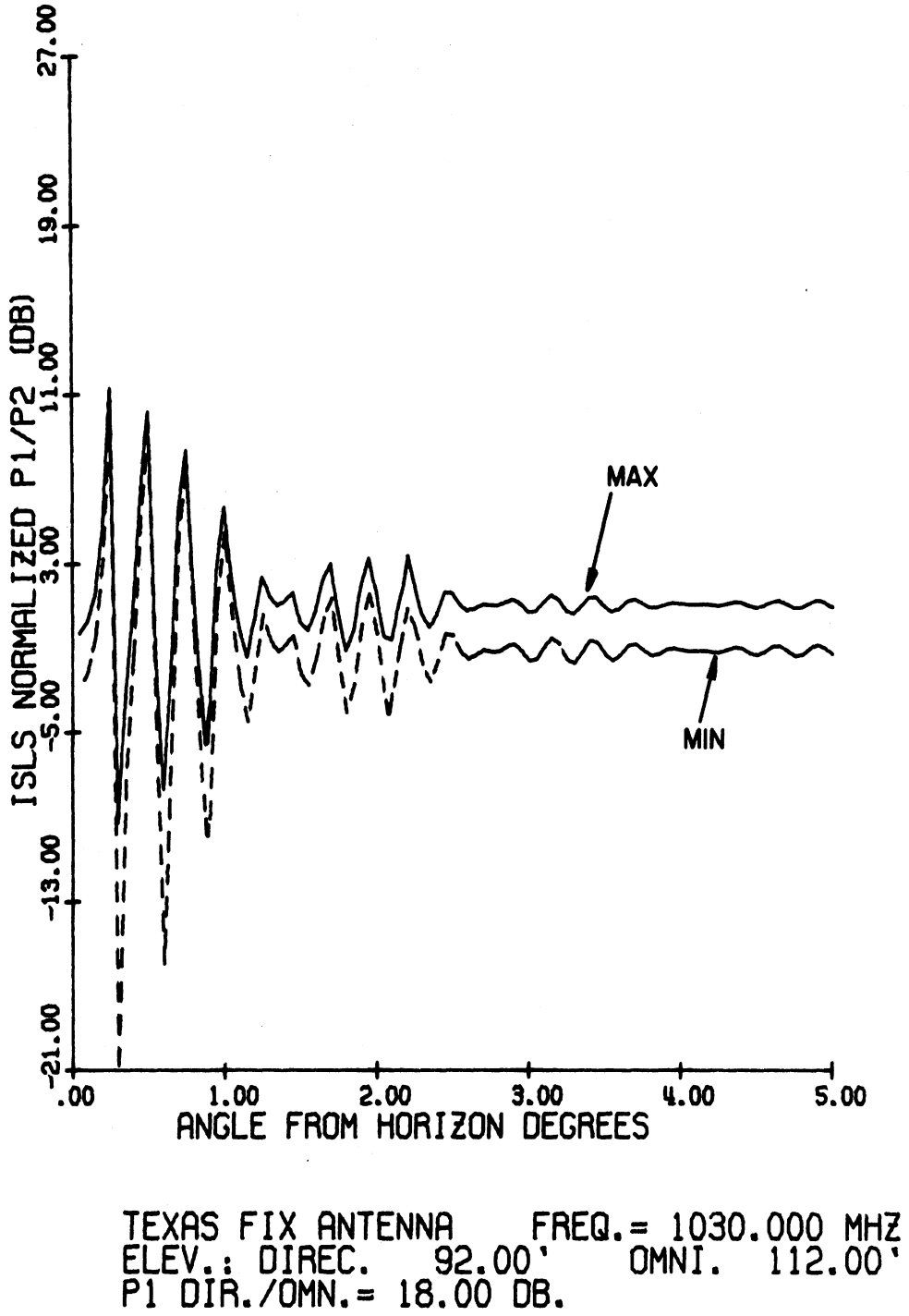

FIG. 53: Normalized pulse ratio envelopes as functions of θ.

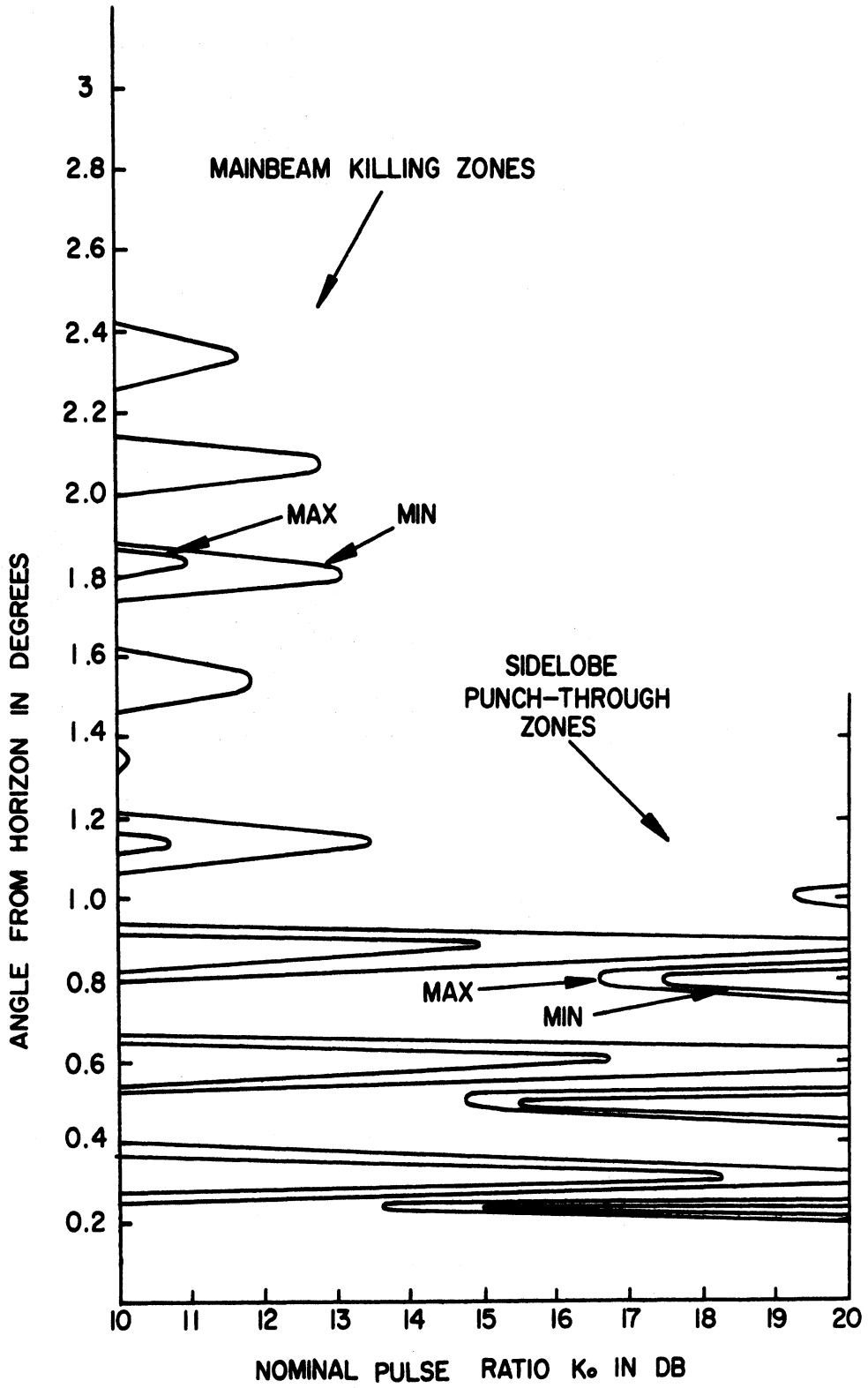

FIG. 54: Mainbeam killing and sidelobe punch-through zones as functions of the nominal pulse ratio for the Texas Instruments Fix antenna. H_d = 92', H_0 = 112', f = 1030 MHz, P1 DIR/OMNI = 18dB, a = 9dB, b = 0dB, L = -25dB.

The effective beamwidths $\alpha_{1MAX}(\theta)$, $\alpha_{1MIN}(\theta)$ as functions of θ are shown in Fig. 55. The beamwidths are obtained for K_0 = 18dB and a = 9dB. For $\theta > 2.5^o$, $\alpha_{1MAX}(\theta) \sim 3.1^o$ and $\alpha_{1MIN}(\theta) \sim 1.4^o$. The corresponding SLS mode value of the effective beamwidth for the same antenna is about 2.6^o.

The number of replies $N_{MAX}(\theta)$, $N_{MIN}(\theta)$ as functions of θ are shown in Fig. 56. For $\theta > 2.5^o$, $N_{MAX}(\theta) \sim 24$, $N_{MIN}(\theta) \sim 11$. For $\theta < 2.5^o$, $N_{MAX}(\theta)$ varies between 33 and 0, $N_{MIN}(\theta)$ varies between 25 and 0. For the same antenna, the saturation value of the number of replies in the SLS mode is about 20.

Figure 57 shows the coverage diagram for the antenna where the maximum free space range in the SLS case is adjusted to 200 nautical miles. It can be seen From Fig. 57 that for the maximum envelope case the maximum range of 250 nautical miles occurs at $\theta \sim 0.18^o$ and the minimum range of 50 nautical miles occurs at $\theta \sim 0.3^o$. The corresponding ranges for the minimum envelope case are found to be 200 and 15 nautical miles, respectively.

4.3.5 NADIF Fix I Antenna.

The heights above ground of the phase centers of the directional and omnidirectional antennas are H_d = 92' and H_0 = 112' respectively. The system uses the Texas Instruments omnidirectional antenna. The free space elevation plane patterns of the directional and omnidirectional antennas are assumed to be identical.

Figure 58 shows $P1(\theta)_{MAX}$, $P1(\theta)_{MIN}$ and $P2(\theta)$ as functions of θ where the 0dB level is adjusted to coincide with the maximum $P1(\theta)_{SLS}$ level in the free space case. For $\theta > 3^o$ the oscillations in the curves may be considered to be negligible.

Figure 59 shows the normalized maximum and minimum envelope pulse ratios as functions of θ. For $\theta > 2.5^o$ the oscillations in the curves may be considered negligible.

Figure 60 shows the main beam killing and sidelobe punch-through zones as functions of the nominal pulse ratio. For K_0 = 18dB, a = 9dB and b = 0dB, there are 3 main beam killing zones and 2 sidelobe punch-through zones in the range of θ shown.

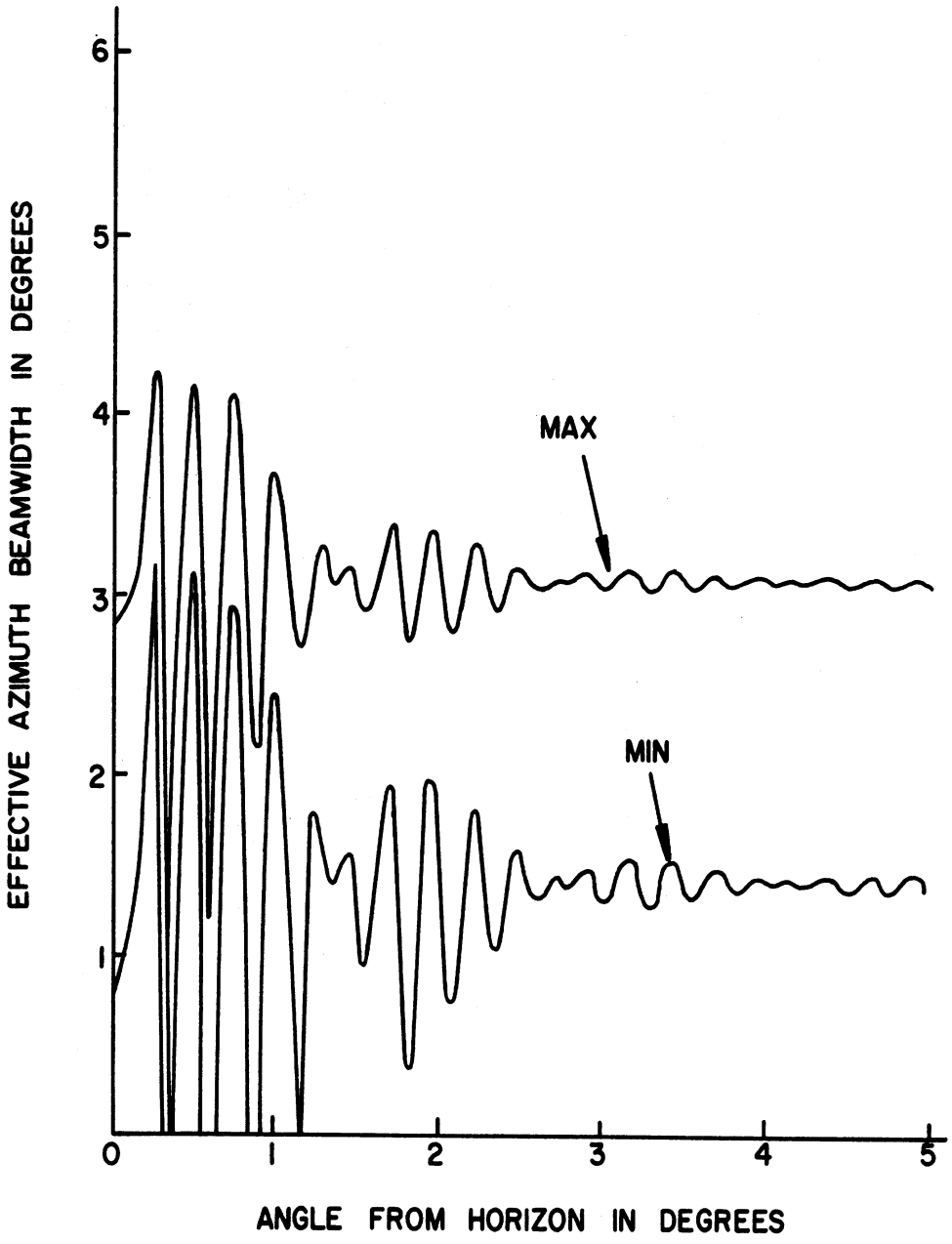

FIG. 55: Effective azimuth beamwidths as functions of the angle from the horizon for the Texas Instruments Fix antenna. H_d = 92', H_0 = 112', f = 1030 MHz, nominal pulse ratio K_0 = 18dB, P1 DIR/OMNI = 18dB.

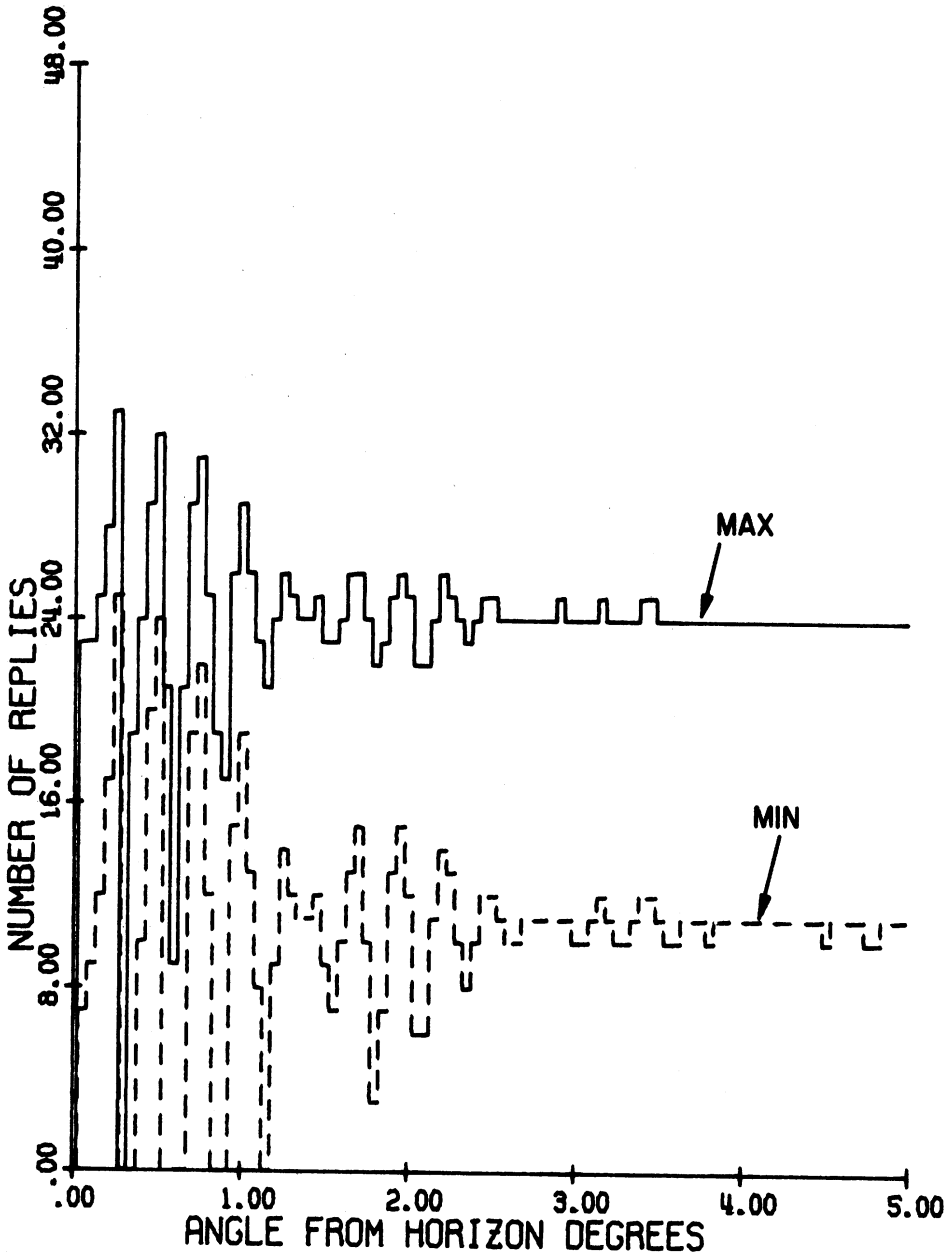

TEXAS FIX ANTENNA FREQ.= 1030.000 MHZ
ELEV.: DIREC. 92.00' OMNI. 112.00'
P1/P2= 18.00 DB P1 DIR./OMN.= 18.00 DB.

FIG. 56: Number of replies as functions of angle from the horizon.

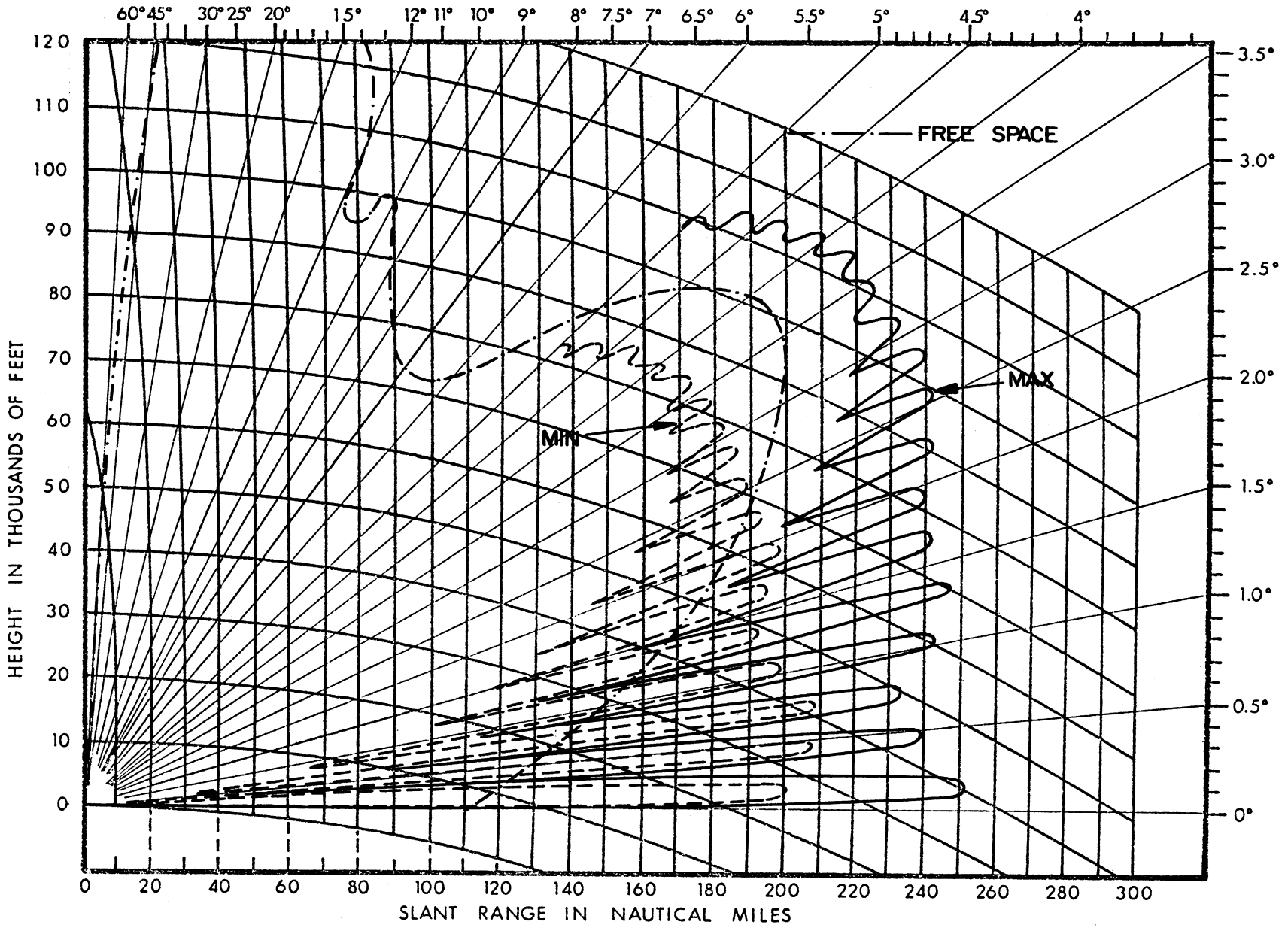

FIG. 57: Coverage diagram for the Texas Instruments Fix antenna: H_d = 108', H_0 = 112', f = 1030 MHz.

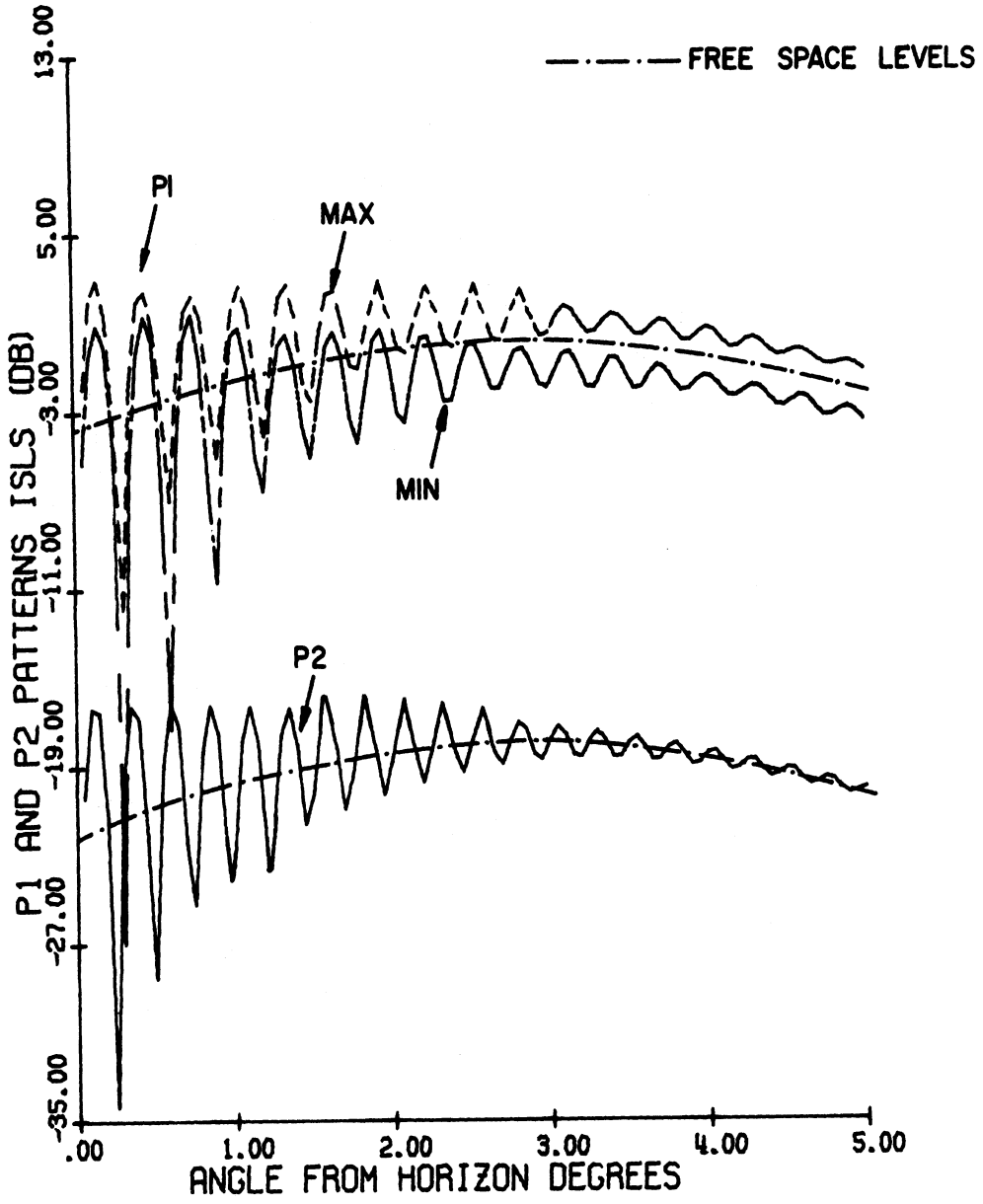

FIG. 58: $P1(\theta)_{MAX}$, $P1(\theta)_{MIN}$ and $P2(\theta)$ as functions of θ.

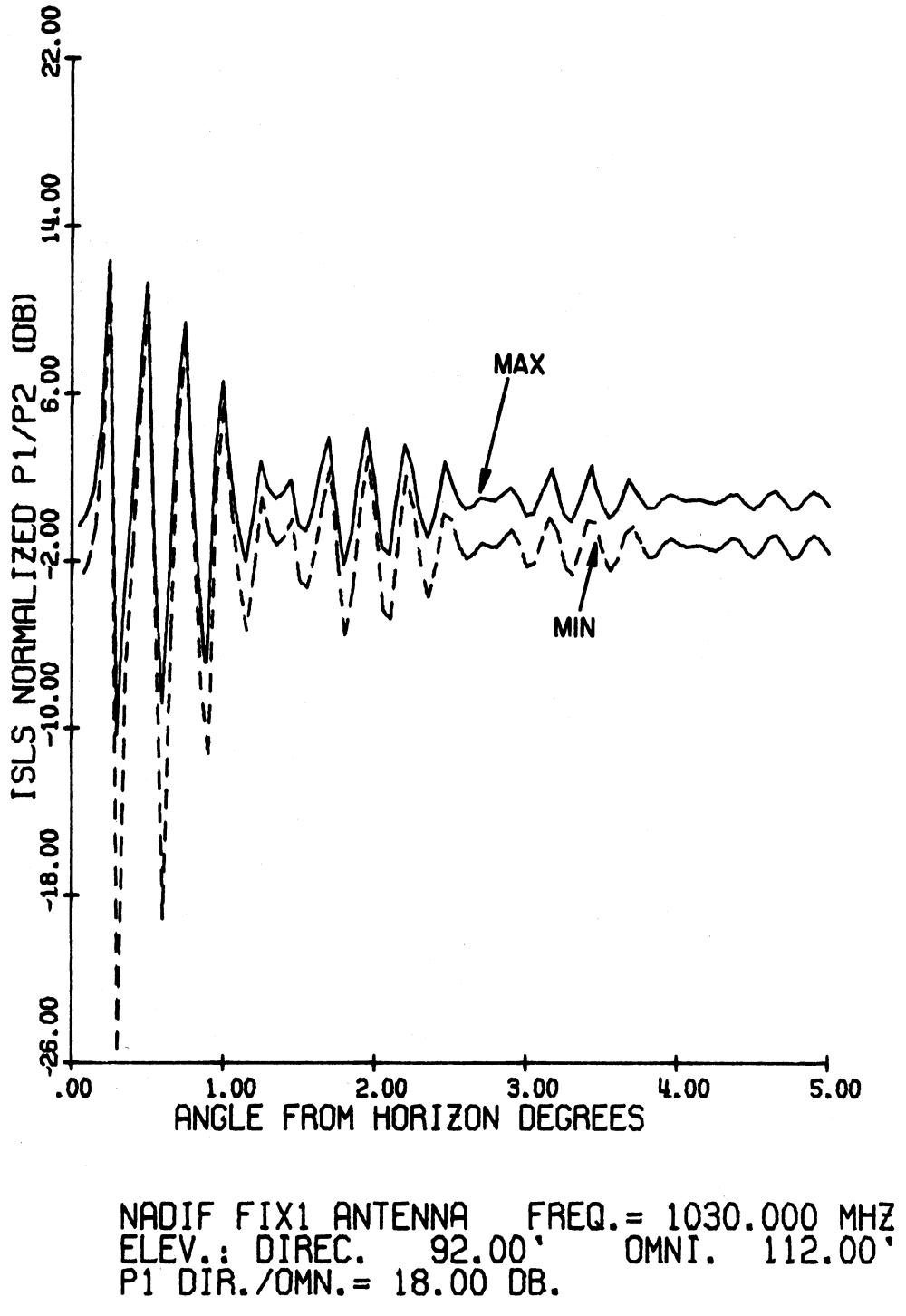

FIG. 59: Normalized pulse ratio envelopes as functions of θ.

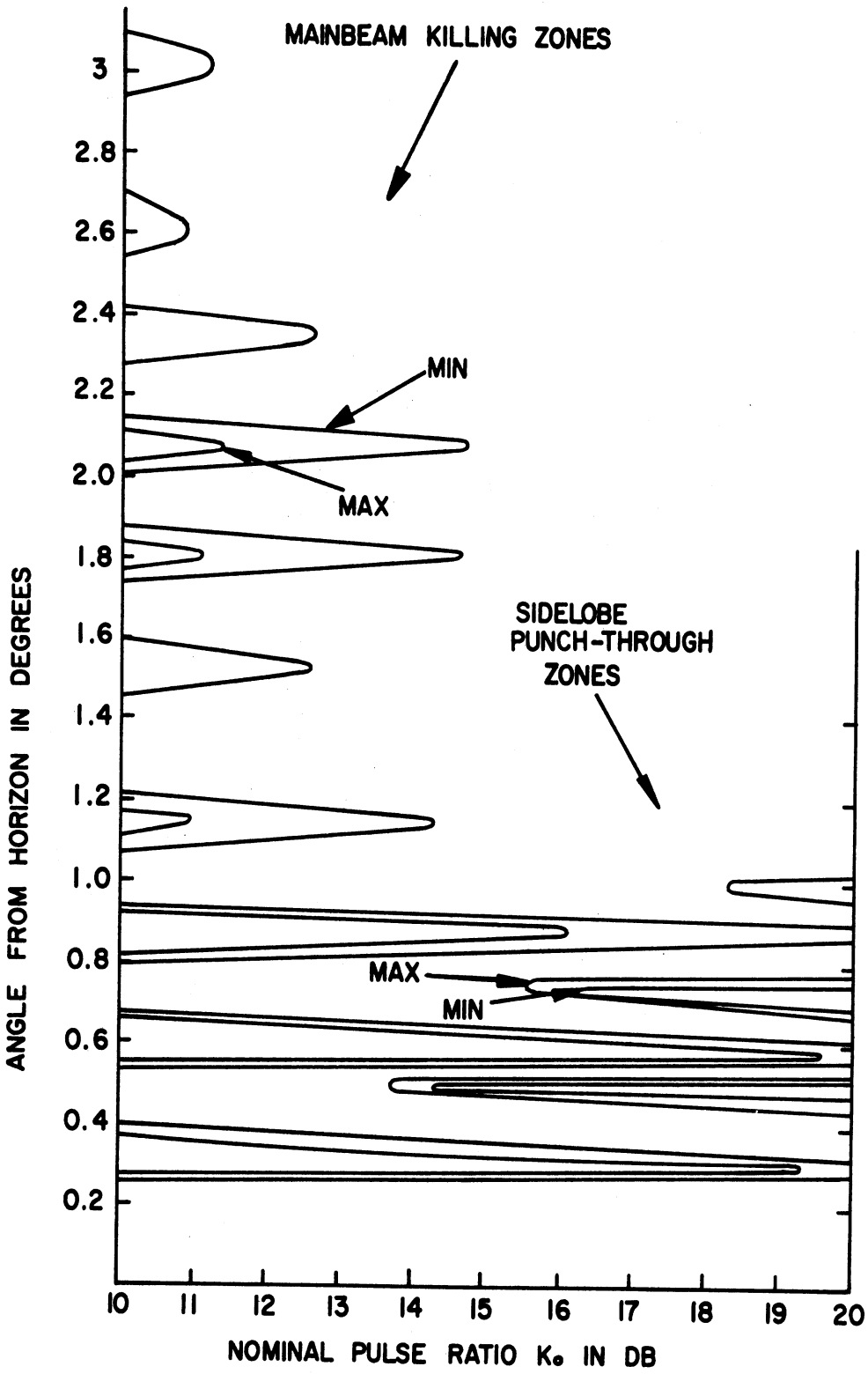

FIG. 60: Mainbeam killing and sidelobe punch-through zones as functions of nominal pulse ratio for NADIF Fix I antenna. H_d = 92', H_0 = 112', f = 1030 MHz, P1 DIR/OMNI = 18dB, a = 9dB, b = 0dB, L = -25dB.

The effective beamwidth $\alpha_{1MAX}(\theta)$, $\alpha_{1MIN}(\theta)$ as functions of θ for the threshold level a = 9dB and nominal pulse ratio K_0 = 18dB are shown in Fig. 61. For $\theta > 2.5^o$, $\alpha_{1MAX}(\theta) \sim 3.1^o$ and $\alpha_{1MIN}(\theta) \sim 1.4^o$. The corresponding SLS mode value of the effective beamwidth for the same antenna is about 2.6^o.

The number of replies $N_{MAX}(\theta)$, $N_{MIN}(\theta)$ as functions of θ are shown in Fig. 62. For $\theta > 2.5^o$, $N_{MAX}(\theta) \sim 24$ and $N_{MIN}(\theta) \sim 10$. For $\theta < 2.5^o$, $N_{MAX}(\theta)$ varies between 35 and 0, $N_{MIN}(\theta)$ varies between 27 and 0. The saturation value of the number of replies is about 20 for the same antenna in the SLS case.

Figure 63 shows the coverage diagram for the antenna where the maximum free space range in the SLS case is adjusted to be 200 nautical miles. It can be seen from the figure that for the maximum envelope case the maximum range of 280 nautical miles occurs at $\theta \sim 0.18$ and the minimum range of 50 nautical miles occurs at $\theta \sim 0.3^o$. The corresponding ranges for the minimum envelope case are 220 and 15 nautical miles respectively.

4.3.6. NADIF Fix II Antenna.

The heights above ground of the phase centers of the directional and omnidirectional antennas are H_d = 92' and H_0 = 111' respectively. It uses the same directional antenna as NADIF Fix I. The omnidirectional antenna used is the Westinghouse omni. Thus the free space elevation plane patterns of the two antennas are not identical.

Figure 64 shows $P1(\theta)_{MAX}$, $P1(\theta)_{MIN}$ and $P2(\theta)$ as functions of θ where the 0dB level is adjusted to coincide with the maximum $P1(\theta)_{SLS}$ level in the free space case. For $\theta > 3^o$ the oscillations in the curves may be neglected.

Figure 65 shows the normalized maximum and minimum envelope pulse ratios as functions of θ. For $\theta > 2.5^o$ the oscillations in the curves may be considered negligible.

Figure 66 shows the main beam killing and sidelobe punch-through zones as functions of the nominal pulse ratio. For K_0 = 18dB, a = 9dB and b = 0dB, there are 1 main beam killing zone and 3 sidelobe punch-through zones in the range of θ shown.

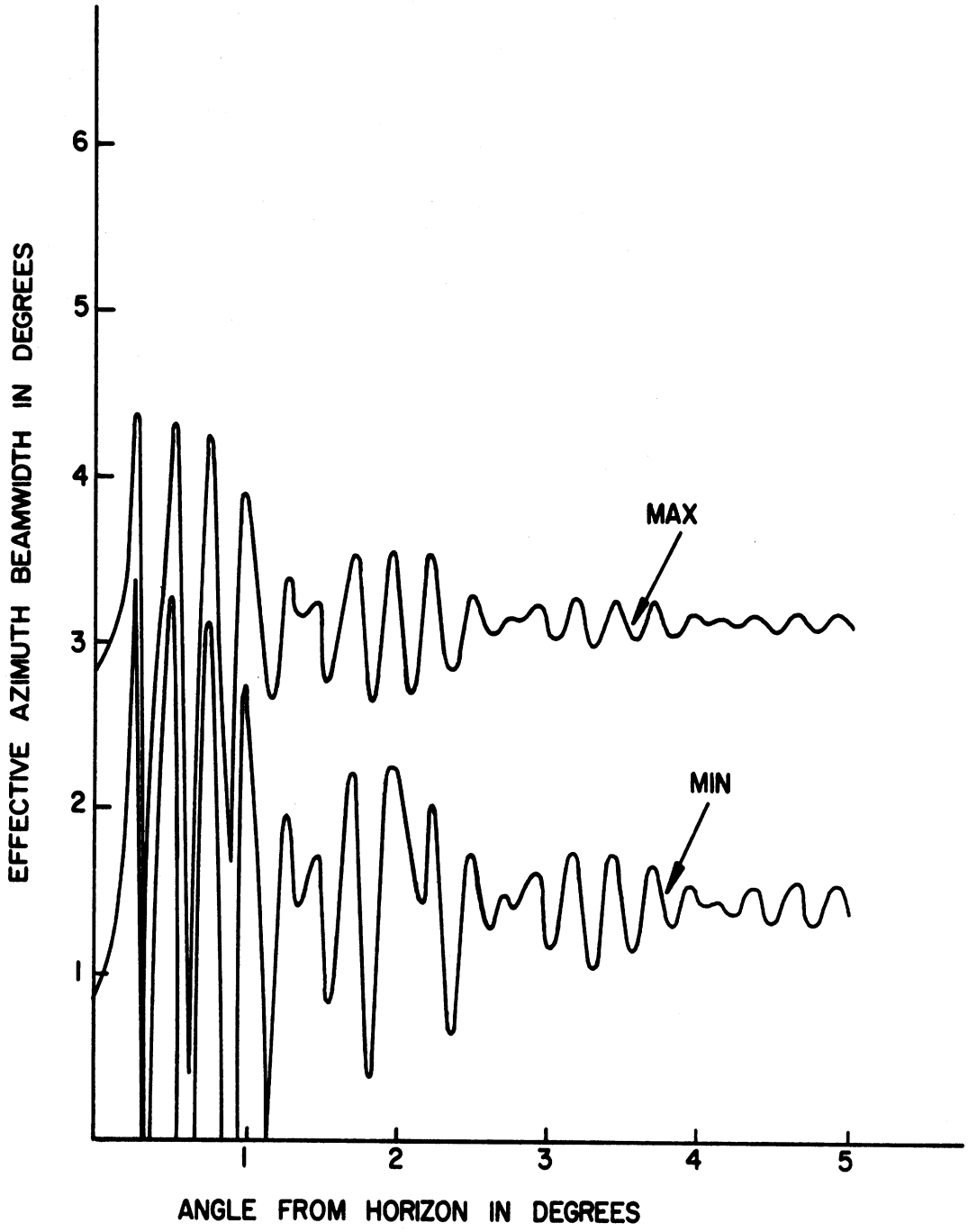

FIG. 61: Effective azimuth beamwidths as functions of the angle from the horizon for the NADIF Fix I antenna. H_d = 92', H_0 = 112', f = 1030 MHz, nominal pulse ratio K_0 = 18dB, P1 DIR/OMNI = 18dB.

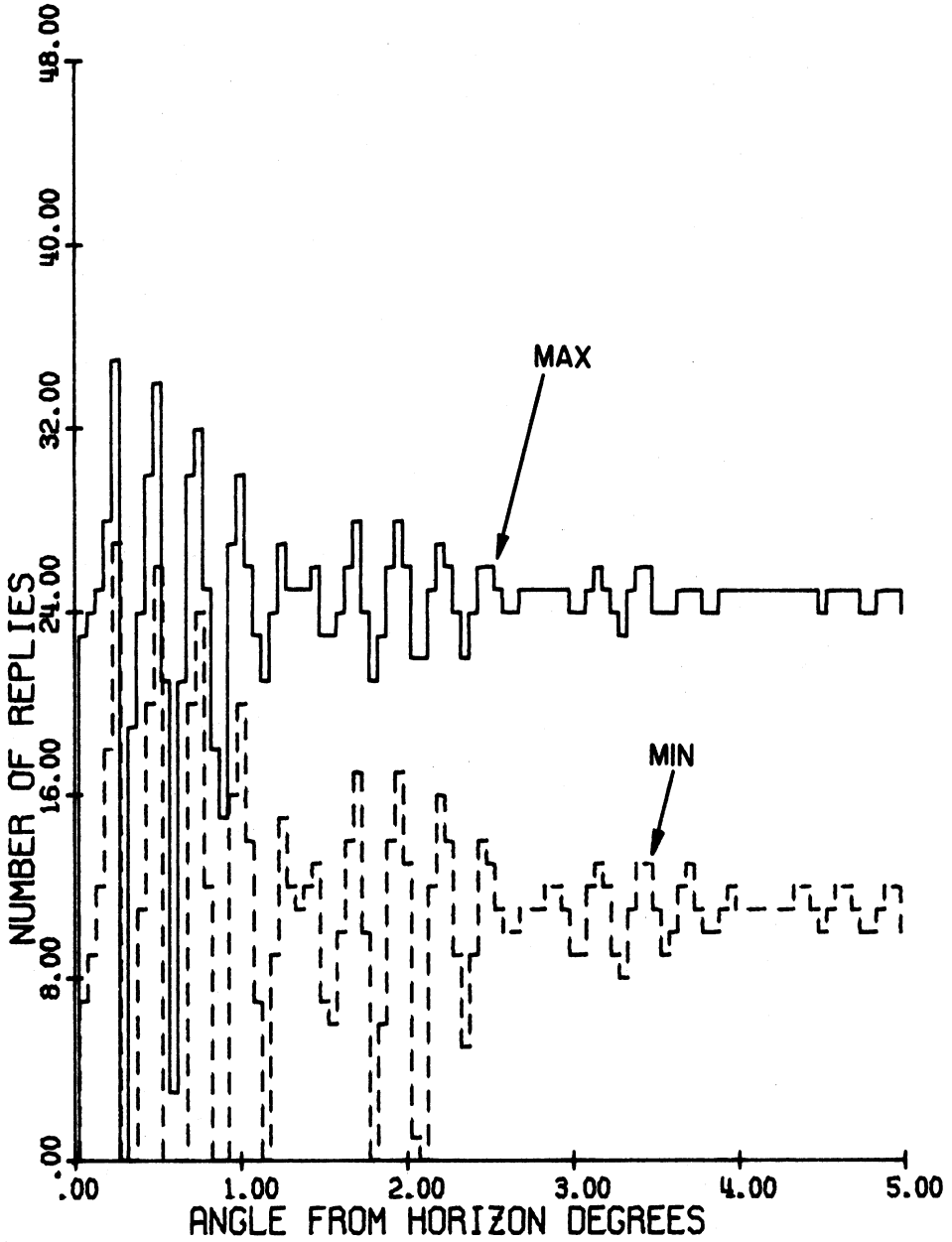

FIG. 62: Number of replies as functions of angle from the horizon.

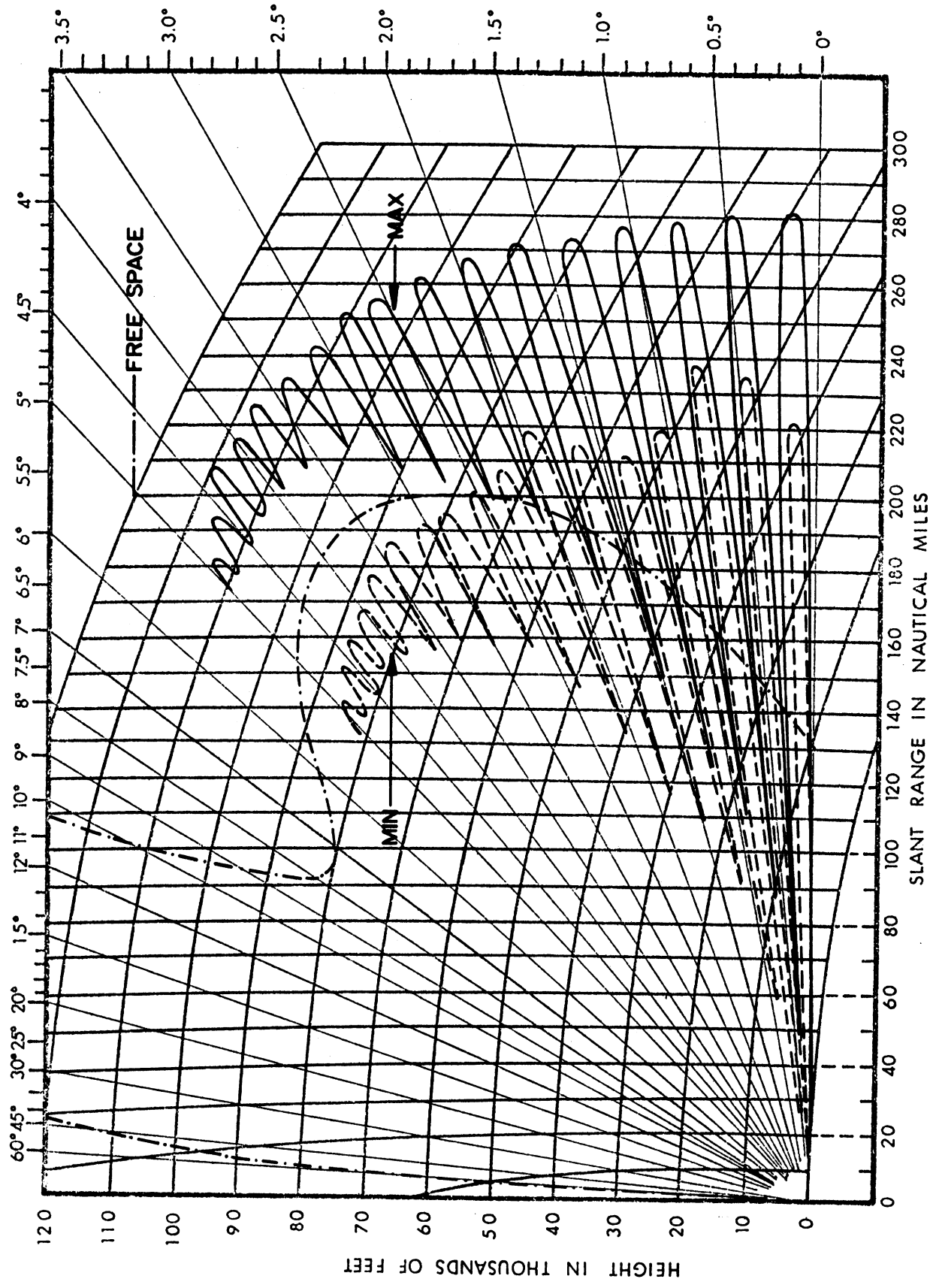

FIG. 63: Coverage diagram for NADIF Fix I, II, and III antennas. H = 92', f = 1030 MHz.

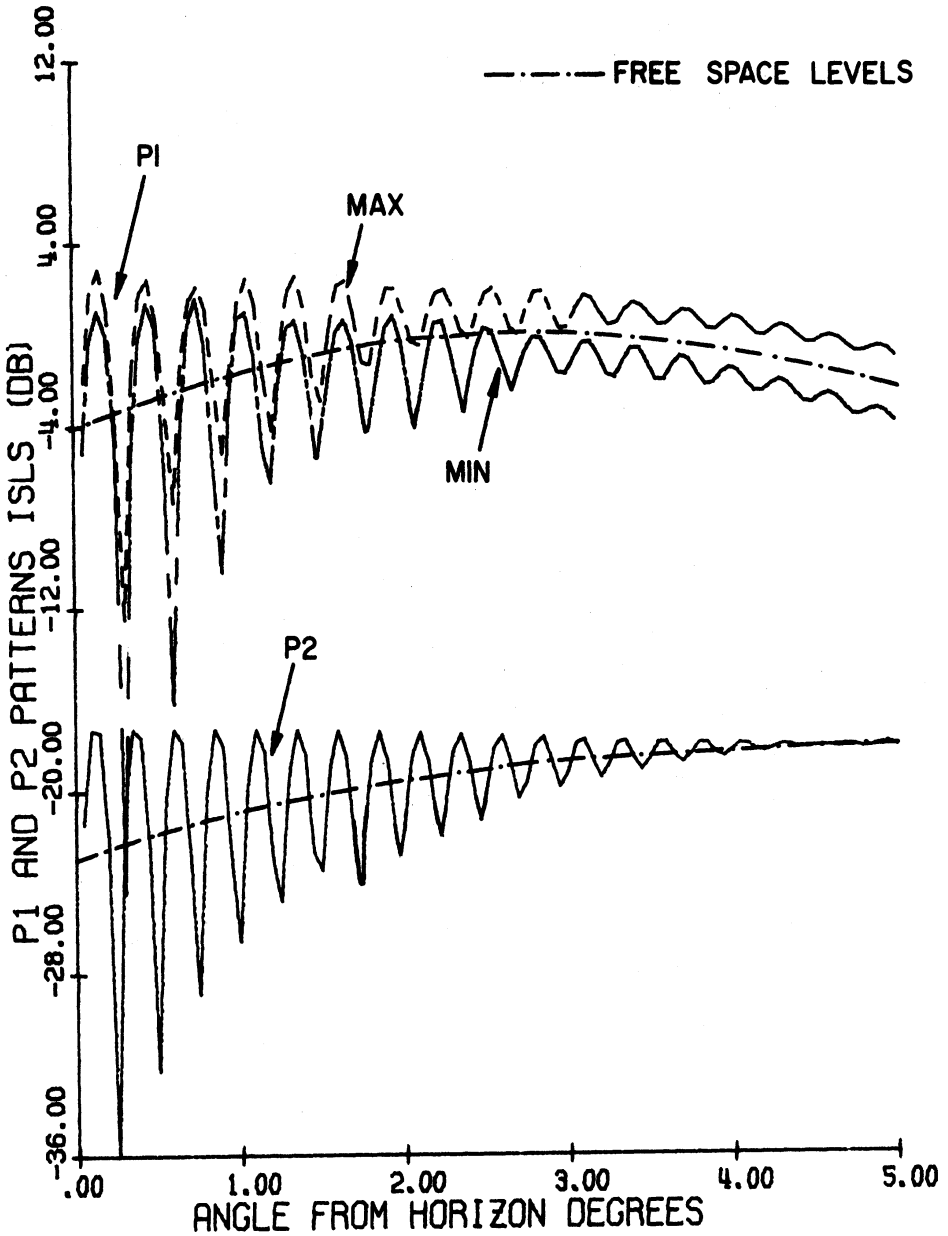

FIG. 64: $P1(\theta)_{MAX}$, $P1(\theta)_{MIN}$ and $P2(\theta)$ as functions of θ.

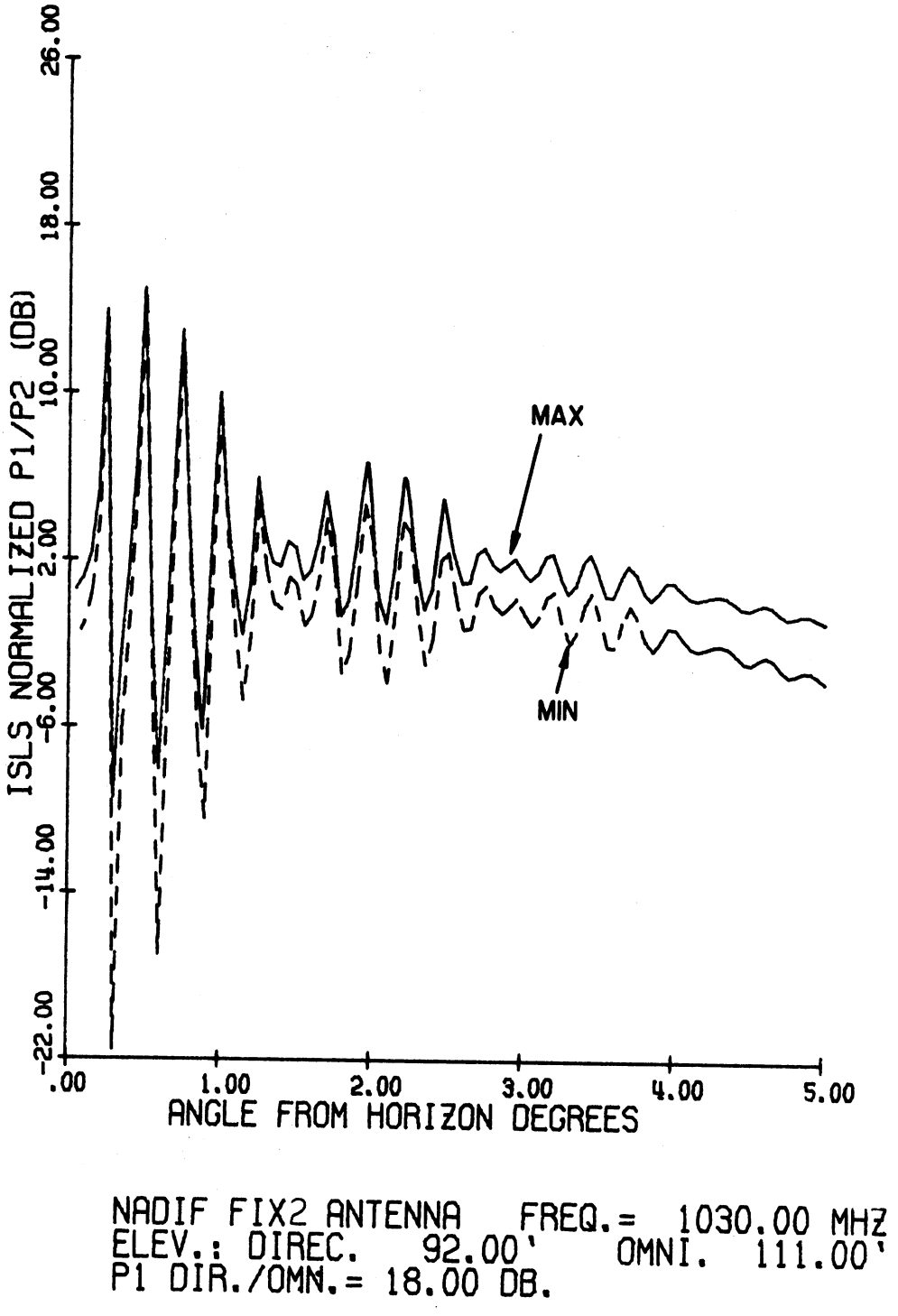

FIG. 65: Normalized pulse ratio envelopes as functions of θ.

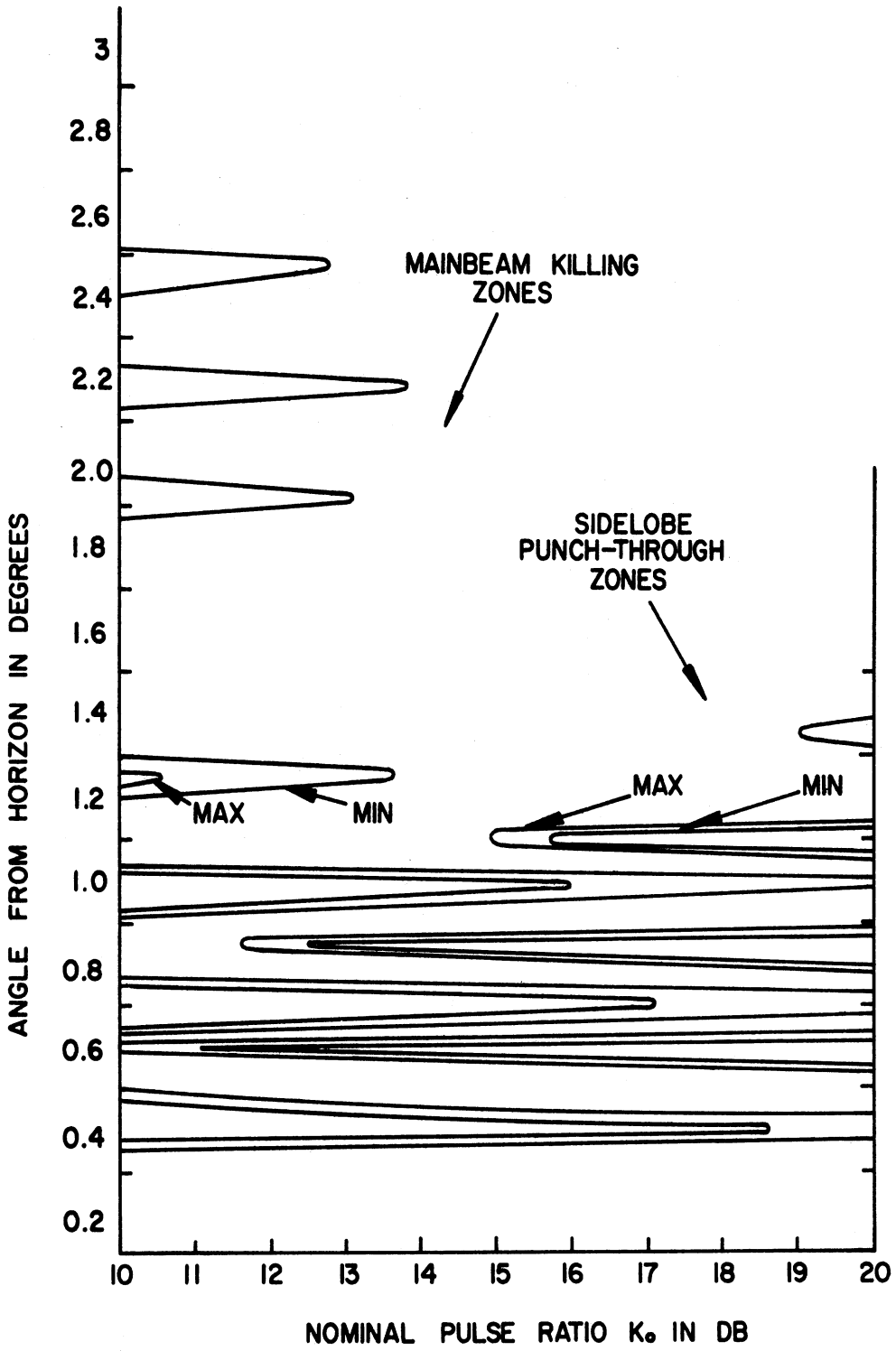

FIG. 66: Mainbeam killing and sidelobe punch-through zones as functions of the nominal pulse ratio for NADIF Fix II antenna. H_d = 92', H_0 = 111', f = 1030 MHz, P1 DIR/OMNI = 18dB, a = 9dB, b = 0dB, L = -25dB.

The effective azimuth beam widths $\alpha_{1MAX}(\theta)$, $\alpha_{1MIN}(\theta)$ as functions of θ for the threshold level a = 9dB and nominal pulse ratio K_0 = 18dB are shown in Fig. 67. For $\theta > 2.5^0$, $\alpha_{1MAX}(\theta) \sim 3^0$, $\alpha_{1MIN}(\theta) \sim 1^0$.

The number of replies $N_{MAX}(\theta)$, $N_{MIN}(\theta)$ as functions of θ are shown in Fig. 68. For $\theta > 2.5$, $N_{MAX}(\theta)$ 22, $N_{MIN}(\theta)$ does not assume a constant value in the range of θ shown in Fig. 68. For $\theta < 2.5^0$, $N_{MAX}(\theta)$ varies between 36 and 0. $N_{MIN}(\theta)$ is found to vary between 28 and 0. The saturation value of the number of replies is about 17 for the same antenna operating in the SLS mode.

The coverage diagram of the antenna is the same as the NADIF Fix I, and is given by Fig. 63.

4.3.7. NADIF Fix III Antenna.

The heights above ground of the phase centers of the directional and omnidirectional antennas are H_d = 92' and H_0 = 110', respectively. It uses the existing small aperture omnidirectional antenna. The free space elevation plane patterns of the directional and omnidirectional antennas are not identical.

Figure 69 shows $P1(\theta)_{MAX}$, $P1(\theta)_{MIN}$ and $P2(\theta)$ as functions of θ, where the 0dB level is adjusted to coincide with the maximum $P1(\theta)_{SLS}$ level in the free space case. For $\theta > 2.5^0$, the oscillations in the $P1(\theta)_{MAX}$, $P1(\theta)_{MIN}$ may be neglected. However, due to the small vertical aperture of the omni antenna, the fluctuations in the $P2(\theta)$ pulse are appreciable throughout the range of θ shown.

Figure 70 shows the normalized maximum and minimum envelop pulse ratios as functions of θ. The oscillations in the curves persist throughout the range of θ shown in Fig. 70.

Figures 71 a and b show the main beam killing and sidelobe punch-through zones as functions of the nominal pulse ratio. For K_0 = 18dB, a = 9dB and b = 0dB, there are 10 main beam killing zones and 12 sidelobe punch-through zones in the range of θ

The effective azimuth beamwidths $\alpha_{1MAX}(\theta)$, $\alpha_{1MIN}(\theta)$ as functions of θ for the threshold level a = 9dB and the nominal pulse ratio K_0 = 18dB are shown in Fig. 72. For $\theta > 10^0$, $\alpha_{1MAX}(\theta) \sim 3.5^0$ and $\alpha_{1MIN}(\theta) \sim 2.2^0$. The corresponding SLS mode saturation value of the effective beamwidth for the same antenna is about 3.1^0.

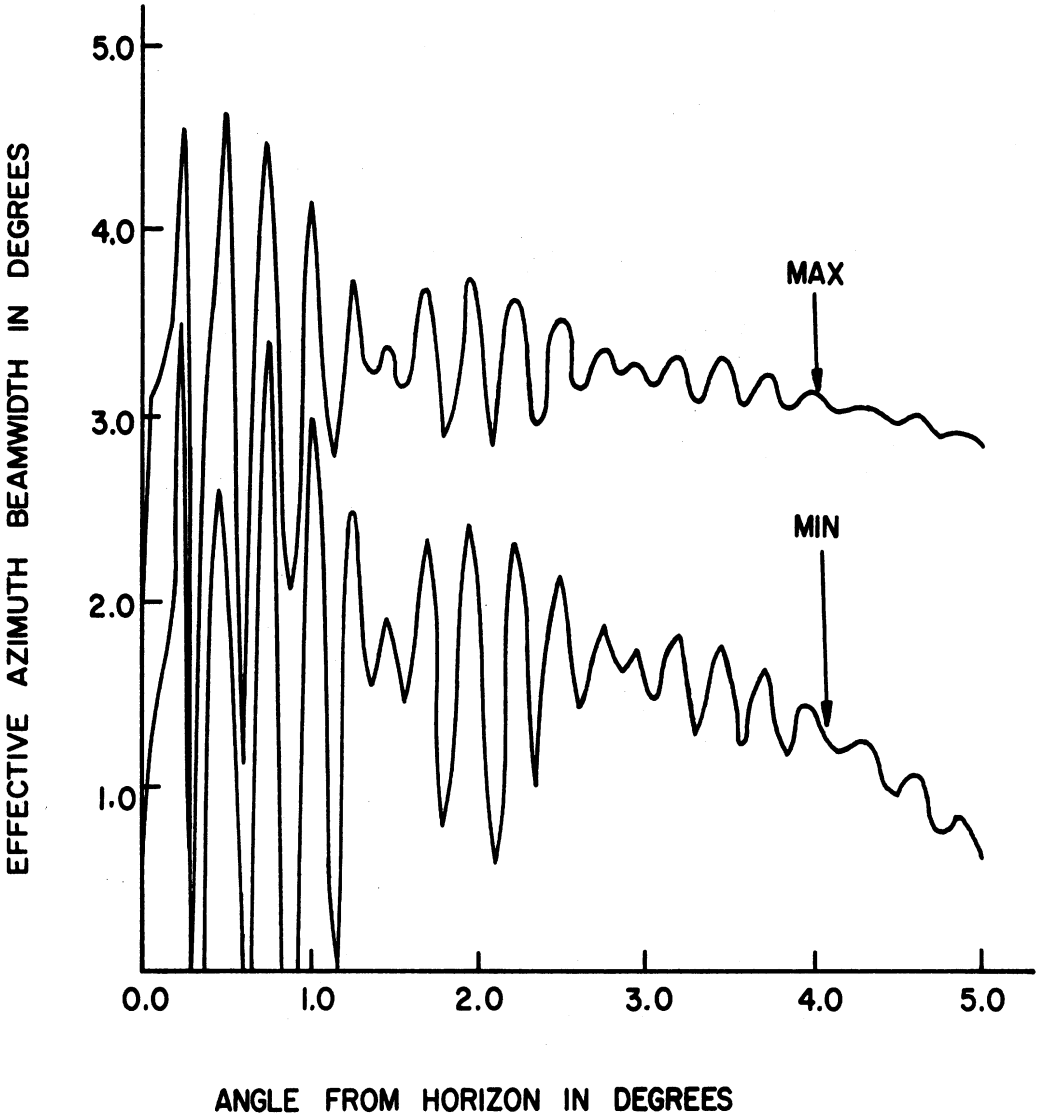

FIG. 67: Effective azimuth beamwidths as functions of angle from the horizon for NADIF Fix II antenna. H_d = 92', H_0 = 110', f = 1030 MHz, nominal pulse ratio K_0 = 18dB, P1 DIR/OMNI = 18dB.

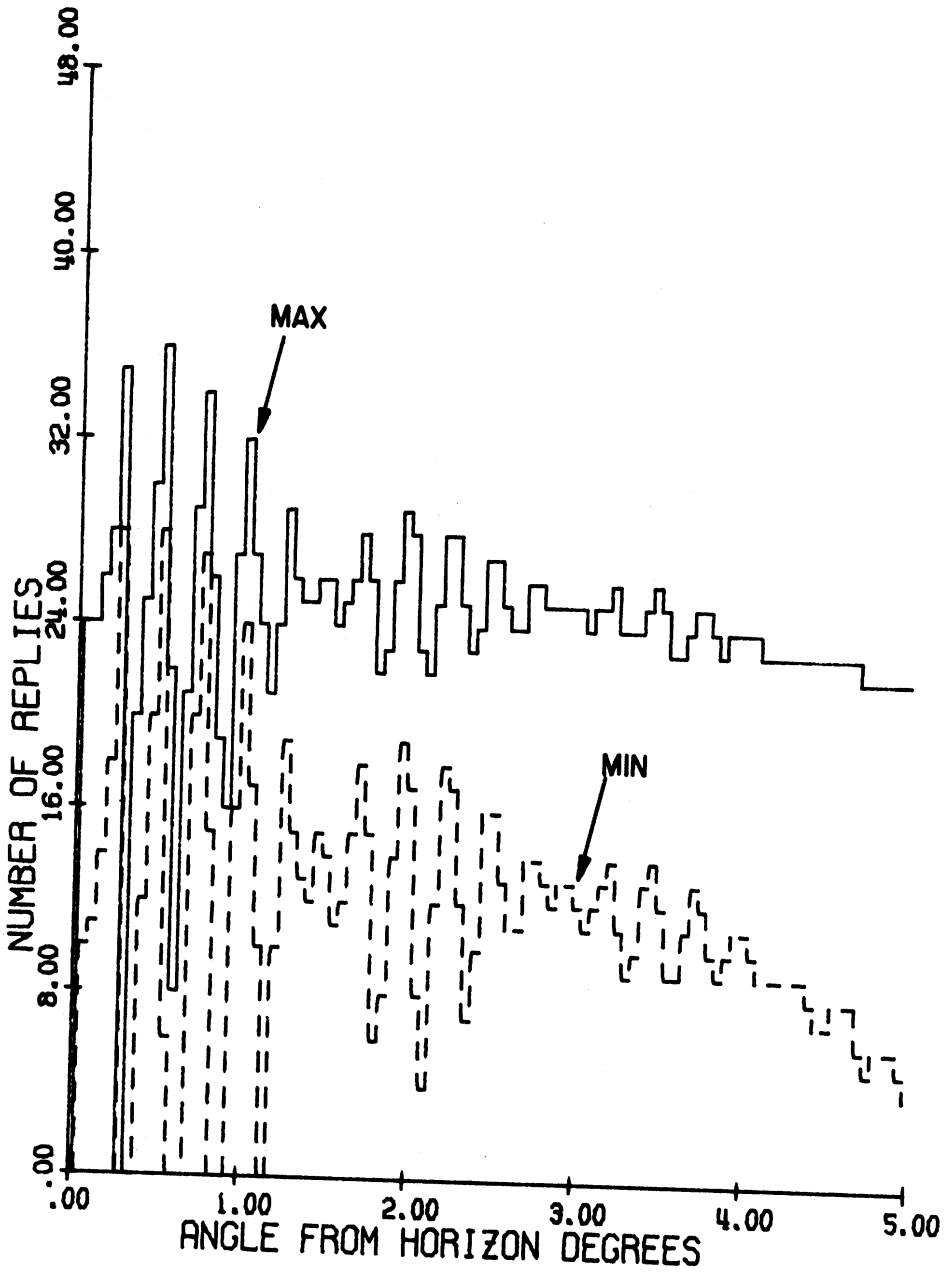

FIG. 68: Number of replies as functions of angle from the horizon.

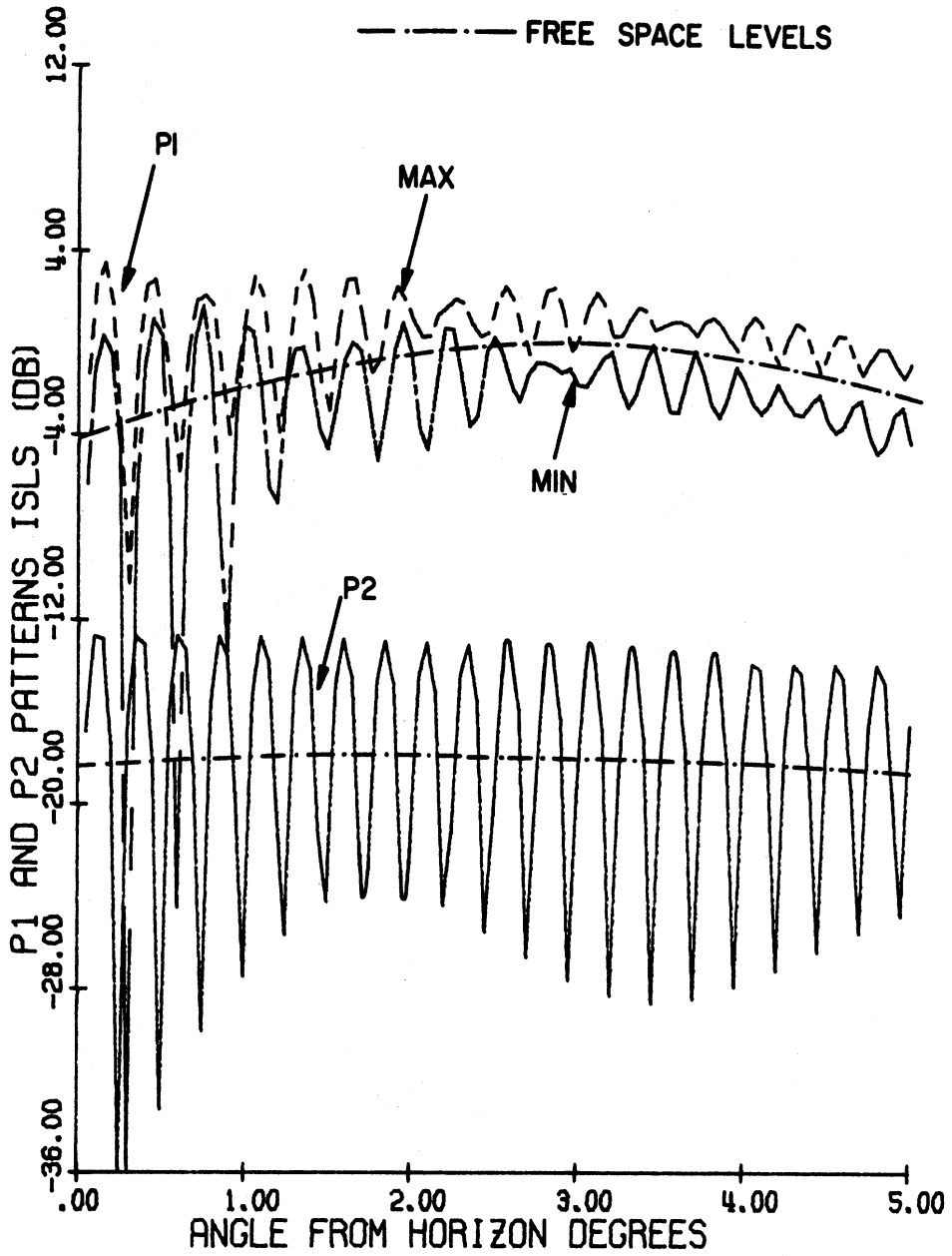

FIG. 69: $P1(\theta)_{MAX}$, $P1(\theta)_{MIN}$ and $P2(\theta)$ as functions of θ.

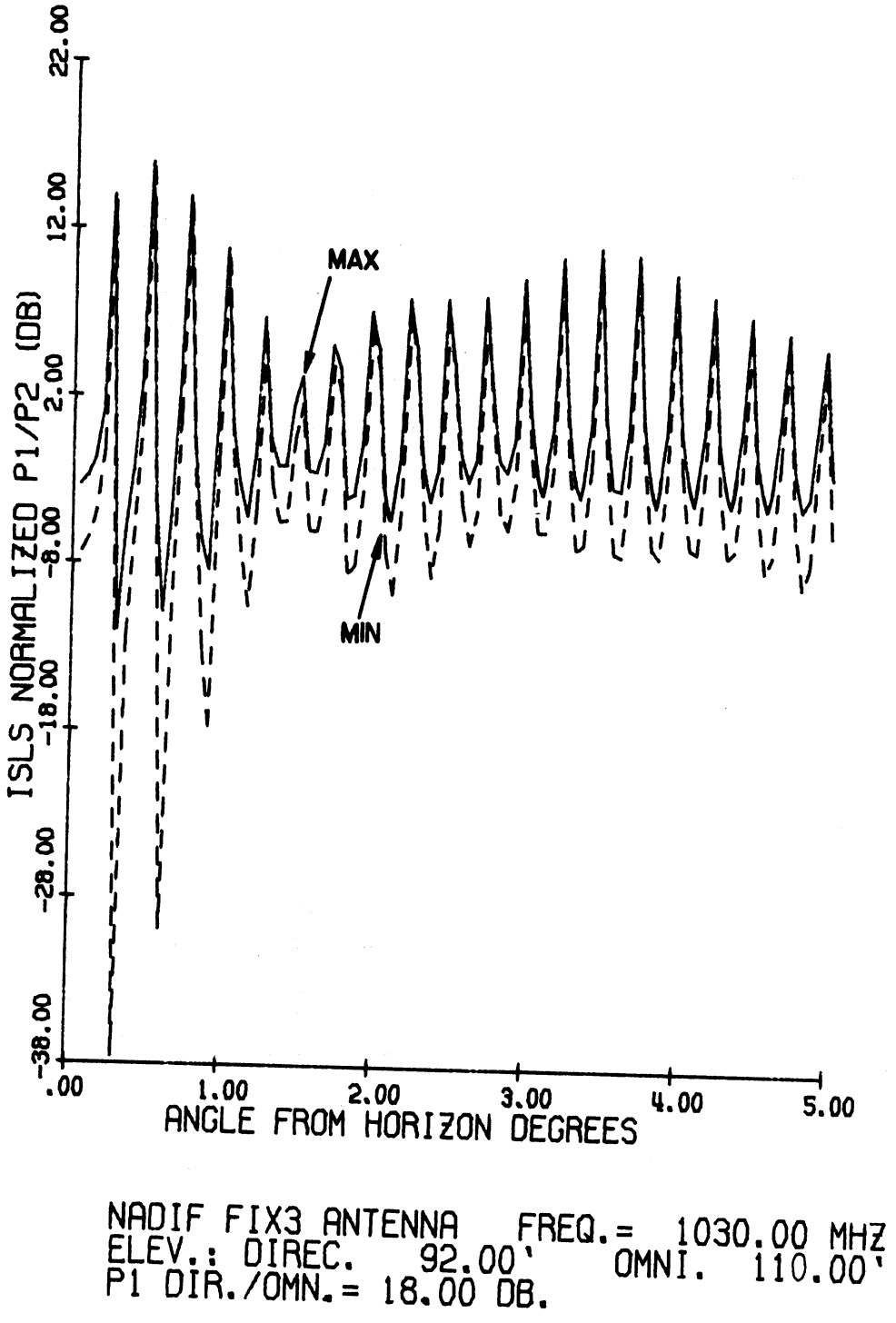

FIG. 70: Normalized pulse ratio envelopes as functions of θ.

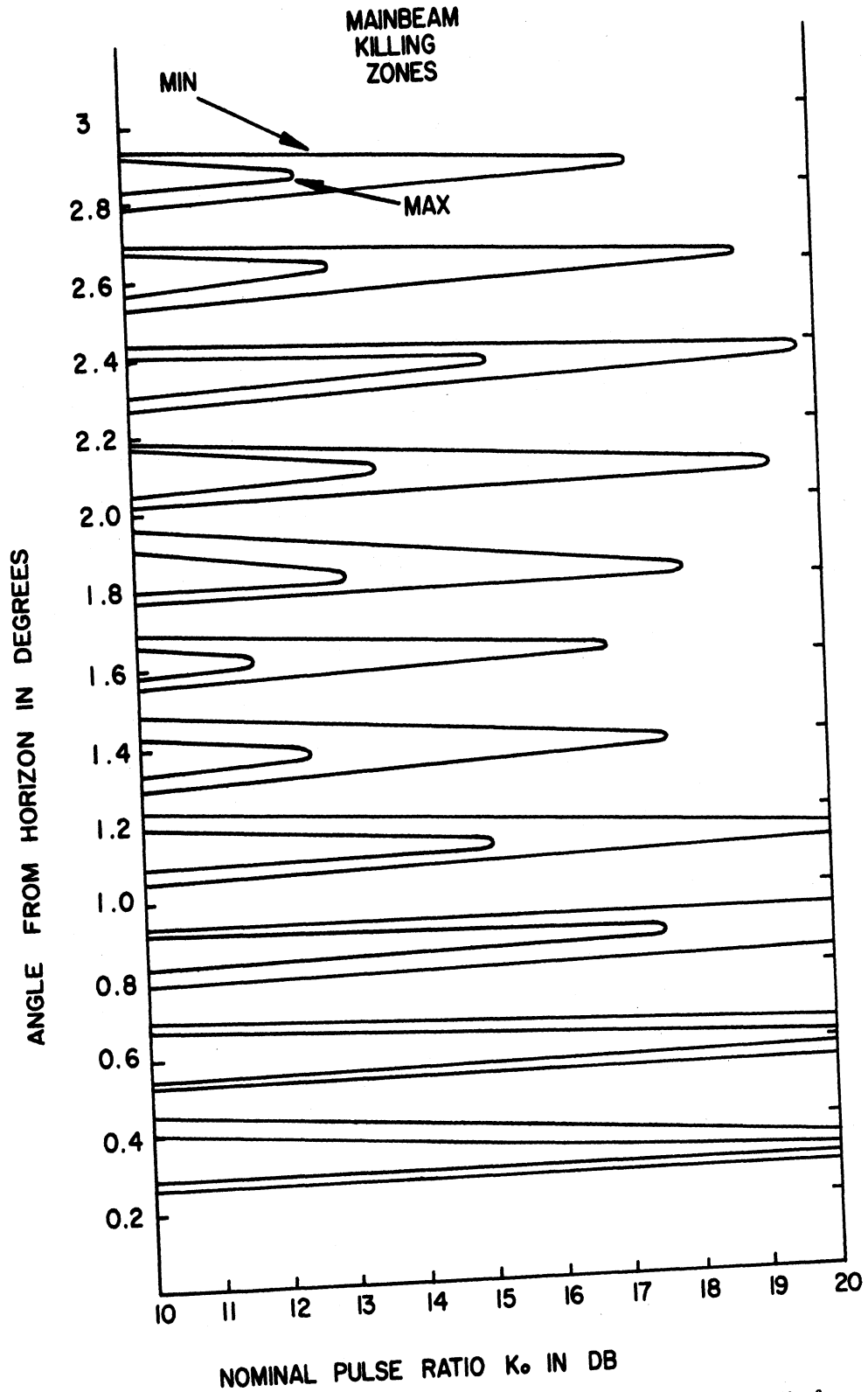

FIG. 71 a: Mainbeam killing zones as functions of nominal pulse ratio for NADIF Fix III antenna. H_d = 92', H_0 = 110', f = 1030 MHz, P1 DIR/OMNI = 18dB, a = 9dB, b = 0dB, L = -25dB.

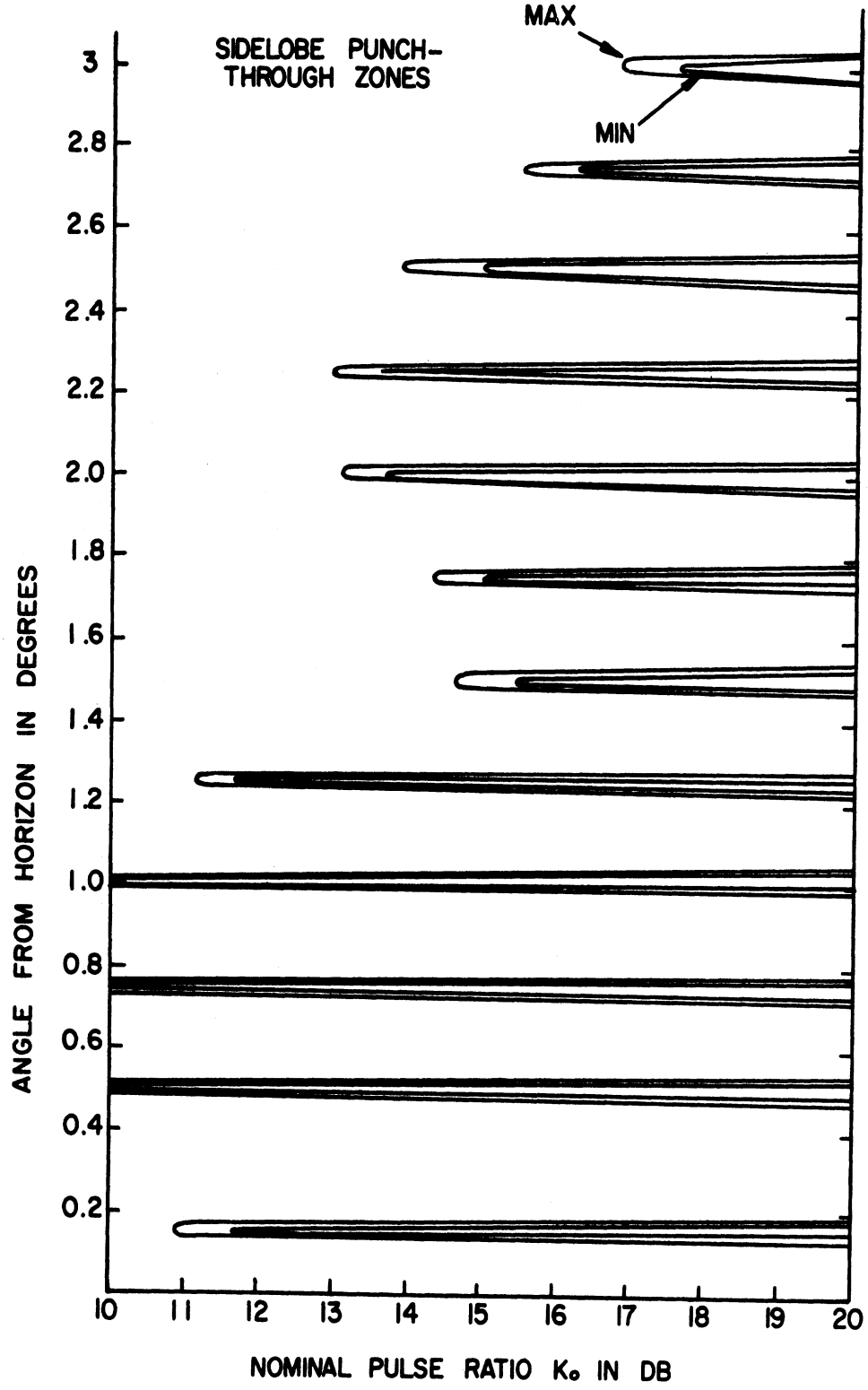

FIG. 71 b: Sidelobe punch-through zones as functions of the nominal pulse ratio for NADIF Fix III antenna. H_d = 92', H_0 = 110', f = 1030 MHz, P1 DIR/OMNI = 18dB, a = 9dB, b = 0dB, L = -25dB.

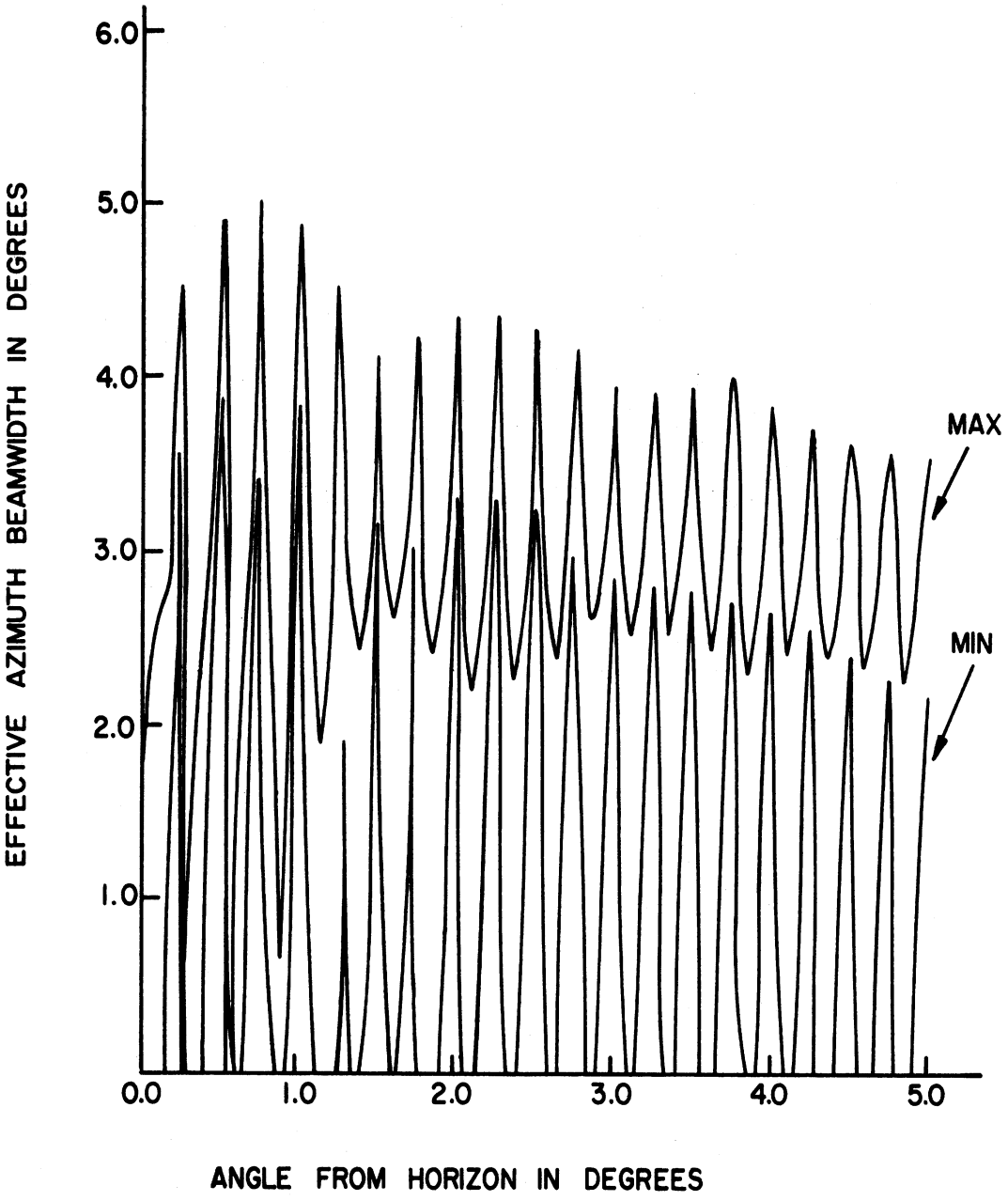

FIG. 72: Effective azimuth beamwidths as functions of the angle from the horizon for the NADIF Fix III antenna. H_1 = 92', H_0 = 110', f = 1030 MHz, nominal pulse ratio K_0 = 18dB, P1 DIR/OMNI = 18dB.

Figure 73 shows the number of replies $N_{MAX}(\theta)$, $N_{MIN}(\theta)$ as functions of θ. The number of replies does not assume constant values within the range of θ shown in Fig. 73. For $\theta > 10^{o}$, $N_{MAX}(\theta) \sim 28$ and $N_{MIN}(\theta) \sim 17$. The corresponding saturation value of the number of replies is about 24 for the same antenna operating in the SLS mode.

The coverage diagram for the antenna is the same as NADIF Fix I and II, and is shown in Fig. 63.

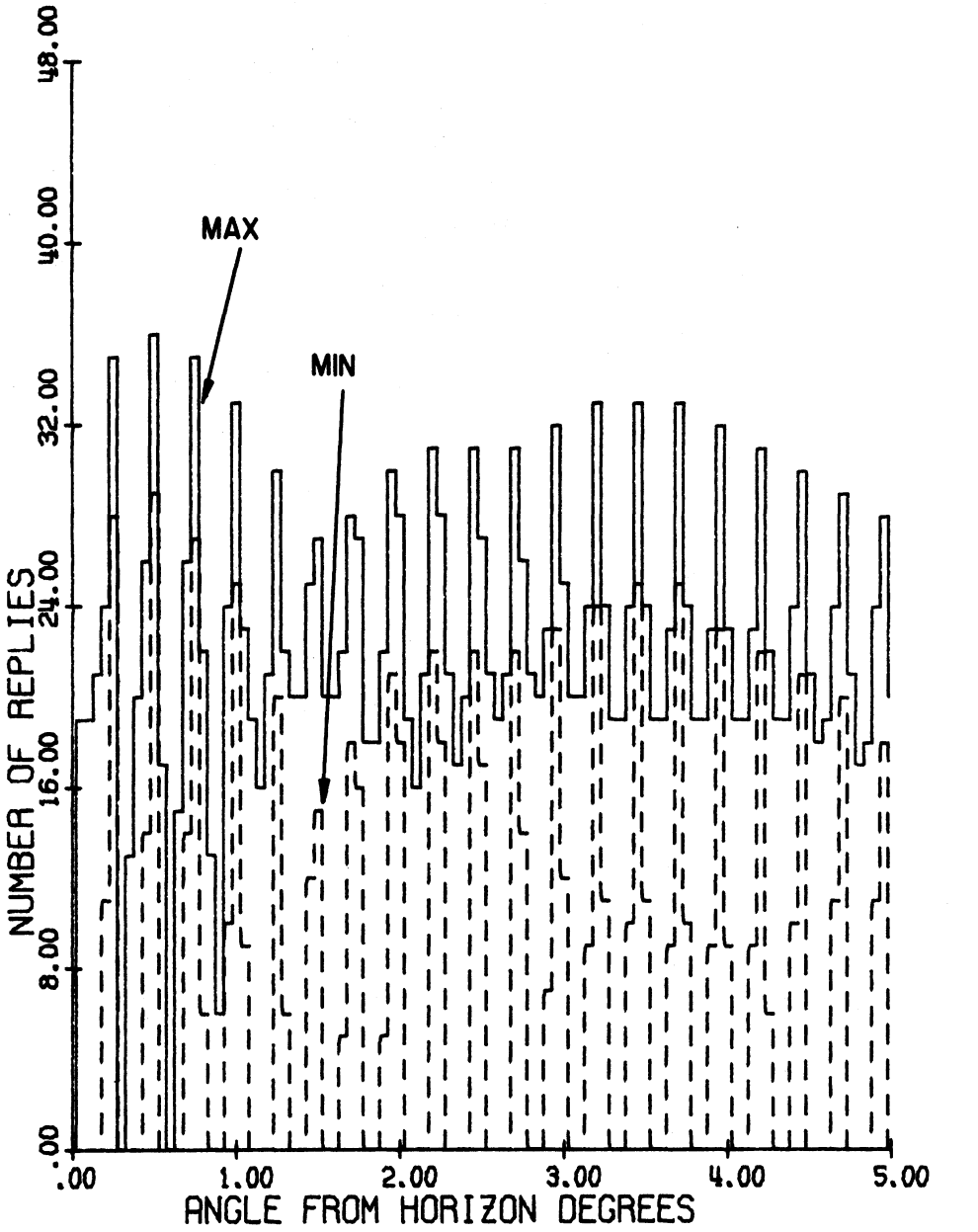

FIG. 73: Number of replies as functions of angle from the horizon.

5. GENERAL DISCUSSION

Detailed numerical results for the ISLS mode performance of ATCRBS using different antenna systems have been given in Section 4. In the present section we give a short discussion of some of the selected results.

5.1 Summary of Important Results

The ISLS mode results given in the previous chapter have been divided into two main groups: one corresponds to the maximum pulse envelope case, and the other to the minimum pulse envelope case. The occurrence of either case depends mainly on the phase relationship between the directional and omnidirectional antennas (see Section 2). Some of the selected important parameters characterizing the overal ISLS mode performance of the ATCRBS in these two cases are shown in Tables 9 and 10, respectively. The tables have been prepared so that the various antenna systems involved may be compared with each other on the basis of different performance criteria. The various symbols used in Tables 9 and 10 are explained as follows:

N_{MB} is the number of main beam killing zones in $0^{o} \leq \theta \leq 5^{o}$ for nominal pulse ratio K_0 = 18 dB and the threshold level a = 9 dB, 1/q = 18 dB,

N_{SL} is the number of sidelobe punch-through zones in $0^{o} \leq \theta \leq 5^{o}$ for nominal pulse ratio K_0 = 18 dB, threshold level b = 0 dB, sidelobe level L = -25 dB and 1/q = 18 dB,

N_{max} is the maximum number of replies in $0^{o} \leq \theta \leq 5^{o}$,

N_{min} is the minimum number of replies in $0^{o} \leq \theta \leq 5^{o}$,

N_f is the number of replies in free space,

R_{max} is the maximum range in nautical miles for ATCRBS in the presence of ground,

R_{min} is the minimum range in nautical miles for ATCRBS in the presence of ground,

R_0 is the maximum SLS mode range in nautical miles for the ATCRBS in free space.

TABLE 9: SUMMARY OF THE ISLS MAXIMUM ENVELOPE MODE PERFORMANCE CRITERIA OF ATCRBS

	Antenna Type	N_{MB}	N_{SL}	N_{max}	N_f	N_{min}	R_{max}	R_0	R_{min}
Terminal	Westinghouse Array	0	2	24	18	9	50.5	40	14
	Texas Inst. Reflector	0	2	25	19	11	44	40	6
	Hazeltine Open Array	0	4	24	19	8	44	40	8
	Existing Hog-Trough	1	7	26	19	0	81	40	5
	Hazeltine E-Scan			19		19	45	40	14
Enroute	Westinghouse Array	0	5	49	37	20	251	200	50
	Texas Inst. Reflector	0	4	50	39	21	220	200	52
	Existing Hog-Trough	2	20	47	38	0	408	200	22
	Texas Fix Reflector	1	3	33	24	0	250	200	50
	NADIF Fix I	2	2	35	24	0	280	200	50
	NADIF Fix II	1	3	36	22	0	280	200	50
	NADIF Fix III	2	12	36	28	0	280	200	50

TABLE 10: SUMMARY OF THE ISLS MINIMUM ENVELOPE MODE PERFORMANCE CRITERIA OF ATCRBS

	Antenna Type	N_{MB}	N_{SL}	N_{max}	N_f	N_{min}	R_{max}	R_0	R_{min}
Terminal	Westinghouse Array	2	2	18	7	0	40	40	7
	Texas Inst. Reflector	2	2	18	7	0	34	40	3
	Hazeltine Open Array	4	3	17	8	0	34	40	5
	Existing Hog-Trough	5	7	20	9	0	62	40	2
	Hazeltine E-Scan			8		8	36	40	12
Enroute	Westinghouse Array	5	4	36	17	0	192	200	28
	Texas Inst. Reflector	6	4	38	16	0	172	200	28
	Existing Hog-Trough	16	13	33	18	0	321	200	18
	Texas Fix Reflector	3	3	25	11	0	200	200	15
	NADIF Fix I	3	2	26	10	0	220	200	15
	NADIF Fix II	3	3	28		0	220	200	15
	NADIF Fix III	8	12	29	17	0	220	200	15

From Tables 9 and 10 it is found that in general, the maximum envelope ISLS mode performance of ATCRBS using any antenna system is superior to the minimum envelope ISLS mode performance. Basically the reason for this is that the received pulse ratio within the main beam region is always larger for the

maximum envelope case at all angles. However, in the maximum envelope case the sidelobe punch-through occurs more frequently. For all the antennas considered, it is found that the operation in the maximum envelope considerably reduces the main beam killing zones in space.

As discussed in Section 2, modes operating in the maximum or the minimum envelopes may be obtained by properly adjusting the phase difference between the directional and omnidirectional antennas. From the results given in Tables 9 and 10, it may be concluded that in almost all cases it is more advantageous to operate in the maximum envelope level, which can be obtained by using the appropriate amount of phase delay between the directional and omnidirectional antenna when radiating the P1 pulses.

5.2 SLS Mode Results

Detailed results of the SLS mode performance of ATCRBS using various antenna systems have been discussed in [1]. For the purpose of comparing the performance of ATCRBS in ISLS and SLS modes we give some selected results of the SLS mode performance in Table 11.

TABLE 11: SUMMARY OF THE PERFORMANCE CRITERIA OF ATCRBS OPERATING IN THE SLS MODE

	Antenna Type	N_{MB}	N_{SL}	N_{max}	N_f	N_{min}	R_{max}	R_0	R_{min}
Terminal	Westinghouse Array	1	2	23	15	0	45	40	10.5
	Texas Inst. Reflector	0	2	23	16	3	39.3	40	11
	Hazeltine Open Array	2	4	23	15	0	39.3	40	4.1
	Existing Hog-Trough	6	6	23	15	0	76	40	4.8
	Hazeltine E-Scan	0	0		16		41	200	13
Enroute	Westinghouse Array	0	4	45	32	6	223.4	200	41.4
	Texas Inst. Reflector	0	4	45	32	8	196.4	200	38.7
	Existing Hog-Trough	10	19	43	30	0	368.4	200	16.8
	Texas Instruments Fix Antennna	3	3	30	20	0	232	200	30
	NADIF Fix I	3	3	32	20	0	252	200	30
	NADIF Fix II	2	4	33	20	0	252	200	30
	NADIF Fix III	3	13	33	20	0	252	200	30

5.3 Comparison of ISLS and SLS Mode Performance

On comparing the results given in Tables 9, 10 and 11, it is found that in general, the quality of SLS mode performance of ATCRBS falls between those of the maximum and minimum envelope cases of the ISLS mode, the maximum envelope mode performance being superior. From the results obtained in the present investigation, it appears that during the ISLS mode of operation it would be advantageous to adjust the relative phase of the directional and omnidirectional antennas such that the system operates at the maximum pulse envelope. The phase adjustment necessary to achieve the maximum in the ISLS P1 pulse envelope might be made by monitoring the signal received by a sensor suitably placed to be in the far field of the two antenna system and at a height equivalent to an elevation angle corresponding to the first maximum in the P1 pulse lobing pattern.

5.4 General Discussion of ISLS Mode Results

Except for the existing hog-trough and Hazeltine open array antennas, it is found that the lobings in the elevation plane patterns of all other antennas in the presence of ground take place mostly in the region $\theta < 5^{o}$. For $\theta > 5^{o}$ the patterns above ground become essentially similar to the corresponding free space patterns; in this region of space the $P1(\theta)_{MAX}$ and $P1(\theta)_{MIN}$ levels occur slightly above and below the free space SLS mode $P1(\theta)$ pulse intensity level. The lobings in the patterns are attributed to the fact that the free space elevation plane patterns have large field gradients below the horizon as well as the fact that for vertical polarization the reflection coefficient is a rapidly decreasing function of θ in the region of interest. The lobings in the region $\theta \leq 2.5^{o}$ are found to be most critical.

The lobings in the patterns continue up to $\theta \sim 20^{o}$ for the existing hog-trough antenna and up to $\theta \sim 10^{o}$ for the Hazeltine open array antenna. The reason for this is that these two antennas have small field gradients. As shown in Table 8, the field gradients associated with them are $0.37dB/1^{o}$ and $1.6dB/1^{o}$ respectively.

The pulse ratio curves show that for most antennas only the first and sometimes the second minima could cause the appearance of mainbeam killing zones if

the value of the nominal pulse ratio K_0 is not too small (i.e., $K_0 > 12$dB, say). Also, only the first and sometimes the second maxima are responsible for sidelobe punch-through zones if K_0 is not too large (i.e., $K_0 \leq 18$dB, say). In the case of the hog-trough and Hazeltine open array antennas the first few maxima and minima would be responsible for the creation of the main beam killing and sidelobe punch-through zones. In general, it has been found that for a given antenna system, the main beam killing zones become a more serious problem when the system operates in the minimum pulse ratio envelope.

The behavior of the oscillations in the coverage diagrams as functions of θ for the different antennas appears to be similar to that of the lobings in the elevation plane patterns of the antennas. For most of the antennas the coverage diagrams oscillate appreciably for $0^o < \theta < 5^o$, for $\theta > 5^o$ the oscillations become negligible and the ranges of the beacon for the maximum and minimum envelope cases are slightly above and below the free space SLS mode range. For the existing hog-trough and Hazeltine open array antennas the oscillations persist up to $\theta \sim 25^o$ and $\theta \sim 10^o$ respectively.

On the basis of the present investigation it is found that with 25dB sidelobe level in the azimuth plane pattern of the antenna the most important parameter characterizing the performance of an antenna is its field gradient in the vertical plane pattern of the antenna below the horizon. Of the antennas studied, the existing hog-trough and the Hazeltine open array antennas have the smallest field gradients; thus the overall performance of these two antennas is poorer than the others. The Hazeltine open array performs better than the existing hog-trough antenna because of its higher field gradient.

Judging from the criteria of Tables 9 and 10, the Westinghouse array,antenna, the Texas Instruments reflector antenna and the Hazeltine E-scan antenna all promise to have superior performance. It is seen that the performance characteristics of the first two antennas are much the same. Tables 9 and 10 show the distinct advantage of having the phase centers of the directional and omnidirectional antennas coincident as does the Hazeltine E-scan antenna. For the enroute system, it is seen that the performance of the Westinghouse array and the Texas Instruments reflector antennas

is generally equal and superior to other enroute systems, especially when judged on the basis of main beam killings, sidelobe punch-throughs and the number of replies. NADIF Fix III results shown in Tables 9 and 10 show the existence of a large number of sidelobe punch-through zones. This is attributed to the use of the existing small aperture omni antenna which has a small field gradient. This indicates that for satisfactory performance, both the directional and omnidirectional antennas should have large field gradients.

6. REFERENCES

[1] J. Zatkalik, D. L. Sengupta and C-T Tai, "SLS Mode Pefformance of ATCRBS with Various Antennas", Technical Report 1, Contract DOT-TSC-17, The University of Michigan Radiation Laboratory Report 012539-1-T, July 1974.

[2] A. Ashley, C. F. Phillips and A. A. Simolunas, "System Capability of Air Traffic Control Radar Beacon System", Department of Transportation, Air Traffic Control Advisory Committee Report, Vol. 2, pp. 287-300, 1969.

[3] N. K. Shaw and A. A. Simolunas, "System capability of air traffic control radar beacon system", Proc. IEEE, Vol. 58, No. 3, 399-407, 1970.

[4] A. Ashley and J. S. Perry, "Beacons", Chapter 38, in Radar Handbook, ed. M. Skolnik, McGraw-Hill Book Co., New York, pp. 38-1 - 38-33, 1970.

[5] "U. S. national standard for the IFF Mark X (SIF)/air traffic control beacon system characteristics", Amendment 1, October 10, 1968 (obtainable from Federal Aviation Administration, Washington, D. C.).

[6] P. R. Drouilhet, "The development of the ATC radar beacon system: past, present, and future", IEEE Trans. on Communications, Vol. Com-21, No. 5, 408-421, 1973.

[7] B. M. Poteat, W. B. Evans, A. W. Markusan, K. W. Connor, K. F. Horenkamp, D. Davis and D. R. Logan, "ATCRBS Antenna Modification Kit: Phase I", Westinghouse Defense and Electronic Systems Center, Systems Development Division, Baltimore, Maryland, July 25, 1973.

[8] P. N. Richardson, "Air Traffic Control Radar Beacon System (ATCRBS) Phase I Final Engineering Report, Report No. UI-855511-F, Texas Instruments, Inc., Dallas, Texas, 1973.

[9] V. Mazzola, P. W. Hannan, E. M. Newman and P. Kendrick, "ATCRBS Antenna Modification Kit, Phase I", Engineering Report No. 10991, Hazeltine Corporation, Greenlawn, New York, 1973.

[10] Frank LaRussa, Private communication, 1973.

[11] R. J. Giannini, J. H. Gutman and P. W. Hannan, "A cylindrical phased-array antenna for ATC interrogation", Microwave Journal, Vol. 16, No. 10, 46-49, 1973.

APPENDIX A
COMPUTER PROGRAM FOR IBM-360, MODEL 67

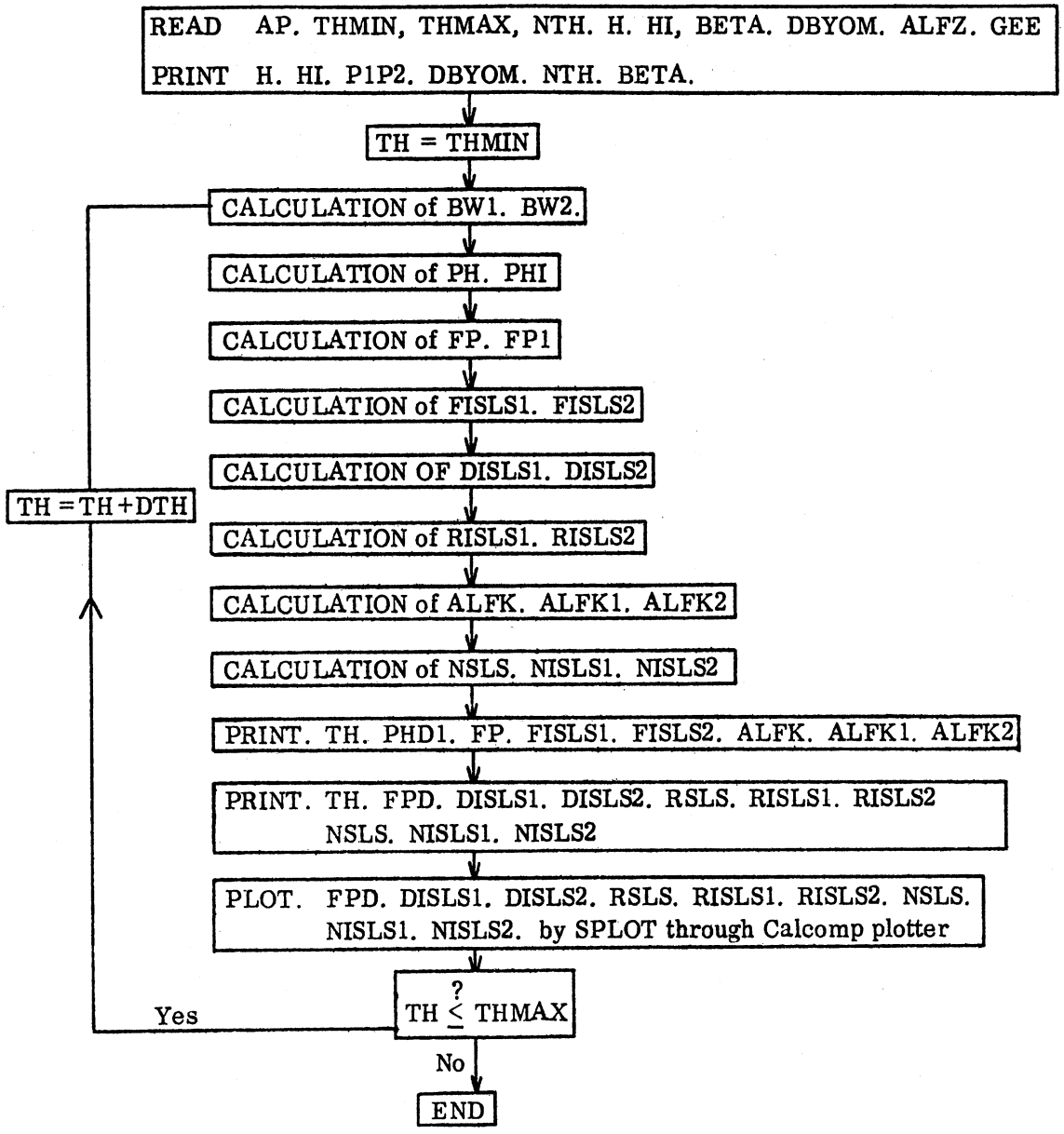

FIG. A-1: Flow diagram for the main program.

List of Some of the Symbols Used

ABS = Absolute value

ALFK = $\alpha_{eff}(\theta)$SLS

ALFK1 = $\alpha_{max}(\theta)$

ALFK2 = $\alpha_{min}(\theta)$

ALOG10 = Log 10

BETA = β

DISLS1 = 20 log 10 (FISLS1)

DISLS2 = 20 log 10 (FISLS2)

DR = $\pi/180.0$

DTH = (THMAX - THMIN)/(NTH-1)

FISLS1 = P1 max(θ)

FISLS2 = P1 min(θ)

FP = P1(θ)SLS for H

FPD = 20 log 10 (FP)

FP1 = P1(θ)SLS for H1. FPD1 = 20 log 10 (FP1)

NSLS = N(θ)SLS

NISLS1 = $N_{max}(\theta)$

NISLS2 = $N_{min}(\theta)$

PH = Fd(θ)

PHD = 20 log 10 PH

PHDI = 20 log 10 PHI

PHI = Fd(-θ)

PI = π

REF = $\rho(\theta)$

RISL1 = DISLS1 - FPD1

RISLS2 = DISLS2 - FPD1

RSLS = PFD - FPD1

SIN1 = specified for each antenna

SQRT = Square root

TH = θ

MAIN PROGRAM

```
C   *** PROGRAM TO ANALIZE THE PERFORMANCE OF BEACON SYSTEMS ***
C
C    *** INPUT QUANTITIES :
C      AP        ANTENNA TYPYE;
C                1    WESTINGHOUSE ANTENNA
C                2    TEXAS INSTRUMENTS ANTENNA
C                3    HAZELTINE ANTENNA
C                4    EXISTING ANTENNA
C                5    NADIF FIX1 ANTENNA
C                6    TEXAS FIX ANTENNA
C                7    HAZELTINE ESCAN ANTENNA
C      THMAX     UPPER LIMIT FOR ELEVATION ANGLE IN PATTERN CALCULATION
C      THMIN     LOWER LIMIT FOR ELEVATION ANGLE IN PATTERN CALCULATION
C      BETA      TILTED ANGLE
C      NTH       NUMBER OF POINTS BETWEEN HORIZONTAL AND THMAX
C      H         ELEVATION OF DIRECTIONAL ANTENNA
C      H1        ELEVATION OF OMNIDIRECTIONAL ANERNNA
C      P1P2      RATIO OF P1 PULSE TO P2 PULSE AMPLITUDES IN DB
C      DBYOM     RATIO OF THE PORTION OF P1 PULSE RADIATED BY THE
C                DIRECTIONAL ANTENNA TO THAT RADIATED BY THE
C                OMNIDIRECTIONAL ANTENNA FOR ISLS CASE
C      ALFZ      NOMINAL BEAMWIDTH
C      GEE       CONSTANT RELATED TO THE SPEED OF ROTATION
       DIMENSION A(7),C(15,8)
       INTEGER AP
       DATA A /4.3738,1.7039,0.4554,1.1036,0.2644,0.6346,0.8108/
       DATA C /-64.85,-135.06,13.02,-64.55,-151.88,-47.04,-91.27,8*0.0,
      1 0.084,0.080,0.500,1.000,0.300,0.860,0.790,0.860,0.960,0.540,
      2 0.230,0.120,0.060,2*0.0,
      3 0.500,1.000,0.885,0.530,11*0.0,
      4 0.084,0.51,0.966,0.780,0.045,10*0.0,
      5 0.01,0.094,0.635,0.99,0.53,0.542,0.515,0.515,0.43,0.465,0.437,
      6 0.327,0.302,0.217,0.153,
      7 0.01,.039,.561,.995,.482,.45,.435,.42,.355,.417,.342,.35,.334
      8,.24,.12,
      9 0.079,0.072,0.03,0.53,0.915,0.945,0.845,0.845,0.315,0.034,5*0.0/
       READ(5,200) AP,THMIN,THMAX,NTH,H,H1,BETA,P1P2,DBYOM,ALFZ,GEE
       IF(NTH.GT.401) NTH=401
       IF (THMAX.GT.90.0) THMAX=90.0
C   *** OPERATING FREQUENCY : F=1030.0 MHZ
       F=1030.0
       PI=3.14159265
       DR=0.017453292
       PP1=-36.0
       PP2=0.0
       RAT1=-15.00
       RAT2=15.000
       NOPMIN=000
       NOPMAX=030
       CONST=4.*PI*F/11808.0
       P1P2=ABS(P1P2)
       DBYOM=ABS(DBYOM)
       QISLS=1.0/(10.0**(DBYOM/20.0))
       BW1=2.32-1./(10.0**((P1P2-DBYOM)/20.0))
       BW2=7.64-BW1
       BW1=20.0*ALOG10(BW1)
       BW2=20.0*ALOG10(BW2)
       DTH=(THMAX-THMIN)/(NTH-1)
       WRITE (6,212)
       GO TO (1,2,3,4,5,6,7), AP
```

main program (cont'd)

```
    1   WRITE (6,201) BETA
        WRITE (7,201) BETA
        NS=7
        B=2.*5.4*F/11808.0
        GO TO 8
    2   WRITE (6,202) BETA
        WRITE (7,202) BETA
        NS=13
        K1=3
        SIN1=0.07846
        GO TO 8
    3   WRITE (6,203) BETA
        WRITE (7,203) BETA
        NS=4
        K1=1
        SIN1=0.22495
        GO TO 8
    4   WRITE (6,204) BETA
        WRITE (7,204) BETA
        NS=5
        K1=3
        SIN1=0.47767
        GO TO 8
    5   WRITE (6,205) BETA
        WRITE (7,205) BETA
        NS=15
        K1=3
        SIN1=0.0583
        GO TO 8
    6   WRITE (6,206) BETA
        WRITE (7,206) BETA
        NS=15
        K1=3
        SIN1=0.0583
        GO TO 8
    7   WRITE (6,207) BETA
        WRITE (7,207) BETA
        NS=10
        K1=4
        SIN1=0.11942
    8   WRITE(6,208) H,H1,P1P2,DBYDM
        WRITE(7,209) H,H1,P1P2,DBYDM,P1P2,NTH
        H=12.0*H
        H1=12.0*H1
        DO 14 N=1,NTH
        TH=THMIN+(N-1)*DTH
        THETA=TH*DR
        SINTH=SIN(THETA)
        SQRT1=SQRT(2.+SINTH**2)
        REF=(3.*SINTH-SQRT1)/(3.*SINTH+SQRT1)
          TB=(TH-BETA)*DR
        SINTB=SIN(TB)
        COSTB=COS(TB)
        TC=(TH+BETA)*DR
        SINTC=SIN(TC)
        COSTC=COS(TC)
        IF (AP.EQ.1) GO TO 11
C   ***FREE SPACE PATTERN FOR ALL EXPECT WESTINGHOUSE
        ARG1=SINTB/SIN1
        ARGN=SINTC/SIN1
```

main program (cont'd)

```
      PH=0.0
      PH1=0.0
      DO 10 K=1,NS
      ARG=PI*(ARG1-K+K1)
      IF (ABS(ARG).LE.0.0349) GO TO 9
      PH=PH+C(K,AP)*SIN(ARG)/ARG
      GO TO 101
    9 PH=PH+C(K,AP)
  101 ARGM=PI*(K1-K-ARGN)
      IF (ABS(ARGM).LE.0.0349) GO TO 102
      PH1=PH1+C(K,AP)*SIN(ARGM)/ARGM
      GO TO 10
  102 PH1=PH1+C(K,AP)
   10 CONTINUE
      GO TO 13
C ***FREE SPACE PATTERN FOR WESTINGHOUSE
   11  COSTH=COS(THETA)
      ARG2=PI*COSTB/2.
      ARG3=PI*SINTB/2.0
      PHZ=SIN(ARG2)*COS(ARG3)/COSTB
      AR2=PI*COSTC/2.0
      AR3=PI*SINTC/2.0
      PHX=SIN(AR2)*COS(AR3)/COSTC
      PH=PHZ*5.4201
      PH1=5.4201*PHX
      DO 12 K=1,NS
      ARG4=K*PI*B*SINTB
      ARGL=K*PI*B*SINTC
      PH=PH+2.*PHZ*A(K)*COS(ARG4+DR*C(K,AP))
      PH1=PH1+2.*PHX*A(K)*COS(DR*C(K,AP)-ARGL)
   12 CONTINUE
      PH=PH/15.686
      PH1=PH1/15.686
   13 IF (ABS(PH).LE.0.016035) GO TO 103
      PHD=20.0*ALOG10(ABS(PH))
      GO TO 104
  103 PHD=-36.00
  104 IF(ABS(PH1).LE.0.016035) GO TO 105
      PHD1=20.0*ALOG10(ABS(PH1))
      GO TO 106
  105 PHD1=-36.00
  106 IF (H.LE.0) GO TO 14
      ETA=PH1*REF/PH
      ARG5=CONST*H*SINTH
      FP=PH*SQRT(1.+ETA**2+2.*ETA*COS(ARG5))
      IF (FP.LE.0.016035) GO TO 107
      FPD=20.0*ALOG10(FP)
      GO TO 108
  107 FPD=-36.0
  108  IF (H1.LE.0.0) GO TO 14
      ARG6=CONST*H1*SINTH
      FP1=PH*SQRT(1.+ETA**2+2.*ETA*COS(ARG6))
      IF (FP1.LE.0.016035) GO TO 109
      FPD1=20.0*ALOG10(FP1)
      FPD2=FPD1-P1P2
      IF (FPD2.LE.-36.00) FPD2=-36.00
      GO TO 110
  109 FPD1=-36.0
      FPD2=FPD1
  110 FISLS1=FP+QISLS*FP1
```

main program (cont'd)

```
      FISLS2=FP-QISLS*FP1
      IF (ABS(FISLS1).LE.0.016035) GO TO 111
      DISLS1=20.0*ALOG10(ABS(FISLS1))
      GO TO 112
  111 DISLS1=-36.0
  112 IF (ABS(FISLS2).LE.0.016035) GO TO 113
      DISLS2=20.0*ALOG10(ABS(FISLS2))
      GO TO 114
  113 DISLS2=-36.0
  114 RSLS=FPD-FPD1
      RISLS1=DISLS1-FPD1
      RISLS2=DISLS2-FPD1
      IF (THETA.EQ.0.0) GO TO 121
      ALFK=(RSLS+P1P2-9.)/12.0735
      ALFK1=(RSLS+P1P2-BW1)/12.0735
      ALFK2=(RSLS+P1P2-BW2)/12.0735
      IF (ALFK.LE.0.0) GO TO 115
      ALFK=2.*ALFZ*SQRT(ALFK)
      GO TO 116
  115 ALFK=0.0
  116 IF(ALFK1.LE.0.0) GO TO 117
      ALFK1=2.*ALFZ*SQRT(ALFK1)
      GO TO 118
  117 ALFK1=0.0
  118 IF (ALFK2.LE.0.0) GO TO 119
      ALFK2=2.*ALFZ*SQRT(ALFK2)
      GO TO 120
  119 ALFK2=0.0
  120 NSLS=ALFK*GEE
      NISLS1=ALFK1*GEE
      NISLS2=ALFK2*GEE
      GO TO 122
  121 ALFK=0.0
      ALFK1=0.0
      ALFK2=0.0
      NSLS=0
      NISLS1=0
      NISLS2=0
  122 WRITE(6,210) TH,PHD,PHD1,FP,FISLS1,FISLS2,ALFK,ALFK1,ALFK2
      WRITE (7,211) TH,FPD2,FPD ,DISLS1,DISLS2,RSLS,RISLS1,RISLS2,
     1NSLS,NISLS1,NISLS2
  14  CONTINUE
  200 FORMAT (1X,I1,2F6.2,I3,/,2F10.4,/,3F10.4,/,2F10.4)
  201 FORMAT ('WESTINGHOUSE ANTENNA TILTED ANGLE=',F4.1,' DEG')
  202 FORMAT ('TEXAS INSTR. ANTENNA TILTED ANGLE=',F4.1,' DEG')
  203 FORMAT ('HAZALTINE ANTENNA    TILTED ANGLE=',F4.1,' DEG')
  204 FORMAT ('EXISTING ANTENNA     TILTED ANGLE=',F4.1,' DEG')
  205 FORMAT ('NADIR FIX1 ANTENNA   TILTED ANGLE=',F4.1,' DEG')
  206 FORMAT ('TEXAS FIX ANTENNA    TILTED ANGLE=',F4.1,' DEG')
  207 FORMAT ('HAZALTINE ESCAN ANT. TILTED ANGLE=',F4.1,' DEG')
  208 FORMAT ('0ELEVATION OF DIRECTIONAL ANTENNA = ',F10.4,' FEET  ',
     1///,'ELEVATION OF OMNIDIRECTIONAL ANTENNA= ',F10.4,' FEET  ',
     2///,'RATIO OF PULSES P1/PI=',F6.2,' DB',
     2///,'P1 THRU DIREC. ANT./P1 THRU OMNI. ANT. (ISLS)=',F6.2,' DB',
     2///,4X,'ANGLE FROM',5X,'FREE SPACE PATTERN',6X,'P A T T E R N ',
     3' A B O V E  G R O U N D',7X,'E F F E C T I V E  B E A M W I ',
     4'D T H ',/,4X,' HORIZON ',3X,'ABOVE HOR.',3X,'BELOW HOR.',3X,
     5'P1 PULSE SLS',4X,'P1 ISLS MAX',4X,'P1 ISLS MIN',3X,'SLS CASE',7X,
     6'ISLS MAX',7X,'ISLS MIN',/)
  209 FORMAT ('ELEV.: DIREC.',F8.2,'''',4X,'OMNI.',F8.2,'''',/,
```

main program (cont'd)

```
     1'P1/P2=',F6.2,' DB P1 DIR./OMN.=',F6.2,' DB.                    ',/,
     1'P1/P2=',F6.2,' DB.',/,
     1'                                          ',/,
     1'ANGLE FROM HORIZON DEGREES',/,
     2'P1 AND P2 PATTERNS SLS (DB)',/,
     3'P1 AND P2 PATTERNS ISLS (DB)',/,
     4'    ISLS NORMALIZED P1/P2 (DB)          ',/,
     5'NUMBER OF REPLIES',/,
     5I4,/,
     7'DEG FROM HOR',1X,'P2 DB',7X,'P1 SLS DB',3X,'P1MAX ISLS',2X,
     8'P1MIN ISLS',2X,'RSLS DB',5X,'RISLS MAX',3X,'RISLS MIN',2X,
     9'NO OF REP SLS',2X,'NISLS MAX',2X,'NISLS MIN',/)
 210 FORMAT (4X,F9.4,1X,E12.4,1X,E12.4,1X,E12.4,4X,E12.4,3X,E12.4,2X,
     1E12.4,3X,E12.4,3X,E12.4)
 211 FORMAT (8E12.4,7X,I3,9X,I3,8X,I3)
 212 FORMAT ('1')
     STOP
     END
```

Program for Graphical Output SPLOT

```
      DIMENSION X(401),X1(800),X2(800),X3(800)
      DIMENSION Y1(401),Y2(401),Y3(401),Y4(401),Y5(401),Y6(401),Y7(401)
      REAL NR1,NR2,NR3
      DIMENSION NR1(800),NR2(800),NR3(800)
      DIMENSION T1(10),T2(10),T3(15),T4(10),T5(10)
      DIMENSION XPRINT(10),YPRNT1(10),YPRNT2(10),YPRNT3(10),YPRNT4(10)
      READ (5,21,END=500) (T1(I),I=1,10)
      READ (5,21) (T2(I),I=1,10)
      READ (5,24) (T3(I),I=1,14)
      READ (5,21) (T4(I),I=1,10)
      READ (5,21) (T5(I),I=1,10)
      READ (5,21) (XPRINT(I),I=1,8)
      READ (5,21) (YPRNT1(I),I=1,8)
      READ (5,21) (YPRNT2(I),I=1,8)
      READ (5,21) (YPRNT3(I),I=1,9)
      READ (5,21) (YPRNT4(I),I=1,8)
      READ (5,22) N
      M1=1
      M2=1
      M3=1
      DO 3 I=1,N
      READ (5,23) X(I),Y1(I),Y2(I),Y3(I),Y4(I),Y5(I),Y6(I),Y7(I)
     1,NNR1,NNR2,NNR3
      IF(I.NE.1) GO TO 100
      NR1(1)=NNR1
      NR2(1)=NNR2
      NR3(1)=NNR3
      X1(1)=X(I)
      X2(1)=X(I)
      X3(1)=X(I)
100   IF((NNR1.EQ.NR1(M1)).AND.(I.NE.N)) GO TO 1
      M1=M1+1
      X1(M1)=(X(I)+X(I-1))/2.0
      NR1(M1)=NR1(M1-1)
      M1=M1+1
      X1(M1)=X1(M1-1)
      NR1(M1)=NNR1
1     IF((NNR2.EQ.NR2(M2)).AND.(I.NE.N)) GO TO 2
      M2=M2+1
      X2(M2)=(X(I)+X(I-1))/2.0
      NR2(M2)=NR2(M2-1)
      M2=M2+1
      X2(M2)=X2(M2-1)
      NR2(M2)=NNR2
2     IF((NNR3.EQ.NR3(M3)).AND.(I.NE.N)) GO TO 3
      M3=M3+1
      X3(M3)=(X(I)+X(I-1))/2.0
      NR3(M3)=NR3(M3-1)
      M3=M3+1
      X3(M3)=X3(M3-1)
      NR3(M3)=NNR3
3     CONTINUE
      CALL PLT(X(2),Y1(2),N-1,X(2),Y2(2),N-1,0.0,0.0,0,XPRINT(1),
     1YPRNT1(1),T1(1),T2(1),T4(1))
      CALL PLT(X(2),Y1(2),N-1,X(2),Y3(2),N-1,X(2),Y4(2),N-1,XPRINT(1)
     1,YPRNT2(1),T1(1),T2(1),T3(1))
      CALL PLT(X(2),Y5(2),N-1,0.0,0.0,0,0.0,0.0,0,XPRINT(1),YPRNT3(2),
     1T1(1),T2(1),T5(1))
      CALL PLT(X(2),Y6(2),N-1,X(2),Y7(2),N-1,0.0,0.0,0,XPRINT(1),
     1YPRNT3(1),T1(1),T2(1),T3(5))
```

SPLOT (cont'd)

```
      CALL PLT(X1(1),NR1(1),M1,0.0,0.0,0,0.0,0.0,0,XPRINT(1),YPRNT4(1)
     1,T1(1),T2(1),T4(1))
      CALL PLT(X2(1),NR2(1),M2,X3(1),NR3(1),M3,0.0,0.0,0,XPRINT(1),
     1YPRNT4(1),T1(1),T2(1),T3(1))
   21 FORMAT(10A4)
   22 FORMAT (I4,/)
   23 FORMAT (8E12.4,7X,I3,9X,I3,8X,I3)
   24 FORMAT (14A4)
  500 STOP
      END
      SUBROUTINE PLT(X1,Y1,N1,X2,Y2,N2,X3,Y3,N3,XPRINT,YPRINT,T1,T2,T3)
      DIMENSION X1(800),X2(800),X3(800)
      DIMENSION Y1(800),Y2(800),Y3(800)
      DIMENSION XPRINT(10),YPRINT(10),T1(10),T2(10),T3(10)
      CALL PLTXMX(10.0)
      CALL PSCALE(5.0,1.0,XMIN,DX,X1,N1,1,X2,N2,1,X3,N3,1)
      CALL PSCALE(5.0,1.0,YMIN,DY,Y1,N1,1,Y2,N2,1,Y3,N3,1)
      CALL PLTOFS(XMIN,DX,YMIN,DY,3.0,3.0)
      CALL PAXIS(3.0,3.0,XPRINT,-30,5.0,0.0,XMIN,DX,1.0)
      CALL PAXIS(3.0,3.0,YPRINT,30,6.0,90.0,YMIN,DY,1.0)
      CALL PLTREC
      IF (N1.EQ.0) GO TO 1
      CALL PLINE(X1,Y1,N1,1,0,0,1.0)
    1 IF (N2.EQ.0) GO TO 2
      CALL PDSHLN(X2,Y2,N2,1,0.1,1.0)
    2 IF (N2.EQ.0) GO TO 3
      CALL PCTRLN(X3,Y3,N3,1,1.0)
    3 CL=PSYMLN(0.15,30)
      CALL PSYMB(5.25-CL/2.,2.0,0.15,T1,0.0,40)
      CALL PSYMB(5.25-CL/2.,1.8,0.15,T2,0.0,40)
      CALL PSYMB(5.25-CL/2.,1.6,0.15,T3,0.0,40)
      CALL PLTEND
      RETURN
      END
```

APPENDIX B
REPORT OF INVENTIONS

A diligent review of the work performed under this contract has revealed no new innovation, discovery, improvement or invention.